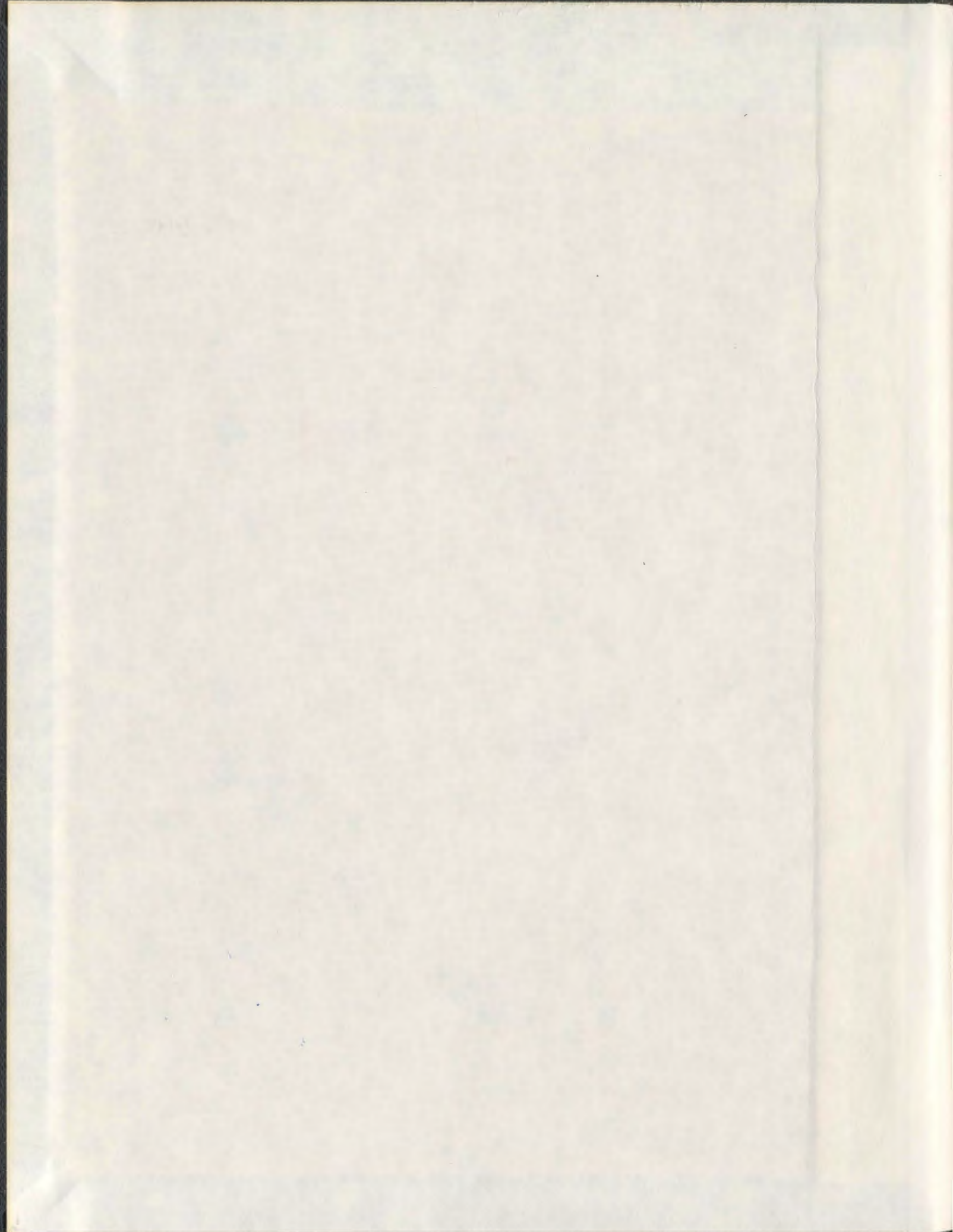
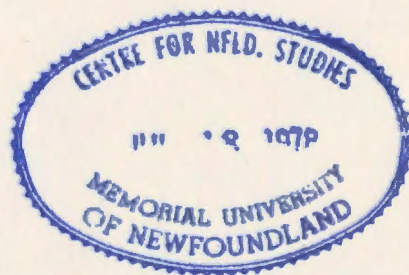


SYNTHESIS AND CHARACTERIZATION OF MOLECULAR
MATERIALS DERIVED FROM DENDRIMERS,
[60] FULLERENE, AND LINEAR π -CONJUGATED OLIGOMERS

MD. ILIAS MAHMUD



001311



**Synthesis and Characterization of Molecular
Materials Derived from Dendrimers, [60]Fullerene,
and Linear π -Conjugated Oligomers**

by

© Md. Ilias Mahmud

A thesis submitted to the
School of Graduate Studies
in partial fulfilment of the
requirements for the degree of
Doctor of Philosophy

Department of Chemistry
Memorial University of Newfoundland

December 2009

St. John's

Newfoundland

Abstract

This thesis reports the studies of a series of novel π -conjugated organic hybrid materials undertaken throughout my PhD research. In the synthetic work, the Cu(I)-catalyzed azide-alkyne [3+2] cycloaddition, one of the most popular click reactions, has been successfully utilized to covalently attach a series of azido-pendant Fréchet-type dendrimers to various alkynylated π -conjugated building blocks, ranging from [60]fullerene, porphyrin, tetrathiafulvalene (TTF) analogues, and linear/star-shaped conjugated phenylene ethynylene oligomers (OPEs), in a modular fashion. The resulting hybrid macromolecules show rich photophysical, electrochemical, and surface morphological properties, which are potentially useful for the application in molecular optoelectronic devices. The most remarkable finding resulting from the "click synthesis" comes from a class of dendro[60]fullerenes, which show interesting surface self-assembly behavior to form controllable nanostructures. The correlation between aggregation behavior and molecular parameters has been examined, and the results indicate that the surface self-assembling properties of these dendro[60]fullerenes are dependent on dendron generation, the nature of the end-groups, and acidity. Moreover, a class of electron-rich polyynes has been synthesized, in which redox active 1,3-dithiole and ferrocenyl end groups are incorporated into the polyynes. Potential of these polyyne-TTF hybrids in making electrochemically active conducting polymer materials has been explored based on voltammetric and spectroscopic characterization. Finally, the thesis work has developed the synthesis of a series of poly(ethylene glycol) (PEG) functionalized conjugated arylene polymers as well as a group of imidazolium-based ionic liquids. These materials are specially

designed for functionalization of single-walled carbon nanotubes (SWNTs) through non-covalent and covalent approaches.

Acknowledgements

I would like to express sincere thanks to my revered supervisor Prof. Yuming Zhao for being a great inspirational mentor during my time at Memorial University. Dr. Zhao is an extraordinary young scientist from whom I have learned a great deal. I am immensely indebted for his generous support in guiding, helping and constantly encouraging me throughout this research effort. He is the most creative person I have had the opportunity so far to work with in a chemistry lab and will never forget his innumerate brilliant ideas. But more importantly Dr. Zhao is a wonderful person. He has created an extremely positive, ambitious, and stimulating research environment in the laboratory that makes it a pleasure to come to work everyday.

It gives me immense pleasure to express my heartfelt thanks to the members of my candidacy examination and supervisory committees, Profs. Graham Bodwell, Robert J. Helleur, Sunil Pansare, and Travis Fridgen, for their time and valuable suggestions. Special thanks to our collaborator, Prof. David W. Thompson for many things, including valuable suggestions, especially in solving the photophysical and photochemical properties of some complex compounds.

I am also thankful to all respectable teachers, and staff at the Department of Chemistry, Memorial University; particularly to Profs. Paris Georghou, Peter Pickup, Raymond Poirier for their encouragement during the course of my research. I also want to thank to the nice people of the Department of Chemistry, especially to Ms. Mary Flinn, Ms. Viola Martin, Ms. Linda Winsor, and many others, though it will be hard to name all of them here.

I am very much grateful to my parents, my wife, my beloved daughter and

my brother, and sister for their unparalleled love. My wife, Afroza Begum, who is an electroanalytical chemist of my department, has been very inspirational and supportive in both academics and life. I am grateful for her understanding and patience, since chemistry joined our hands.

Last, but certainly not the least, I would like to thank my colleagues who have helped me in so many ways during this research. All of my lab mates, especially Guang Chen and Li Wang, for being very supportive over the years on various aspects of materials analysis and I feel very fortunate to have worked with them.

To everyone else I did not mention, thanks for making my time enjoyable at Memorial University. I wish everyone all the best in future.

Contents

Acknowledgements	ii
Acknowledgements	iv
List of Schemes	x
List of Tables	xiv
List of Abbreviations and Symbols	xv
1 Introduction	1
1.1 Nanomaterials Chemistry: Significance, Opportunities and Challenges	1
1.2 Development of Click Chemistry	5
1.2.1 Essential Criteria for Click Reactions	7
1.2.2 Types of Click Reactions	8
1.3 Cu-Catalyzed Alkyne-Azide Coupling (CuAAC)	10
1.3.1 Mechanism of CuAAC Reaction	13
1.3.2 Catalysts for CuAAC	15
1.3.3 Roles of Base and Ligand in CuAAC	18

1.3.4	CuAAC in Multicomponent One-Pot Synthesis	19
1.3.5	Microwave(MW)-Assisted CuAAC	21
1.3.6	CuAAC in Solid-Phase Synthesis	22
1.4	Recent Advances in Material Synthesis Based on CuAAC	23
1.4.1	Macromolecular and Supramolecular Synthesis Based on CuAAC	24
1.4.2	CuAAC Based Surface Functionalization	38
1.4.3	Synthesis of Well-defined Hydrogel Networks via CuAAC . . .	42
1.4.4	Functionalization of [60]Fullerene via CuAAC	46
1.4.5	Functionalization of Carbon Nanotubes via CuAAC	46
1.5	Outline of this thesis	49
2	Dendro[60]fullerenes: Modular Synthesis and Controllable Supramolec- ular Self-Assembly	52
2.1	Introduction	52
2.2	Objectives of This Project	63
2.3	Results and Discussions	64
2.3.1	Synthesis	64
2.3.2	Structures and Electrochemical Properties of Dendro[60]fullerenes	67
2.3.3	Electronic Absorption and Emission Properties of Dendro[60]fullerenes	70
2.3.4	Interfacial Self-Assembling Behavior of Dendro[60]fullerenes .	73
2.4	Conclusions	79
2.5	Experimental Part	80
3	Dendrimer Functionalized π-Conjugated Macromolecules	101
3.1	Introduction	101

3.2	Objectives of the Project	106
3.3	Results and Discussions	106
3.3.1	Synthesis of Dendrimer-Functionalized <i>meso</i> -Porphyrins . . .	106
3.3.2	Synthesis of Dendrimer-Functionalized TTFAQs	107
3.3.3	Synthesis of Dendrimer-Functionalized Linear OPEs	109
3.3.4	Attempted Synthesis of Dendrimer-Functionalized Star-Shaped OPEs	112
3.3.5	Characterizations of Dendrimer-Functionalized <i>meso</i> -Porphyrins	116
3.3.6	Characterizations of Dendrimer-Functionalized TTFAQs . . .	120
3.3.7	Characterizations of Dendrimer-Functionalized Linear OPEs .	124
3.4	Conclusions	127
3.5	Experimental Part	127
4	Synthesis and Properties of Electroactive Polyynes	153
4.1	Introduction	153
4.2	Objectives of the Project	159
4.3	Results and Discussions	161
4.3.1	Synthesis	161
4.3.2	Characterizations	166
4.4	Conclusions	173
4.5	Experimental Part	174
5	Design and Synthesis of π-Conjugated Polymers and Task-specific Ionic Liquids for Carbon Nanotube Functionalization	191
5.1	Introduction	191

5.2	Objectives of the Project	196
5.3	Results and Discussions	199
5.3.1	Synthesis of Ethylene Glycol Functionalized Phenylene Ethynylene Polymers	199
5.3.2	Synthesis of Task-specific Imidazolium Ionic Liquids	202
5.3.3	Supramolecular Interactions Between SWNTs and Conjugated Polymers	203
5.4	Conclusions	207
5.5	Experimental Part	208
6	Conclusions and Future Work	224
	Bibliography	227

List of Schemes

1.1	A hetero Diels-Alder type click reaction.	8
1.2	A nucleophilic ring opening click reaction.	9
1.3	Sharpless' asymmetric dihydroxylation as a click reaction.	9
1.4	A Heck-type cyclization click reaction.	10
1.5	A thiol-ene coupling (TEC) reaction as click reaction.	10
1.6	Comparison of uncatalyzed and Cu-catalyzed Huisgen 1,3-dipolar cycloaddition reactions.	11
1.7	Microwave-assisted one-pot CuAAC reaction.	13
1.8	Mechanism of the CuAAC reaction.	14
1.9	Click reaction catalyzed by Cu turnings or wire.	17
1.10	Alkyne coupling side-reactions commonly observed in CuAAC reactions.	19
1.11	A one-pot three-component CuAAC reaction.	20
1.12	A one-pot synthesis of a triazol-substituted glycoconjugate from D- glucose.	20
1.13	A one-pot Wittig-Knoevenagel-Diels-Alder-CuAAC reaction.	21
1.14	A solid-phase CuAAC reaction.	23
1.15	Convergent synthesis of dendrimers using the CuAAC reaction.	24

1.16	Synthesis of a diblock dendrimer via the CuAAC reaction.	25
1.17	Pre- and post-functionalization poly(<i>p</i> -phenylene ethynylene)s (PPEs) via the CuAAC reaction.	27
1.18	Preparation of functional thiophene monomer by click chemistry. . . .	28
1.19	Preparation of functionalized PEDOT by click chemistry.	29
1.20	Synthesis of a dendrinoized polymer via the CuAAC reaction.	29
1.21	Synthesis of cyclic dendronized polymer via an REMP click reaction.	30
1.22	A cascade functionalization of synthetic polymers using CuAAC reaction.	31
1.23	Orthogonal multi-functionalization of random co-polymers.	31
1.24	Synthesis of neoglycopolymers via a “co-click” strategy.	32
1.25	Matyjaszewski’s one-pot, multi-catalytical, three step strategy for telechelic polystyrene synthesis.	33
1.26	Jérôme’s domino-type strategy for dimethyl amino functionalized Polymer.	34
1.27	Orthogonal tandem strategy for the synthesis of triblock-copolymers.	35
1.28	“Click cyclization” to make well-defined macrocyclic polymers. . . .	35
1.29	Synthesis of a flavin-functionalized polymer by click chemistry and self-assembly with DAP.	36
1.30	Block copolymer synthesis using the CuAAC and ROMP reactions. .	37
1.31	Modification of SAM surfaces using CuAAC reactions.	39
1.32	CuAAC based layer-by-layer assembly of ultra-thin polymer multilayer films.	39
1.33	Synthesis of conjugated polymers by CuAAC reactions.	40

1.34	Coupling of azide-pendant ligands to the surface of pre-formed liposomes via CuAAC.	41
1.35	Click reactions among PEG-based building blocks to form hydrogels.	42
1.36	3-D hydrogel networks constructed by CuAAC.	43
1.37	Synthesis of polymer-peptide conjugate 143 via CuAAC.	44
1.38	Formation of horse albumin (HA)-based hydrogels via CuAAC.	45
1.39	Functionalization of SWNTs with polystyrenes via CuAAC.	48
1.40	Functionalization of MWNTs via CuAAC.	49
1.41	Covalent attachment of cyclodextrins to SWNTs via CuAAC.	49
2.1	Self-Assembling supramolecular nanostructures from a C ₆₀ Derivative.	56
2.2	Synthesis of C ₆₀ -rich dendrimers via click chemistry.	59
2.3	Fullerene hexakis-adducts prepared by CuAAC reaction.	60
2.4	Fréchet-type Azide-Pendant Dendrimers.	65
2.5	Synthesis of dendrofullerene 175-179 through click chemistry.	66
3.1	Proposed molecular switch behavior for dendrimer-functionalized phenylacetylene-TTFAQ 191	105
3.2	Synthesis of alkyne pendant porphyrin 193 and dendroporphyrins 194-196 via a click reaction.	107
3.3	Attachment of dendrimers to extended-TTFAQ via CuAAC reactions.	108
3.4	Synthesis of dendrimer functionalized OPEs 210-213	110
3.5	Synthesis of dendrimer-functionalized linear PPE oligomers (219-222).	111
3.6	Synthesis of star-shaped OPE 228	114
3.7	Attempted synthesis of dendrimer-functionalized star-shaped OPE 228a	115

4.1	Tobe's synthesis of cyclo[n]carbons (243ad) by laser-desorption time-of-flight.	158
4.2	Cyclic polyynes were supposed as intermediates of [60] fullerenes. . .	158
4.3	Two polyynes synthetic approaches via Hay coupling and a modified Fritsch-Buttenberg-Wiechell (FBW) rearrangement.	159
4.4	Synthesis of phosphonate 257	161
4.5	Synthesis of dithiafulvenyl (DTF) endcapped tetrayne 262 and diyne 263	162
4.6	Synthesis of DTF endcapped hexaynes 266	163
4.7	Synthesis of DTF endcapped diynes 271	164
4.8	Synthesis of ferrocenyl endcapped polyynes.	165
4.9	Proposed polymerization pathways for 285 via oxidative coupling or topochemically controlled 1,4-addition.	168
5.1	Synthesis of ethylene glycol ether functionalized PPE 288	200
5.2	Synthesis of ethylene glycol ether functionalized PPB 289	201
5.3	Synthesis of a foldamer-type phenylene ethylene polymer 290	202
5.4	Synthesis of imidazolium and pyrene containing ionic liquids.	203

List of Tables

2.1	Electronic and emission properties of dendrofullerenes.	72
3.1	Photophysical data for free base porphyrin 193 , 194 , and 196	117
3.2	Electrochemical data of porphyrins 193-196	118

List of Abbreviations and Symbols

1D	one-dimensionally
2D	two-dimensionally
A	acceptor
Å	angstrom(s)
AFM	atomic force microscopy
APCI	atmospheric pressure chemical ionization
aq	aqueous
Bu	butyl
calcd	calculated
cm	centimeter(s)
CV	cyclic voltammetry
D	donor
d	doublet

DBU	1,8-diazabicyclo[5.4.0]undec-7-ene
dec	decomposed
DFT	density functional theory
DMF	<i>N,N</i> -dimethylformamide
DMSO	dimethyl sulfoxide
E_g	bandgap energy
EL	electroluminescence
Et	ethyl
FBW	Fritsch-Buttenberg-Wiechell
FET	field effect transistor
FTIR	Fourier transform Infrared (spectroscopy)
g	gram(s)
HMBA	4-hydroxymethylbenzoic acid
h	hour(s)
HOMO	highest occupied molecular orbital
IL	ionic liquid
IR	infrared (spectroscopy)

ITO	indium tin oxide
LCD	liquid crystal display
LCMS	liquid chromatography-mass spectrometry
LDA	lithium diisopropylamide
LED	light emitting diode
LHMDS	lithium hexamethyldisilazide
LUMO	lowest unoccupied molecular orbital
m	multiplet
<i>m/z</i>	mass to charge ratio
mA	milliampere(s)
MALDI-TOF	matrix assisted laser desorption/ionization-time of flight
Me	methyl
mg	milligram(s)
MHz	megahertz
min	minute(s)
mL	milliliter(s)
mmol	millimole(s)

mol	mole(s)
mp	melting point
MS	mass spectrometry
NBS	<i>N</i> -bromosuccinimide
NLO	nonlinear optical
nm	nanometer
NMR	nuclear magnetic resonance (spectroscopy)
ODCB	<i>ortho</i> -dichlorobenzene
OFET	organic field effect transistor
OLED	organic light emitting diode
OPE	oligo(<i>p</i> -phenyleneethynylene)
OP	oligo(<i>p</i> -phenylene)
OPV	oligo(<i>p</i> -phenylene vinylene)
OPV	Organic Photovoltaics
OT	oligo(α -thiophene)
<i>p</i>	<i>para</i>
PA	poly(acetylene)

PCBM	[6,6]-phenyl C61-butyric acid methyl ester
PCC	pyridinium chlorochromate
PDA	poly(diacetylene)
PEG	poly(ethylene glycol)
PEGA	poly(ethylene glycol dimethylacrylamide)
Ph	phenyl
PL	photoluminescence
PPE	poly(<i>p</i> -phenyleneethynylene)
PPB	poly(<i>p</i> -phenylenebutadienylene)
ppm	parts per million
PPP	poly(<i>p</i> -phenylene)
PPV	poly(<i>p</i> -phenylenevinylene)
PTA	poly(triacetylene)
PVC	poly(vinyl chloride)
rt	room temperature
s	second(s) or singlet
satd	saturated

SEC	size exclusion chromatography
STC	standard test conditions
t	triplet
TDI	toluene diisocyanate
TBAF	tetra- <i>n</i> -butylammonium fluoride
TBTA	tris-[(1-benzyl-1H-1,2,3-triazol-4-yl) methyl]amine
TCEP	tris(2-carboxyethyl)phosphine
Tf	trifluoromethanesulfonyl
THF	tetrahydrofuran
THPTA	tris(hydroxypropyltriazolylmethyl)amine
TIPS	triisopropylsilyl
TIPSA	triisopropylsilylacetylene
TLC	thin-layer chromatography
TMEDA	tetramethylethylenediamine
TMS	trimethylsilyl
TMSA	trimethylsilylacetylene
TTF	tetrathiafulvalene

TTFAQ	<i>N,N,N',N'</i> -tetrathiafulvaleneanthraquinone
UV-Vis	ultraviolet-visible
UI	ultrasonic irradiation
UV-Vis-NIR	ultraviolet-visible-near infrared (spectroscopy)
V	volt(s)
W	watt(s)
XRD	X-ray diffraction
δ	chemical shift
λ_{em}	maximum emission wavelength
λ_{maz}	maximum absorption wavelength

Chapter 1

Introduction

1.1 Nanomaterials Chemistry: Significance, Opportunities and Challenges

The term “nano” has already been deeply rooted in the present sciences and technologies, despite the fact that a clear definition to distinguish nanoscience and nanotechnology from other scientific disciplines is not existing. Generally speaking, nanoscience refers to the study of phenomena and the manipulation of materials on the atomic to molecular and macromolecular scales. Materials fabricated on this scale (1 to 100 nm) tend to show physical, chemical and biological properties and phenomena that are unique or unprecedented compared to their macroscopic counterparts.¹ The origin of such a “nano effect” or “quantum effect” has been broadly discussed and well established in numerous literature sources, and the “nano” approach has become extremely popular in modern materials science to design and exploit novel materials whose structural dimensions are intermediate between isolated

atoms and bulk macroscopic materials, in order to tune-up, modify, or sometimes even to reverse the properties of various materials.

At the very heart of nanoscience and nanotechnology are the rational design of nanostructured materials and integration of them in relevant device applications. Ever since the early conceptualization by Eric Drexler and Norio Taniguchi, the focuses on nanoscience and nanotechnology have enormously reshaped the landscapes of chemistry, biology, electrical engineering, materials technology, and other scientific disciplines. For example, understanding of how the flagella of *E. coli* works gave the inspiration to construct molecular motors, while the phenomenon of facile electron transfer through a molecular wire or junction was exploited with new meanings analogous to macroscopic electronic units (*i.e.* molecular electronics). It has been widely accepted that the design of functional nanostructures will form the basis on which future molecular electronics and photonics will be developed. In the meantime, investigations on many naturally existing supramolecular structures, although too complex to be mimicked by current synthetic chemistry, have promoted researchers to envisage new directions that current research would be heading for.

One of the greatest scientific challenges of the 21st century is the development of functional materials with well-defined properties and high degrees of structural order.² In order to meet the rising demand for such advanced materials, new ways and more robust techniques for material preparation are desirable. By modifying the skeletal structure of a molecule or altering the position of a functional group, synthetic chemists now can achieve control over the physical properties of various molecular materials and their interactions with other materials.³ In this respect, organic nanomaterials that contain extensive and well defined π -conjugated backbones

have found a wide range of applications in modern electronics, optoelectronics and photonics, such as organic light-emitting diodes (OLEDs), optical non-linearity controlled telecommunications apparatus, organic thin-film transistors (OTFTs), photodynamic therapies (PDT), optical amplifiers, lasers, and organic photovoltaics (OPVs) or solar cells.⁴

Consider two new molecular materials reported in recent chemistry literature as examples. Perepichka *et al.* recently demonstrated the use of two air-stable isomeric tetrathienoanthracenes (**1** and **2**) to fabricate thin-film transistors by both solution processing and vacuum evaporation techniques with very high thermal stability (up to 400 °C), hole mobilities up to $7.4 \times 10^{-2} \text{ cm}^2 \text{ V}^{-1} \text{ S}^{-1}$ and very high on/off ratios of 1×10^8 for vacuum-deposited films.⁵ Both molecules self-assembled through π -stacking into high-quality thin films (see Figure 1.1).

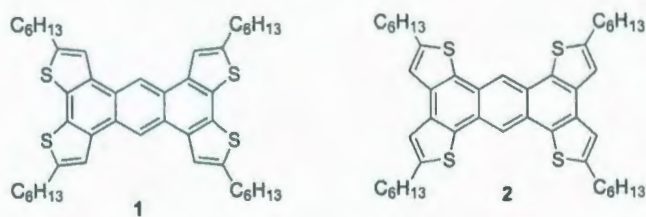


Figure 1.1: Air-stable heteroarenes for thin film organic transistors.

Perylene tetracarboxylic diimides **3** and arylene ethynylene macrocycles **4** were reported by Moore *et al.* in 2008 to self-assemble into 1-dimensional, highly organized supramolecular structures. Potential applications of these materials in nanoscale optoelectronic devices were envisioned in light of their efficient exciton diffusion and charge-transport abilities (see Figure 1.2).⁶

Richard Feynman, one of the most eminent physicists of the last century, began

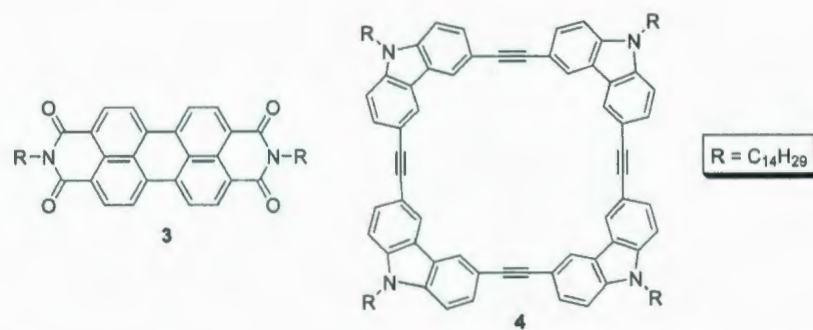


Figure 1.2: Aromatic building blocks for 1D nanostructures developed by Moore.

his famous lecture series in 1959 to the physical society with, *there is plenty of room at the bottom, not just room at the bottom, what I demonstrate is that there is plenty of room that you can decrease the size of things in a practical way.* There is no doubt that this ingenious prophecy has caused the most profound impact in modern science and technology—the rise of nanotechnology. One of the goals of nanotechnology is to acquire superior properties or unprecedented functions by constructing ultra-miniaturized devices. Initially, nanomaterials applied in molecular devices were mainly inorganic species, whereas organic molecules were virtually invisible on the radar. Over the past two decades, however, the research on organic based nanomaterials has advanced substantially, owing to the advantages such as innumerate choices of molecular structures for property optimizations, low cost of building materials, high flexibilities, and ease of processing and compatibilities. Nevertheless, the use of organic molecules in nanodevices is still being hampered by a number of bottlenecks. Among them, how to prepare functional nanomaterials in a controllable manner (*e.g.* well-defined, molecular arrangements, solid-phase ordering, and regular film formation) poses a significantly challenging barrier to practical device fabrication.⁶

Currently, there are two popular approaches for the fabrication of nanoscale materials and devices, namely *bottom-up* and *top-down*. From the synthetic chemist's viewpoint, the bottom-up approach is more appealing, since synthetic chemists are well equipped with a vast number of synthetic methodologies to manipulate various molecular building blocks. In addition, the full-fledged knowledge about supramolecular chemistry has also offered an effective toolbox for precisely and conveniently assembling molecular components into larger functional superstructures. To be useful in the synthesis of nanomaterials, the reactions utilized are generally expected to be high yielding, selective, fast, compatible and environmentally friendly, and are better to end with little or no byproducts. These criteria are aptly fulfilled by the popularized "click chemistry" concept originally developed by Sharpless and co-workers. In the following section, the concept of click chemistry and its recent application in materials chemistry will be briefly reviewed.

1.2 Development of Click Chemistry

If synthetic chemists aim their goals mainly at molecular properties, for example, better pharmaceutical activities or improved photonic absorptivities, then it is logical for them to avoid using complicated synthetic strategies in their experimental maneuvers, unless there are no other choices to achieve the analogous properties.⁷ The synthesis of bioactive natural products has constituted the most intriguing framework of organic chemistry for many decades. However, the synthesis of many of these natural products requires the formation of a large number of contiguous carbon-carbon bonds, which is generally tedious, expensive, and in many cases slow in

reaction rate due to lower thermodynamic driving force, and intolerance to particular experimental conditions. On the other hand, natural products and their analogues are not the only molecules that can give rise to useful biological properties. There are certainly plenty of alternatives that are readily accessible through facile and efficient synthesis; especially, reactions that proceed under benign conditions with fast rates and a high thermodynamic driving force. The use of such kinds of reactions can significantly shorten the period of discovery and production of molecules with desired properties. In this respect, preference is given to carbon-heteroatom bond forming reactions. If one looks around at Nature's examples, there are some advantages to making carbon-heteroatom bonds over carbon-carbon bonds. For example nucleic acids, proteins, and polysaccharides are enzymatically condensed polymeric products that are made up of small subunits linked together through carbon-heteroatom bonds in aqueous media.^{7,8} This concept gave birth to the new field of "click chemistry" in the late 1990s, focusing on synthetic methodologies that lead to easy preparation of complex substances by joining small units together via carbon-heteroatom linkages.⁷ The goal of such kind of "click reactions" has been aimed at making a number of fast, reproducible, selective, and modular building blocks that would work reliably in both small and large-scale applications. In this sense, "click chemistry" is in fact nothing but a synthetic philosophy. According to Sharpless, the concept of click chemistry was inspired by the observation of various special biological events in nature, which generates "smart materials" by ligating simple modular units. For example, the 1,4-disubstituted 1,2,3-triazole linkage resulting from a "click reaction" possesses useful topological and electronic features similar to nature's ubiquitous amide connectors (see Figure 1.3).⁹



Figure 1.3: Triazole linker that mimics natural amide connector.

1.2.1 Essential Criteria for Click Reactions

In 2001, a critical review article was published by Sharpless and co-workers on “click chemistry”,⁷ in which a set of stringent criteria was laid out for categorizing “click reactions” in an unambiguous way. Basically, a click reaction must be:

- Modular and of wide application scope
- High yielding
- Generating inoffensive byproducts that can be removed by nonchromatographic methods
- Stereospecific (but not necessarily enantioselective)

In addition, the click reaction is required to possess characteristics including:

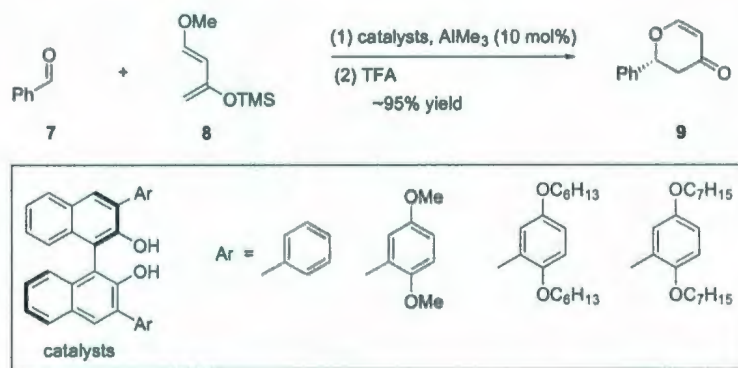
- Simple reaction conditions
- Readily available starting materials and reagents
- Using no solvent or a solvent that is benign (such as water)
- Simple product isolation

Thermodynamically, a click reaction should have a significant driving force. Usually, if the ΔG° is greater than 20 kcal/mol, the reaction can proceed to completion rapidly and yield almost exclusively a single product. In a sense, the reaction can be perceived as “spring-loaded” for a single trajectory. Other preferred features for a click reaction include stability of the reaction product under normal physiological conditions and high atom economy.

1.2.2 Types of Click Reactions

Based on the criteria laid out by Sharpless, a number of special organic reactions have been identified as click reactions. The following section lists the most common representatives of carbon-heteroatom bond forming click reactions.

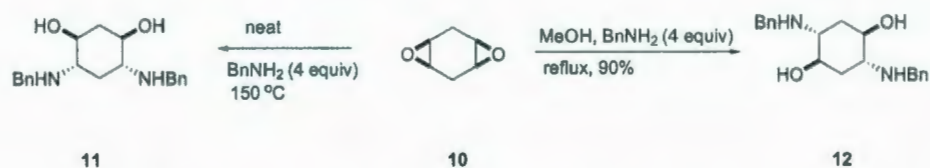
(1) Certain cycloaddition reactions involving unsaturated compounds, for example, 1,3-dipolar cycloaddition and hetero Diels–Alder reactions (see Scheme 1.1).¹⁰



Scheme 1.1: A hetero Diels–Alder type click reaction.

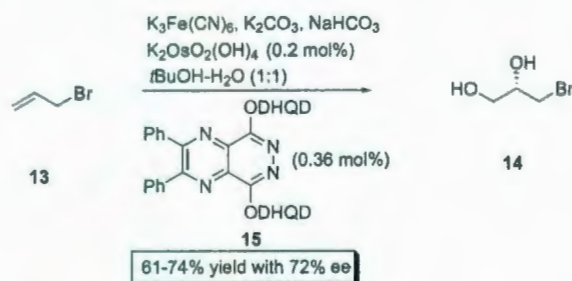
(2) Some nucleophilic substitution reactions involving the ring–opening of strained heterocyclic electrophiles, such as aziridines, epoxides, aziridinium ions, and episul-

fonium ions. For example, Sharpless and co-workers demonstrated the nucleophilic ring-opening of a diepoxide by an amine could be considered as an efficient click reaction (see Scheme 1.2).⁷



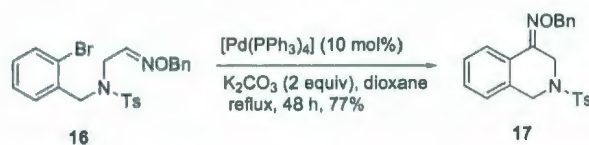
Scheme 1.2: A nucleophilic ring opening click reaction.

(3) Addition reactions to carbon-carbon multiple bonds, especially oxidative addition reactions, such as epoxidation, aziridination, and dihydroxylations, as well as Michael addition of Nu-H reactants. An example of this type of click reaction is the dihydroxylation reaction developed by Sharpless in 1994 (see Scheme 1.3).¹¹



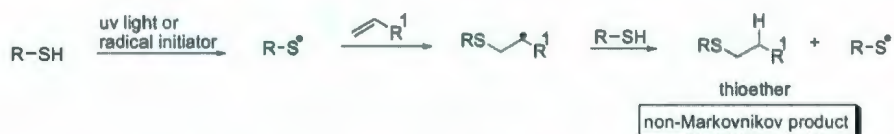
Scheme 1.3: Sharpless' asymmetric dihydroxylation as a click reaction.

(4) Some non-aldol type carbonyl reactions, such as the formation of aromatic heterocycles, oxime ethers, thioureas, amides and hydrazones, can be viewed as click reactions. For example, a non-aldol six-membered-ring formation by Heck-type cyclization as demonstrated by Tanaka *et al.* presents a good example of this type of click reaction (see Scheme 1.4).¹²



Scheme 1.4: A Heck-type cyclization click reaction.

(5) Most recently, a new type of thiol-ene coupling (TEC) reactions has received much attention as a valuable addition to the toolbox of click chemistry. The major advantage of this reaction over other types of click reaction is the absence of metal catalysts, which may eventually render TEC based reactions more compatible with *in vivo* experiments. The photochemically/thermally induced version of TEC follows a radical mechanism, resulting in the formation of an anti-Markovnikov product-thioether as shown in Scheme 1.5.¹³

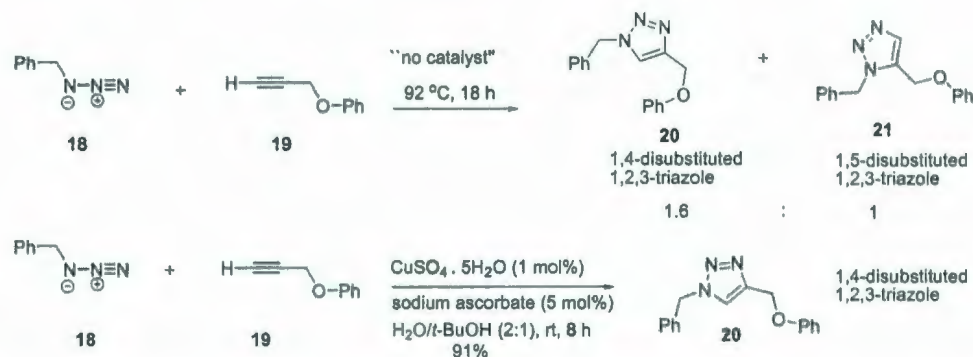


Scheme 1.5: A thiol-ene coupling (TEC) reaction as click reaction.

1.3 Cu-Catalyzed Alkyne-Azide Coupling (CuAAC)

Among numerous click reactions developed in the literature so far, the 1,3-dipolar cycloaddition of azide and alkyne has received enormous attention due to its reliability, specificity, and biocompatibility. In fact, the study of this type of click reaction has become so popular and widely adopted by the synthetic community in recent years that it is regarded as the “cream of the crop” of all the click reactions.

The [3+2] cycloaddition of azide and alkyne, generally referred to as azide/alkyne cycloaddition (AAC), is not new. The original reaction was reported by Dimroth in the early 1900s. In the 1970s, Rolf Huisgen investigated and popularized this reaction by improving the compatibility and stereoselectivity. However, the mechanism of this reaction, along with the potential, generality, and application, had not been fully explored in the ensuing decades. In Huisgen's protocol, the reaction tends to afford a mixture of 1,4 and 1,5-disubstituted triazole isomeric products (see Scheme 1.6). Various attempts thereafter to achieve control over stereoselectivity failed until Sharpless and co-workers devised the protocol of using Cu(I) as an efficient catalyst to exclusively form 1,4-disubstituted 1,2,3-triazole as the only product (see Scheme 1.6).¹⁴

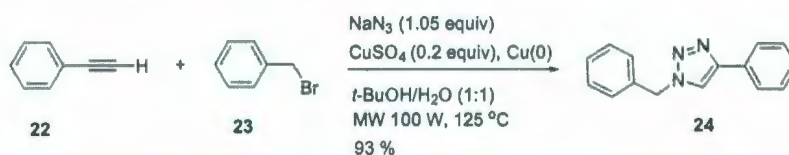


Scheme 1.6: Comparison of uncatalyzed and Cu-catalyzed Huisgen 1,3-dipolar cycloaddition reactions.

Like all other types of click reactions, the CuAAC has a uniquely large thermodynamic driving force of at least 20 kcal/mol, as well as some other appealing features as outlined below:

- The CuAAC reaction can be performed with remarkable tolerance to oxygen, aqueous environment, and most organic and inorganic functional groups.
- The Cu(I) catalyst promotes the reaction rate to *ca.* $k = 10^7$, making the reaction conveniently fast at room temperature. Furthermore, the reaction rate can be accelerated by addition of suitable ligands (*i.e.* ligand-accelerated-catalysis).
- The reaction is almost unaffected by the steric and electronic properties of the substrates. For example, various substituted terminal alkynes react well with azides bearing alkyl (primary, secondary, or tertiary), aromatic, or even heteroaromatic groups.
- The reaction is compatible with water as the solvent. Actually, it has been reported that water is a better solvent than other common organic solvents for CuAAC for several reasons. First, water is a good heat sink and has a convenient boiling temperature, which is particularly suitable for large-scale synthesis. Second, water offers a great leverage for differentiating the reactivities of the competing polarizable and nonpolarized species. Third, the CuAAC reaction proceeds at a much higher rate in an aqueous medium than in an organic one. The reason could be that the free energies of organic molecules become substantially greater when poorly solvated in water, which gives rise to increased reactivity. Therefore, CuAAC reactions are commonly performed in water or mixed-solvent systems containing water mixed with aprotic solvents (*e.g.* acetonitrile, THF, DMSO, halogenated solvents, CHCl_3 , THF or hexane) or protic solvents (MeOH, EtOH, *t*-BuOH).¹⁵ As an example, Scheme 1.7 shows

a three-component, one-pot CuAAC reaction that affords good to excellent yields within 15 min in 1:1 water/*t*-BuOH under microwave irradiation.¹⁶



Scheme 1.7: Microwave-assisted one-pot CuAAC reaction.

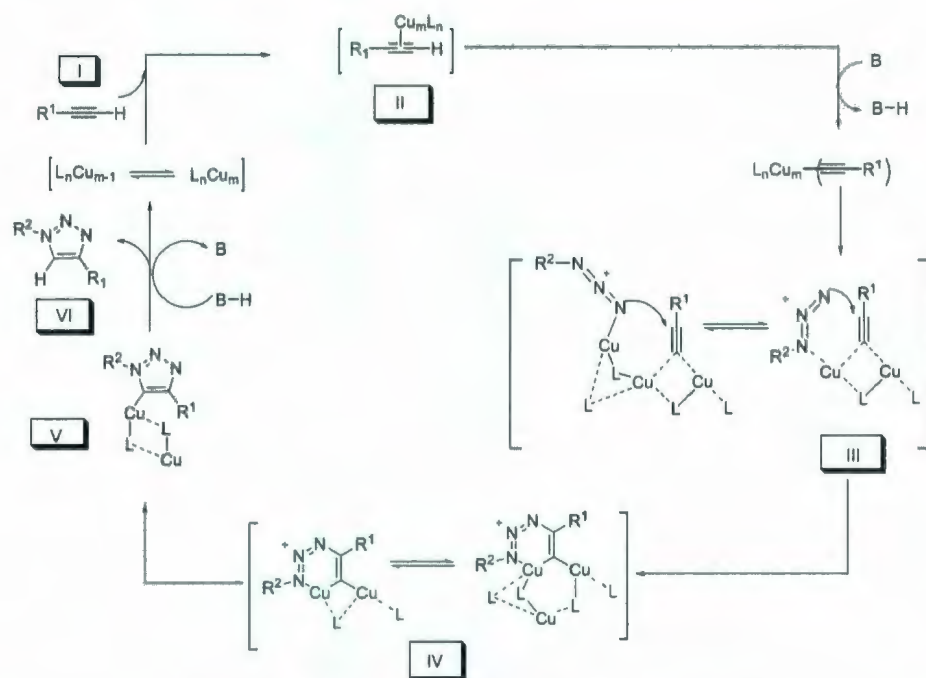
1.3.1 Mechanism of CuAAC Reaction

Experimentally, the following main features of CuAAC reaction have been identified:

1. In the CuAAC, a rate acceleration of up to 10^7 is observed over that of an uncatalyzed AAC reaction, while the 1,4-regioselectivity of CuAAC is exclusive.
2. Kinetic studies reveal that the CuAAC reaction follows second-order kinetics with respect to Cu(I) species (*i.e.* $k \propto [\text{Cu(I)}]^2$). This result suggests that the rate-limiting step of the mechanism may involve the formation of a cluster intermediate containing two copper centers.^{17,18}
3. A significant autocatalytic effect can be observed in the cases where multiple triazoles are formed.¹⁹ This feature is suggestive of an intermolecular ligand effect.¹⁸
4. The formation of copper acetylide appears to be a key step, although the primary structure and the direct activity of such a moiety in the transition state cannot be exactly predicted. The difficulty arises from the fact that there are too many possible interactions (*e.g.* π -complexation, multiple copper species) as

well as numerous known possible structures of copper acetylides. Nevertheless, density functional theory (DFT) calculations have indicated that the formation of a copper acetylene complex results in a substantial lowering of the pKa value of acetylene by 9.8 units. This effect could be the major contribution of copper acetylide to rate acceleration.²⁰

- The reaction rate is significantly decreased with increasing amounts of copper catalyst.



Scheme 1.8: Mechanism of the CuAAC reaction.

Based on the experimental observations, Sharpless and co-workers first proposed a stepwise mechanism for the CuAAC reaction in 2002.¹⁴ The key step of this mechanism is a direct conversion of a di-copper acetylide intermediate into a copper-

triazole intermediate. This mechanism was later revised by Finn and Fokin through DFT studies, in which a Cu-containing six-membered ring intermediate was proposed for the cycloaddition step. Most recently, Bock *et al.* made another modification on this mechanism based on some new experimental findings.^{9,18} Scheme 1.8 depicts the most up-to-date mechanism for the CuAAC reaction. The key steps of this mechanism proceed through the formation of copper acetylide, followed by a six-membered metallocycle **IV** as a key intermediate, which leads to the product 1,2,3-triazole **VI** after reductive elimination.

1.3.2 Catalysts for CuAAC

A large variety of copper-based catalysts have been developed to promote CuAAC reactions, among which Cu(I) salts (*e.g.* CuI and CuBr) or coordination complexes of copper (*e.g.* Cu(CH₃CN)₄PF₆, (EtO)₃P·CuI, Cu(PPh₃)₃Br, Cu(OTf)·C₆H₆) are the most commonly employed ones.¹⁷ The coordination complexes of copper are particularly designed to suit organic media, where Cu(I) salts usually have very poor solubility, so as to give the best performance in either deoxygenated organic solvents or mixed solvent systems involving water.

Generally 0.25–2.00 mol% of catalyst loading is necessary for the CuAAC reaction. It is, however, important to maintain the level of Cu(I) species throughout the course of the reaction. Cu(I) is thermodynamically unstable and susceptible to oxidation to form catalytically inactive Cu(II) or to disproportionation to form Cu(0) and Cu(II) respectively.¹⁹ This is indeed problematic to the CuAAC reaction, since the presence of Cu(II) can catalyze unwanted oxidative homocoupling of alkynes, leading to the

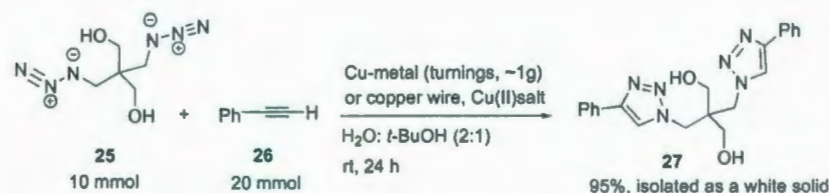
formation of bis(butadiyne) byproducts and reducing the efficiency of cycloaddition.¹⁷

Apart from using Cu(I) species directly, the addition of a sacrificial reducing agent like sodium ascorbate, in combination with Cu(II) salt, such as copper(II) sulfate pentahydrate or copper(II) acetate, can generate Cu(I) *in situ* as an effective catalyst. In these catalyst systems, sodium ascorbate is normally used in 3 to 10-fold excess with respect to CuSO₄.⁹ In addition to ascorbate salts, the use of other reducing agents such as hydrazine and tris(2-carboxyethyl)phosphine (TCEP) has also been reported.^{21,22}

The sacrificial reducing agent approach is economical and can be performed in an aqueous environment without the involvement of base or protecting groups.^{9,23} The main drawback of this method, however, is the possibility of overreduction to form Cu(0). One way to solve the problem is to control the ratio of Cu(II)/reducing agent. Addition of Cu(I) stabilizing reagents, for example, tris(hydroxypropyltriazolylmethyl)amine (THPTA), can greatly improve the yield and purity of the product,^{9,24} since soft ligands like THPTA can effectively stabilize Cu(I) in a way analogous to copper(I)-containing proteins in biological systems.^{9,19,25}

In 2002, Sharpless and co-worker developed a simple method to produce catalytic amount of Cu(I) through comproportionation of Cu(II) and Cu(0).¹⁷ As illustrated in Scheme 1.9, a small piece of copper metal (wire or turnings) was added to the reaction mixture containing Cu(II) species under shaking or stirring at room temperature for 12–48 h to catalyze a click reaction between diazide **25** and phenylacetylene **26**, resulting in an excellent yield.

Active Cu(I) catalysts can also be generated by oxidizing copper metal with amine salts.^{20,23} This method simplifies the reaction conditions but has some drawbacks.



Scheme 1.9: Click reaction catalyzed by Cu turnings or wire.

In particular, it is rather time-consuming and requires excess amounts of copper. Moreover, the reaction medium must be slight acidic in order to dissolve metallic copper. This could be detrimental when acid-sensitive functional groups are present in the reactants.

Recently, stable and readily accessible copper nanoclusters, copper/cuprous oxide nanoparticles,²³ and Cu(I)-modified zeolites^{17,26} have been found to produce excellent catalysis for CuAAC. Especially, Cu(I)-modified zeolites (highly porous aluminosilicate minerals with enormous surface areas) have shown some advantages over other Cu(I) catalysts. CuAAC reactions catalyzed by Cu(I)-zeolite systems can thus proceed without the use of ligands and often result in higher yields (roughly 13% higher) and faster rates (3 times) than those catalyzed by Cu(I) salts. Moreover, the use of Cu(I)-zeolites tends to yield purer products with lower copper contamination. This feature fulfills the requirement for “traceless organic synthesis”, and therefore can be conveniently applied in combinatorial screening studies.

Besides various copper-based catalysts, catalytic systems involving other transition metals, for example, Pt(II), Pd(II), and Ru(II) have been reported in the recent literature.²⁷ These transition metal catalysts, although more expensive than copper, can catalyze the cycloaddition of azides with both terminal and internal alkynes, hence greatly expanding the synthetic scope of AAC reactions.

1.3.3 Roles of Base and Ligand in CuAAC

If the CuAAC reaction is conducted in a non-basic solvent, such as acetonitrile, a suitable amount of base (generally 1–5 equivalents to alkyne/azide) is often added to accelerate the reaction.²⁴ The most commonly used bases include triethylamine, 2,6-lutidine and *N,N*-diisopropylethylamine (DIPEA) (Figure 1.4). The exact role of bases in accelerating the CuAAC reaction is not clear yet, but it has been reported that addition of a base may give rise to some beneficial effects, such as stabilizing the Cu(I) species, facilitating the formation of acetylide anions,²⁸ suppressing byproduct formation and increasing reaction yield.²⁸

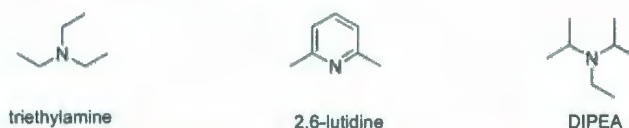


Figure 1.4: Bases commonly employed in CuAAC reactions.

Besides the bases, other stabilizing ligands illustrated in Figure 1.5 are known to have a benevolent effect of accelerating the CuAAC reaction.¹⁹ In particular, the reactions utilizing some polyvalent ligands exhibit unusually high reaction rates.¹⁹ Of note is that some CuAAC reactions forming di- or poly-triazoles can be autocatalytic, since the nitrogenous products are hypothesized to serve as rate-accelerating ligands for Cu(I). The major roles of ligands in CuAAC reactions are believed to be stabilizing Cu(I) through complexation and preventing the formation of byproducts originating from Glaser, Straus and Eglinton homocoupling reactions as shown in Scheme 1.10.²⁴

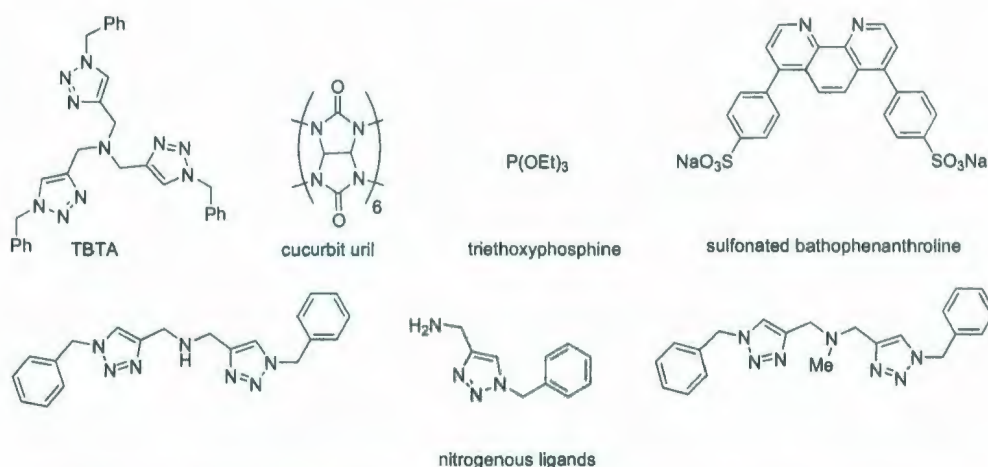
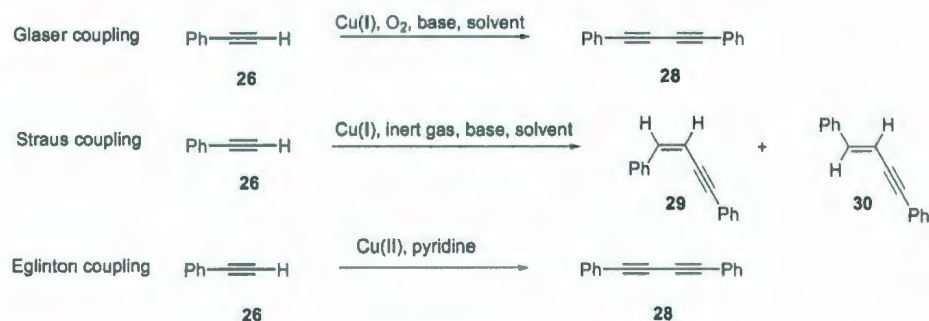


Figure 1.5: Examples of ligands capable of accelerating CuAAC reactions.

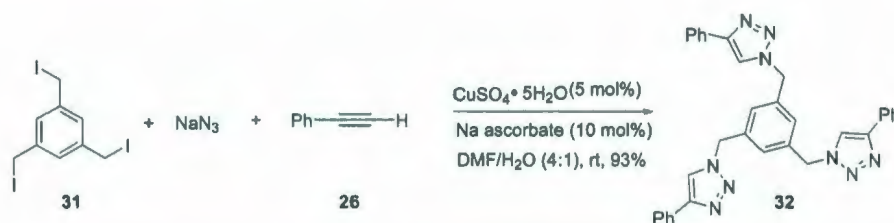


Scheme 1.10: Alkyne coupling side-reactions commonly observed in CuAAC reactions.

1.3.4 CuAAC in Multicomponent One-Pot Synthesis

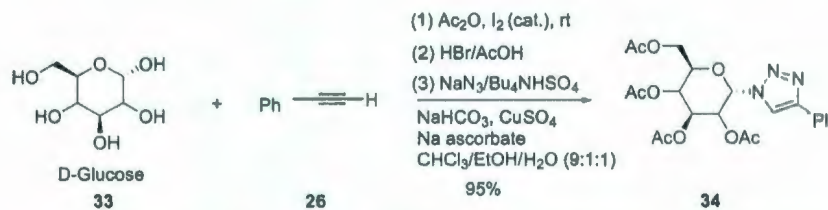
Although several organic azides are quite stable and termed as bioorthogonal, low-molecular weight azides are unstable and difficult to handle. Moreover, small molecules with several azido functionalities have to be handled carefully. One way to solve this problem is to apply the so called “one-pot CuAAC protocol”. For example, the reaction shown in Scheme 1.11 is a one-pot three-component click reaction, which involves two steps: (i) an organic halide is converted *in situ* to respective organic azide; (ii) the azide is immediately consumed through the CuAAC reaction in the

presence of a terminal alkyne and Cu(I).



Scheme 1.11: A one-pot three-component CuAAC reaction.

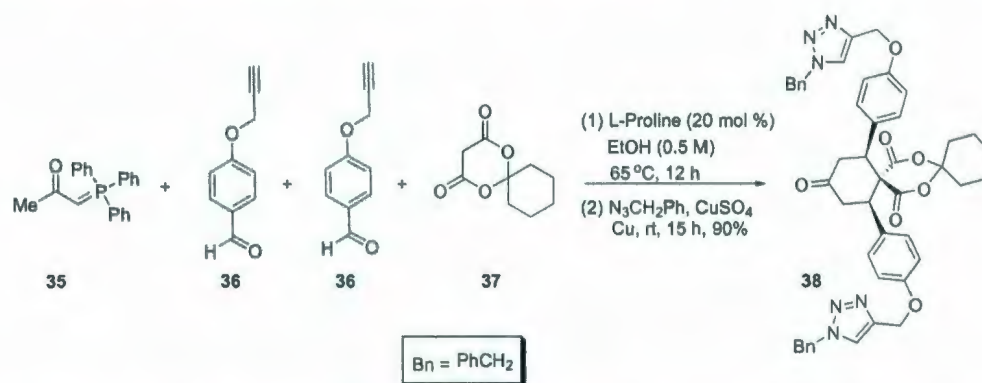
The one-pot protocol is particularly convenient and suitable for the CuAAC involving aliphatic azides. An excess amount of NaN_3 can be added to achieve a better yield, without interfering with the click reaction. Scheme 1.12 illustrates a one-pot synthesis of triazolylglycosides (**34**) from unprotected monosaccharides. In this case, a sequence of acetate protection, bromination, and azide generation in the presence of acetylides, produces the expected triazole product in good yield after four individual reaction steps in one pot. Selectivity and minimum byproduct formation are two keys to the success of combining these reactions in one pot.



Scheme 1.12: A one-pot synthesis of a triazol-substituted glycoconjugate from D-glucose.

Recently, a four-component one-pot protocol, which involves a sequence of Wittig olefination, Knoevenagel condensation, Diels-Alder reaction, and CuAAC reaction

has been developed (see Scheme 1.13). This reaction works very well with numerous organic azides and the yields are generally very high.



Scheme 1.13: A one-pot Wittig-Knoevenagel-Diels-Alder-CuAAC reaction.

1.3.5 Microwave(MW)-Assisted CuAAC

Microwave-assisted organic synthesis has become very popular since 1986, owing to the advantages of high yield, reduced reaction time, and clean product formation. The rate enhancement observed from microwave chemistry might stem from the efficient dielectric heating that creates an inverted temperature gradient.¹⁶ Although CuAAC reactions normally do not require elevated temperature, microwave chemistry can dramatically reduce the reaction time from over 12 h to less than 1 h, with the yields remaining at almost the same level as those undertaken under typical conditions. These outcomes substantiate that the microwave heating is non-selective in accelerating the rates of the click reaction and other side reactions.¹⁶

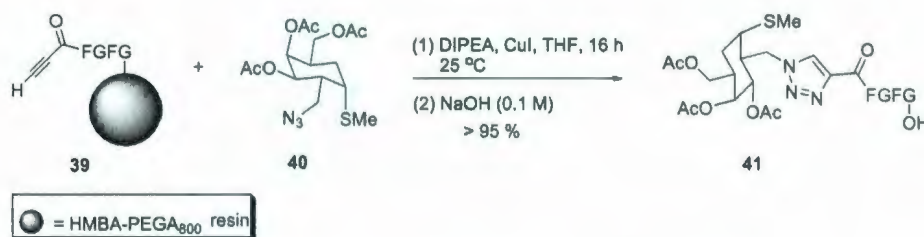
Microwave-assisted CuAAC has the same wide scope and bioorthogonality to all known organic functional groups as those of room-temperature reactions. Moreover,

microwave heating does not affect the reaction yield and ease of product isolation. These merits provide a possible means to overcome some barriers encountered in aqueous synthetic environment. Especially, for room-temperature CuAAC reactions, where products are either insoluble in water/alcohol mixtures or too soluble to isolate by aqueous work-up, the microwave-assisted CuAAC protocol can provide an efficient approach to rapidly obtain desired products in anhydrous organic solvents with extremely low catalyst loading.

1.3.6 CuAAC in Solid-Phase Synthesis

The efficiency of the CuAAC reaction allows it to be effectively utilized on the solid-phase, which leads to attractive implications in combinatorial synthesis and drug discovery.¹⁷ Also, the CuAAC reaction can be utilized as a powerful methodology to modify the surface properties of various solid substrates such as resins or metals, allowing a wide range of functionalities to be “clicked” on the surface under mild conditions in high yields. The benefits of CuAAC in solid-phase synthesis arise from the insensitivity that CuAAC shows towards various experimental conditions, types of solid substrates, and in subsequent surface modifications. Both Cu(I) and Cu(II) salt/sodium ascorbate systems are able to effectively catalyze the reaction in the solid phase or at the interface. For solid-phase synthesis on resin support, using the reaction shown in Scheme 1.14 as an example, THF, DMF, and acetonitrile/DMSO are commonly used solvents, and the resin support can be either polar matrices, such as poly(ethylene glycol)s (PEGs), or non-polar matrices, such as polystyrenes. A major limitation of CuAAC in the solid-phase synthesis is the oxidative alkyne

homocoupling that produces diyne as the byproduct. However, triazole formation on azide-substituted resins has recently been reported to proceed with high yields and no byproduct formation even at an alkyne concentration of 1.25 M. Presently, solid-phase “click chemistry”, which is still in its infancy, is envisioned to offer a powerful toolbox for modern combinatorial and materials chemistry in light of its reliability and robustness.



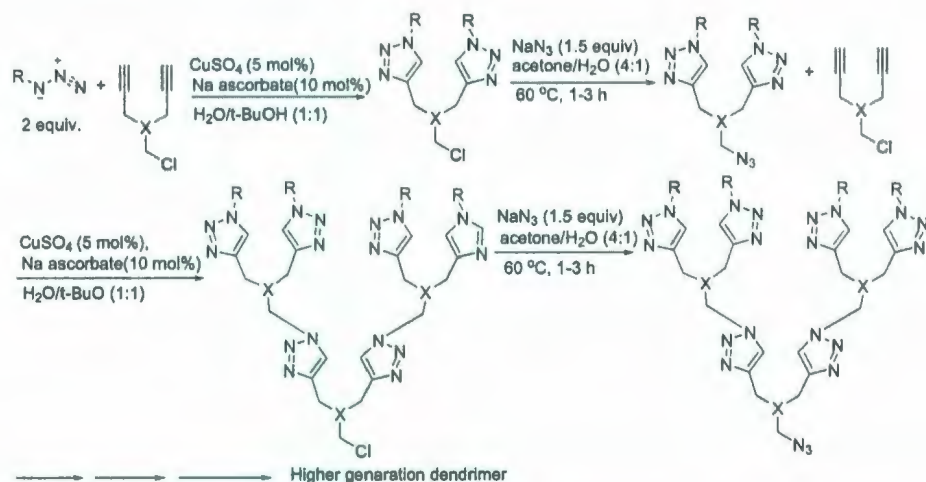
Scheme 1.14: A solid-phase CuAAC reaction.

1.4 Recent Advances in Material Synthesis Based on CuAAC

As discussed previously, a major challenge in current materials science lies in how to achieve “smart” materials with a high-degree of structural order and well-defined properties. This requires the development of facile synthetic methodologies that are task-specific and capable of tackling molecules of great complexity and demanding compatibility. For this reason, awareness of the significance and importance of the CuAAC reaction for material synthesis was immediately aroused after the first report on CuAAC by Sharpless and co-workers. In a recent review article co-authored

by Hawker, Folkin, Finn, and Sharpless, a special homage was paid to Sr. John Conforth whose inspirational idea of using rapid, modular, and efficient reactions to synthesize polymers was given the credit for seeding the concept of click chemistry.²⁹ The following text will briefly review the application of click reactions in modern materials chemistry.

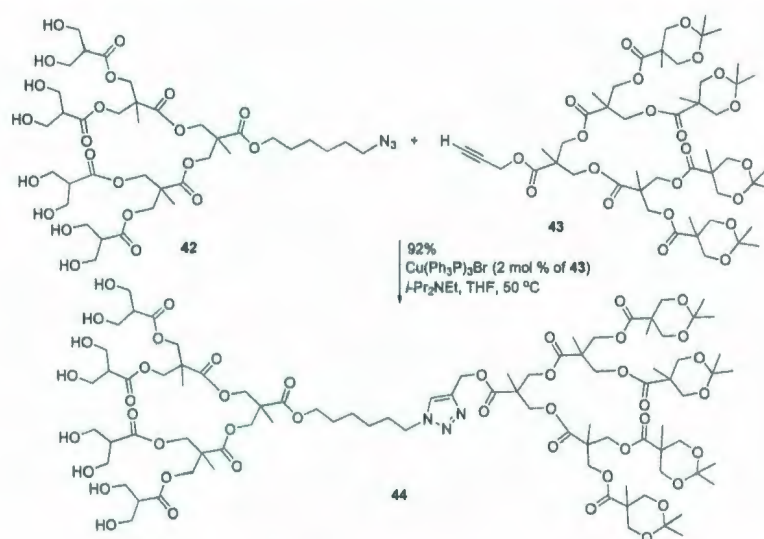
1.4.1 Macromolecular and Supramolecular Synthesis Based on CuAAC



Scheme 1.15: Convergent synthesis of dendrimers using the CuAAC reaction.

Paul Flory first synthesized dendrimers in 1941 by an iterative approach,³⁰ but problems with purification and lengthy chromatographic separations of impure products have posed significant challenges to synthetic dendrimer chemistry. These challenges can be adequately addressed by the “fidelity” that click reactions exhibit. Hawker, Fokin, and Sharpless pioneered the development of a “click” strategy for the

convergent synthesis of dendrimers (see Scheme 1.15).¹⁹ In their work, triazole-linked dendrimers of high purity and excellent yields were successfully synthesized using the CuAAC reaction. Owing to the use of stoichiometric quantities of reactants and almost quantitative conversion efficiency, the click approach effectively circumvented the laborious purification efforts commonly encountered in dendrimer synthesis.



Scheme 1.16: Synthesis of a diblock dendrimer via the CuAAC reaction.

Chemically differentiated dendrimers allow for the introduction of diverse functional groups (*e.g.* drug targeting moiety, diagnostic label) at specific positions of nanostructured systems. However, the synthesis of such type of block dendrimers is by no means trivial. Using the CuAAC click reaction, Hawker and co-workers prepared a triazole-linked unsymmetrical diblock dendrimer in 2005 (Scheme 1.16).³¹ The high efficiency and selectivity of the CuAAC reaction make it possible to link two dendritic blocks (42 and 43) together without using any protecting strategies.

Motivated by the successes of dendrimer synthesis, Finn *et al.* applied this

CuAAC reaction to the synthesis of linear polymers and even three-dimensional polymeric networks. Figure 1.6 lists several examples of polymers prepared by CuAAC reactions.³²

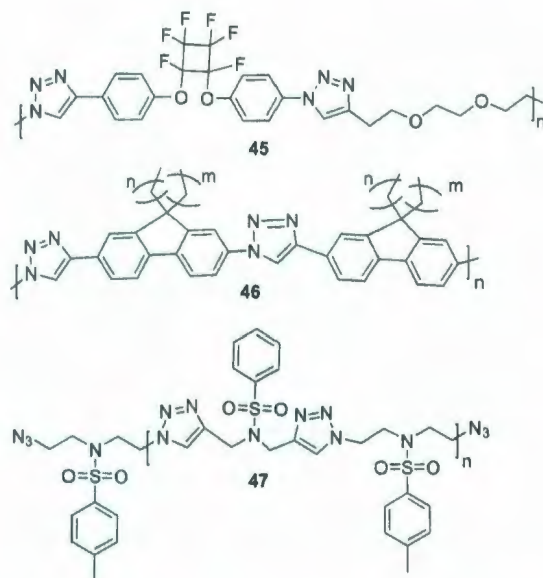
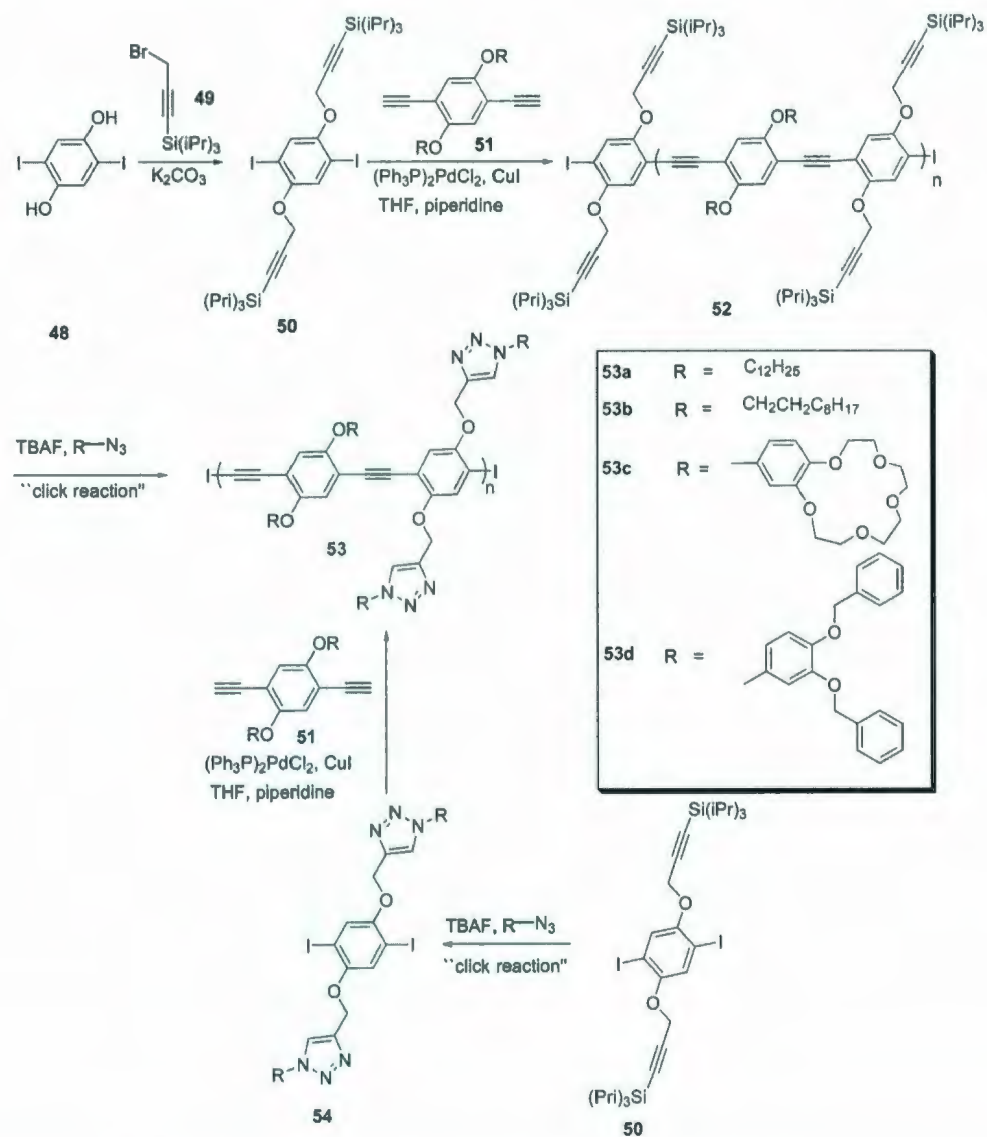


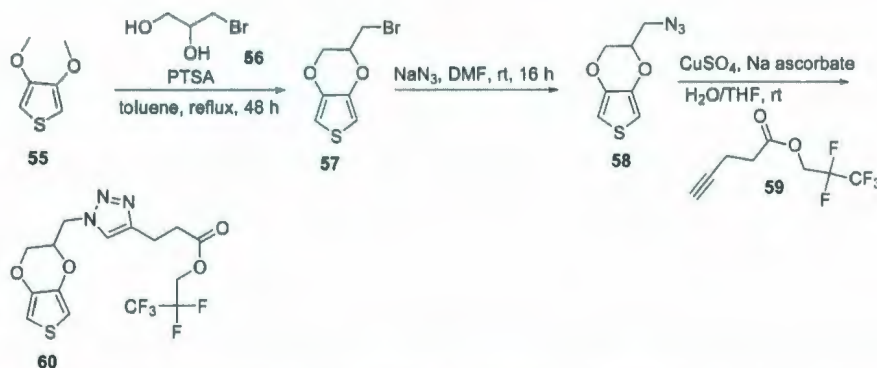
Figure 1.6: Linear polymers synthesized by CuAAC reactions.

As a matter of fact, polymer science has probably been the biggest beneficiary since the inception of “click chemistry”. The main challenges experienced in polymer formation/functionalization are the random coil formation usually observed in large molecules, dramatic solubility changes and substantial steric hindrance to the reacting functional groups. The CuAAC click reaction has demonstrated particular suitability in addressing these challenges. In general, CuAAC click reaction provides an efficient route not only to assemble the polymeric backbone, but to enable facile end-group functionalization, polymer-to-polymer coupling, and polymer backbone grafting.



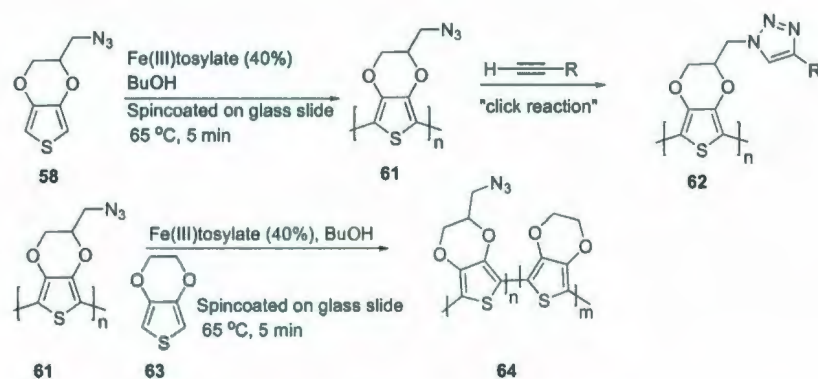
Scheme 1.17: Pre- and post-functionalization poly(*p*-phenylene ethynylene)s (PPEs) via the CuAAC reaction.

In 2005, Uwe Bunz demonstrated the construction of some functional poly(*p*-phenyleneethynylene)s (PPEs **53**) through the CuAAC click reaction.³³ Two techniques, namely pre- and post-functionalization, were explored as exemplified in Scheme 1.17. In the post-functionalization technique, a specific polymer backbone is postsynthetically fabricated. This technique allows for the introduction of a variety of functional groups in the final step after polymerization, and it is particularly advantageous in terms of introducing functional groups that might not be compatible with harsh polymerization conditions. The main disadvantage of this method is that the synthesized polymer cannot be corrected if there is any error in the structure. In the pre-functionalization technique, the polymerization is placed at the last step, implemented from a specific monomer. Errors in functionalization of a monomer can be easily corrected by appropriate purification or functionalization. It has been demonstrated that the CuAAC click reaction is suitable for both pre- and post-functionalization methods.



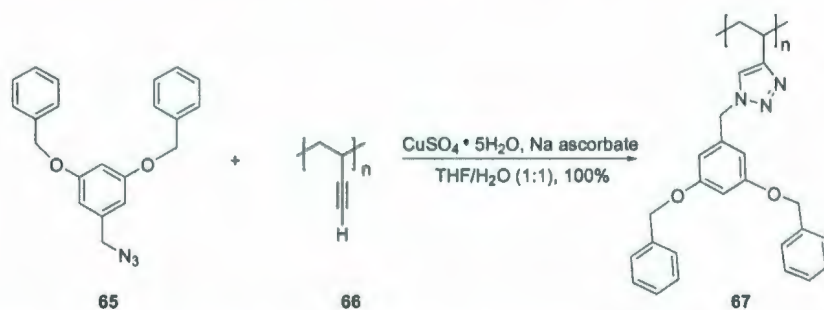
Scheme 1.18: Preparation of functional thiophene monomer by click chemistry.

In 2008, Hvilsted and co-workers synthesized a group of new highly conductive



Scheme 1.19: Preparation of functionalized PEDOT by click chemistry.

polymer films based on poly(3,4-ethylenedioxythiophene)s (PEDOTs).³⁴ Conducting materials based on PEDOTs have shown some special advantages, such as very high electrical conductivity and particular stability in aqueous environments. A CuAAC based “click” protocol was utilized for postpolymerization functionalization of PEDOTs to produce conductive polymers in the presence of various functional groups on the polymer backbones (see Schemes 1.18 and 1.19).



Scheme 1.20: Synthesis of a dendrinoized polymer via the CuAAC reaction.

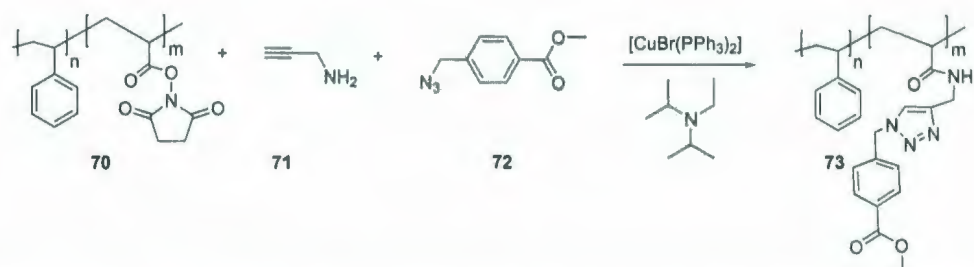
Polymers with multiply functionalized side chains are of great interest to material chemists. One appealing representative is the dendrimer-grafted polymers. Usually this type of macromolecule can be made through both convergent and divergent



Scheme 1.21: Synthesis of cyclic dendronized polymer via an REMP click reaction.

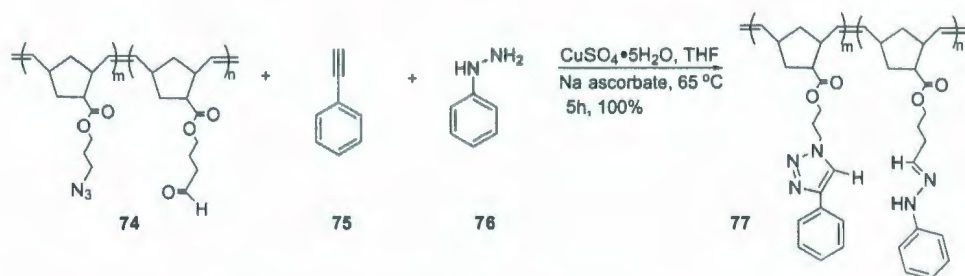
synthetic strategies. The convergent strategy has to face the challenge of increasing steric hindrance, while the divergent strategy often suffers from incorrect structures. By using the CuAAC reaction, the problems arising from both divergent and convergent methods can be properly addressed. For example, in 2004, Fréchet and co-workers synthesized an interesting class of dendritic macromolecules by using the so-called “graft-to” technique to functionalize a pre-formed terminal alkyne pendant polymeric backbone with azide-pendant dendrimers up to the third generation through the CuAAC reaction (see Scheme 1.20).³⁵ The almost quantitative yields of the click functionalization contrast sharply the poor efficiencies displayed by other non-click strategies. Grubbs and Fréchet *et al.* have recently demonstrated the first direct synthesis of cyclic dendronized polymers via ring-expansion metathesis polymerization (REMP) of a dendronized macromonomer. Atomic force microscopic (AFM) imaging has confirmed the cyclic topology, revealing uniform cyclic features with no detectable linear polymer contaminants (see Scheme 1.21).³⁶

C. J. Hawker and co-workers explored this idea further by undertaking some efficient cascade side-chain functionalization of macromolecular moieties (see Scheme



Scheme 1.22: A cascade functionalization of synthetic polymers using CuAAC reaction.

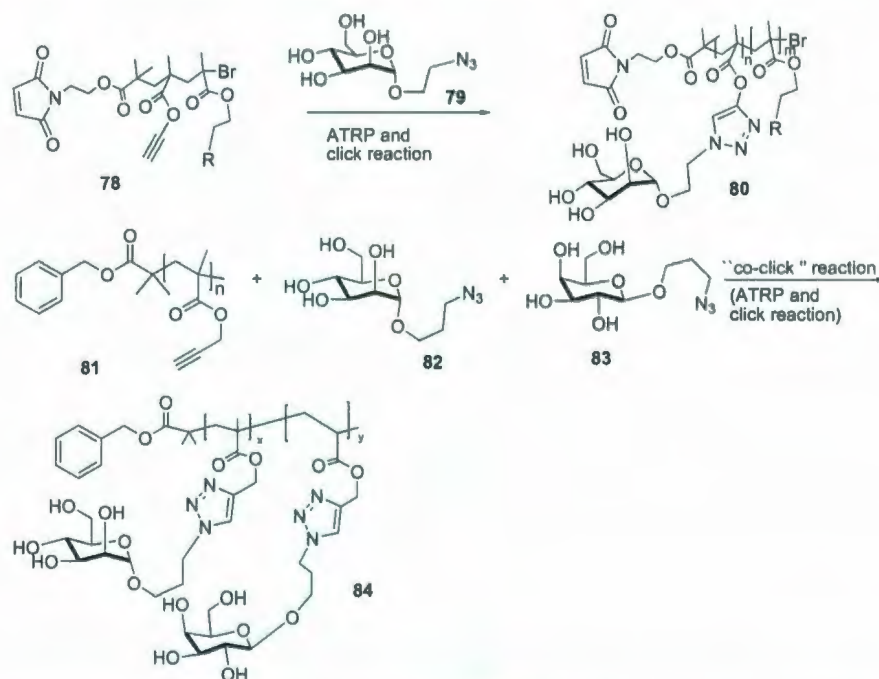
1.22), which is far better than any other reactions previously reported.³⁵



Scheme 1.23: Orthogonal multi-functionalization of random co-polymers.

The CuAAC type click chemistry in combination with a living polymerization technique, for example, ring-opening metathesis polymerization (ROMP), can be used as a powerful tool for the preparation of multi-functionalized random copolymers, since the combination of CuAAC and ROMP gives satisfactory control over such polymer properties as polydispersity, molecular weight, functional group tolerance and others. For example, Weck and co-workers have demonstrated a modular approach to achieve multi-functionalization of a polymer backbone in quantitative yield.³⁷ In this investigation, the ROMP technique was used to construct a polymeric scaffold first, and then it was multi-functionalized by the CuAAC and hydrazone formation

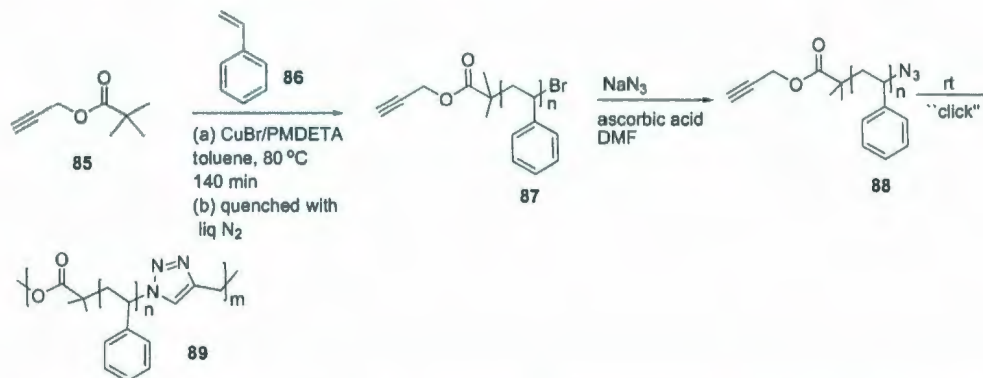
reactions as shown in Scheme 1.23. This one-pot technique paved the way for direct multi-functionalization of a properly designed co-polymer backbone through orthogonal reactions (CuAAC and hydrazone formation).



Scheme 1.24: Synthesis of neoglycopolymers via a "co-click" strategy.

Neoglycopolymers are a class of biopolymers derived from sugars. They have attracted enormous interest, because they show favorable interactions with a protein receptor, known as the "glycoside cluster effect". For this reason, neoglycopolymers have been envisaged to find applications in medicinal science.³⁸ In 2006, Haddleton and co-workers demonstrated an efficient synthesis of a neoglycopolymers by grafting an azido pendant sugar on polymers bearing alkyne functionality through the CuAAC reaction (see Scheme 1.24).³⁹ The ATRP (Atom Transfer Radical Polymerization) reaction used in synthesizing the polymers is a living polymerization of the

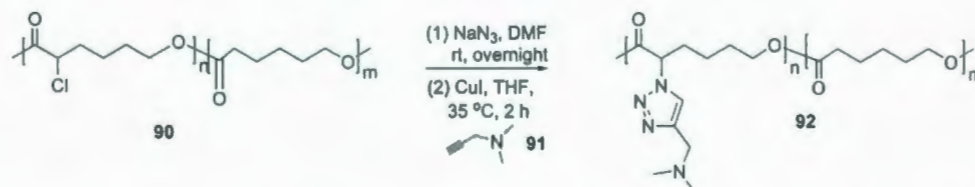
formation of carbon-carbon bond through transition metal catalyst.^{38,40} This reaction featured high yield and easy reaction procedures. It was therefore anticipated that the click approach could provide access to a variety of complex polymeric structures that show significant application potentials in nanomedicine.



Scheme 1.25: Matyjaszewski's one-pot, multi-catalytical, three step strategy for telechelic polystyrene synthesis.

The CuAAC type click reaction has also been applied to the synthesis of some important polymers using "one-pot" non-tandem or tandem strategies. In 2005, Matyjaszewski reported an elegant one-pot, multi-catalytic, three step strategy, in which atom transfer radical polymerization (ATRP), *in situ* azidation, and CuAAC were combined to synthesize a telechelic polystyrene polymer (see Scheme 1.25).⁴¹ Unfortunately, the synthesis ended with relatively limited success due to the poor performance of click chemistry in this case. The authors reasoned that a possible competing side reaction between inorganic azide and terminal alkynyl group, resulting in the production of *N*-substituted triazoles as the byproduct, could be the culprit. To solve this problem, Jérôme and co-workers developed a domino-type reaction strategy,

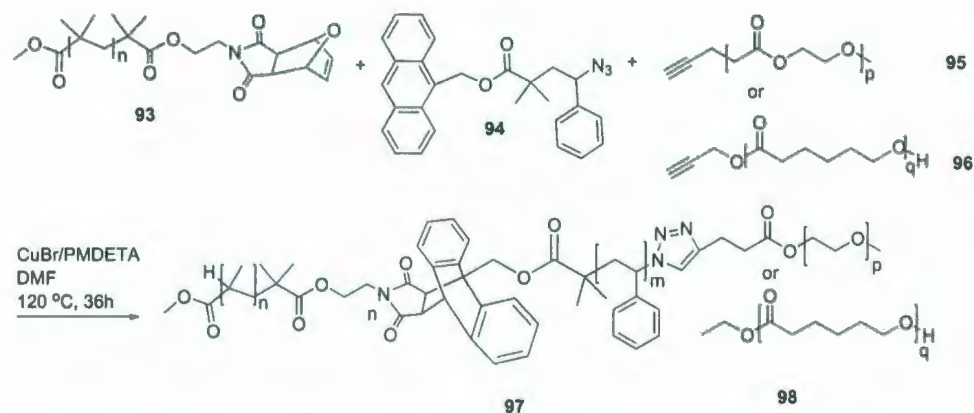
which combined an *in situ* azide formation and subsequent click reaction of pendant groups along the polymeric backbone (see Scheme 1.26).⁴² The later method led to a significantly increased reaction yield.



Scheme 1.26: Jérôme's domino-type strategy for dimethyl amino functionalized Polymer.

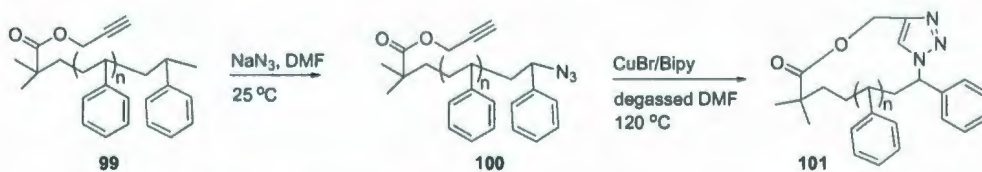
Owing to its particular efficiency, the CuAAC reaction can also be readily used in combination with traditional polymerization or other known chemical reactions to afford useful one-pot strategies for material synthesis. Recently, Tunca and co-workers reported the preparation of a series of elegant amphiphilic triblock-copolymers via a “special one-pot click” strategy, which enlisted two types of CuAAC reactions and a Diels–Alder reaction.⁴³ As illustrated in Scheme 1.27, the synthesis was accomplished by making use of a bifunctional and dual-purpose polystyrene building block at one end and an anthracene functionality at the other.

Macrocyclic polymers are an important class of polymers that capture significant interest. Efforts for synthesis of macrocyclic polymers have long been underway, as these kind of polymers are anticipated to show some unique topological and physical properties. Macrocyclic polymers are commonly prepared by cyclization of linear precursors, and this method usually suffers from poor yields and competitive side reactions. As a result, tedious purification procedures are generally required. In



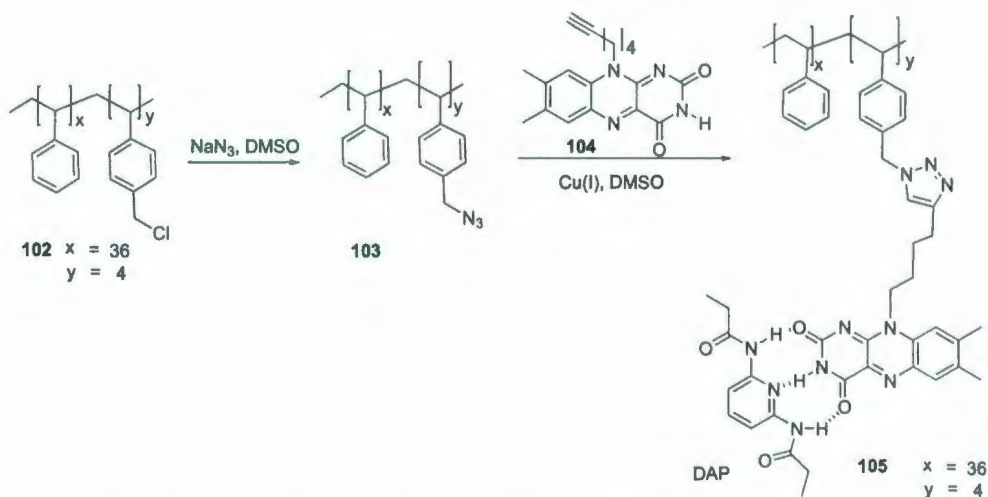
Scheme 1.27: Orthogonal tandem strategy for the synthesis of triblock-copolymers.

2006, Scott M. Grayson demonstrated the synthesis of some macrocyclic polymers using the CuAAC reaction (Scheme 1.28).⁴⁴ The end-group modification of **99** led to azido-terminated polymer **100**, which cyclized through an intramolecular CuAAC to afford macrocyclic polymer **101** in an almost quantitative yield. As such, tedious purification procedures were effectively averted.



Scheme 1.28: "Click cyclization" to make well-defined macrocyclic polymers.

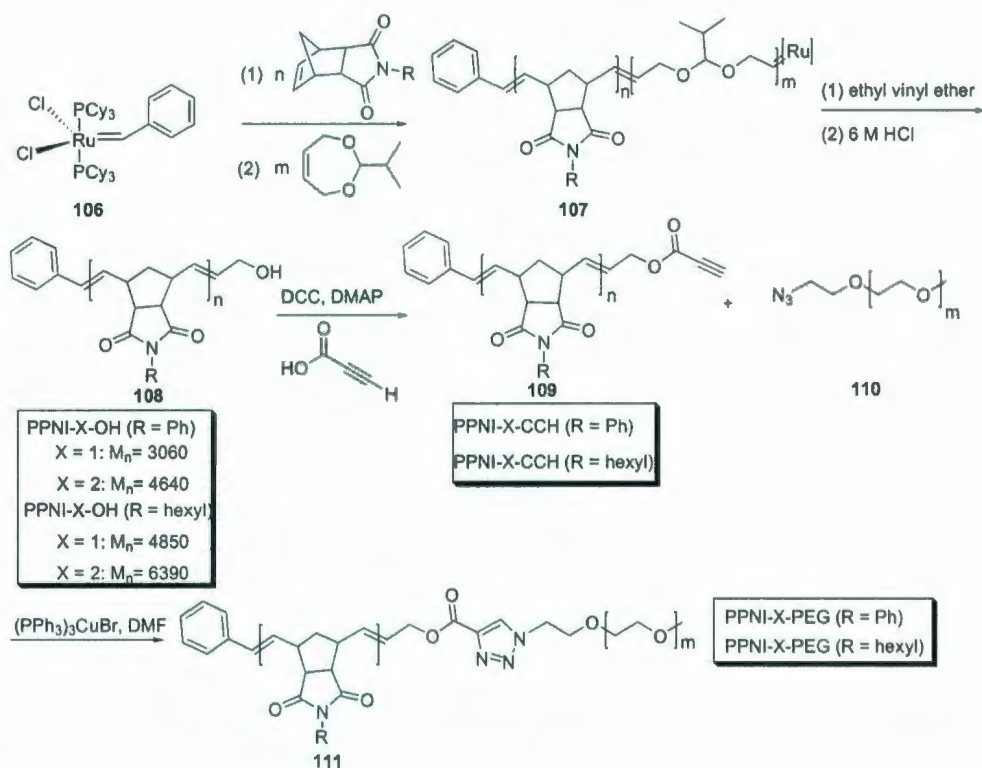
In biological systems, many recognition events, such as H-bonding, π - π stacking, and electrostatic interactions, are often exploited in various enzymatic processes to control and monitor the protonation and oxidation states of an important cofactor's activity.⁴⁵ Moreover, the incorporation of recognition elements in various molecular systems is often advantageous in the development of redox-active molecular devices



Scheme 1.29: Synthesis of a flavin–functionalized polymer by click chemistry and self–assembly with DAP.

and various model systems with potential application ranging from chromatography to biosensing.⁴⁵ Using the CuAAC reaction, a flavin functionalized polymer was synthesized and its self–assembly was demonstrated by Carroll and co-workers in 2005 (see Scheme 1.29). The experiment provided valuable information about the effects of a polymeric environment on flavin binding sites in both neutral and reduced states.³⁵

Amphiphilic block copolymers can form macromolecular architectures through supramolecular self–assembly, leading to controllable nanoscopic objects, such as ordered micellar structures in solution or microphase–separated structures in the bulk. Block copolymers can be synthesized via numerous well–established convergent synthetic approaches, in which each individual polymer block is made by a suitable polymerization technique that provides the best architectural control. In 2008, Kilbinger demonstrated a convergent route for the synthesis of an interesting diblock polymer 111 using the CuAAC and ring opening metathesis polymerization (ROMP)



Scheme 1.30: Block copolymer synthesis using the CuAAC and ROMP reactions.

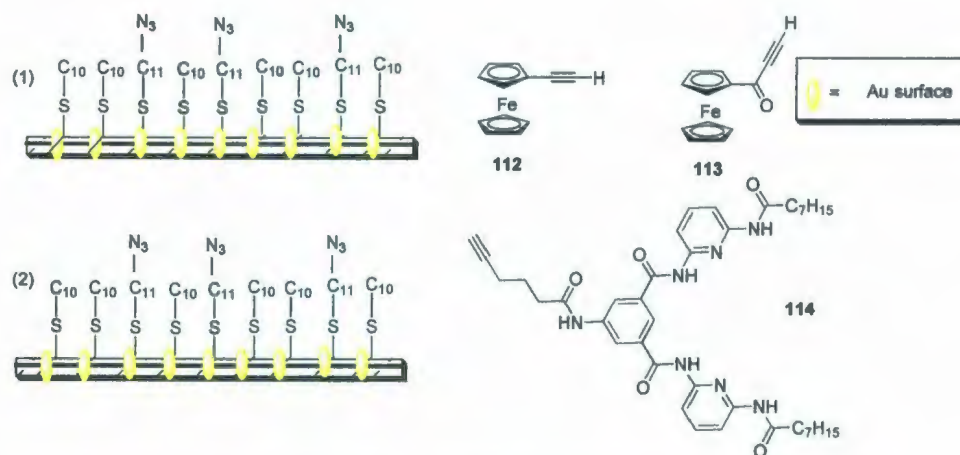
reactions as shown in Scheme 1.30.⁴⁶

In summary, click chemistry, particularly the CuAAC reaction, has shown great power in constructing complex macromolecular structures containing a large variety of functional groups, ranging from variously shaped dendrimers, multisegmented block-copolymers, rod-coil-block co-polymers, star-polymers, graft-polymers, polymer-brushes, and cross-linked capsules and others.⁴⁶ The high yield of the CuAAC click reaction is the key to successful synthesis, and in principle nearly every polymeric structure can be obtained by using properly planned click strategies.

1.4.2 CuAAC Based Surface Functionalization

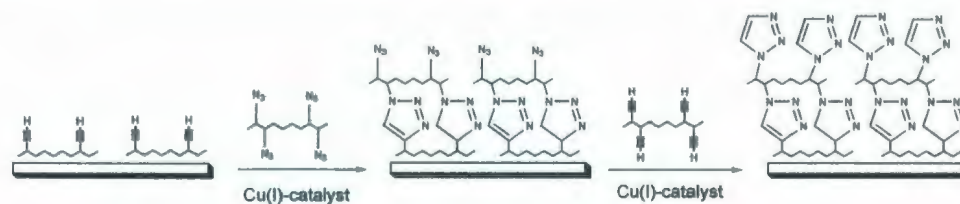
The CuAAC reaction has been demonstrated to be particularly efficient in interfacial functionalizations, because an important feature of CuAAC is the reduced or enforced distance between reactants, resulting in enhanced reaction rates.¹⁸ This particular aspect of CuAAC has been exploited for interfacial functionalizations in numerous ways; for example, click functionalization within the pocket of enzymes (protein profiling, the so-called ABPP), micropatterning induced by AFM tips, or direct microcontact printing. Usually surfaces or interfaces represent a chronic source of incomplete reactions. The advent of the CuAAC reaction has auspiciously opened up an easy and rapid access to various functionalized surfaces having reproducible surface densities. In the past few years, the CuAAC type click reaction has been successfully applied in functionalization or modification of surfaces, such as self-assembled monolayers (SAMs), polymer resins, layer-by-layer assemblies, block copolymer (BCP) micelles, liposomes, polymersomes, and others. The following text will discuss on a number of selected examples in the recent literature.

Chidsey and co-workers pioneered the preparation of SAMs on gold surface using “click chemistry” to anchor electroactive ferrocene derivatives.⁴⁷ In this work, an azido-functionalized SAM was prepared via adsorption of 11-azidoundecanethiol mixed with decanethiol. Then click reactions of ferrocene alkyne **112** and **113** on the azido-functionalized surface were effected, resulting in corresponding ferrocene-functionalized surfaces (see Scheme 1.31).⁴⁸ Through a similar strategy, Zirbs and co-workers have recently modified the surface of Au-bound azido-SAMs by coupling azido-SAMs with a terminal alkyne functionalized, highly polar hydrogen bonding



Scheme 1.31: Modification of SAM surfaces using CuAAC reactions.

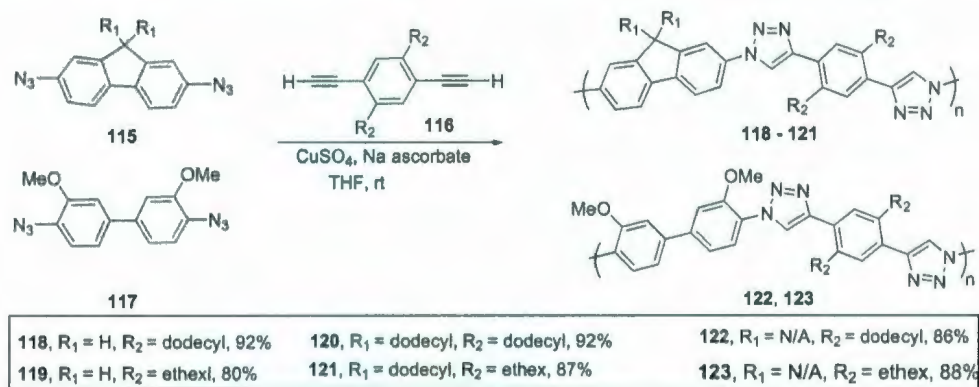
system, **114** (Scheme 1.31).⁴⁹ Interestingly, the extent of functionalization of these two examples, that is, the amount of azido moieties bound to the surface, was satisfactory (up to 20%), which provided an efficient proof of the broad applicability of the CuAAC reaction towards attachment of supramolecular receptors to the surface.



Scheme 1.32: CuAAC based layer-by-layer assembly of ultra-thin polymer multilayer films.

Controllable polymer thin films are of great importance due to their broad potential applications, such as in thin-film electronics. Multilayered thin-films of diverse compositions can be generated using the layer-by-layer technique. Although thin-film assembly of polyelectrolyte (PE) films directed by non-covalent interactions

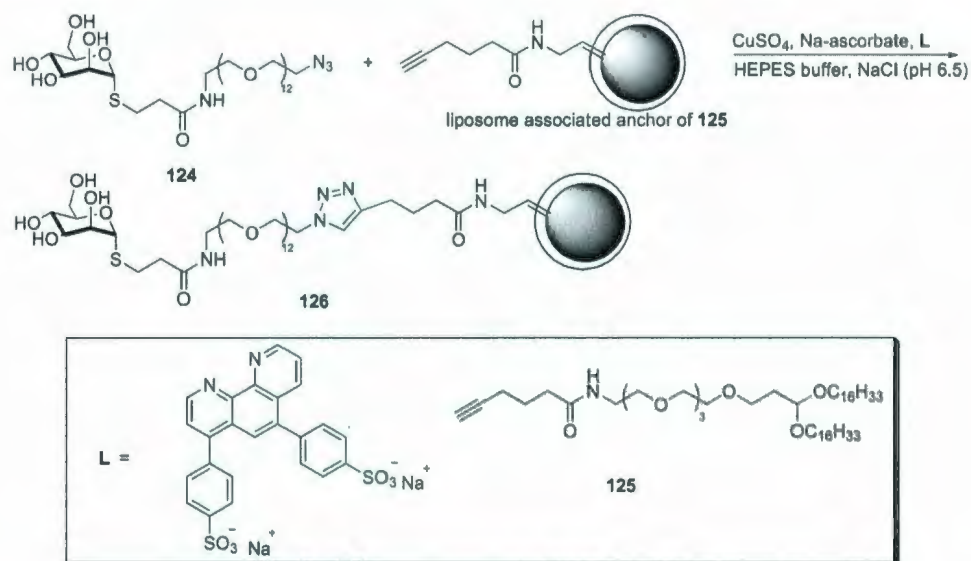
(e.g. electrostatic or hydrogen bonding) are most popular, thin-film assembly by means of covalent bonding does offer some special advantages. In particular, thin films assembled in a covalent manner give very high stability, since the cross-linked polymer networks and the films usually do not disassemble in varying solution environments. In such a surface functionalization technique, the CuAAC reaction is used to construct the grafting of a polymer film in a layer-by-layer fashion. For instance, Caruso and co-workers prepared layer-by-layer polymer films using the CuAAC reaction as shown in Scheme 1.32,⁵⁰ in which azide and alkyne polymers were coupled in a stepwise fashion onto a pre-functionalized alkyne-containing surface and vice-versa. Excellent efficiency for surface functionalization was achieved.



Scheme 1.33: Synthesis of conjugated polymers by CuAAC reactions.

Another strategy for surface functionalization is to use a heated AFM cantilever tip to produce high local heating, which enables reversible and/or irreversible writing of nanostructures on the surface of thin films.⁵¹ In 2006 Uwe Bunz's group reported the synthesis of conjugated polymers via the CuAAC protocol shown in Scheme 1.33.⁵² CuAAC of diazide **115** with diyne **116** in THF in the presence of copper sulfate

and sodium ascorbate efficiently produced conjugated polymers **118–121** at room temperature in very good yield. Another diazide **117** was reacted with **116** under the same CuAAC click conditions to produce polymers **122** and **123** in excellent yield. After the preparation of the conjugated polymers, functional nanopatterns on the polymer thin films were produced with the help of a heated AFM cantilever tip. The essence of this strategy is the absence of tackiness and ripping, which makes this kind of nanostructured semiconducting materials suitable for many practical applications.

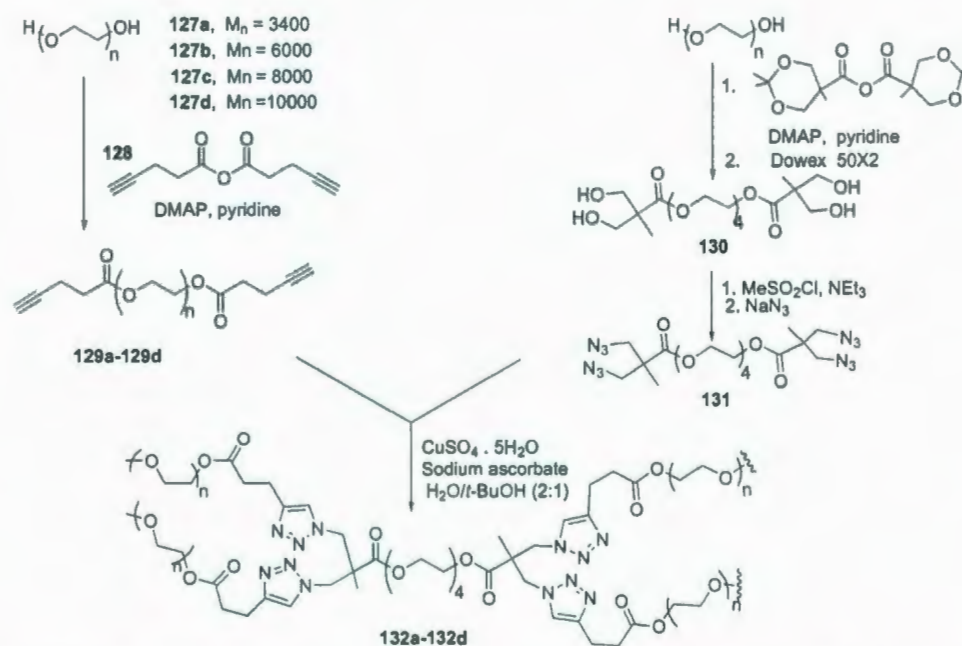


Scheme 1.34: Coupling of azide-pendant ligands to the surface of pre-formed liposomes via CuAAC.

Liposomes have self-closed vesicular structures made up of phospholipid bilayers and they are of particular interest to material and biological chemists. The applications of liposomes range from membrane models and diagnostics to drug/gene delivery.⁵³ It was found that when liposomes were conjugated with a water-soluble

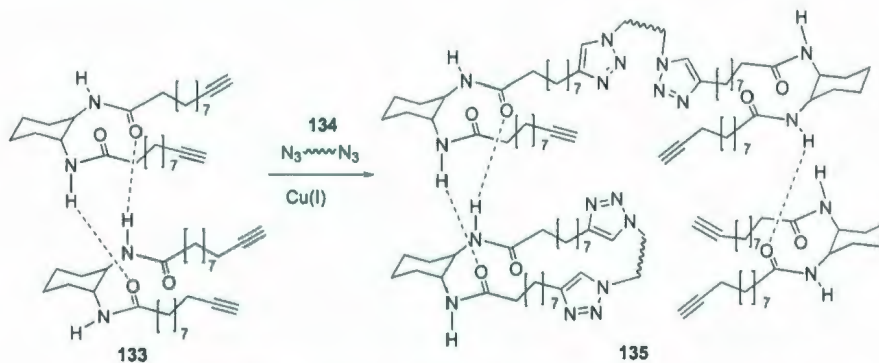
polymer, for example poly(ethylene glycol) (PEG), the complex could achieve an increased circulation time in blood. The preparation of immunoliposomes, the so-called synthetic peptide-based vaccines, are of significant interest in this context, and in many studies, polymers are used to conjugate with liposomes, forming bioconjugates as simple and potential drug delivery systems. In 2006 Schuber reported a chemoselective conjugation method based on the CuAAC reaction for the coupling of azido-pendant ligands to a pre-formed liposome surface already carrying alkynyl functional groups (see Scheme 1.34).⁵³ Because of the mild conditions of the click reaction, the lipid-membranes were found intact during and after the course of functionalization, with only the outer surface modified.

1.4.3 Synthesis of Well-defined Hydrogel Networks via CuAAC



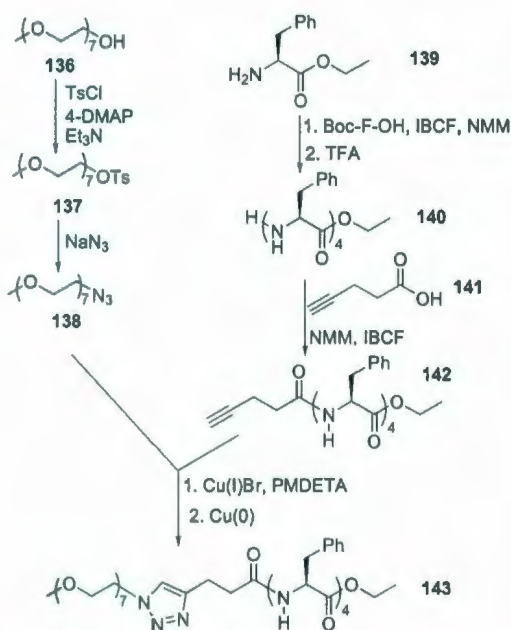
Scheme 1.35: Click reactions among PEG-based building blocks to form hydrogels.

Cross-linked hydrogels are appealing materials for numerous biomedical applications, such as drug delivery and tissue engineering scaffolds,⁵⁴ since they can self-assemble into fibrous networks driven by non-covalent forces such as dipole-dipole, van der Waals, and H-bonding interactions.⁵⁵ The traditional synthetic methods for hydrogel materials utilize uncontrolled radical based cross-linking reactions, which tend to result in some poorly defined structures. Therefore, it is difficult to relate the network structures to the physical properties of the gel materials. In order to overcome this challenge, Hawker and co-workers explored the synthesis of some PEG-based hydrogel materials using the CuAAC reactions shown in Scheme 1.35.⁵⁶ The resulting hydrogels were characterized by well-defined networks and significantly improved mechanical properties.



Scheme 1.36: 3-D hydrogel networks constructed by CuAAC.

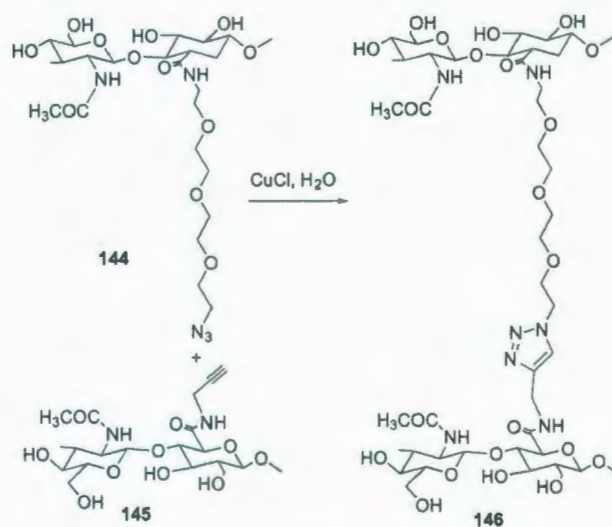
Finn and co-workers recently synthesized some low-molecular weight organogelators based on undecynylamide of *trans*-1,2-diaminocyclohexane by means of CuAAC reaction (Scheme 1.36).³⁸ In this case, the 1,2,3-triazole rings formed after the CuAAC click reactions assisted the formation of 3-D hydrogel networks.



Scheme 1.37: Synthesis of polymer-peptide conjugate **143** via CuAAC.

Another interesting type of hydrogels, recently reported by Dave J. Adams, was based on a conjugate of poly(ethylene oxide) (PEO) tetraphenylalanine and peptides synthesized via a CuAAC reaction between an alkyne pendant peptide and an azide pendant PEO oligomer (see Scheme 1.37).⁵⁷ The THF solution of the click product, conjugate **143**, was afterwards subjected to dialysis against water, leading to supramolecular self-assemblies in well-defined nanotube structures.

Generally speaking, the use of CuAAC for hydrogel synthesis has some special advantages over other methods. First, enhanced mechanical properties of the gels can be attained, as a result of the controlled nature of click reactions. Secondly, hydrogels produced by click reactions, such as CuAAC, feature environmental stability as well as tolerance to various functional groups. This enables the incorporation of a large variety of additives and facilitates flexible chemical tailoring of the hydrogel



Scheme 1.38: Formation of horse albumin (HA)-based hydrogels via CuAAC.

structures. As an example, Crescenzi and co-workers recently reported an elegant procedure for the preparation of hydrogels most suitable for tissue engineering.⁵⁸ The key step in the synthesis is a CuAAC reaction that links the arms of two polysaccharide chains (see Scheme 1.38).

1.4.4 Functionalization of [60]Fullerene via CuAAC

Buckminster C_{60} fullerene is an interesting carbon allotrope with extremely small size (*ca.* 0.7 nm in diameter), aesthetic spherical shape, and an extended 3-D π -conjugated system. C_{60} behaves like an electronegative polyene molecule, capable of reversibly accepting up to six electrons to become a stable poly anions. For example, C_{60} could be doped by alkali metals to form a superconducting materials M_3C_{60} .⁵⁹

C_{60} has many potential applications in molecular devices (*e.g.* photovoltaics, nonlinear optics), molecular machinery, supramolecular chemistry, and nanomedicine (photodynamic therapeutic agents), to name a few.⁶⁰ The main challenges of handling C_{60} is its strong tendency for aggregation and poor solubility in many solvents. Covalent modifications of C_{60} can substantially improve the processibility of C_{60} , producing C_{60} derivatives with interesting physical and electronic properties.

There are numerous reactions that can be used to prepare C_{60} derivatives. However, the application of the CuAAC reaction to prepare functionalized C_{60} derivatives has only been recently exploited mainly by the Nierengarten and Zhao group. Since this topic is closely related to the work to be discussed in Chapter 2 of this thesis, a detailed literature review will therefore be provided in the introduction section of Chapter 2.

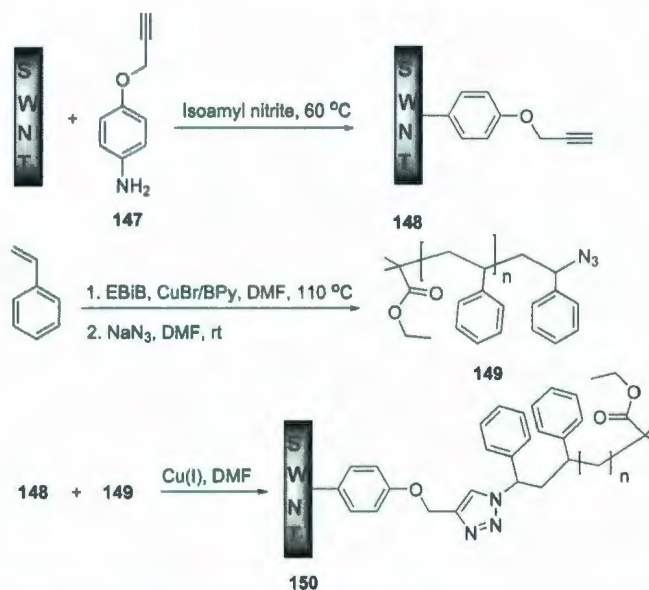
1.4.5 Functionalization of Carbon Nanotubes via CuAAC

As an important class of carbon allotropes with paramount importance compared to fullerenes, carbon nanotubes (particularly single-walled carbon nanotubes, SWNTs) exhibit extraordinary mechanical, electrical and photophysical properties that can

be exploited in the design of sensors,^{61,62} molecular electronics,^{63,64} field emission displays,⁶⁵ ultra-strong materials,⁶⁶ and so on. In some nanotube-based devices, techniques for *in-situ* growth of SWNTs in the solid phase are followed,^{67,68} while in many other applications solution-phase processing of SWNTs is essential so as to achieve appropriate assemblies, quantitative dispersions, and proper orientations of SWNTs within the host matrices.⁶⁹ However, the handling of carbon nanotubes in solution is not an easy task because of the insoluble nature of carbon nanotubes in most solvents.^{70,71} To overcome this barrier, several initiatives have been taken, including non-covalent functionalizations with various surfactants and π -rich organic molecules such as polymers⁷² and dendrimers,⁷³ conjugated oligomers,⁷⁴ porphyrins,⁷⁵ and pyrene derivatives.⁷⁰

Covalent functionalization presents an useful approach to modify the properties of SWNTs.⁷⁶⁻⁸¹ In comparison to the non-covalent method, the covalent approach has some special merits. First, covalent modification can introduce a variety of functional groups onto the surface of SWNTs with known organic reactions, and the resulting functionalized SWNTs generally have very good stability in organic solvents.⁸² Second, the covalent approach can lead to high degrees of functionalization and hence substantially increase the solubility and compatibility of SWNTs. Moreover, covalently functionalized SWNTs have been found to possess considerably reduced cytotoxicity, making biological or medicinal uses possible.^{81,82}

The first example of using CuAAC to functionalize SWNTs was reported by Adronov and co-workers in 2005.⁷¹ In this work, they first performed an arenediazonium radical reaction that attached alkynyl groups to the sidewall of SWNTs as shown in Scheme 1.39. Next, azido-pendant polystyrenes **149** prepared

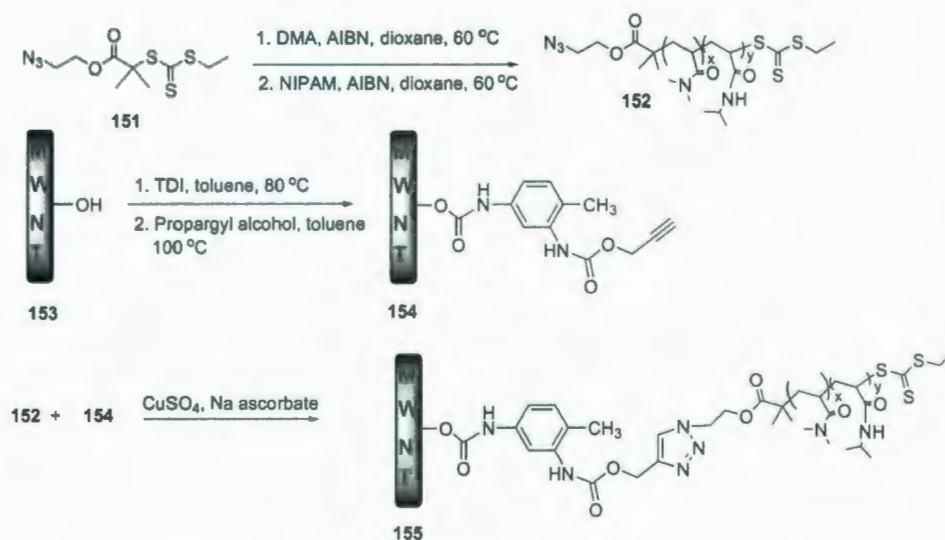


Scheme 1.39: Functionalization of SWNTs with polystyrenes via CuAAC.

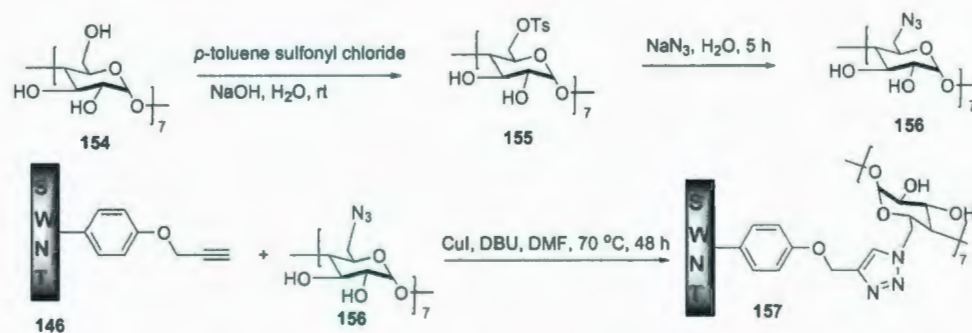
by a controllable ATRP approach were “clicked” to functionalized SWNTs **148** via a CuAAC reaction, giving rise to polymer functionalized SWNTs **150**. The advantage of this methodology is the full control over the length and architecture of the polymers attached to the sidewall of SWNTs.

Lately, the Adronov group further demonstrated the functionalization of multi-walled carbon nanotubes (MWNTs) using a “graft to” polymerization technique, in which an azido-pendant diblock copolymer **152** was clicked to alkyne-decorated MWNTs **154** through the CuAAC reaction as shown in Scheme 1.40.⁸³

Recently, Zheng and co-workers explored the use of click reaction to covalently attach cyclodextrin to SWNTs.⁸² As shown in Scheme 1.41, the resulting functionalized SWNTs were proposed to function as novel artificial receptors. This work together with other relevant examples in the literatures underscores the great applicability of CuAAC in covalent functionalizations of SWNTs with a wide spectrum of polymeric



Scheme 1.40: Functionalization of MWNTs via CuAAC.



Scheme 1.41: Covalent attachment of cyclodextrins to SWNTs via CuAAC.

moieties.

1.5 Outline of this thesis

This PhD thesis describes four major projects focusing on the synthesis and characterization of various novel π -conjugated organic materials. As a modular click strategy based on the CuAAC reaction has been utilized to a great extent in my

synthetic work, the recent progress of click chemistry in relevant fields has just been reviewed in the preceding sections of this chapter.

Detailed experimental investigations are discussed in Chapters 2 to 5.

Chapter 2 introduces the synthesis and molecular properties of a series of amphiphilic dendro[60]fullerenes. In synthesizing these molecules, a CuAAC click strategy was successfully implemented. The photophysical and electrochemical properties of the dendro[60]fullerenes were studied by UV-Vis and fluorescence spectroscopic and cyclic voltammetric techniques. Due to their amphiphilic nature, these molecules were expected to serve as interesting supramolecular building blocks. Their acidity dependent self-assembly behaviors on mica surface were studied by AFM. These molecules yielded interesting surface morphologies, which appear to be significantly dependent on three key parameters, dendrimer generation, peripheral group, and acidity of the medium. Detailed correlations between molecular structures and the photophysical, electrochemical properties, and self-assembling outcomes were examined and discussed.

In Chapter 3, various carbon-rich, π -conjugated dendritic architectures were covalently attached to a series of linear phenylene ethynylene oligomers, π -extended tetrathiafulvalene derivatives (TTFAQs), and porphyrins through the CuAAC reaction. The photophysical and electrochemical properties of these molecules were studied by UV-Vis, fluorescence spectroscopic, and cyclic voltammetric techniques. Relevant structure-property relationships are established and compared with literature results. Materialization of these new hybrid compounds has not only provided models for investigation of dendrimer encapsulated redox-active moieties, but also offered a useful insight into the design principle of dendrimer-based molecular

optoelectronic devices.

Chapter 4 investigates the synthesis and properties of a series of electroactive polyynes. A number of transition metal catalyzed homo/cross coupling reactions were employed to prepare these highly unsaturated molecules. The properties of these compounds were investigated by electronic spectroscopic and cyclic voltammetric techniques. Of particular interest, relatively stable solid thin films were successfully prepared on the surface of electrode through electrochemically induced polymerization. Possible mechanisms for the thin film formation and implications in electronic device fabrication are discussed in this chapter.

Chapter 5 explores the functionalization of SWNTs by both non-covalent and covalent approaches in order to improve solubility and processability. In the first part a series of π -conjugated polymers have been synthesized and used for non-covalent functionalization of SWNTs. The solubility and processability of these polymer-CNTs conjugates increased significantly and the nature of supramolecular interactions between SWNTs and polymers was investigated by AFM, UV-Vis and Raman spectroscopy. In the second part of this chapter, a group of task-specific imidazolium based ionic liquids were synthesized. These ionic liquids are expected to be suitable media for covalent functionalization of SWNTs.

Finally, a concluding summary on this thesis work and perspectives for future work are given in Chapter 6.

Chapter 2

Dendro[60]fullerenes: Modular Synthesis and Controllable Supramolecular Self-Assembly

2.1 Introduction

Supramolecular chemistry, pioneered by Lehn and co-workers, has become an extensively pursued discipline in modern chemistry. It is widely believed that supramolecular self-assembly holds the key to spontaneous construction of devices and machines which are well-defined and preprogrammed on the nanometer scale and beyond.^{84,85} The formation of a super-structure via self-assembly of small molecular building blocks is thermodynamically favored and involves a delicate balance between strong covalent bonds that hold the molecular building blocks together and the reversible intermolecular forces that assemble them. How to build up supramolecular

self-assemblies in a controllable manner is a challenging, but highly rewarding task because in nanoscale device fabrications controlled microscopic architectures are prerequisite to achieving advanced or even unprecedented performances.⁸⁶

Of the numerous molecular building blocks investigated in the recent literature, C₆₀ fullerene and dendrimers constitute two important classes owing to their unique molecular shapes and multiple properties.⁸⁷ Dendrimers possess highly branched molecular backbones with nearly perfect molecular shapes and many end groups exposed at their globular periphery.³⁰ Such features allow flexible tuning of molecular shapes, functionalities, and intermolecular interactions. An interesting example is given in Figure 2.1, where a propeller shaped amphiphilic dendritic structure, based on a conformationally flexible aromatic segment, self-assembled into well-defined discrete nanostructures in the solid state or at the interface. TEM imaging clearly shows the formation of discrete nanoparticles (Figure 2.2) with a uniform diameter on the molecular length scale (6 nm).⁸⁸ The nanoparticles were assumed to assemble through weak $\pi - \pi$ interactions among these novel amphiphiles. Usually flat aromatic compounds, irrespective of their molecular shapes, have a strong tendency to form long (rod-like) 1-D nanostructures due to directional $\pi - \pi$ stacking in a columnar fashion. However, when dendritic structures are introduced to the periphery of a flat system, such as in **158a** or **158b**, the intermolecular interactions and favorable molecular packing geometry are considerably altered, resulting in the formation of nano-assemblies in higher dimension.

C₆₀ fullerene is an interesting carbon allotrope with an aesthetic spherical shape, extremely small size (ca. 0.7 nm in diameter), and extended π -system. Ever since its discovery in 1985, C₆₀ has become one of the most intensively investigated

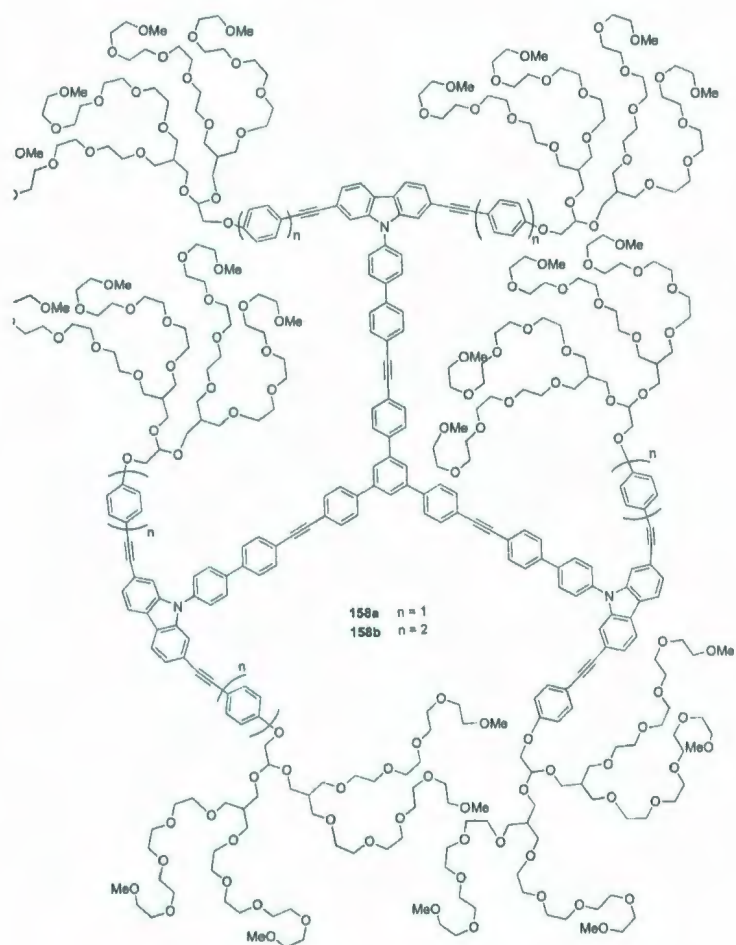


Figure 2.1: Propeller shaped aromatic amphiphiles.

carbon species. This is mainly due to its intriguing molecular structure and rich electronic/photophysical properties. To explore the full scale of its application potentials, it is crucially important to have certain criteria strictly fulfilled. When C_{60} -based materials are used in various device applications, for example, C_{60} based bulk heterojunction (BHJ) photovoltaic cells, specific micro- and nanoscopic ordering in the solid state or at the interface is required.^{60,89} Such ordering of C_{60} is, however, not easy to control due to some unavoidable barriers, especially, the fact that C_{60}

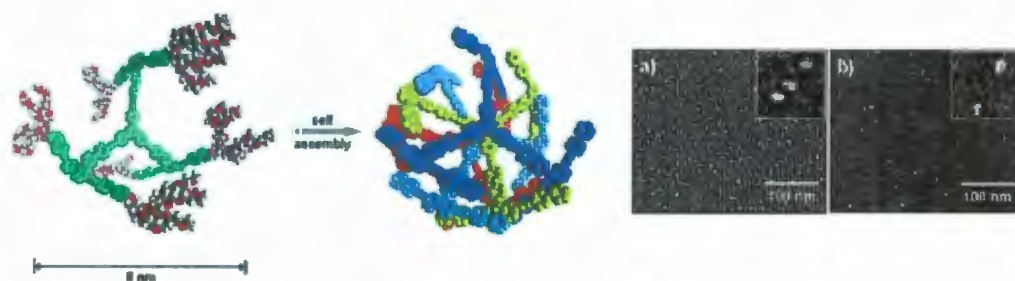


Figure 2.2: A propeller-shaped aromatic amphiphiles with dendrimers as end-capping groups.

tends to strongly aggregate via $\pi - \pi$ stacking. It results in a lack of directional interactions in case of nano- or microscopic ordering of C_{60} as can be observed for metal-ligand complexation or hydrogen bonding. To induce some attributes of directional interactions on the barren C_{60} cage, methods of applying templates or attachments of molecular functional groups are commonly used. Nevertheless, successes in this respect are somewhat limited so far.⁹⁰

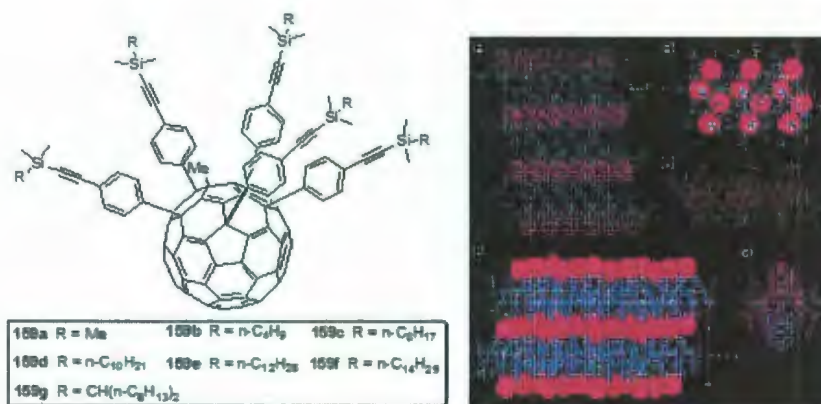
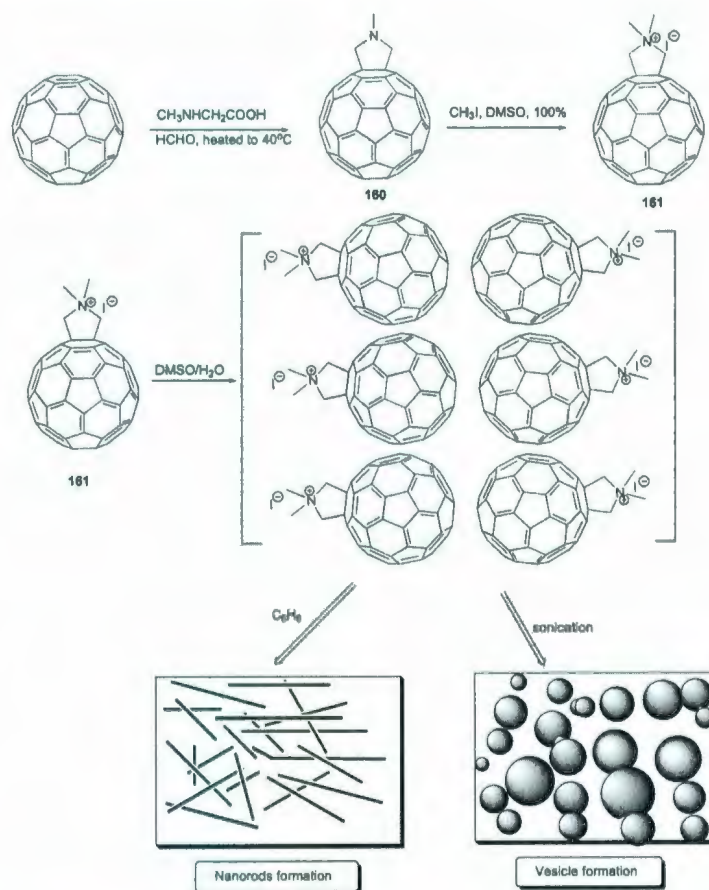


Figure 2.3: Conical shaped fullerene derivatives.

Nakamura *et al.* recently demonstrated the synthesis of a type of “shuttle-cock”

shaped C_{60} adducts with different molecular appendages. These C_{60} derivatives self-assembled into distinct nanometer-scale objects, such as columns and lamellae (see Figure 2.3), which could be regulated by certain parameters, including reaction conditions, size and peripheral groups.⁹¹



Scheme 2.1: Self-Assembling supramolecular nanostructures from a C_{60} Derivative.

Amphiphilic C_{60} derivatives containing ionic moieties or polar groups have been known to produce nanostructures with defined shapes in the solid state or at interfaces (*e.g.* spheres, vesicles, needles, and tubules).^{92,93} Take Nakamura's

work as an example. The sizes and shapes of these surface morphologies were also found to be dependent on several factors, such as molecular structures and experimental conditions.^{92,94} Tour *et al.* investigated the surface morphological outcomes of some ionic fullerene derivatives.⁹⁴ As shown in Scheme 2.1, C₆₀-N,N'-dimethylpyrrolidinium iodide was synthesized and then let self-assemble under different conditions, affording either nanorods (14–120 nm in diameter) when subjected to self-assembly in benzene or vesicles upon sonication (10–70 nm in diameter).

The self-assembly behaviors of C₆₀ derivatives discussed above are optimistic in the sense that some sort of regulation on supramolecular self-assembly becomes possible through the variation of certain parameters. However, complete supramolecular self-assembly of C₆₀ derivatives in a strictly controllable manner has not been achieved yet. The exact role of C₆₀ in dictating the supramolecular behavior is also under debate. It is therefore imperative to examine a wider range of C₆₀ adducts with diverse functionalities for a clear understanding. In this perspective, inclusion of dendritic groups to the C₆₀ cage could be an effective means to attain controllable supramolecular properties. The study of dendrimer/C₆₀ hybrid systems, generally referred to as dendro[60]fullerenes, has attracted significant research interest in recent years.^{60,95,96} C₆₀ gives such a convenient core for the growth of dendrimers that variable degrees of addition within the C₆₀ core have become possible. The resulting dendritic hybrids are usually spherical in shape, producing globular macromolecular systems even with low-generation dendrons. By embedding C₆₀ cages in the middle of dendritic structures, stabilizing effects on the excited states and/or charge-separation species (*e.g.* radical anions) can be attained, which offers a useful approach

to optimize the photophysical and photonic properties of C_{60} -based molecular materials.⁹² For this reason, dendrofullerenes have been successfully exploited in many recent designs of new functional materials, for example, stable monomolecular films at air-water interface and light-harvesting systems for artificial photosynthetic mimics.^{92,97}

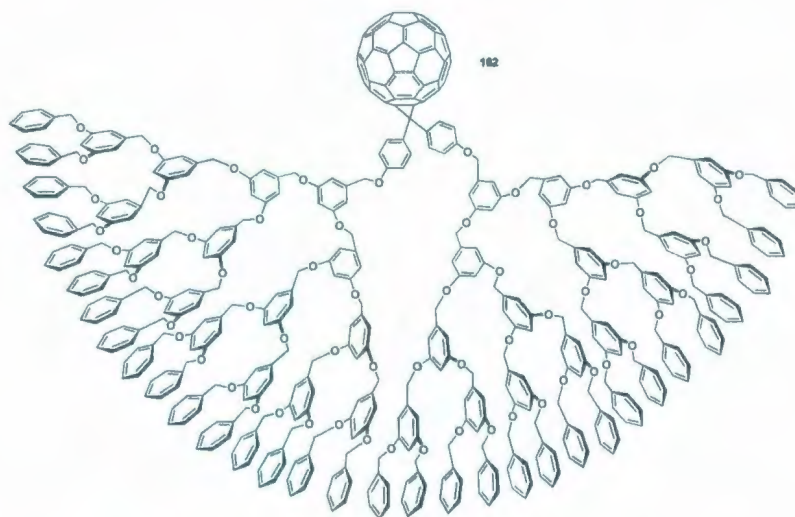
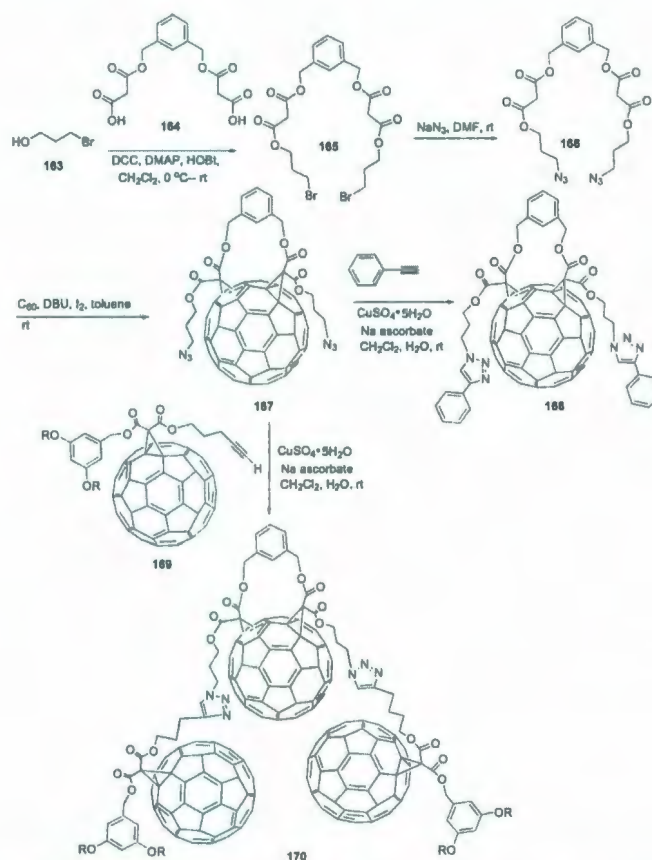


Figure 2.4: First dendro[60]fullerene synthesized by Fréchet.

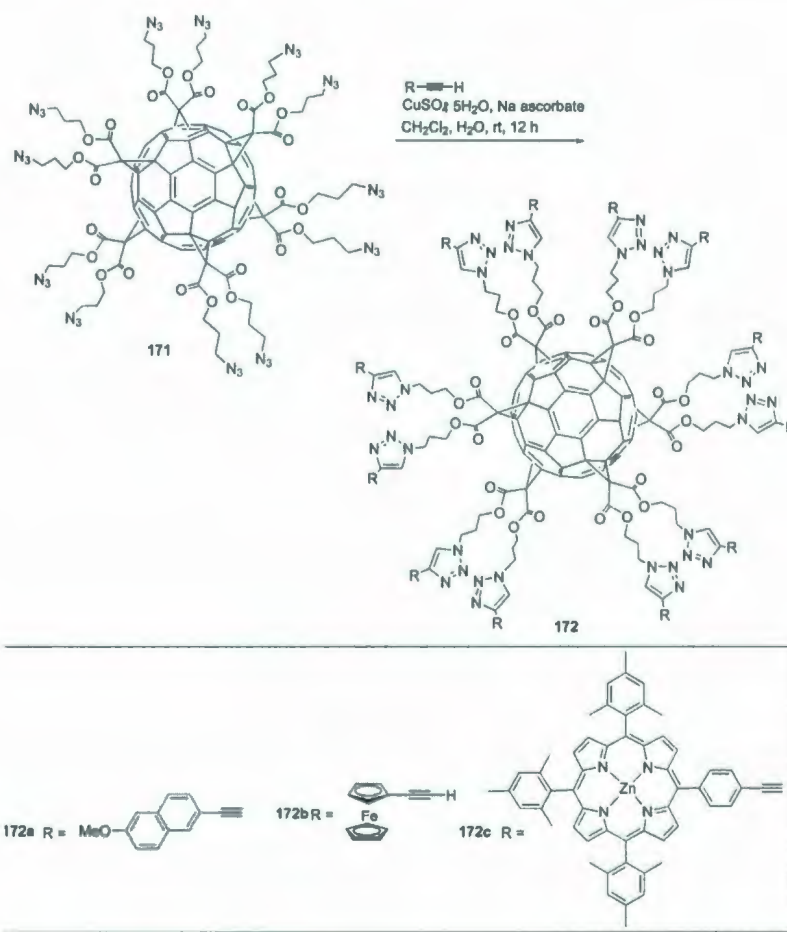
The first dendrofullerene **162** was prepared by Fréchet's group in 1993 as shown in Figure 2.4. Since then, a large variety of dendrofullerenes have emerged in the literature, with the dendron structures varying from Fréchet to Newkome and depsipeptide types. Nierengarten and Hirsch's groups are the two most inspirational and active teams in the field of dendrofullerene chemistry.^{60,95,96}

Among various synthetic methods used for dendrofullerenes, the CuAAC-type click reaction has been proven particularly advantageous.^{97,98} The three most significant challenges facing the synthesis of dendrofullerenes are: (i) low yield, (ii)

harsh reaction conditions, and (iii) troublesome byproduct separation. In principle, all of these difficulties can be properly addressed by using click chemistry. To exploit the potency of click chemistry, Nierengarten *et al.* have recently applied the CuAAC protocol to successfully prepare a series of dendrofullerenes as shown in Schemes 2.2 and 2.3.^{97,98} Worth particular remark is that in synthesizing **172**, twelve building blocks onto the core of C₆₀ have been anchored through a one-pot reaction. The overall yield of this click reaction is 62% (96% per reaction), testifying to the remarkable efficiency of CuAAC in the assembly of sophisticated dendrofullerene structures.



Scheme 2.2: Synthesis of C₆₀-rich dendrimers via click chemistry.



Scheme 2.3: Fullerene hexakis-adducts prepared by CuAAC reaction.

Aside from the synthesis, the application of dendrofullerenes as building blocks for preparing nanoscale architectures has also gained growing attention in recent study. As both C_{60} and dendrimers have attributes to form ordered structures in the solid state or at interfaces, both could provide an augmented effect for controlling supramolecular self-assembly. One very interesting example of dendrofullerenes, which gave controlled ordering of C_{60} in supramolecular nanostructures, is shown in Figure 2.5. In this work, Conyers *et al.* demonstrated the synthesis of dendrofullerene

173 (“buckysome”), where the phospholipid functions have been mimicked by investigating the biological role of a novel globular amphiphile (AF-1). Figure 2.5 shows the TEM image of AF-1 in citrate and PBS buffers. In the citrate buffer, predominantly vesicular nanostructures are formed in the sizes ranging from 75-100 nm irrespective of the methods of preparation (sonication, vortexing and extrusion). In the presence of PBS buffer, although 75-100 nm vesicles (see Figure 2.5, C) were observed to form, they were much less abundant.

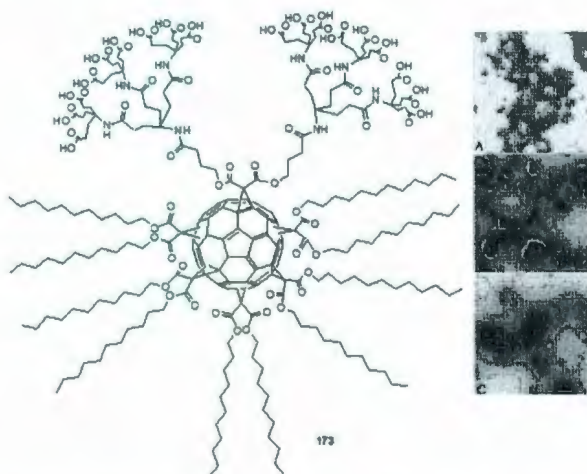


Figure 2.5: **173** and its TEM image (A: **173** was treated with citrate buffer, scale bar is 500 nm and in B and C: **173** was treated with PBS buffer, scale bar is 100 nm)

Most recently, a dynamically polydisperse supramolecular assembly of dendrofullerenes has been reported by Martín *et al.* (see Figure 2.6). AFM imaging clearly shows the formation of well-organized nanostructures (5-15 nm), which were formed by the self-assembly of dendrofullerene **174** through $\pi - \pi$ and van der Waals

interactions.⁸⁷ In the structure of 174, a type of donor-acceptor complex was formed between the curved (concave) aromatic surface of the electron donating 2-[9-(1,3-dithiol-2-ylidene)anthracen-10(9H)-ylidene]-1,3-dithiole tetrathiafulvalenes (extended TTFs) and the electron-accepting convex exterior of [60]fullerene with a significant binding constant (as high as 10^3 M^{-1}). The combination of supramolecular and electronic reciprocity between the host and guest molecules in this case has enabled the supramolecular assembly to act as self-organized electroactive materials.

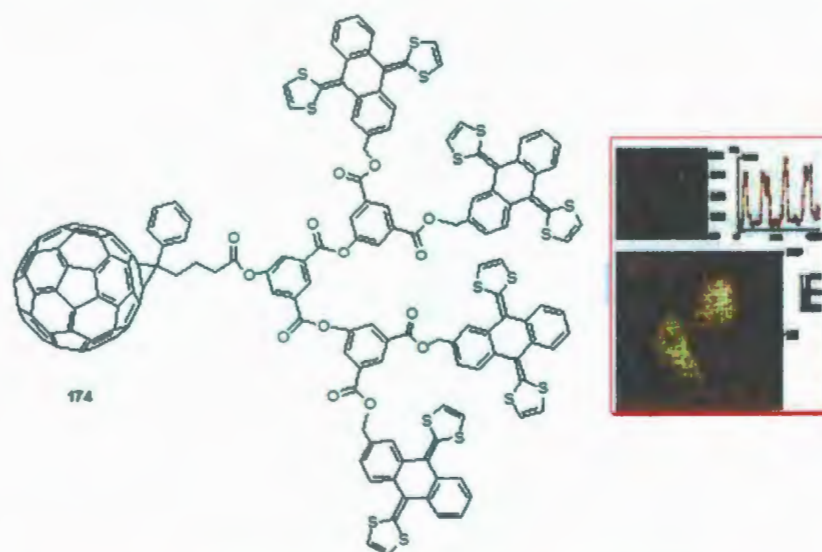


Figure 2.6: Electroactive supramolecular dendrofullerene 174.

From the above examples of controlled formation of dynamically polydisperse supramolecular nanospheres, it is clear that dendrofullerenes are suitable for the formation of supramolecular nanomaterials.⁸⁷ However to explore the full application potentials, synthesis and property investigations of a broad range of dendrofullerenes are imperative.

2.2 Objectives of This Project

To control and regulate the size of supramolecular nanostructures in the solid state or at interfaces is one of the aims of this project. However, a clear understanding of the role of various non-covalent forces for supramolecular nanostructures formation obviously requires proper strategies for the control and manipulation of self-assembly. This field has not been given careful attention so far. The underdevelopment of the field might be due to two main reasons: (1) the synthesis of dendro[60]fullerenes is not easy and usually requires multi-step synthesis and tedious purification procedures, and (2) the self-assembly of C_{60} derivatives is often complicated by the involvement of intricate intermolecular forces, the nature of which is difficult to understand.⁶⁰ To shed light on this problem, in the beginning of this work, it was planned to apply CuAAC click chemistry to allow easy access to a series of dendro[60]fullerene amphiphiles. Then, controlled generation of supramolecular nanostructures by solvophobicity-directed self-assembly would be explored. A series of Fréchet-type dendrimer functionalized C_{60} derivatives were designed, in which the dendrons and C_{60} moieties are covalently linked by a 1,2,3-triazole unit via the CuAAC reaction (see Figure 2.7). With these new 1,2,3-triazole-linked fullerodendrimers, the self-assembling behavior on the surface of mica could be investigated by atomic force microscopy (AFM). The detailed results will be discussed in this chapter.

In a long-term objective, the modified dendrofullerenes are expected to serve as mimics for artificial photosynthetic systems. For this purpose, the dendritic shielding effect on the photophysical and electrochemical properties were also investigated.

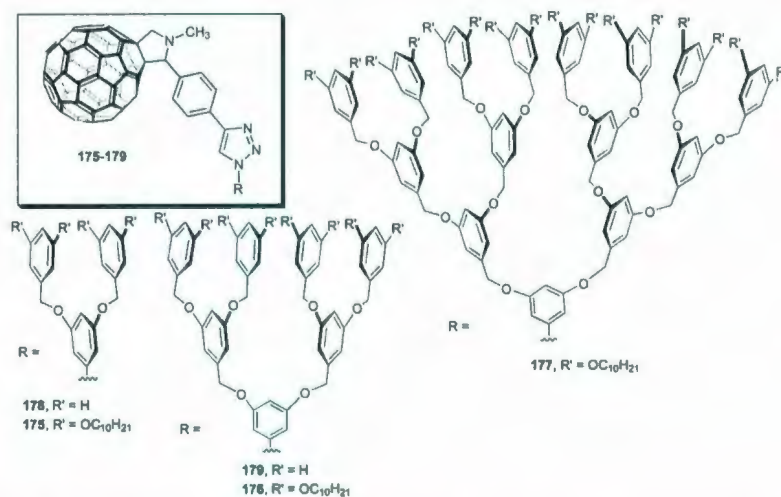


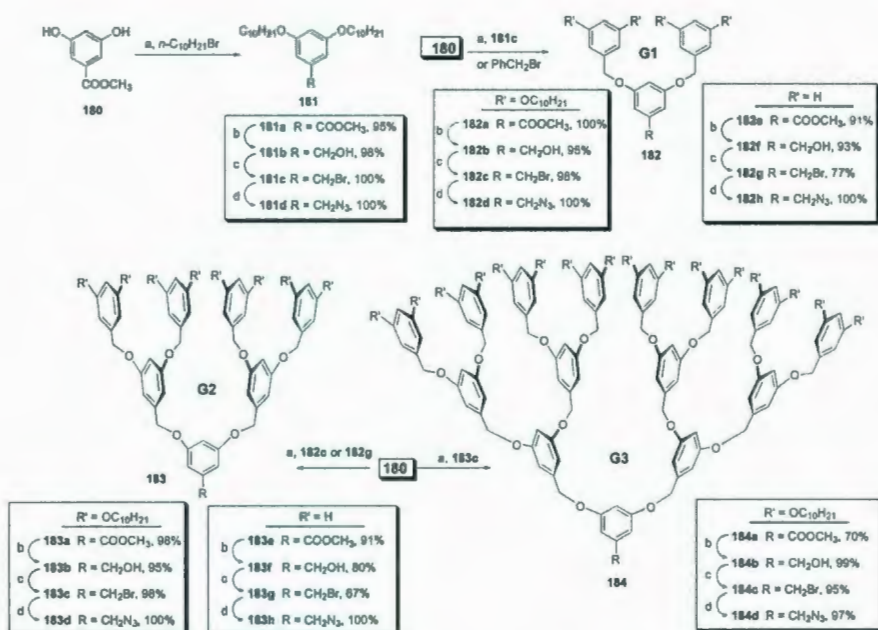
Figure 2.7: Dendrofullerenes (175-179) with and without peripheral decyl chains.

2.3 Results and Discussions

2.3.1 Synthesis

Two series of Fréchet-type dendrons (182-184) were synthesized following a modified literature protocol (see Scheme 2.4).⁶⁰ Two sets of dendrimers, with and without peripheral decyl chains, were prepared. The inclusion of peripheral decyl chains was intended to play an effective role in controlling the supramolecular self-assembling outcomes. Scheme 2.4 outlines the synthetic details.

3,5-Dihydroxybenzoic acid was esterified with MeOH under acidic conditions to yield compound **180** in a quantitative yield. Benzoate **180** was subjected to a Williamson etherification reaction with *n*-decylbromide in the presence of a phase-transfer catalyst, 18-crown-6, to yield compound **181a** in 95% yield. The ester group of **181a** was reduced to the corresponding benzyl alcohol in 98% yield by LiAlH₄ in dry THF. Primary alcohol **181b** was converted into alkyl bromide **181c** in an

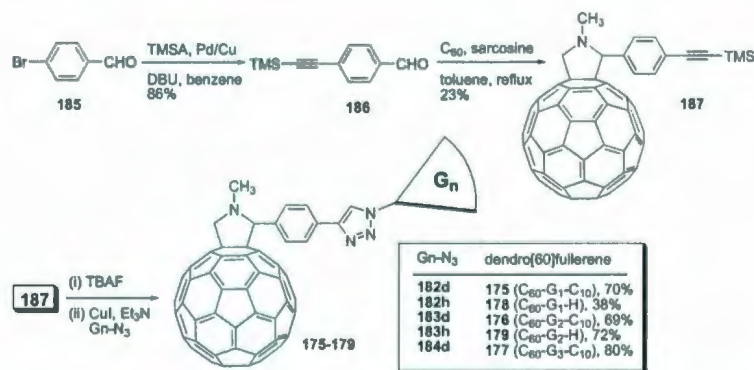


Scheme 2.4: Fréchet-type Azide-Pendant Dendrimers.

almost quantitative yield, when subjected to PPh_3 and CBr_4 (Appel reaction). Alkyl bromide **181c** was then transformed to alkyl azide **181d** by reacting it with NaN_3 . For producing the first generation dendrons, dihydroxy ester **180** was subjected to a Williamson etherification reaction with alkyl bromide **181c** or benzyl bromide under the same reaction conditions as used for the synthesis of **181a**. These common reaction protocols were followed in subsequent reactions for the preparation of dendrimers from the first to third generation (**182-184**). Satisfactory yields were attained.

Note that the azido-attached dendrons are precursors for the CuAAC reaction. To prepare various dendrofullerenes, alkynylated [60]fullerene was also prepared. In this work, fullerene-alkyne **187** was prepared through a 1,3-dipolar cycloaddition reaction, commonly known as the "Prato" protocol for fullerene functionalization. As shown

in Scheme 2.5, TMSA benzaldehyde **186**, sarcosine, and pristine fullerene were mixed in dry toluene under reflux for 24 h. Sarcosine and TMSA benzaldehyde produced an azomethine ylide *in situ*, which reacted with the [6,6] double bond of C₆₀ through a [3 + 2] cycloaddition to produce silyl protected alkynyl C₆₀ derivative **187**. The silyl group was removed *in situ* using TBAF and then subjected to CuAAC click reaction with respective azido-attached dendrons to form a series of dendrofullererenes **175-179**. Purification of these products was done by standard flash chromatographic techniques. The yields after column separation were satisfactory and sometimes were dependent on the solubility of products. For example, the yield of a poorly soluble dendrofullerene, **178**, was 38%, whereas the yield of **177**, which has far better solubility due to decyl chains, reached 80%.



Scheme 2.5: Synthesis of dendrofullerene **175-179** through click chemistry.

2.3.2 Structures and Electrochemical Properties of Dendro[60]fullerenes

The molecular structures of the dendrofullerenes were characterized by various spectroscopic techniques, including $^1\text{H-NMR}$, $^{13}\text{C-NMR}$, FT-IR, and high-resolution MALDI-TOF mass spectrometry. The high-resolution MALDI-TOF mass spectra clearly showed molecular ion peaks of these dendrofullerenes (175-179), while $^1\text{H-NMR}$ gives the most useful data to identify the triazole functional group formed after the CuAAC click reaction (see Figure 2.8). The formation of 1,2,3-triazole linker was also proved by the stretching bands at $2050\text{-}2150\text{ cm}^{-1}$ in the IR spectra. $^{13}\text{C-NMR}$ was however not so useful as the other methods in structure elucidation, mainly as a result of the low solubility of the dendrofullerenes.

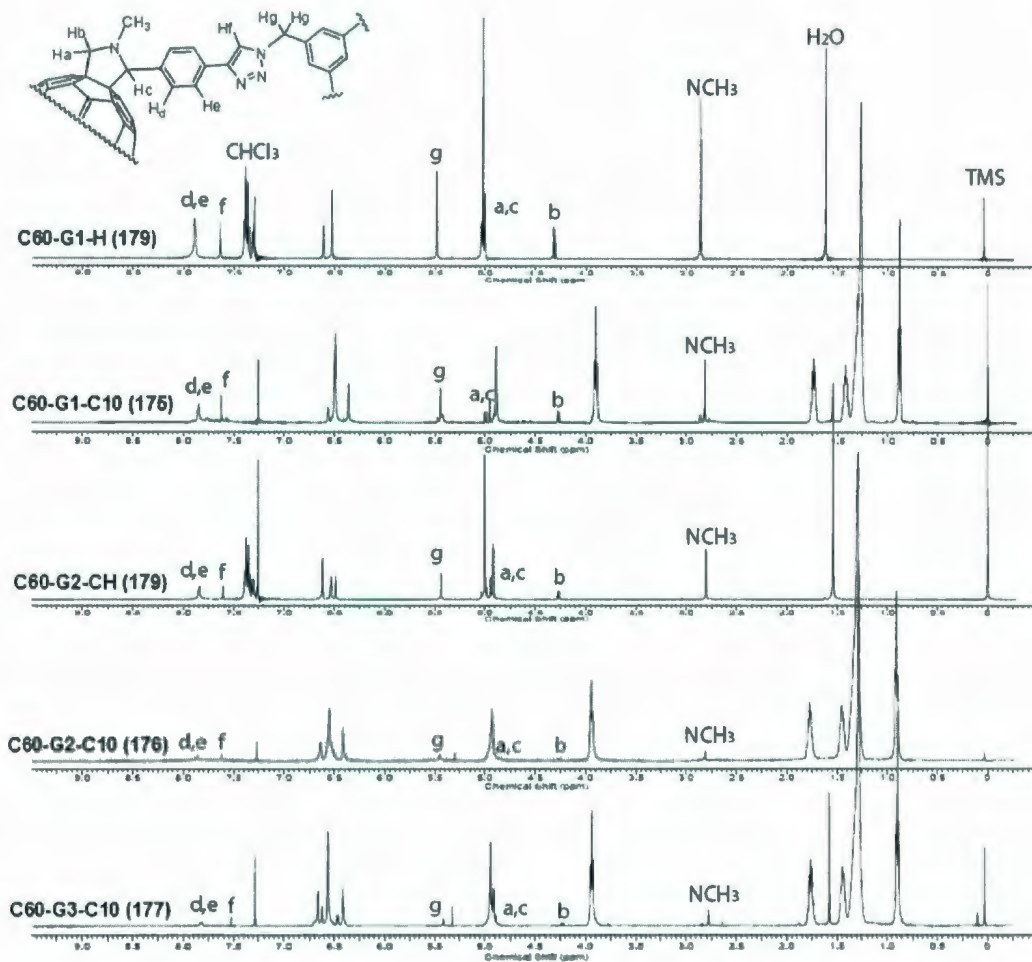


Figure 2.8: $^1\text{H-NMR}$ of dendro[60]fullerenes 175-179.

Figure 2.8 gives the $^1\text{H-NMR}$ spectra of dendrofullerenes **175-179**, where key proton signals corresponding to the linkage groups were highlighted and assigned. An interesting feature shown in this Figure is that the chemical shifts remain almost unchanged as the generation of dendrimers increases. This observation indicates that the linkage groups are experiencing similar chemical environments in different dendron generations.

The electrochemical behavior on dendrofullerenes **175-179** was conducted by cyclic voltammetry, and the detailed voltammograms are given in Figure 2.9. In the positive potential region of the voltammograms, dendro[60]fullerenes did not lead to any appreciable redox currents. However, the negative potential window presents different scenarios. All four dendrofullerenes display very rich redox patterns, which somehow resemble the redox features of pristine C_{60} .⁹⁹ The quasi-reversible redox wave pairs are ascribed to the sequential reductions on the C_{60} cage.^{99,100} For the dendrofullerenes bearing the first generation dendrons, such as **175** and **178**, at least three quasi-reversible redox waves were observed in the reduction window of their cyclic voltammograms.

The cyclic voltammograms of the dendrofullerenes bearing the second generation dendrons are complex and difficult to make clear assignment. Although the three redox peaks in their voltammograms can be distinguished and assigned to sequential reductions of the C_{60} cage, they are irreversible in nature. This can be explained by the shielding (steric crowding) imposed by higher generation dendrons around the C_{60} cage. As reported previously by Ito, bulky dendrons could act as barriers that hinder electron transfer at the C_{60} core of dendrofullerenes.¹⁰¹ In this sense, the patterns of CV observed in our experiments are consistent with other cases of dendrofullerenes

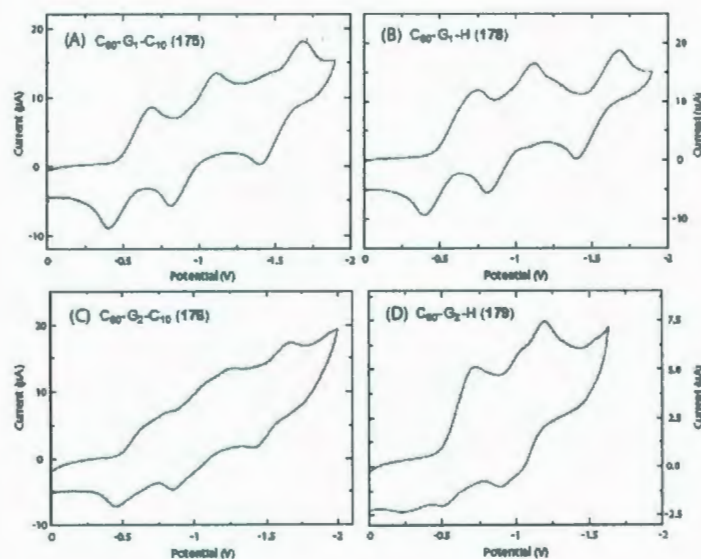


Figure 2.9: Cyclic voltammograms of dendro[60]fullerenes 175, 176, 178 and 179.

reported in the literature. The 1,2,3-triazole ring is an electron-accepting functional group. However, evidence for redox features arising from the triazole group was not found in the cyclic voltammetric analysis.

2.3.3 Electronic Absorption and Emission Properties of Dendro[60]fullerenes

Electronic absorption properties of the synthesized dendrofullerenes were investigated by UV-Vis spectroscopy. Figure 2.10 shows the normalized UV-Vis absorption spectra measured in CHCl_3 at room temperature, and Table 2.1 lists the detailed photophysical data. In the spectra, the prominent absorption shoulder bands in the 300-520 nm region are the characteristic $\pi \rightarrow \pi^*$ electronic transitions of the C_{60} core.¹⁰² The absorption shoulders for different dendrofullerenes in this region are a little bit different in shape, which might be accounted for by dendron effects. It is

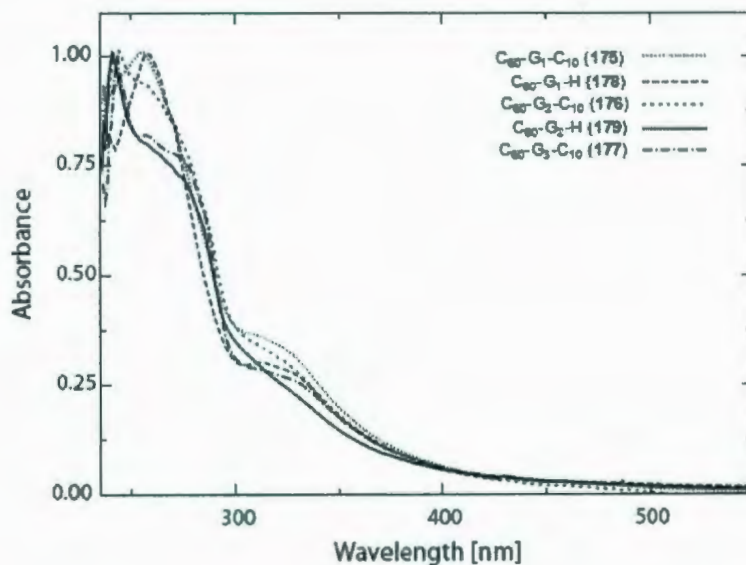


Figure 2.10: UV-Vis. absorption of dendro[60]fullerenes.

likely that the variation in the generation and functionality of the dendron moiety results in different aggregation behavior of the dendrofullerenes in solution.

It has been discussed previously that, due to the extended π -systems, C_{60} tends to aggregate via π - π stacking forces. This makes pristine [60]fullerenes show limited photophysical activities, since the aggregation of fullerenes results in a rapid deactivation of the excited states. Dendrimers with branching and peripheral groups could reasonably induce some shielding effect to retard the aggregation of C_{60} , thereby slowing down the deactivation of the excited states of [60]fullerenes. This leads to the so-called “long-lived” charge-separated states. The absorption maxima and the absorptions range were found to be almost similar for all dendrofullerenes having dendrons from the first to the third generation. This observation suggests there is no significant electronic communication between the dendron and the C_{60} core

Entry	Absorption			Emission	
	λ_{abs} (nm)	ϵ ($10^6 \text{ M}^{-1} \text{ cm}^{-1}$)	E_{op} (cm)	λ_{em} (nm)	E_{em} (cm)
187	258	2.2	38760	400	25000
	329	0.63	30395	470	21230
178	256	0.84	39060	338	29590
	312	0.26	32050	351	28490
175	255	2.3	39220	338	29590
	320 (sh)	0.77	31250	352	28410
				470	21280
179	270 (sh)	2.8	37040	430	23260
	328 (sh)	0.89	30490	590	16950
176	270	3.8	37040	400	25000
	320	1.4	31250	467	21410
177	275	6.6	36360	435	22990
	325	2.2	30770	460	21740

Table 2.1: Electronic and emission properties of dendrofullerenes.

through the triazole linker. Similar behavior has already been observed in related phenylenevinylene-based dendrimers.¹⁰³

2.3.4 Interfacial Self-Assembling Behavior of Dendro[60]fullerenes

One of the main aims of the “click” syntheses of dendro[60]fullerenes is to study their supramolecular interfacial self-assembly. It was mentioned in previous sections that [60]fullerenes are bulky, totally hydrophobic in nature, and particularly insoluble in some organic solvents. In the designed dendro[60]fullerenes, with relatively polar dendritic structures, it was envisioned that these molecules would show amphiphilicity in certain organic solvents. There are two regions of different nature upon solvation: the C₆₀ cage shows little penchant for solubilization (solvophobic), whereas the Fréchet-type dendrons are more solvent-friendly (solvophilic). Certainly, this amphiphilic nature will be an important element for exploring supramolecular aggregation.¹⁰⁴⁻¹⁰⁶ The shapes of dendrofullerenes are also important factors in dictating their aggregation behavior. In the literature, several theoretical models have been developed to predict the morphological features of assemblies by amphiphiles.^{107,108} Based on these theories, five most probable self-assembling morphologies were envisaged initially when the shape of amphiphiles (e.g. dendrofullerenes) was taken into consideration (see Figure 2.11).

Supramolecular assemblies of the dendro[60]fullerenes were formed on mica surface by the spin-coating method at a spin rate of 2000 rpm. Several drops of diluted solutions (10^{-5} to 10^{-6} M) of the dendro[60]fullerenes in chloroform were first spin-cast on a finely cleaved mica surface at room temperature. The surface samples were then rinsed with chloroform and kept spinning for a few more minutes. The morphologies of assemblies by dendrofullerenes were examined by atomic force microscopy (AFM) operated in the tapping-mode (non-contact mode).

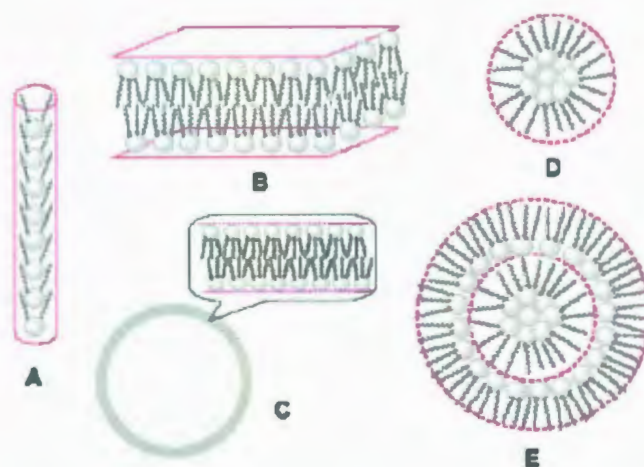


Figure 2.11: Most probable morphologies of dendro[60]fullerene supramolecular assemblies.

As discussed previously, the triazole-linked dendrofullerenes are supposed to show characteristics of amphiphilicity in common nonpolar organic solvents. If this were the case, it could eventually direct these molecules to form self-assemblies of defined shape and geometry. Generally, self-assembly is an energy-independent mechanism and the driving forces are usually H-bonding, van der Waals forces, and $\pi - \pi$ interactions. For the dendrofullerenes prepared in this work, in addition to the apparent $\pi - \pi$ stacking forces, hydrogen bonding is also envisioned to play a role in self-assembly, in view of the presence of good hydrogen bonding acceptors in the molecular structure, 1,2,3-triazole and pyrrolidine groups. With this in mind, it was also anticipated that the aggregation behavior of the dendrofullerene amphiphiles would be sensitive to pH value.

Figure 2.12 shows the AFM images that depict the surface morphologies of the supramolecular assemblies by dendro[60]fullerenes prepared under neutral conditions.

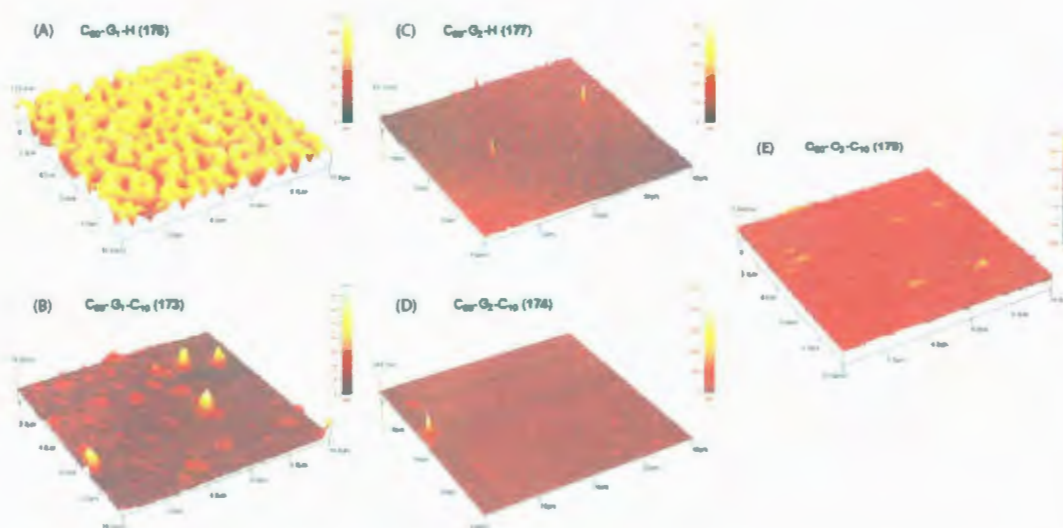


Figure 2.12: Surface morphologies of dendro[60]fullerenes in neutral condition.

The surface morphologies of **178** show closely packed and cross-linked worm-like nanocylindrical structures. The heights of these cylindrical nanostructures were measured to be around 40-100 nm. Dendro[60]fullerene **178** has wedge-like molecular shape. According to a theoretical packing model for amphiphilic molecules proposed by Tsonchev *et al.*, “wedge-like” molecules prefer to pack themselves into “cylindrical micelles”. It is therefore normal for wedges to stack into cylinders, if they are packed co-axially along a straight line.¹⁰⁷ It was also theoretically modeled that the molecular span for dendro[60]fullerene **178** is around 2.5 nm. Hence, the cylindrical nanostructures (40-100 nm) must have been formed in a multiple-layer architecture. The surface self-assembly of dendro[60]fullerene **179** is very different from **178**. Nanostructures assembled by the molecules of **177** produce some semi-spheroid nanoaggregates on the surface, which are random in size. Due to increased span of this higher-generation dendritic amphiphile, the molecular size of **179** does not

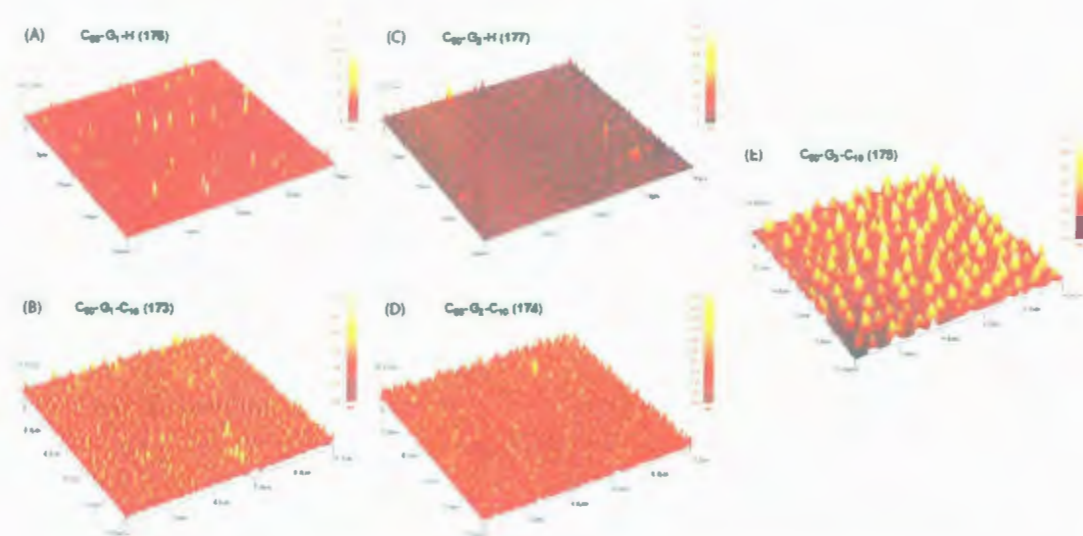


Figure 2.13: Surface morphologies of dendro[60]fullerenes in acidic condition.

resemble the “wedge”, as opposed to 178. Instead, the shape of 179 is more suitable to be defined as a “truncated cone”. According to Tsonchev’s theoretical packing model, truncated cones prefer to pack in a spherical geometry. Experimentally, however, the surface morphology revealed by AFM is random and undefined. The other three dendro[60]fullerenes 175, 176, and 177 produced amorphous thin-films with randomly structured aggregates across the surface. The peripheral decyl chains of these dendro[60]fullerenes are supposed to facilitate the assembly in lamellar structures, leading to the formation of amorphous thin-films on the surface.

At this stage, however, it was little bit disappointing that no discrete spherical micellar nanostructures from the interfacial self-assembly of dendro[60]fullerenes 175–179 were observed under neutral conditions, which contradicts the prediction based on known theoretical packing models.¹⁰⁷ The supramolecular surface self-assembling outcome from the same dendrofullerenes under acidic conditions were

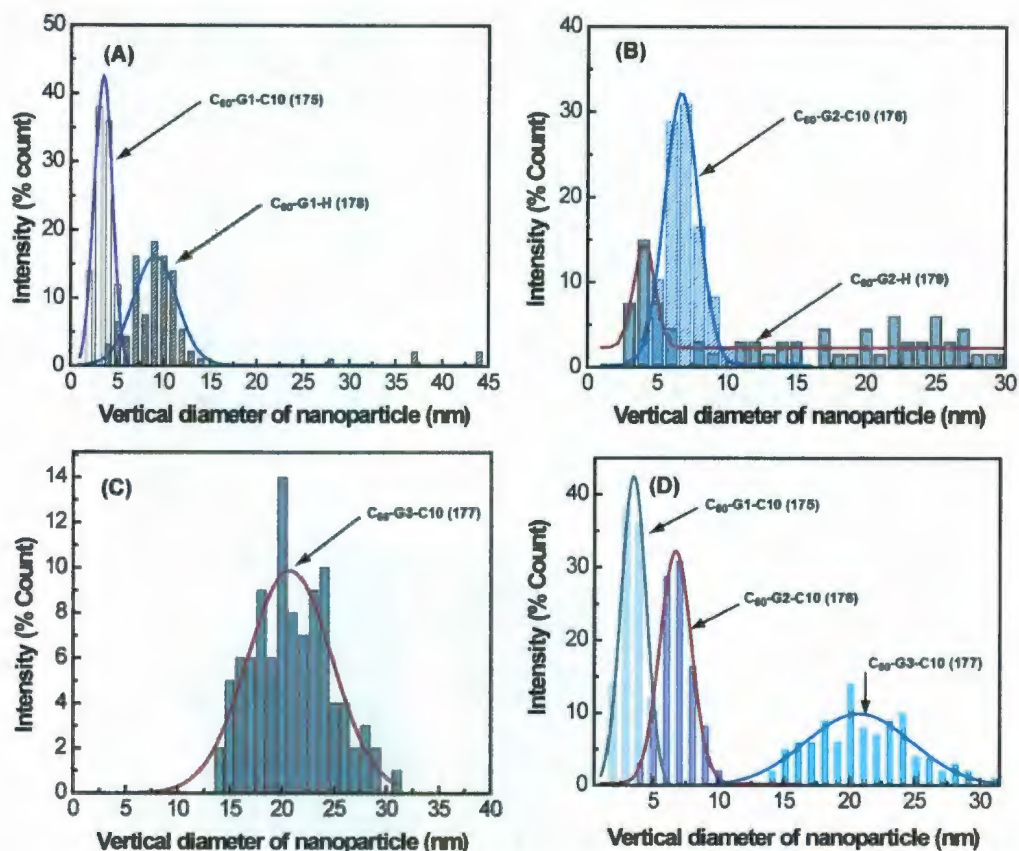


Figure 2.14: Height analysis of the nanospheres assembled by dendro[60]fullerenes under acidic conditions.

markedly different from those conducted under neutral conditions. Similar spin-coating procedures on freshly cleaved mica surface were adopted using acidified solutions of dendrofullerenes 175-179 in chloroform. Trifluoroacetic acid (TFA) was added in excess to the solution of dendrofullerenes and then spin-coated at room temperature. The interfacial self-assemblies of these dendro[60]fullerenes on mica surfaces were studied by AFM (see Figure 2.13). Unlike those in neutral conditions, all the acidified dendro[60]fullerenes produced discrete spherical nanoaggregates. It

could be assumed at this stage that the strong acid might have protonated the nitrogen atoms in 1,2,3-triazole rings and/or that of pyrrolidine rings, thereby enhancing the inherent solvophobicity to a greater extent.

One key finding from this work is that self-assembling behavior of the synthesized dendro[60]fullerene amphiphiles can reach up to a controllable level regulated by such factors as the nature of dendron, balance of solvophobicity and solubility, acidity of medium, and the peripheral groups of dendron. Figure 2.14 reveals that dendrofullerenes having dendrons without alkyl chains formed nanospheres, the sizes of which are significantly large and varying. Dendrofullerenes having alkyl chains in their dendrons on the contrary produced ordered arrays of nanospheres, which are comparatively uniform in dimension. In order to make more clear assignments of the possible morphologies and hierarchical orders from these interfacial self-assemblies, statistical analysis of the vertical diameters of the nanospheres measured by AFM have been performed and illustrated in Figure 2.14. In all these cases, dendrofullerenes having no alkyl peripheral groups give much wider size distributions than dendro[60]fullerenes with decyl peripheral groups.

In Figure 2.14A, it is seen that the size distributions of the nanospheres from the first generation dendro[60]fullerene with decyl chains, **175**, is lower (0–5 nm) than those from the first generation dendro[60]fullerene without decyl chains, **178** (0–15 nm). This effect is greater for the second generation dendro[60]fullerenes. The size distribution of nanospheres (0–10 nm) formed by dendro[60]fullerene with decyl chains, **176**, is narrower than that of dendro[60]fullerene without decyl chains, **179** (0–30 nm). Obviously these peripheral decyl chains influence the size distribution by forming an insulating layer around nanoaggregates. The phenyl peripheral groups in

dendro[60]fullerenes (**178** and **179**) produce sufficient affinity for stacking with the C₆₀ cage, resulting in multi-layered aggregates and comparatively wider size distribution.

It was observed that the size distributions of spherical micelles formed from the dendro[60]fullerenes with decyl chains are narrower and monodispersed. Moreover, based on the average sizes of the nanospheres (from statistical analysis) and estimated diameter of monolayer micelles (from molecular modeling), it is reasonable to believe that these dendrofullerenes prefer to form monolayered or in some cases bilayered micelles. The decyl chains function as an insulating layer between the monolayered micelles and prevent further aggregation to form multilayered micelles. The size distribution of nanospheres of the third generation dendro[60]fullerenes is broad, likely due to increased flexibility of the dendron in **177**. Figure 2.14D shows that there is a clear trend that the average sizes of the spherical micelles assembled by dendro[60]fullerenes with decyl chains progressively increases with growing dendron generation, indicating a control over the assemblies by molecular parameters.

2.4 Conclusions

In this chapter, a series of 1,2,3-triazole-linked dendro[60]fullerenes have been successfully synthesized using a modular CuAAC reaction. Photophysical and electrochemical properties of these compounds were studied by UV-Vis spectroscopic and cyclic voltammetric analysis. More interesting results were obtained from the amphiphilic self-assembling behavior of these compounds. Self-assembly of dendro[60]fullerenes produced some well-defined spherical shapes and the sizes were controllable at the molecular (bottom-up) level. It was found that three

molecular parameters played important roles: acidity, dendron size (generation), and the nature of peripheral group. From detailed examination of the surface morphology, it is believed that under controlled conditions (up to certain dendrimer generations, peripheral groups, etc.), dendro[60]fullerene molecules can be tuned to give four different self-assembly morphologies, namely, multilayered cylinders, lamella, monolayered spherical micelles, and multilayered spherical micelles. This finding presents a plausible bottom-up approach to construct defined nanostructures. Further exploration along this direction would benefit the research of C_{60} and dendrimer based functional nanomaterials.

2.5 Experimental Part

General procedures and methods

Chemicals and reagents were purchased from commercial suppliers and used as-received unless noted otherwise. [60]Fullerene(purity 99.5+%) was purchased from MTR Ltd. THF was distilled from sodium/benzophenone. Et_3N , benzene, and toluene were distilled from LiH. Tetrabutylammonium fluoride (1 M in THF) was purchased from Aldrich. Palladium catalyst $Pd(PPh_3)_2Cl_2$ was prepared from $PdCl_2$ according to literature procedures. All reactions were performed in standard, oven-dried glassware, and palladium-catalyzed Sonogashira reactions were done under N_2 atmosphere. Evaporation and concentration were performed at H_2O -aspirator pressure. Flash column chromatography was carried out with silica gel 60 (230-400 mesh) from VWR International. Thin-layer chromatography (TLC) was carried out with silica gel 60 F_{254} covered on plastic sheets and visualized by UV light or

KMnO₄ stain. Melting points (mp) were measured with a Fisher-Johns melting point apparatus and are uncorrected. ¹H and ¹³C NMR spectra were measured on the Bruker Avance 500 MHz spectrometer. Chemical shifts (δ) are reported in parts per million (ppm) downfield from the signal of internal reference SiMe₄. Coupling constants (J) are given in Hertz. Infrared spectra (IR) were recorded on a Bruker Tensor 27 spectrometer. UV-Vis spectra were recorded on an Agilent 8453 spectrophotometer. APCI mass spectra (MS) were measured on an Agilent 1100 series LCMSD spectrometer, and MALDI-TOF mass spectra on an Applied Biosystems Voyager instrument with dithranol as the matrix. Cyclic voltammetric experiments were performed on an Epsilon electrochemical analyzer, and AFM imaging was conducted on a QScope 250 scanning probe microscope in non-contact (tapping) mode. Fluorescence spectra were measured in deoxygenated CHCl₃ at ambient temperature using a Quantamaster 10000 fluorometer.

Synthesis of methyl 3,5-bis(decyloxy)benzoic acid ester 181a

To a 100 mL round-bottom flask were added methyl 3,5-dihydroxybenzoic acid ester **180** (500 mg, 3.00 mmol), 1-bromodecane (2.65 g, 12.0 mmol), K₂CO₃ (3.40 g, 25.0 mmol), 18-crown-6 (157 mg, 6.00 \times 10⁻⁴ mol) in acetone (150 mL). The mixture was refluxed for 24 h and then cooled to room temperature. The solvent was evaporated in vacuo, and the residue was dissolved in CH₂Cl₂. The solution of the product mixture was sequentially washed with H₂O, dilute aq. NaOH (1 M), and H₂O again. The organic layer was dried over MgSO₄, concentrated in vacuo, and the resulting crude product was purified by flash chromatography using hexanes/CH₂Cl₂ (3:1) to afford compound **181a** (1.27 g, 2.83 mmol, 95%) as white needle-like crystals.

Mp 52-53 °C; IR (neat): 2921, 2850, 1722, 1599 cm^{-1} ; ^1H NMR (500 MHz, CDCl_3): δ 7.16 (d, $J = 2.6$ Hz, 2H, ArH), 6.63 (t, $J = 2.5$ Hz, 1H, ArH), 3.97 (t, $J = 6.6$ Hz, 4H, O- CH_2), 3.89 (s, 3H, ester CH_3), 1.77 (m, 4H, decyl CH_2), 1.44 (m, 4H, decyl CH_2), 1.38-1.23 (m, 24H, decyl CH_2), 0.88 (t, $J = 6.9$ Hz, 6H, decyl CH_3); ^{13}C NMR (125 MHz, CDCl_3): δ 167.3 ($\text{C}=\text{O}$), 160.5 (Ar CO), 132.1, 107.9, 106.9, 68.6 (OCH_2), 52.5 (OCH_3), 32.2, 29.9, 29.8, 29.7, 29.6, 29.5, 26.0, 23.0, 14.4 (decyl CH_3); APCI-MS (positive mode) m/z calcd for $\text{C}_{28}\text{H}_{48}\text{O}_4$ 448.4, found 449.3 [$\text{M} + \text{H}$] $^+$.

Synthesis of 3,5-bis(decyloxy)benzyl alcohol 181b

A solution of **181a** (1.00 g, 2.23 mmol) in dry THF (40 mL) was added to a 100 mL round-bottom flask cooled at 0 °C. A pre-cooled slurry of LiAlH_4 (169 mg, 4.45 mmol) in dry THF (10 mL) was then added dropwise. After addition of LiAlH_4 , the reaction mixture was stirred at room temperature for 2 h, then quenched with a small amount of H_2O to consume excess LiAlH_4 and neutralized with aq. HCl (1 M). The solvent (THF) was removed in vacuo, and the resulting content was extracted with ethyl acetate and washed with a saturated NH_4Cl solution. The organic layer was dried over MgSO_4 and filtered. Evaporation of the solvent in vacuo afforded compound **181b** (921 mg, 2.19 mmol, 98%) as a white solid. Mp 29-31 °C; IR (neat): 3364 (br, OH), 2919, 2851, 1590, 1466, 1128 cm^{-1} ; ^1H NMR (500 MHz, CDCl_3): δ 6.48 (m, 2H, ArH), 6.37 (m, 1H, ArH), 4.56 (s, 2H, benzylic CH_2), 3.91 (t, $J = 6.6$ Hz, 4H, O- CH_2), 2.69 (br s, 1H, OH), 1.77 (m, 4H, decyl CH_2), 1.46 (m, 4H, decyl CH_2), 1.41-1.24 (m, 24H, decyl CH_2), 0.92 (t, $J = 6.8$ Hz, 6H, decyl CH_3); ^{13}C NMR (125 MHz, CDCl_3): δ 160.6 (Ar $\text{C}-\text{O}$), 143.5, 105.2, 100.7, 68.2 (OCH_2), 65.3 (benzylic CH_2), 32.1, 29.82, 29.80, 29.64, 29.56, 29.5, 26.3, 22.9, 14.3 (decyl CH_3); APCI-MS

(positive mode) m/z calcd for $C_{27}H_{48}O_3$ 420.4, found 421.3 $[M + H]^+$ and 444.3 $[M + Na]^+$.

Synthesis of 3,5-bis(decyloxy)benzyl bromide **181c**

A solution of **181b** (300 mg, 0.714 mmol) and CBr_4 (356 mg, 1.07 mmol) in CH_2Cl_2 (30 mL) was added to a 100 mL round-bottom flask, and to this mixture was dropwise added a solution of PPh_3 (281 mg, 1.07 mmol) in CH_2Cl_2 at 0 °C. The content was then kept under stirring at room temperature for 3 h. The solvent was removed in vacuo and the resulting residue was purified by flash chromatography using hexanes/ CH_2Cl_2 (5:1) to yield compound **181c** (345 mg, 0.715 mmol, 100%) as white shiny crystals. Mp 26-27 °C; IR (neat): 2923, 2853, 1596, 1165, 1057 cm^{-1} ; 1H NMR (500 MHz, $CDCl_3$): δ 6.53 (m, 2H, Ar-H), 6.40 (m, 1H, Ar-H), 4.42 (s, 2H, benzylic CH_2), 3.94 (t, $J = 6.6$ Hz, 4H, O- CH_2), 1.78 (m, 4H, decyl CH_2), 1.46 (m, 4H, decyl CH_2), 1.42-1.23 (m, 24H, decyl CH_2), 0.91 (t, $J = 6.9$ Hz, 6H, decyl CH_3); ^{13}C NMR (125 MHz, $CDCl_3$): δ 160.7 (Ar C-O), 139.8, 107.7, 101.6, 68.4 (O- CH_2), 34.0 (benzylic CH_2), 32.2, 29.9, 29.8, 29.7, 29.6, 29.5, 26.3, 23.0, 14.4 (CH_3); APCI-LCMS (positive mode) m/z calcd for $C_{27}H_{47}O_2^{79}Br$ (^{81}Br) 482.3 (484.3), found 483.3 (485.3) $[M + H]^+$.

Synthesis of G1-C10 dendron **182a**

G1-C10 dendron **182a** (1.31 g, 1.35 mmol, 100%) was prepared as white needle-like crystals from methyl 3,5-dihydroxybenzoic acid ester **180** (231 mg, 1.38 mmol), **181c** (2.00 g, 4.15 mmol), K_2CO_3 (762 mg, 5.52 mmol), and 18-crown-6 (72.0 mg, 2.80 mmol) following the same etherification procedure as described in the synthesis of **181a**. Mp 58-59 °C; IR (neat): 2922, 2853, 1726, 1595, 1163, 1051 cm^{-1} ; 1H NMR

(500 MHz, CDCl₃): δ 7.32 (d, $J = 2.6$ Hz, 2H, Ar-H), 6.82 (m, 1H, Ar-H), 6.59 (m, 4H, Ar-H), 6.44 (m, 2H, ArH), 5.00 (s, 4H, benzylic CH₂), 3.96 (t, $J = 6.6$ Hz, 8H, decyl O-CH₂), 3.92 (s, 3H, ester CH₃), 1.80 (m, 8H, decyl CH₂), 1.48 (m, 8H, decyl CH₂), 1.43-1.26 (m, 48H, decyl CH₂), 0.93 (t, $J = 6.9$ Hz, 12H, decyl CH₃); ¹³C NMR (125 MHz, CDCl₃): δ 166.9 (C=O), 160.8, 160.0 (Ar C-O), 138.8, 132.2, 108.6, 107.4, 105.9, 101.1, 70.5, 68.2 (one benzylic O-CH₂ and one decyl O-CH₂), 52.3 (ester CH₃), 32.2, 29.84, 29.82, 29.7, 29.6, 29.5, 26.3, 22.9, 14.3 (decyl CH₃); APCI-MS (positive mode) m/z calcd for C₆₂H₁₀₀O₈ 972.7, found 973.7 [M + H]⁺.

Synthesis of G1-C10 dendron 182b

G1-C10 dendron **182b** (476 mg, 0.500 mmol, 98%) was prepared as a white solid from **182a** (500 mg, 0.514 mmol) and LiAlH₄ (100 mg, 2.63 mmol) following the same reduction procedure as described in the synthesis of **181b**. Mp 47-48 °C; IR (neat): 3500-3200 (br, OH), 2922, 2853, 1596, 1455, 1161 cm⁻¹; ¹H NMR (500 MHz, CDCl₃): δ 6.62 (m, 2H, Ar-H), 6.55 (m, 5H, Ar-H), 6.41 (m, 2H, Ar-H), 4.96 (s, 4H, benzylic CH₂), 4.64 (s, 2H, benzylic CH₂), 3.95 (t, $J = 6.6$ Hz, 8H, decyl O-CH₂), 1.78 (m, 8H, decyl CH₂), 1.46 (m, 8H, decyl CH₂), 1.40-1.25 (m, 48H, decyl CH₂), 0.90 (t, $J = 6.9$ Hz, 12H, decyl CH₃); ¹³C NMR (125 MHz, CDCl₃): δ 160.8, 160.5 (two Ar C-O), 143.7, 139.3, 106.03, 106.01, 101.6, 101.1 (six aromatic carbon signals), 70.4, 68.4, 65.6 (two benzylic O-CH₂ and one decyl O-CH₂), 32.2, 29.88, 29.86, 29.7, 29.62, 29.56, 26.4, 23.0, 14.4 (decyl CH₃); APCI-MS (positive mode) m/z (%) calcd for C₆₁H₁₀₀O₇ 944.8, found 945.7 [M + H]⁺.

Synthesis of G1-C10 dendron 182c

G1-C10 dendron **182c** (314 mg, 0.312 mmol, 98%) was prepared as white shiny

crystals from **182b** (300 mg, 0.318 mmol), CBr_4 (264 mg, 0.795 mmol), and PPh_3 (208 mg, 0.795 mmol) following the same bromination procedure as described in the synthesis of **181c**. Mp 42-43 °C; IR (neat): 2922, 2853, 1594, 1457, 1162, 1052 cm^{-1} ; ^1H NMR (500 MHz, CDCl_3): δ 6.70 (m, 2H, Ar-H), 6.64 (m, 4H, Ar-H), 6.62 (m, 1H, Ar-H), 6.51 (m, 2H, Ar-H), 4.99 (s, 4H, benzylic CH_2), 4.45 (s, 2H, benzylic CH_2), 4.01 (t, $J = 6.5$ Hz, 8H, decyl O- CH_2), 1.86 (m, 8H, decyl CH_2), 1.56 (m, 8H, decyl CH_2), 1.51-1.34 (m, 48H, decyl CH_2), 1.02 (t, $J = 7.0$ Hz, 12H, decyl CH_3); ^{13}C NMR (125 MHz, CDCl_3): δ 160.7, 160.2 (two Ar C-O), 139.7, 139.0, 108.2, 105.8, 102.3, 100.9, 70.2, 68.1 (one benzylic O- CH_2 and one decyl O- CH_2), 33.6 (benzylic CH_2Br), 32.1, 29.82, 29.80, 29.64, 29.55, 29.49, 26.3, 22.9, 14.3 (decyl CH_3); APCI-MS (positive mode) m/z calcd $\text{C}_{61}\text{H}_{99}\text{O}_6$ ^{79}Br (^{81}Br) 1006.7 (1008.7), found 1007.7 (1009.7) $[\text{M} + \text{H}]^+$.

Synthesis of G1-C10 dendron **182d**

A solution of **182c** (200 mg, 0.199 mmol) and NaN_3 (139 mg, 2.14 mmol) in DMSO (5 mL) was added in a 100 mL round-bottom flask and heated up to 80-85 °C for 30 h. Afterwards, the content was cooled to room temperature and then quenched with slow addition of water (exothermic). The mixture was extracted with CH_2Cl_2 (20 mL) and the organic layer was sequentially washed with H_2O and a saturated NH_4Cl solution and then dried over MgSO_4 , and filtered. Removal of the solvent in vacuo afforded **182d** (192 mg, 0.198 mmol, 100%) as pale yellow liquid. IR (neat): 2923, 2853, 2099, 1595, 1457, 1164, 1058 cm^{-1} ; ^1H NMR (500 MHz, CDCl_3): δ 6.64-6.54 (m, 7H, ArH), 6.45 (m, 2H, ArH), 4.98 (s, 4H, benzylic CH_2), 4.28 (s, 2H, benzylic CH_2), 3.97 (t, $J = 6.6$ Hz, 8H, decyl O- CH_2), 1.81 (m, 8H, decyl CH_2), 1.49 (m, 8H,

decyl CH₂), 1.44-1.26 (m, 48H, decyl CH₂), 0.94 (t, *J* = 6.9 Hz, 12H, decyl CH₃); ¹³C NMR (125 MHz, CDCl₃): δ 160.8, 160.5 (2 Ar C-O), 139.0, 137.8, 107.4, 105.9, 102.1, 101.1, 70.4, 68.3 (one benzylic O-CH₂ and one decyl O-CH₂), 55.0 (benzylic CH₂N₃), 32.1, 29.83, 29.81, 29.7, 29.6, 29.5, 26.3, 22.9, 14.3 (CH₃); APCI-MS (positive mode) *m/z* calcd for C₆₁H₉₉O₆N₃ 969.8, found 970.8 [M + H]⁺.

Synthesis of G2-C10 dendron 183a

G2-C10 dendron **183a** (1.03 g, 0.510 mmol, 98%) was prepared as a white solid from methyl 3,5-dihydroxybenzoic acid ester **180** (87.0 mg, 0.521 mmol), **182c** (1.58 g, 1.57 mmol), K₂CO₃ (273 mg, 1.98 mmol), and 18-crown-6 (26.0 mg, 0.100 mmol) following the same etherification procedure as described in the synthesis of **181a**. Mp 68 °C; IR (neat): 2923, 2853, 1725, 1595, 1161, 1052 cm⁻¹; ¹H NMR (500 MHz, CDCl₃): δ 7.33 (m, 2H, Ar-H), 6.79 (m, 1H, Ar-H), 6.72 (m, 4H, ArH), 6.62 (m, 10H, Ar-H), 6.46 (m, 4H, Ar-H), 4.95 (m, 12H, benzylic O-CH₂), 3.96 (m, 23H, overlap of benzylic O-CH₂, decyl O-CH₂ and ester CH₃), 1.82 (m, 16H, decyl CH₂), 1.51 (m, 16H, decyl O-CH₂), 1.47-1.32 (m, 96H, decyl CH₂), 0.99 (t, *J* = 7.1 Hz, 24H, decyl CH₃); ¹³C NMR (125 MHz, CDCl₃): δ 167.0 (C=O), 160.8, 160.5, 160.0 (three Ar CO), 139.2, 139.1, 108.7, 107.8, 107.4, 106.7, 106.1, 102.0, 101.2 (eight aromatic carbon signals), 70.5 (benzylic O-CH₂), 66.4 (decyl O-CH₂), 52.5 (ester CH₃), 32.2, 29.88, 29.86, 29.7, 29.62, 29.57, 26.4, 23.0, 14.4 (decyl CH₃); MALDI-TOF MS (dithranol as the matrix) *m/z* calcd for C₁₃₀H₂₀₄O₁₆ 2022.5, found 2017.3 [M]⁺.

Synthesis of G2-C10 dendron 183b

G2-C10 dendron **183b** (484 mg, 0.243 mmol, 98%) was prepared as a white solid from **183a** (500 mg, 0.247 mmol) and LiAlH₄ (37.0 mg, 0.980 mmol) following the

same reduction procedure as described in the synthesis of **181b**. Mp 124-125 °C; IR (neat): 3600-3200 (br, OH), 2922, 2852, 1595, 1453, 1159, 1054 cm^{-1} ; ^1H NMR (500 MHz, CDCl_3): δ 6.70 (m, 4H, Ar-H), 6.61 (m, 12H, Ar-H), 6.55 (m, 1H, Ar-H), 6.46 (m, 4H, Ar-H), 4.95 (s, 8H, benzylic O- CH_2), 4.94 (s, 4H, benzylic O- CH_2), 4.60 (s, 2H, benzylic O- CH_2), 3.97 (t, $J = 6.5$ Hz, 16H, decyl O- CH_2), 1.82 (m, 16H, decyl CH_2), 1.51 (m, 16H, decyl CH_2), 1.47-1.30 (m, 96H, decyl CH_2), 0.97 (t, $J = 6.9$ Hz, 24H, decyl CH_3); ^{13}C NMR (125 MHz, CDCl_3): δ 160.6, 160.3, 160.1 (three Ar C-O), 143.9, 139.5, 139.2, 106.4, 105.83, 105.75, 101.7, 101.3, 101.0 (nine aromatic carbon signals), 70.2, 70.0, 68.2 65.2 (three benzylic O- CH_2 and one decyl O- CH_2), 32.1, 29.8, 29.7, 29.6, 29.5, 26.3, 22.9, 14.3 (decyl CH_3); MALDI-TOF MS (dithranol as the matrix) m/z calcd for $\text{C}_{129}\text{H}_{204}\text{O}_{15}$ 1994.5, found 1992.9 $[\text{M}]^+$.

Synthesis of G2-C10 dendron **183c**

G2-C10 dendron **183c** (490 mg, 0.238 mmol, 98%) was prepared as white needle-like crystals from **183b** (500 mg, 0.251 mmol), CBr_4 (125 mg, 0.376 mmol), and PPh_3 (99.0 mg, 0.380 mmol) following the same bromination procedure as described in the synthesis of **181c**. Mp 118-119 °C; IR (neat): 2922, 2853, 1595, 1453, 1162, 1053 cm^{-1} ; ^1H NMR (500 MHz, CDCl_3): δ 6.70 (m, 4H, Ar-H), 6.65 (m, 2H, Ar-H), 6.60 (m, 1H, Ar-H), 6.58 (m, 8H, Ar-H), 6.43 (m, 6H, Ar-H), 4.99 (s, 4H, benzylic O- CH_2), 4.98 (s, 8H, benzylic O- CH_2), 4.44 (s, 2H, benzylic CH_2Br), 3.96 (t, $J = 6.5$ Hz, 16H, decyl O- CH_2), 1.79 (m, 16H, decyl CH_2), 1.47 (m, 16H, decyl CH_2), 1.42-1.26 (m, 96H, decyl CH_2), 0.91 (t, $J = 6.9$ Hz, 24H, decyl CH_3); ^{13}C NMR (125 MHz, CDCl_3): δ 160.8, 160.5, 160.3 (three Ar CO), 140.0, 139.24, 139.18, 108.5, 106.7, 106.0, 102.4, 101.9, 101.1 (nine aromatic carbon signals), 70.5, 70.4, 68.3 (two benzylic O- CH_2

and one decyl O-CH₂), 33.8 (benzylic CH₂Br), 32.2, 29.9 (2 ×), 29.7, 29.60, 29.55, 26.3, 23.0, 14.4 (CH₃); MALDI-TOF MS (dithranol as the matrix) *m/z* calcd for C₁₂₉H₂₀₃O₁₄ ⁷⁹Br 2058.4, found 2054.9 [M]⁺.

Synthesis of G2-C10 dendron 183d

G2-C10 dendron **183d** (244 mg, 0.121 mmol, 100%) was prepared as pale-yellow liquid from **183c** (250 mg, 1.21 mmol) and NaN₃ (79.0 mg, 1.21 mmol) following the same procedure as described in the synthesis of **181d**. IR (neat): 2922, 2853, 2099, 1595, 1455, 1163, 1053 cm⁻¹; ¹H NMR (500 MHz, CDCl₃): δ 6.71 (m, 4H, ArH), 6.64-6.56 (m, 13H, Ar-H), 6.44 (m, 4H, Ar-H), 5.01 (s, 4H, benzylic O-CH₂), 4.99 (s, 8H, benzylic O-CH₂), 4.29 (s, 2H, benzylic CH₂N₃), 3.97 (t, *J* = 6.5 Hz, 16H, decyl O-CH₂), 1.80 (m, 16H, decyl CH₂), 1.48 (m, 16H, decyl CH₂), 1.42-1.24 (m, 96H, decyl CH₂), 0.93 (t, *J* = 6.9 Hz, 24H, decyl CH₃); ¹³C NMR (125 MHz, CDCl₃): δ 160.8, 160.5, 160.4 (three Ar CO), 139.3, 139.2, 137.9, 107.5, 106.6, 106.0 (six aromatic carbon signals observed), 70.4, 70.3, 68.3 (two benzylic O-CH₂ and one decyl O-CH₂), 55.1 (benzylic CH₂N₃), 32.2, 29.9, 29.8, 29.7, 29.6, 29.5, 26.3, 22.9, 14.4 (CH₃); MALDI-TOF MS (dithranol as the matrix) *m/z* calcd C₁₂₉H₂₀₃O₁₄N₃ 2019.5, found 2017.5 [M]⁺.

Synthesis of G3-C10 dendron 184a

G3-C10 dendron **184a** (910 mg, 22.1 mmol, 66%) was prepared as a waxy solid from methyl 3,5-dihydroxybenzoic acid ester **180** (55.0 mg, 0.329 mmol), **183c** (2.02 g, 0.981 mmol), K₂CO₃ (181 mg, 1.31 mmol), and 18-crown-6 (8.60 mg, 0.033 mmol) following the same etherification procedure as described in **181a**. IR (neat): 2924, 2854, 1723, 1595, 1451, 1163, 1053 cm⁻¹; ¹H NMR (500 MHz, CDCl₃): δ 7.33 (m,

2H, Ar-H), 6.85 (m, 1H, Ar-H), 6.72 (m, 12H, Ar-H), 6.61-6.57 (m, 22H, Ar-H), 6.42 (m, 8H, Ar-H), 5.04 (s, 4H, benzylic O-CH₂), 4.99 (s, 8H, benzylic O-CH₂), 4.97 (s, 16H, benzylic O-CH₂), 3.94 (m, 32H, decyl O-CH₂), 1.77 (m, 32H, decyl CH₂), 1.46 (m, 32H, decyl CH₂), 1.29-1.35 (m, 192H, decyl CH₂), 0.90 (t, $J = 6.7$ Hz, 48H, decyl CH₃); ¹³C NMR (125 MHz, CDCl₃): δ 166.9 (C=O), 160.9, 160.8, 160.5, 160.3 (four Ar CO), 139.6, 139.3, 132.5, 109.0, 107.8, 106.5, 106.0, 102.0 101.7 (nine aromatic carbon signals, three coincidental peaks not observed), 70.4, 70.3, 68.3 (two benzylic and one decyl O-CH₂, two coincidental peaks not observed), 55.1 (ester CH₃), 32.2, 29.9, 29.8, 29.7, 29.6, 29.5, 26.3, 22.9, 14.4 (CH₃); MALDI-TOF MS (dithranol as the matrix) m/z calcd for C₂₆₆H₄₁₂O₃₂ 4122.1, found 4121.1 [M]⁺.

Synthesis of G3-C10 dendron 184b

G3-C10 dendron **184b** (505 mg, 1.23 mmol, 99%) was prepared as a waxy solid from **184a** (511 mg, 1.24 mmol) and LiAlH₄ (23.5 mg, 0.621 mmol) following the same reduction procedure as described in the synthesis of **183b**. IR (neat): 3398 (br, OH), 2922, 2853, 1595, 1452, 1160, 1054 cm⁻¹; ¹H NMR (500 MHz, CDCl₃): δ 6.67 (m, 12H, ArH), 6.62 (m, 1H, Ar-H), 6.59-6.55 (m, 20H, Ar-H), 6.50 (m, 2H, Ar-H), 6.39 (m, 10H, Ar-H), 4.96 (s, 4H, benzylic O-CH₂), 4.94 (s, 8H, benzylic O-CH₂), 4.93 (s, 16H, benzylic O-CH₂), 4.63 (s, 2H, benzylic O-CH₂), 4.59 (s, 1H, OH), 3.93 (t, $J = 6.7$ Hz, 32H, decyl O-CH₂), 1.77 (m, 32H, decyl CH₂), 1.42 (m, 32H, decyl CH₂), 1.40-1.26 (m, 192H, decyl CH₂), 0.87 (t, $J = 6.7$ Hz, 48H, decyl CH₃); ¹³C NMR (125 MHz, CDCl₃): δ 161.0, 160.7, 160.6, 160.5 (four Ar CO), 139.7, 139.5, 139.4 128.9, 128.0, 127.0, 107.0, 106.6, 105.5, 102.0, 101.5, 101.0 (12 aromatic carbon signals), 70.4, 70.3, 70.2, 68.5, 65.8 (four benzylic and one decyl O-CH₂), 32.2, 29.9, 29.8,

29.7, 29.6, 29.5, 26.3, 22.9, 14.4 (CH₃); MALDI-TOF MS (dithranol as the matrix) m/z calcd for C₂₆₅H₄₁₂O₃₁ 4093.1, found 4106.7 [M + H]⁺.

Synthesis of G3-C10 dendron 184c

G3-C10 dendron **184c** (434 mg, 0.104 mmol, 95%) was prepared as a waxy solid from **184b** (450 mg, 0.110 mmol), CBr₄ (54.6 mg, 0.164 mmol), and PPh₃ (43.3 mg, 0.165 mmol) following the same bromination procedure as described in the synthesis of **181c**. IR (neat): 2922, 2853, 1594, 1453, 1161, 1053 cm⁻¹; ¹H NMR (500 MHz, CDCl₃): δ 6.74 (m, 8H, Ar-H), 6.69 (m, 2H, Ar-H), 6.63-6.61 (m, 25H, Ar-H), 6.58 (m, 2H, Ar-H), 6.44 (m, 8H, Ar-H), 5.02 (s, 2H, benzylic CH₂Br), 5.01 (s, 8H, benzylic O-CH₂), 4.99 (s, 16H, benzylic O-CH₂), 4.46 (s, 4H, benzylic O-CH₂), 3.98 (t, $J = 6.7$ Hz, 32H, decyl O-CH₂), 1.86 (m, 32H, decyl CH₂), 1.50 (m, 32H, decyl CH₂), 1.49-1.35 (m, 192H, decyl CH₂), 0.96 (t, $J = 6.7$ Hz, 48H, decyl CH₃); ¹³C NMR (125 MHz, CDCl₃): δ 161.0, 160.8, 160.7, 160.5 (four Ar C-O), 139.7, 139.4, 139.3, 108.7, 107.9, 106.9, 106.6, 106.2, 102.7, 102.3, 101.9, 100.7 (12 aromatic carbon signals), 70.7, 70.5, 68.3, 68.2 (three benzylic and one decyl O-CH₂, one coincidental peak not observed), 34.2 (benzylic CH₂Br), 32.2, 29.9, 29.8, 29.7, 29.6, 29.5, 26.3, 22.9, 14.4 (CH₃); MALDI-TOF MS (dithranol as the matrix) m/z calcd for C₂₆₅H₄₁₁⁷⁹BrO₃₀ 4155.0, found 4012.5 [M - C₁₀H₂₁]⁺.

Synthesis of G3-C10 dendron 184d

G3-C10 dendron **184d** (265 mg, 0.064 mmol, 97%) was prepared as a waxy solid from **184c** (275 mg, 0.066 mmol) and NaN₃ (43.0 mg, 0.660 mmol) following the same procedure as described in the synthesis of **183d**. IR (neat): 2923, 2853, 2099, 1595, 1455, 1162, 1055 cm⁻¹; ¹H NMR (500 MHz, CDCl₃): δ 6.72 (m, 12H, Ar-

H), 6.61-6.59 (m, 22H, Ar-H), 6.46 (m, 3H, Ar-H), 6.45 (m, 8H, Ar-H), 5.01 (s, 4H, benzylic O-CH₂), 4.99 (s, 8H, benzylic O-CH₂), 4.98 (s, 16H, benzylic O-CH₂), 4.29 (s, 2H, benzylic CH₂N₃), 3.97 (t, *J* = 6.7 Hz, 32H, decyl O-CH₂), 1.80 (m, 32H, decyl CH₂), 1.48 (m, 32H, decyl CH₂), 1.47-1.45 (m, 192H, decyl CH₂), 0.93 (t, *J* = 6.7 Hz, 48H, decyl CH₃); ¹³C NMR (125 MHz, CDCl₃): δ 160.9, 160.8, 160.5, 160.4 (four Ar C-O), 139.9, 139.7, 139.4, 139.3, 107.0, 106.9, 106.2, 106.0, 102.4, 102.1, 101.5, 101.3 (12 aromatic carbon signals), 70.4, 70.3, 68.3, 68.2 (three benzylic and one decyl O-CH₂), 55.2 (benzylic CH₂N₃), 32.2, 29.9, 29.8, 29.7, 29.6, 29.5, 26.3, 22.9, 14.4 (CH₃); MALDI-TOF MS (dithranol as the matrix) *m/z* calcd for C₂₆₅H₄₁₁N₃O₃₀ 4118.1, found 4087.3 [M - N₂]⁺.

Synthesis of G1-H dendron 182e

G1-H dendron **182e** (1.98 g, 5.69 mmol, 95%) was prepared as white shiny crystals from methyl 3,5-dihydroxybenzoic acid ester **180** (1.00 g, 6.00 mmol), benzyl bromide (4.07 g, 24.0 mmol), K₂CO₃ (3.40 g, 24.0 mmol), and 18-crown-6 (156 mg, 0.600 mmol) following the same etherification procedure as described in the synthesis of **181a**. Mp 144-145 °C; IR (neat): 3032, 2950, 1719, 1594, 1153, 1054 cm⁻¹; ¹H NMR (500 MHz, CDCl₃): δ 7.43-7.20 (m, 10H, ArH), 7.30 (d, *J* = 2.6 Hz, 2H, Ar-H), 6.80 (t, *J* = 2.6 Hz, 1H, Ar-H), 5.07 (s, 4H, benzylic CH₂), 3.90 (s, 3H, ester CH₃); ¹³C NMR (125 MHz, CDCl₃): δ 166.9 (C=O), 160.0 (Ar C-O), 136.7, 132.3, 128.8, 128.3, 127.8, 108.6, 107.5, 70.5 (benzylic CH₂), 52.5 (ester CH₃); APCI-MS (negative mode) *m/z* calcd for C₂₂H₂₀O₄ 348.1, found 347.0 [M - H]⁻.

Synthesis of G1-H dendron 182f

G1-H dendron **182f** (855 mg, 2.46 mmol, 93%) was prepared as a white solid

from **182e** (1.00 g, 2.87 mmol) and LiAlH₄ (218 mg, 11.5 mmol) following the same reduction procedure as described in the synthesis of **181b**. Mp 81-82 °C; IR (neat): 3321 (br, OH), 3032, 2904, 2870, 1592 cm⁻¹; ¹H NMR (500 MHz, CDCl₃): δ 7.46-7.28 (m, 10H, Ar-H), 6.60 (m, 2H, Ar-H), 6.53 (m, 1H, Ar-H), 5.01 (s, 4H, benzylic CH₂), 4.58 (s, 2H, benzylic CH₂), 1.86 (br s, 1H, OH); ¹³C NMR (125 MHz, CDCl₃): δ 160.5 (Ar C-O), 143.7, 137.1, 128.9, 128.3, 127.8, 106.1, 101.6 (seven aromatic carbon signals), 70.4, 65.6 (two benzylic OCH₂); APCI-MS (positive mode) *m/z* calcd for C₂₁H₂₀O₃ 320.1, found 343.1 [M + Na]⁺.

Synthesis of G1-H dendron **182g**

G1-H dendron **182g** (460 mg, 1.20 mmol, 77%) was prepared as white shiny crystals from **182f** (500 mg, 1.56 mmol), CBr₄ (571 mg, 1.72 mmol), and PPh₃ (451 mg, 1.72 mmol) following the same bromination procedure as described in the synthesis of **181c**, Mp 83-84 °C. IR (neat): 3032, 2927, 2875, 1594 cm⁻¹; ¹H NMR (500 MHz, CDCl₃): δ 7.48-7.50 (m, 10H, Ar-H), 6.87 (d, *J* = 2.6 Hz, 2H, Ar-H), 6.80 (m, 1H, Ar-H), 5.16 (s, 4H, benzylic CH₂), 4.56 (s, 2H, benzylic CH₂); ¹³C NMR (125 MHz, CDCl₃): δ 160.4, 141.1, 136.9, 128.9, 128.4, 127.8, 108.5, 102.5 (eight aromatic carbon signals), 70.5 (benzylic O-CH₂), 33.9 (benzylic CH₂Br); APCI-MS (negative mode) *m/z* calcd for C₂₁H₁₉O₂ ⁷⁹Br (⁸¹Br) 382.1 (384.1), found 381.2 (383.1) [M - H]⁻.

Synthesis of G1-H dendron **182h**

G1-H dendron **182h** (62.7 mg, 0.182 mmol, 100%) was prepared as white solid from **182g** (69.8 mg, 0.182 mmol) and NaN₃ (118 mg, 1.82 mmol) following the same procedure as described in the synthesis of **181d**, Mp 69-70 °C. IR (neat): 3033, 2930,

2097, 1594, 1497, 1150, 1080 cm^{-1} ; ^1H NMR (500 MHz, CDCl_3): δ 7.54-7.40 (m, 10H, Ar-H), 6.70 (m, 1H, Ar-H), 6.66 (m, 2H, Ar-H), 5.12 (s, 4H, benzylic O- CH_2), 4.33 (s, 2H, benzylic CH_2N_3); ^{13}C NMR (125 MHz, CDCl_3): δ 160.5 (Ar C-O), 137.9, 136.9, 128.8, 128.3, 127.9, 107.4, 102.1 (seven aromatic carbons), 70.3 (benzylic CH_2O), 55.0 (benzylic CH_2N_3); APCI-MS (positive mode) m/z calcd for $\text{C}_{21}\text{H}_{19}\text{O}_2\text{N}_3$ 345.1, found 345.3 $[\text{M}]^+$.

Synthesis of G2-H dendron 183e

G2-H dendron **183e** (210 mg, 0.272 mmol, 91%) was prepared as white crystals from methyl 3,5-dihydroxybenzoic acid ester **180** (50.0 mg, 0.300 mmol), **182g** (344 mg, 0.900 mmol), K_2CO_3 (165 mg, 1.20 mmol), and 18-crown-6 (7.80 mg, 0.030 mmol) following the same etherification procedure as described in the synthesis of **181a**. Mp 98-99 $^\circ\text{C}$; IR (neat): 3030, 2874, 1712, 1593 cm^{-1} ; ^1H NMR (500 MHz, CDCl_3): δ 7.51-7.37 (m, 22H, Ar-H), 6.85 (m, 1H, Ar-H), 6.76 (m, 4H, Ar-H), 6.66 (m, 2H, Ar-H), 5.09 (s, 8H, benzyl O- CH_2), 5.06 (s, 4H, benzyl O- CH_2), 3.97 (s, 3H, ester CH_3); ^{13}C NMR (125 MHz, CDCl_3): δ 166.9 ($\text{C}=\text{O}$), 160.4, 159.9 (two Ar C-O), 139.1, 137.0, 132.3, 128.8, 128.2, 127.7, 108.7, 107.4, 106.6, 101.9 (10 aromatic signals), 70.3 (benzylic O- CH_2), 52.5 (ester CH_3); APCI-MS (positive mode) m/z calcd for $\text{C}_{50}\text{H}_{44}\text{O}_8$ 772.3, found 773.4 $[\text{M} + \text{H}]^+$.

Synthesis of G2-H dendron 183f

G2-H dendron **183f** (3.41 mg, 4.58 mmol, 80%) was prepared as colorless liquid from **183g** (4.42 g, 5.72 mmol) and LiAlH_4 (869 mg, 22.9 mmol) following the same reduction procedure as described in the synthesis of **181b**. IR (neat): 3404 (br, OH), 3032, 2873, 1593, 1497, 1147 cm^{-1} ; ^1H NMR (500 MHz, CDCl_3): δ 7.43-7.27 (m, 20H,

Ar-H), 6.66 (d, $J = 2.6$ Hz, 4H, Ar-H), 6.61 (m, 2H, Ar-H), 6.57 (m, 2H, Ar-H), 6.51 (m, 1H, Ar-H), 5.03 (s, 8H, benzylic O-CH₂), 4.96 (s, 4H, benzylic O-CH₂), 4.39 (s, 2H, benzylic O-CH₂) (OH signal was not observed due to rapid proton exchange); ¹³C NMR (125 MHz, CDCl₃): δ 160.5, 160.4 (two Ar C-O), 139.6, 137.1, 128.9, 128.3, 127.8, 106.7, 106.1, 101.9, 101.7 (nine aromatic carbon signals, one coincidental peak not observed), 70.4, 70.3, 65.6 (three benzylic O-CH₂); APCI-MS (positive mode) m/z calcd for C₄₉H₄₄O₇ 744.3, found 745.4 as [M + H]⁺.

Synthesis of G2-H dendron 183g

G2-H dendron **183g** (380 mg, 0.471 mmol, 67%) was prepared as white needle-like crystals from **183f** (523 mg, 0.703 mmol), CBr₄ (350 mg, 1.05 mmol), and PPh₃ (276 mg, 1.05 mmol) following the same bromination procedure as described in the synthesis of **181c**. Mp 125-126 °C; IR (neat): 3030, 2879, 1559 cm⁻¹; ¹H NMR (500 MHz, CDCl₃) δ 7.43-7.28 (m, 20H, Ar-H), 6.66 (m, 4H, Ar-H), 6.61 (d, $J = 2.6$ Hz, 2H, Ar-H), 6.57 (m, 2H, ArH), 6.51 (m, 1H, Ar-H), 5.03 (s, 8H, benzylic O-CH₂), 4.96 (s, 4H, benzylic O-CH₂), 4.40 (s, 2H, benzylic CH₂Br); ¹³C NMR (125 MHz, CDCl₃): δ 160.5, 160.3 (two Ar CO), 140.1, 137.1, 128.9, 128.3, 127.8, 108.5, 106.7, 102.5, 102.0 (nine aromatic carbon signals, one coincidental signal not observed), 70.5, 70.4 (two benzylic O-CH₂), 33.9 (benzylic CH₂Br); APCI-MS (positive mode) m/z calcd for C₄₉H₄₃O₆ ⁷⁹Br (⁸¹Br) 806.2 (808.2), found 807.3 (809.3) [M + H]⁺.

Synthesis of G2-H dendron 183h

G2-H dendron **183h** (142 mg, 0.185 mmol, 100%) was prepared as a white solid from **183g** (150 mg, 0.186 mmol) and NaN₃ (121 mg, 1.86 mmol) following the same procedure as described in the synthesis of **181d**. Mp 109-110 °C; IR (neat): 3032,

2922, 2095, 1593, 1051 cm^{-1} ; ^1H NMR (500 MHz, CDCl_3): δ 7.45-7.28 (m, 20H, Ar-H), 6.67 (m, 4H, Ar-H), 6.57 (m, 2H, Ar-H), 6.55 (m, 1H, ArH), 6.54 (m, 2H, Ar-H), 5.03 (s, 8H, benzylic O- CH_2), 4.97 (s, 4H, benzylic O- CH_2), 4.25 (s, 2H, benzylic CH_2N_3); ^{13}C NMR (125 MHz, CDCl_3): δ 160.8, 160.7 (two Ar C-O), 139.7, 138.3, 137.3, 129.1, 128.6, 128.1, 107.8, 107.0, 102.4, 102.2 (10 aromatic carbon signals), 70.7, 70.6 (two benzylic O- CH_2), 55.3 (benzylic CH_2N_3); APCI-MS (positive mode) m/z calcd for $\text{C}_{49}\text{H}_{43}\text{O}_6\text{N}_3$ 769.3, found 770.4 $[\text{M} + \text{H}]^+$ and 787.4 $[\text{M} + \text{H}_3\text{O}]^+$.

Synthesis of 4-(trimethylsilylethynyl)benzaldehyde (186)

An oven-dried round-bottom flask was purged with N_2 and to it were added 4-bromobenzaldehyde **185** (530 mg, 2.86 mmol), $\text{Pd}(\text{PPh}_3)_2\text{Cl}_2$ (100 mg, 14.3 mmol), CuI (54.5 mg, 28.6 mmol), and DBU (521 mg, 3.40 mmol) in dry benzene (10 mL) under the protection of N_2 . TMSA (563 mg, 5.70 mmol) in benzene (3 mL) was added dropwise for 0.5 h, and the reaction mixture was kept under reflux for another 0.5 h. After cooling down to room temperature, the mixture was filtered through a Celite^R plug. The resulting organic solution was concentrated in vacuo to give the crude product, which was purified by silica flash chromatography using hexanes/ethyl acetate (25:1) to afford compound **186** (509 mg, 2.51 mmol, 86%) as a pale yellow solid. IR (neat): 2957, 2737, 2156, 1699, 1600, 1563 cm^{-1} ; ^1H NMR (500 MHz, CDCl_3): δ 10.01 (s, 1H, CHO), 7.82 (d, $J = 8.8$ Hz, 2H, Ar-H), 7.61 (d, $J = 8.8$ Hz, 2H, Ar-H), 0.28 (s, 9H, $(\text{Si}(\text{CH}_3)_3)$); ^{13}C NMR (125 MHz, CDCl_3): δ 191.6 ($\text{C}=\text{O}$), 135.9, 132.7, 129.6, 104.1, 99.2, 0.1 ($\text{Si}(\text{CH}_3)_3$); GC-MS m/z (%) calcd for $\text{C}_{12}\text{H}_{14}\text{OSi}$ 202.1, found 201.8 (16, $[\text{M}]^+$), 187 (100, $[\text{M} - \text{CH}_3]^+$).

Synthesis of C_{60} adduct **187**

To an oven-dried round-bottom flask purged with N₂ were charged C₆₀ (712 mg, 9.89 × 10⁻⁴ mol), benzaldehyde **186** (100 mg, 0.500 mmol), and sarcosine (446 mg, 5.00 mmol) in dry toluene (70 mL). The mixture was refluxed for 24 h. Afterwards, the solvent was evaporated off under reduced pressure, and the residue was purified by silica chromatography using hexanes/toluene (4:1) to afford compound **187** (108 mg, 0.114 mmol, 23%) as a dark brown solid. Mp >300 °C; IR (neat): 2947, 2840, 2782, 2159 cm⁻¹; ¹H NMR (500 MHz, CDCl₃): δ 7.78 (br s, 2H, ArH), 7.52 (d, *J* = 8.3 Hz, 2H, ArH), 5.00 (d, *J* = 9.6 Hz, 1H), 4.95 (s, 1H), 4.29 (d, *J* = 9.0 Hz, 1H), 2.82 (s, 3H, NCH₃), 0.25 (s, 9H, Si(CH₃)₃); ¹³C NMR (125 MHz, CDCl₃): δ 156.0, 153.8, 153.1, 152.8, 147.33, 147.31, 146.6, 146.40, 146.36, 146.30, 146.26, 146.22, 146.18, 146.14, 145.99, 145.97, 145.77, 145.64, 145.62, 145.51, 145.43, 145.39, 145.35, 145.31, 145.28, 145.27, 145.21, 144.37, 144.68, 144.43, 144.41, 143.20, 143.06, 142.74, 142.67, 142.63, 142.61, 142.31, 142.27, 142.18, 142.14, 142.08, 142.06, 141.91, 141.7, 141.6, 140.28, 140.25, 140.01, 139.64, 137.4, 136.9, 136.6, 135.9, 135.8 (totally 55 carbon signals observed for the 58 chemically nonequivalent sp² fullerene carbons), 132.4, 132.3, 123.6 (three signals observed for the four aryl carbons), 105.1, 95.3 (two alkylnl carbons), 89.3 (CH), 69.0 (CH₂), 40.0 (NCH₃), 0.2 (Si(CH₃)₃); MALDI-TOF MS (dithranol as the matrix) *m/z* calcd for C₇₄H₁₉NSi 949.1287, found 950.7477 [M + H]⁺.

General synthetic procedure for triazole-linked dendro[60]fullerenes **175-179** via the CuAAC reaction

To a solution of compound **187** (1 equiv) in THF was added TBAF (1 equiv, 1 M in THF), and the mixture was stirred at room temperature for 5 min. To this mixture

were added CuI (0.3 equiv) and azido-dendron (1 equiv). The reaction mixture was kept under stirring at room temperature overnight. The solvent (THF) was then removed in vacuo, and the residue was diluted in CHCl₃, washed with saturated NH₄Cl solution, and dried over anhydrous MgSO₄. Suction filtration followed by flash chromatography using hexanes/CHCl₃ (1:1) and then hexanes/CHCl₃/ethyl acetate (10:2:1) afforded the corresponding dendro[60]fullerene product.

Synthesis of dendro[60]fullerene **175**, C₆₀-G1-C10

Dendro[60]fullerene **175** (115 mg, 0.062 mmol, 72%) was prepared according to the general CuAAC reaction procedure, using compound **187** (80.0 mg, 0.084 mmol), TBAF (0.08 mL, 1 M in THF), CuI (1.6 mg, 0.008 mmol), and azido-dendron **182d** (81.6 mg, 0.084 mmol). The isolated product was dark brown waxy solid. IR (neat): 3032, 2929, 1594 cm⁻¹; ¹H NMR (500 MHz, CDCl₃): δ 7.86 (m, 4H), 7.63 (s, 1H, triazole H), 6.57 (m, 1H), 6.50 (m, 6H), 6.36 (m, 2H), 5.45 (s, 2H), 4.99 (d, *J* = 6.9 Hz, 1H), 4.95 (s, 1H), 4.89 (s, 4H), 4.27 (d, *J* = 6.9 Hz, 1H), 3.95 (t, *J* = 6.5 Hz, 8H), 2.82 (s, 3H), 1.74 (m, 8H), 1.42 (m, 8H), 1.37-1.25 (m, 48H), 0.88 (t, *J* = 6.9 Hz, 12H). Meaningful ¹³C NMR spectrum could not be acquired due to low concentration. MALDI-TOF MS (dithranol as the matrix) *m/z* calcd for C₁₃₂H₁₁₂N₄O₆ 1849.9, found 1848.8 [M]⁺.

Synthesis of dendro[60]fullerene **178**, C₆₀-G1-H

Dendro[60]fullerene **178** (34.2 mg, 0.028 mmol, 38%) was prepared according to the general click reaction procedure, using compound **187** (70.0 mg, 0.074 mmol), TBAF (0.07 mL, 1 M in THF), CuI (1.40 mg, 0.007 mmol), and azido-dendron **182h** (25.5 mg, 0.074 mmol). The isolated product was dark-brown solid. IR(neat): 2921,

2852, 2782, 1595, 1451 cm^{-1} ; ^1H NMR (500 MHz, CDCl_3): δ 7.90 (m, 4H), 7.64 (s, 1H, triazole H), 7.44-7.27 (m, 10H), 6.61 (m, 1H), 6.53 (m, 2H), 5.49 (s, 2H), 5.03 (d, $J = 9.6$ Hz, 1H), 5.02 (s, 4H), 5.00 (s, 1H), 4.31 (d, $J = 9.6$ Hz, 1H), 2.86 (s, 3H, NCH_3); ^{13}C NMR (125 MHz, CDCl_3): δ 160.7 (Ar C-O), 156.5, 154.3, 153.6, 153.5, 148.2, 147.6, 147.0, 146.7, 146.6, 146.53, 146.50, 146.43, 146.41, 146.37, 146.20, 145.81, 145.80, 145.7, 145.60, 145.55, 145.49, 145.43, 145.0, 144.9, 144.67, 144.66, 143.4, 143.3, 143.0, 142.84, 142.78, 142.6, 142.5, 142.44, 142.40, 142.39, 142.33, 142.31, 142.27, 142.2, 142.1, 142.0, 141.8, 140.5, 140.4, 140.2, 137.3, 137.1, 136.9, 136.8, 136.6, 136.2, 136.0 (totally 53 signals were observed out of 58 sp^2 carbons on the C_{60} cage and two phenyl carbons in this region), 131.0, 128.9, 128.4, 127.8, 120.0, 114.2, 107.5, 102.5 (eight aromatic carbon signals were observed out of 12 aromatic carbons), 83.6 (NCHPh on the pyrrolidine ring), 70.4, 70.3 (two O-CH_2 , 69.4 (NCH_2 on the pyrrolidine ring), 54.6 (CH_2N), 40.3 (NCH_3); MALDI-TOF MS (dithranol as the matrix) m/z calcd for $\text{C}_{92}\text{H}_{300}\text{O}_2\text{N}_4$ 1222.2, found 1223.3 $[\text{M} + \text{H}]^+$.

Synthesis of dendro[60]fullerene **176**, C_{60} -G2-C10

Dendro[60]fullerene **176** (126 mg, 0.043 mmol, 69%) was prepared according to the general click reaction procedure, using compound **187** (60.0 mg, 0.063 mmol), TBAF (0.060 mL, 1 M in THF), CuI (1.20 mg, 0.006 mmol), and azido-dendron **183d** (127 mg, 0.063 mmol). The isolated product was dark-brown waxy solid. IR (neat): 2924, 2854, 1597, 1464 cm^{-1} ; ^1H NMR (500 MHz, CDCl_3): δ 7.87 (m, 4H), 7.62 (s, 1H, triazole H), 6.64 (m, 4H), 6.55-6.51 (m, 13H), 6.41 (m, 4H), 5.45 (s, 2H), 5.30 (s, 1H), 4.93 (m, 13H), 4.26 (d, $J = 9.6$ Hz, 1H), 3.94 (t, $J = 6.4$ Hz, 16H), 2.81 (s, 3H), 1.78 (m, 16H), 1.46 (m, 16H), 1.42-1.25 (m, 96H), 0.91 (t, $J = 6.3$ Hz, 24H);

Meaningful ^{13}C NMR spectrum could not be acquired due to low concentration and significant line broadening. MALDI-TOF MS (dithranol as the matrix) m/z calcd for $\text{C}_{200}\text{H}_{214}\text{O}_{14}\text{N}_4$ 2897.6, found 2894.5 $[\text{M}]^+$.

Synthesis of dendro[60]fullerene 179, C_{60} -G2-H

Dendro[60]fullerene **179** (63.0 mg, 0.038 mmol, 70%) was prepared according to the general click reaction procedure, using compound **187** (52.0 mg, 0.055 mmol), TBAF (0.06 mL, 0.006 mmol, 1M in THF), CuI (1.00 mg, 0.005 mmol), and azido-dendron **183h** (42.0 mg, 0.055 mmol). The isolated product was a dark brown waxy solid. IR (neat): 3033, 2930, 1594 cm^{-1} ; ^1H NMR (500 MHz, CDCl_3): δ 7.84 (m, 4H), 7.61 (s, 1H, triazole H), 7.44-7.28 (m, 20H), 6.62 (m, 4H), 6.53 (m, 3H), 6.49 (s, 2H), 5.44 (s, 2H), 5.00 (s, 8H), 4.99 (d, $J = 9.6$ Hz, 1H), 4.94 (s, 1H), 4.92 (s, 4H), 4.27 (d, $J = 9.6$ Hz, 1H), 2.81 (s, 3H); Meaningful ^{13}C NMR spectrum could not be acquired due to low concentration. MALDI-TOF MS (dithranol as the matrix) m/z calcd for $\text{C}_{120}\text{H}_{54}\text{N}_4\text{O}_6$ 1647.4, found 1646.9 $[\text{M}]^+$.

Synthesis of dendro[60]fullerene 177, C_{60} -G3-C10

Dendro[60]fullerene **177** (147 mg, 0.029 mmol, 80%) was prepared according to the general click reaction procedure, using compound **187** (35.0 mg, 0.037 mmol), TBAF (0.04 mL, 0.004 mmol, 1 M in THF), CuI (1.00 mg, 0.005 mmol), and azido-dendron **184d** (120 mg, 0.029 mmol). The isolated product was dark-brown waxy solid. IR (neat): 3417, 2925, 2854, 1619, 1550, 1466 cm^{-1} ; ^1H NMR (500 MHz, CDCl_3): δ 7.83 (m, 4H), 7.5 (s, 1H, triazole H), 6.67 (m, 8H), 6.66 (m, 4H), 6.62 (m, 20H), 6.55-6.41 (m, 5H), 6.41 (m, 8H), 5.45 (s, 2H), 5.30 (s, 1H), 4.95 (s, 16H), 4.93 (m, 9H), 4.89 (m, 4H), 4.26 (d, $J = 9.6$ Hz, 1H), 3.94 (t, $J = 6.5$ Hz, 32H), 2.78 (s,

3H), 1.79 (m, 32H), 1.45 (m, 32H), 1.42-1.25 (m, 192H), 0.91 (t, $J = 6.4$ Hz, 48H);
Meaningful ^{13}C NMR spectrum could not be acquired due to low concentration and
significant line broadening. MALDI-TOF MS (dithranol as the matrix) m/z calcd for
 $\text{C}_{336}\text{H}_{422}\text{N}_4\text{O}_{30}$ 4996.2, found 4993.3 $[\text{M}]^+$.

Chapter 3

Dendrimer Functionalized π -Conjugated Macromolecules

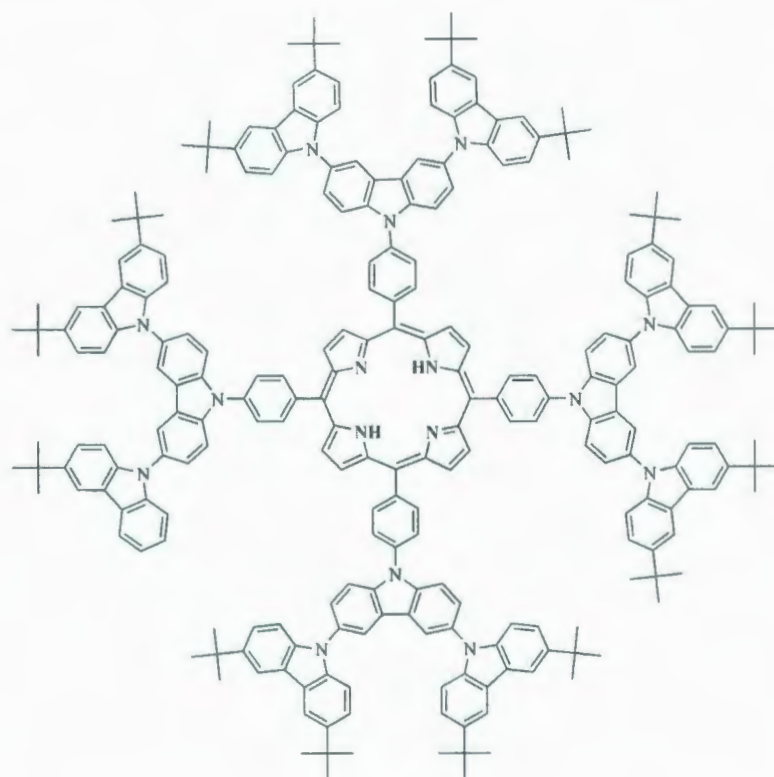
3.1 Introduction

As reviewed in Chapter 2, dendrimers are nanometer-size macromolecules having well-defined tree-like structures¹⁰⁹ and, as a result, they are used as novel building blocks to be attached to various π -conjugated systems to form functional macromolecules with interesting properties, such as special redox and electroluminescent properties.^{110,111} For the last two decades, material chemists have invested substantial effort into the study of dendrimer-functionalized macromolecules. For example, dendrimers attached with porphyrins and tetrathiafulvalenes (TTFs) have been explored to mimic the redox properties of natural heme species, as well as to understand long-distance electron transfer reactions.^{109,112} Another interesting aspect is that some unique properties may arise from dendritic groups, owing to their highly rigid and branched

structures. In the presence of higher generation dendrimers, it is only the surface groups of dendrimers that are in contact with the environment, and therefore they are a crucial factor to be considered in molecular design and tailoring for dendrimer-based materials.^{109,110}

Linear π -conjugated oligomers and polymers were previously investigated for making molecular devices, such as organic solar cells,¹¹³ and thin-film transistors.¹¹⁴ However, the effectiveness of using them directly was not very satisfactory.¹¹⁵ Considering the structural properties of dendrimers, such as their 3-D shape, rigidity, monodispersity, their attachment to these oligomers and polymers could improve the performance of the resulting molecular materials. In this respect, some suitably substituted, rigid π -conjugated dendrimers (porphyrin/oligomer-cored dendrimers) have already been reported to attain enhanced electrical, photophysical and morphological properties,^{4,115,116} which are indeed beneficial for practical uses.

In this category, a variety of dendrimer-appended porphyrins have been synthesized mainly to investigate and clarify the redox properties of heme, and on the basis of which efficient artificial light-harvesting compounds with behavior similar to natural photosynthetic systems can be developed.¹¹⁰ For instance, in 2005, S. Campagna and co-workers demonstrated the synthesis of compound **188**, which has a porphyrin core at the center and carbazole-based dendron as branches (see Figure 3.1). Compound **188** displayed very rich oxidation behavior, whereas the reversible processes were dominated by the carbazole unit.¹¹⁰ Of particular interest here is that the emission spectrum of **188** showed features typical of porphyrin and was independent of excitation wavelength. This behavior suggests that the porphyrin sub-unit acted as an "energy-trap", while the peripheral carbazole sub-unit ("antenna") transferred



188

Figure 3.1: A porphyrin-cored carbazole dendrimer

collected light energy quantitatively to the core. The photophysical behavior of **188** is similar to that of the reaction center of photosynthetic antennae in purple bacteria.¹¹⁷ Obviously, the dendritic structures contribute to improved light-harvesting efficiency. Moreover, compound **188** showed electroluminescence properties in solution at room temperature, which was attributed to the twisted intramolecular charge-transfer excited states of the porphyrin-cored carbazole units.¹¹⁰

Aside from porphyrin, tetrathiafulvalenes (TTFs) constitute another important class of π -conjugated systems which show strong electron donating properties. The simple TTF molecule as shown in Scheme 3.2 is capable of forming electrically

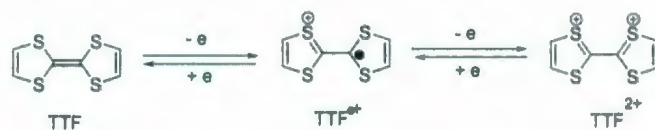


Figure 3.2: Two electron-donor TTF-system building blocks.

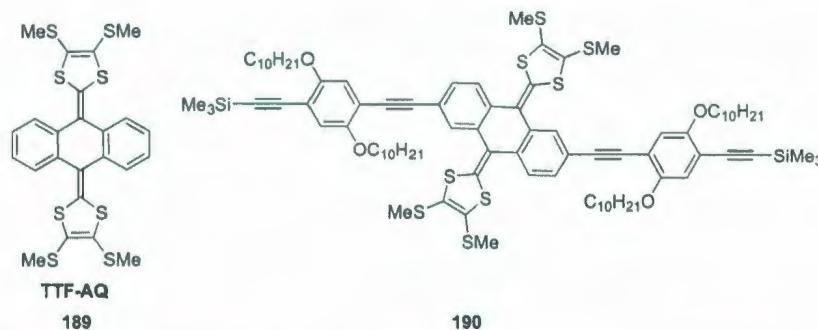
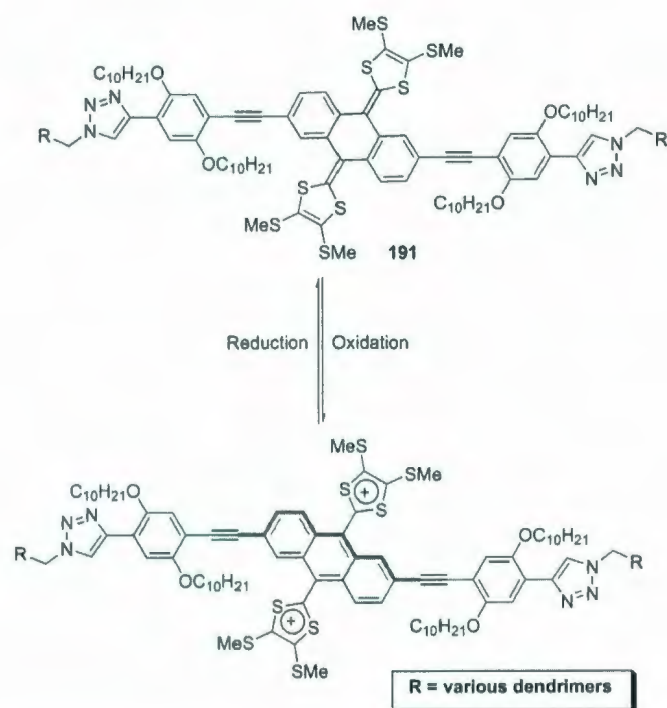


Figure 3.3: TTFAQ 189 and phenylacetylene-expanded TTFAQ 190.

conductive charge-transfer complexes, well-known as organic metals, because it can successively release two electrons upon oxidation to form a stable TTF radical cation and dication.¹¹⁸ Since its discovery in 1970, there have been a large number of research activities invested on expanding the family of TTF derivatives. Currently, the design of TTF-based materials is mainly focused on improving solid-state contact, producing better electron-donating and charge transfer properties, and increasing structural dimensionality. A popular approach toward this goal is to use various spacers (ester, vinylene, ether, and linear π -systems) to extend the conjugation path or to anchor TTF groups to π -conjugated molecules.¹¹⁸ Among various π -extended TTFs, the 9,10-bis(1,3-dithiol-2-ylidene)-9,10-dihydroanthraquinone derivatives (TTFAQs) show the most significant outcome in tuning electron donating abilities. TTFAQs (see Figure 3.3) possess a highly distorted non-aromatic ground-state structure. After sequential releasing of two electrons (see Scheme 3.1), it can form a very stable



Scheme 3.1: Proposed molecular switch behavior for dendrimer-functionalized phenylacetylene-TTFAQ **191**.

dication by gaining aromaticity at the central anthracene and the two dithiolium rings. It is therefore envisioned that the TTFAQ unit offers an active redox core for development of electronic materials. For example, a redox-switchable molecular wire **191** (see Scheme 3.1) was proposed and pursued in our recent study. In this system, the incorporation of dendrimers to TTFAQ should lead to new redox properties useful for optoelectronic applications. In view of the presence of terminal alkyne in **190**, the attachments of dendrimers to **190** was planned to be executed via a click reaction as demonstrated in Chapter 2. Again, to better understand the effects of attaching dendrimers to π -conjugated systems, a group of linear and star-shaped phenylacetylene oligomers have also been synthesized and investigated.

3.2 Objectives of the Project

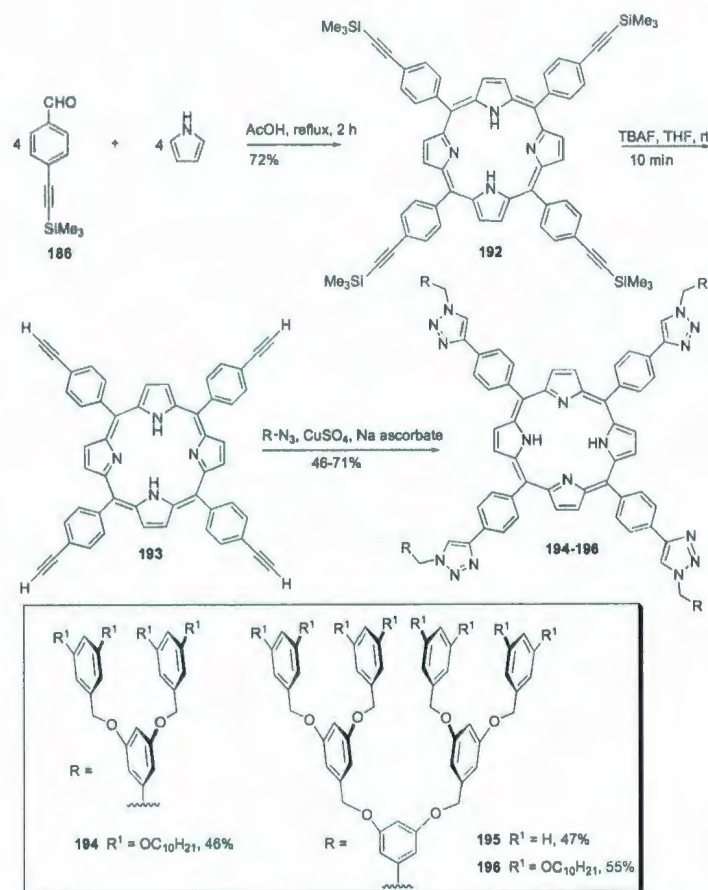
The main objective of this project is to develop efficient modular synthetic methods to prepare a series of dendrimer-attached extended π -conjugated systems. Click chemistry was planned to be used as a key tool for attachment of dendrimer to complex conjugated molecules, including porphyrin, linear phenylene ethynylene oligomers (OPEs), and TTFAQs. In addition, relevant study of the properties was also planned to be performed by electrochemistry, UV-Vis, and fluorescence spectroscopy. In a long-term view, the study is anticipated to establish structure-property relationships and assist the design of advanced organic electro-/chromophores in the field of molecular-based optoelectronics; for example, organic solar cells and molecular switches are particularly targeted by our group at the present stage.

3.3 Results and Discussions

3.3.1 Synthesis of Dendrimer-Functionalized *meso*-Porphyrins

Silyl protected tetraphenyl *meso*-porphyrin **192** was synthesized through a one-pot reaction (Alder-Longo condensation) between four molecules of TMSA-benzaldehyde **186**, and four molecules of pyrrole, with a yield of 72% (see Scheme 3.2). In the next step, the *meso*-porphyrin was deprotected by TBAF in dry THF. The deprotected terminal alkyne was subjected to CuAAC reactions with a series of azido-dendrimers under the catalysis of CuSO₄ and sodium ascorbate in DMF/THF/Et₃N to yield dendrimer functionalized *meso*-porphyrins **194-196**. The yields of the click reactions were 46-55%, which is satisfactory considering the instability of deprotected free-base

porphyrin **193**.

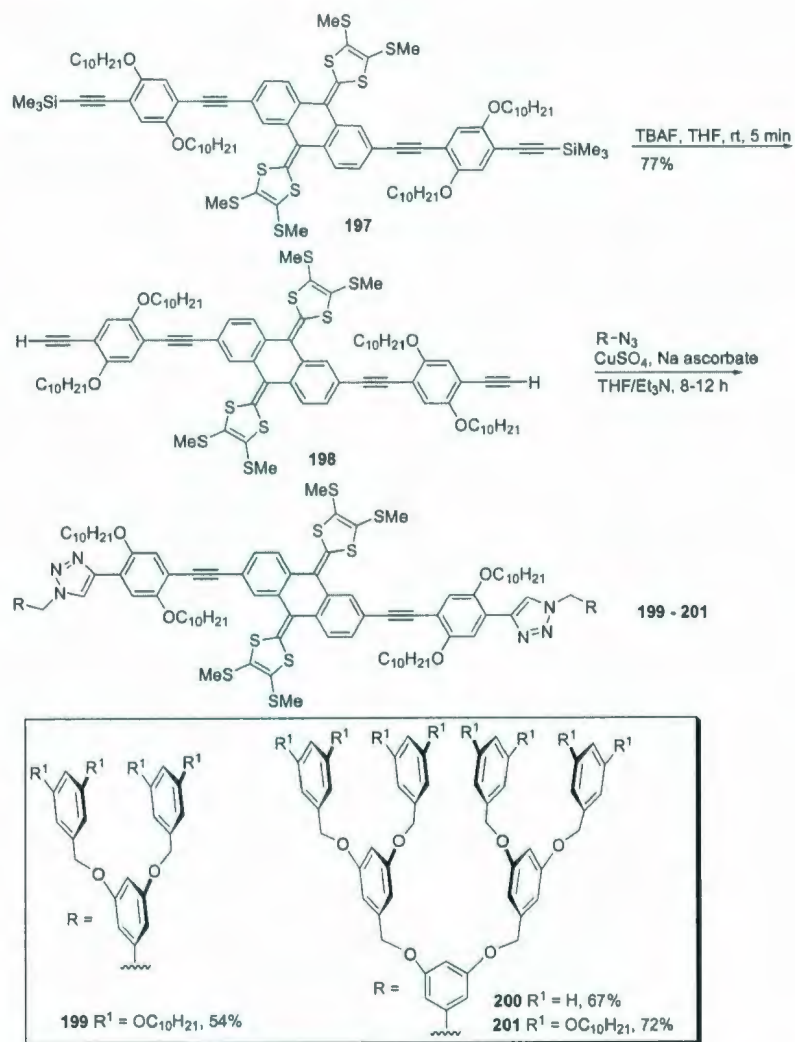


Scheme 3.2: Synthesis of alkyne pendant porphyrin **193** and dendroporphyrins **194-196** via a click reaction.

3.3.2 Synthesis of Dendrimer-Functionalized TTFAQs

As shown in Scheme 3.3, TTFAQ **197** was prepared using the method previously reported by our group.¹¹⁸ Removal of the TMS groups in **197** with TBAF in dry THF afforded compound **198** in 77% yield. The deprotected TTFAQ **198** was then

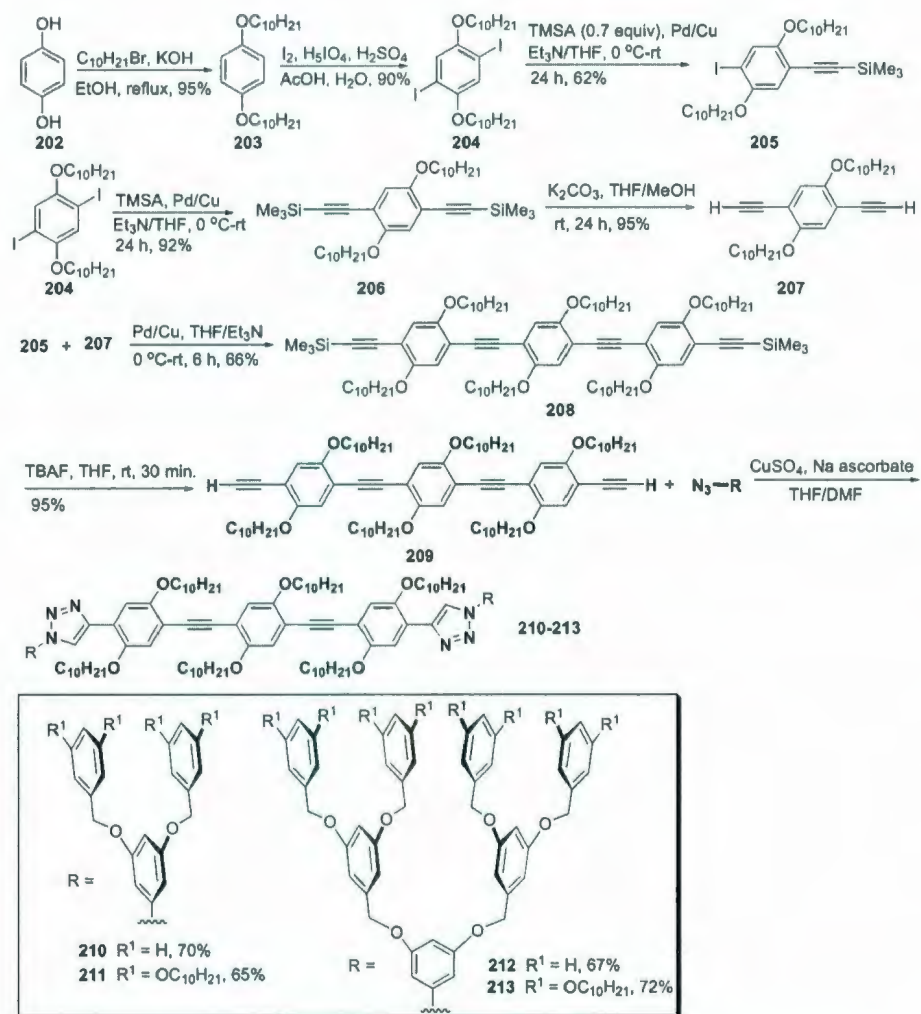
subjected to CuAAC reaction with azido-dendrimers in a similar manner to the syntheses of dendroporphyrins **194-196**, affording dendrimer functionalized TTFAs **199-201** in satisfactory yields.



Scheme 3.3: Attachment of dendrimers to extended-TTFAQ via CuAAC reactions.

3.3.3 Synthesis of Dendrimer-Functionalized Linear OPEs

Dendrimer functionalized linear phenylene ethylene oligomers **210-213** were synthesized starting from dihydroquinone **202** (see Scheme 3.4), which was subjected to a Williamson etherification reaction with decyl bromide to give compound **203** in 90% yield. An acid catalyzed iodination reaction produced diiodo compound **204**. After a selective Sonogashira coupling between compound **204** and TMSA, a monoalkynylated arene **205** was obtained in 62% yield. Double Sonogashira coupling between compound **204** and more than *two* equivalents of TMSA yielded compound **206** in 92% yield. The silyl groups of **206** were removed with K_2CO_3 to give compound **207** in 95% yield. Compound **207** was subjected to another Pd-catalyzed Sonogashira coupling reaction with 2 molar equivalents of **205** to give linear OPE **208** in 85% yield. Compound **208** was deprotected using K_2CO_3 to form compound **209** in 95% yield. Cu(I)-catalyzed cycloaddition reaction between azide-pendant dendrimers of different generations and the terminal alkynylated linear OPE **209** eventually produced a series of dendrimer-functionalized OPEs **210-213** in satisfactory yields, ranging from 65 to 72%.



Scheme 3.4: Synthesis of dendrimer functionalized OPEs 210-213.

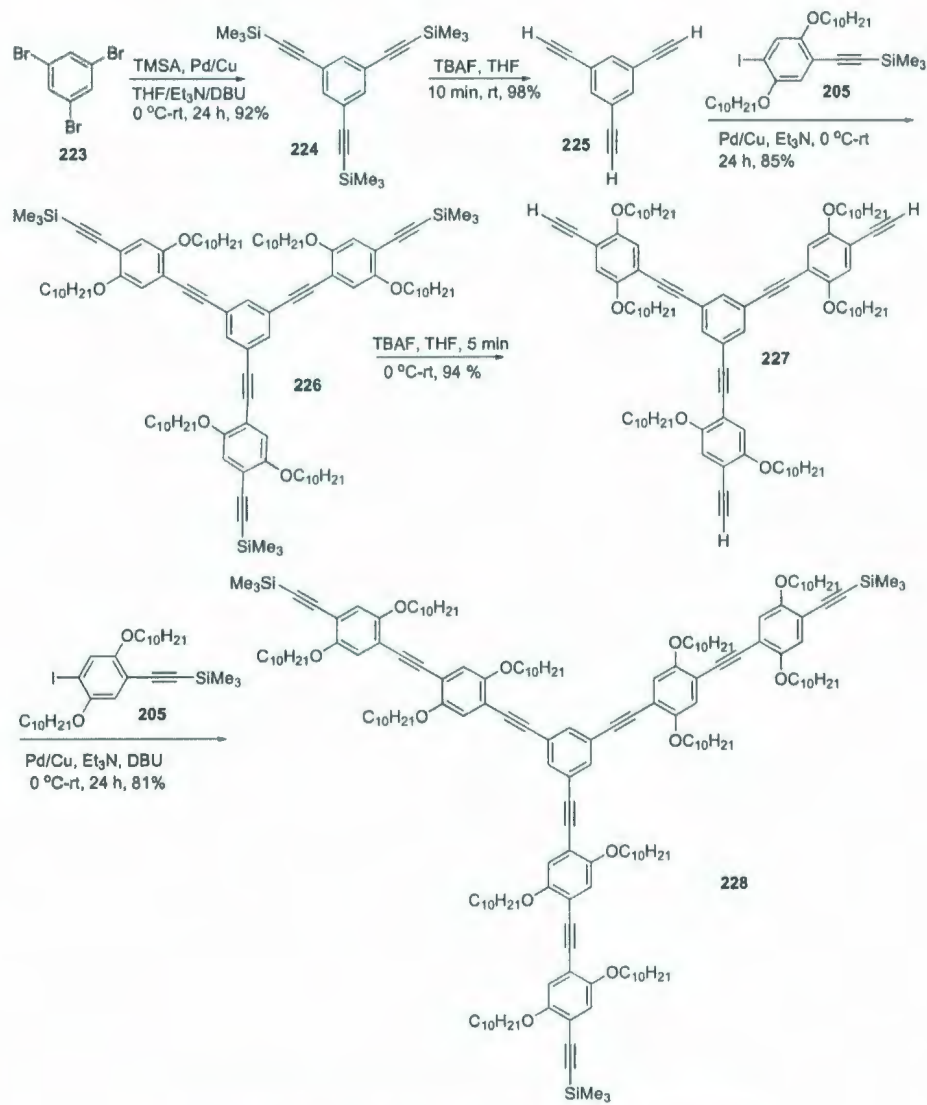
free hydroxyl groups to which biologically active molecules (carbohydrate, peptides, etc.) could be attached by Williamson etherification reactions for the study of novel dendrimer-oligomer bio-conjugates.

3.3.4 Attempted Synthesis of Dendrimer-Functionalized Star-Shaped OPEs

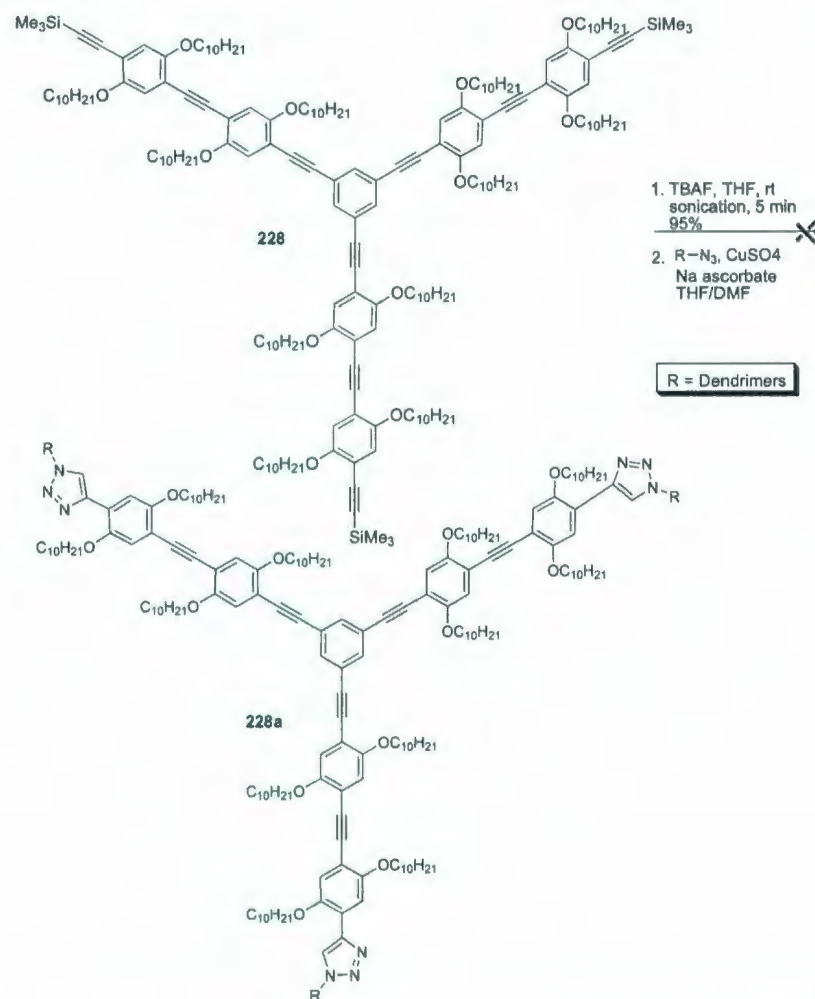
Aside from linear-shaped OPEs, a star-shaped OPE framework was also targeted. Commercially available 1,3,5-tribromobenzene (**223**) was used as the starting material shown in Scheme 3.6. The synthesis involved multiple steps of transition-metal-catalyzed cross-coupling reactions. The purification of the OPE intermediates was done by using standard flash chromatographic techniques, and the yields were satisfactory.

In the synthesis, a Pd-catalyzed Sonogashira reaction between compound **223** and TMSA first afforded compound **224** in 92% yield. Deprotection of the TMS groups of **224** with K_2CO_3 produced compound **225**, which was subjected to a Pd-catalyzed Sonogashira reaction with compound **205** to produce star-shaped OPE **226** in 85% yield. Removal of the TMS groups of compound **226** with TBAF in THF at low temperature afforded OPE **227** in 94% yield. Compound **227** was then subjected to another Sonogashira reaction to produce oligomer **228** in 81% yield. The terminal silyl groups in **228** were deprotected using TBAF at low temperature to produce the precursor for a click reaction (Scheme 3.7). The previously synthesized azide-pendant Fréchet-type dendrimers were used to construct dendrimer-functionalized star-shaped OPE oligomer **228a** through the CuAAC reaction. Unfortunately, the

click reaction did not lead to the formation of dendrimer-functionalized star-shaped OPEs (see Scheme 3.7). A likely reason is due to incomplete reaction (either one or two dendrons were attached by click reaction instead of three) or alkyne homo-coupling side reactions. Modification of the reaction conditions is necessary.



Scheme 3.6: Synthesis of star-shaped OPE **228**.



Scheme 3.7: Attempted synthesis of dendrimer-functionalized star-shaped OPE **228a**.

3.3.5 Characterizations of Dendrimer-Functionalized *meso*-Porphyrins

The dendrimer functionalized porphyrins **194-196** were characterized by UV-Vis, fluorescence, and cyclic voltammetric analyses in order to understand their electronic and electrochemical properties.

The UV-Vis absorption spectra for dendrimer-functionalized free base porphyrins are shown in Figure 3.4, and detailed steady-state photophysical data are given in Table 3.1. The porphyrin molecules display two characteristic absorption bands in the UV-Visible spectra, namely B (Soret) and Q bands, which are assigned to $\pi \rightarrow \pi^*$ transitions of the porphyrin rings.¹¹⁹ The absorption spectrum for free base porphyrin with four terminal alkyne groups **193** is characterized by the strongly-absorbing Soret (B) band at 425 nm (usually 429 nm in unsubstituted free base porphyrins, that originates from $S_0 \rightarrow S_2$ absorption, and two weaker Q bands at 545 nm (usually at 558 nm $S_0 \rightarrow S_1(1)$ absorption) and 571 nm (usually at 598 nm $S_0 \rightarrow S_1(0)$ absorption).^{119,120} It is clear that the absorption bands were blue-shifted in the UV-Vis spectrum of **193**. The blue-shift is more pronounced in porphyrins functionalized with dendrimers, **194-196**. In **194**, **195**, and **196**, the Soret band appeared at 418, 422, and 413 nm respectively, whereas the Q band appeared as a single band at 534, 530, and 529 nm respectively.

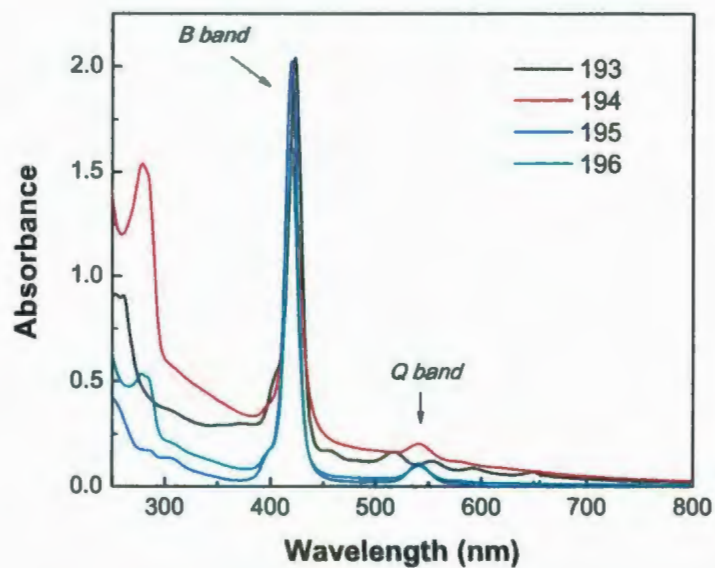


Figure 3.4: Absorption spectra of free base porphyrins **193**, **194**, **195**, and **196**.

entry	Abs. λ_{max} (nm)	Em. λ_{max} (nm)
free base porphyrin	429 (Soret); 558, 598 (Q-band)	602, 655
193	425 (Soret); 545, 571 (Q-band)	660, 720
194	414 (Soret); 528 (Q-band)	–
195	418 (Soret); 534 (Q-band)	564, 568
196	413 (Soret); 529 (Q-band)	584, 592

Table 3.1: Photophysical data for free base porphyrin **193**, **194**, and **196**

The blue shifts in dendrimer functionalized porphyrins could be explained by the electron-withdrawing effects of the four triazole functionalities. From the previous reports of dendritic porphyrins, it seems that 1,2,3-triazole impedes the electronic interaction between dendrimers and porphyrins.^{120,121} For higher generation dendrimer-functionalized free base porphyrins, this shift is more pronounced. This could be explained by the steric effect, that is higher generation dendrimers would reasonably pose higher dendritic encapsulation, which makes a firm insulating layer around the centrally localized porphyrin core.

The electrochemical properties of dendrimer functionalized *meso*-porphyrins were characterized by CV (see Figure 3.5 and Table 3.2). Significant line-broadening is observed for dendrimer-functionalized porphyrins **194** and **196**, which makes their voltammogram too featureless to decipher. However, porphyrin **195** still shows a characteristic patterns of three distinctive reversible redox couples.

entry	<i>Ox.</i> (V)		<i>Red.</i> (V)		
	E_{pa}	E_{pc}	E_{pa}	E_{pc}	
193	+0.79, +1.33	–	-1.09, -1.43	-1.21, -1.57, -1.76	
194	–	–	–	–	
195	+0.79, +1.33	–	-1.24, -1.43	-1.36, -1.71	
196	–	–	–	–	

Table 3.2: Electrochemical data of porphyrins **193-196**

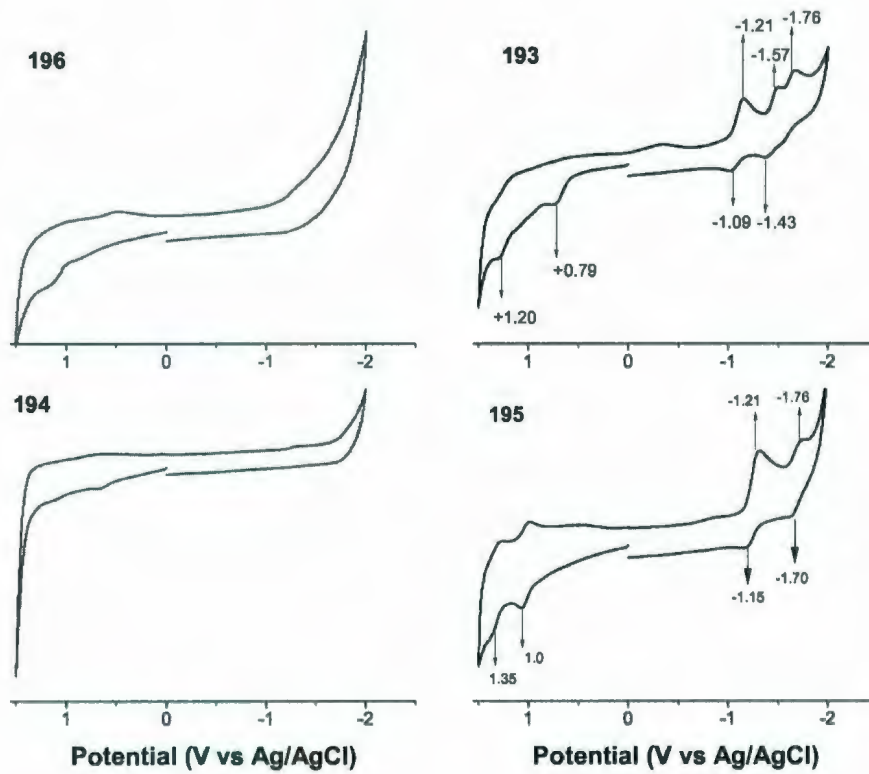


Figure 3.5: Cyclic voltammograms of free base porphyrins 193, 194, 195, and 196.

3.3.6 Characterizations of Dendrimer-Functionalized TTFAQs

The electronic properties (absorption and emission) of dendrimer-functionalized TTFAQs were studied by UV-Vis and fluorescence spectroscopic techniques. The UV-Vis absorption spectra of **199**, **200**, and **201** are shown in Figure 3.6. In addition to two absorption bands of a typical TTFAQ derivative **197** at λ_{max} 355 and 455 nm, two additional peaks appear at around λ_{max} 240 and 280 nm for compounds **199-201**, which are assigned to the absorption of the dendron groups attached. The similar low-energy absorption profiles of **199-201** signify very weak ground-state electronic interactions between the dendrons and the TTFAQ core. A slight blue-shift of low-energy bands by around 1-11 nm, however, is observed, when comparing dendro-TTFAQs **199-201** with TTFAQ core **197**.

The lowest-energy absorption band (λ_{max}) in TTFAQ, **189**, is found at 456 nm and was assigned to the $\pi \rightarrow \pi^*$ transition.¹¹⁸ In **190**, due to increased conjugation and decreased HOMO-LUMO gap, a bathochromic shift by 11 nm is observed relative simple TTFAQ, **189**.¹¹⁸ This shift is relatively lower than that of linear molecules with similar conjugation. This can be reasoned based on the nonplanarity of an TTFAQ; in other words, the TTFAQ molecules become more twisted with dendrimer attachments, such that orbital interactions through C \equiv C and 1,2,3-triazole functionality are weakened. Moreover, within the conjugated π -frameworks of compounds **199-201**, the electronic role of triazole as weak acceptors should not be overlooked. As a matter of fact, the dendro-TTFAQs present a series of donor-acceptor (D-A) system. Nevertheless, the D-A electronic interactions in these molecules are very small, indicating a low degree of π -electron delocalization

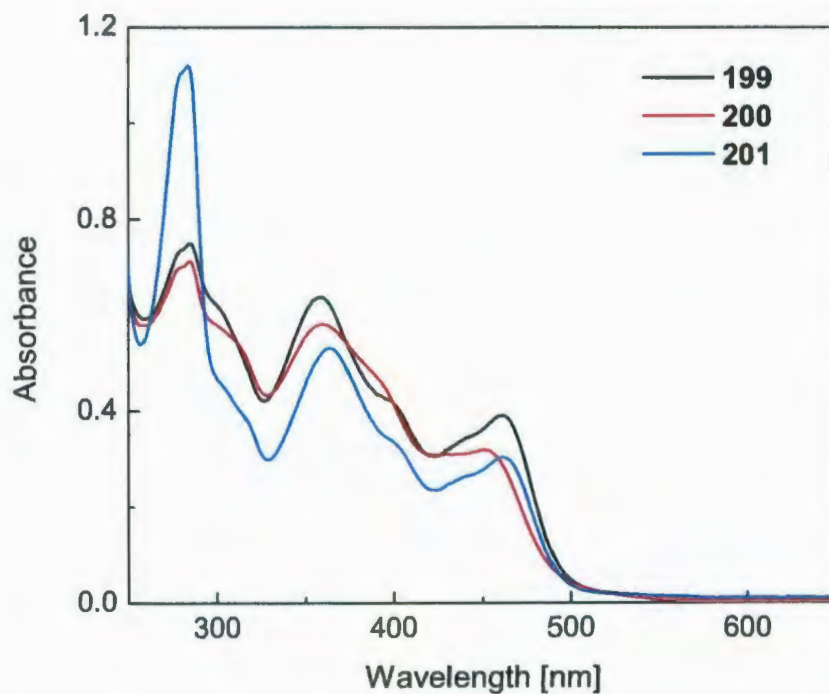


Figure 3.6: Absorption spectra of dendrimer-functionalized TTFAQs **199-201** in CHCl_3 .

along the non-planar TTFAQ and acetylene backbone. The 11 nm hypsochromic shift displayed by **200** could be explained due to enhanced π -stacking in dendritic structures, which further exacerbate the non-planarity of the molecule and decrease π -conjugation. However, for **199** and **201**, steric hindrance arising from bulky *n*-decyl peripheral groups could possibly have alleviated π -stacking to some extent. As such the molecules are more twisted than that of **200**. This hypothesis is in line with the spectral shift observed for the second lowest-energy absorption bands of compounds **199-201** compared with the band at 367 nm for **197**.

The emission spectrum ($S_1 \rightarrow S_0$ transition) of **199** shows two closely positioned bands at 490 and 477 nm respectively (see Figure 3.7). Blueshifts by 27 and 40 nm are observed when compared with TTFAQ **197** (517 and 420 nm). Almost similar fluorescence emissions were observed at 520 nm for **200** and 518 nm for **197** in comparison to **197**. These results suggest no significant enhancement of electronic interactions in the excited states of **199-201**.

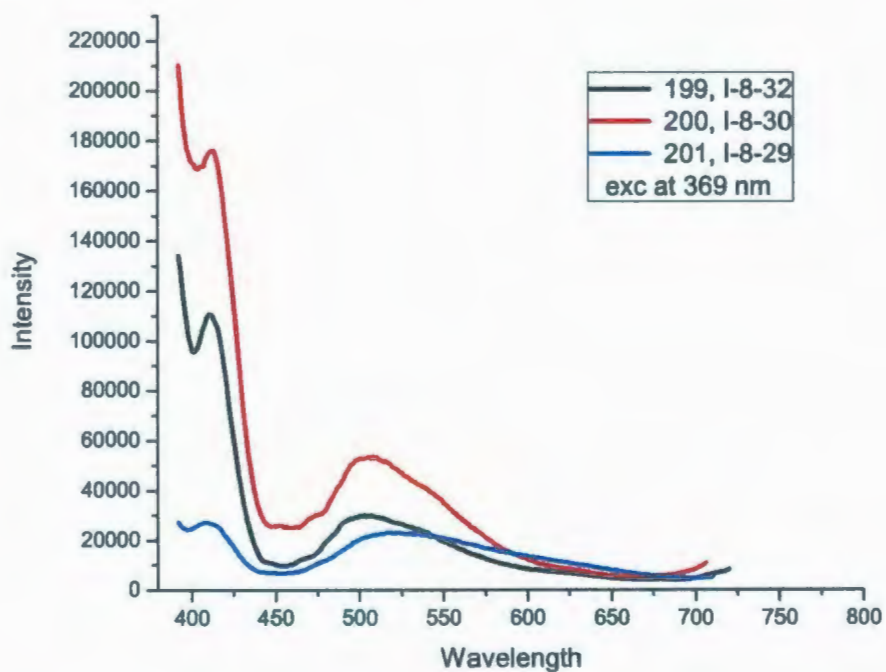


Figure 3.7: Emission spectra of dendrimer-functionalized TTFAQs **199-201** in CHCl_3 .

The electrochemical properties of dendrimer functionalized TTFAQs **199-201**

were studied by cyclic voltammetry (CV) and the acquired data are compared with those of TTFAQ 189 and phenylacetylene-extended TTFAQ 190, which were previously investigated by our group.¹¹⁸ Generally, an electron-withdrawing group attached to the TTFAQ core will raise the oxidation potentials E^{ox} , whereas an electron donating group will result in decreased E^{ox} .

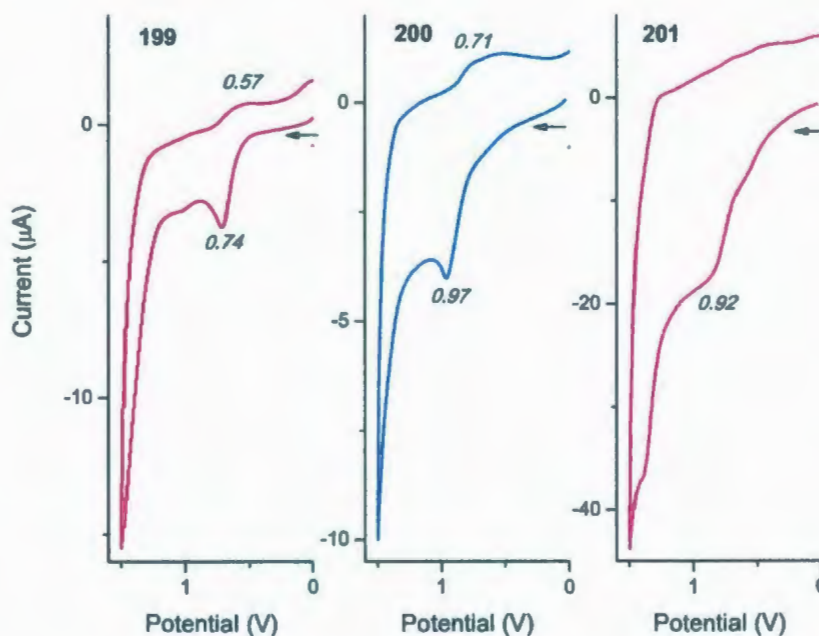


Figure 3.8: Cyclic voltammogram of compounds 199, 200 and 201 recorded in $\text{CHCl}_3\text{-MeCN}$ (4:1, v/v) at rt; Bu_4NBF_4 (0.1M) as supporting electrolyte, glassy carbon as working electrode, Pt wire as counter electrode, and Ag/AgCl as reference, scan rate 100 mV/s.

From the CV plots of 199–201 (see Figure 3.8), it is seen that all the derivatives

feature a typical quasi-reversible wave pair due to simultaneous two-electron oxidation of the TTFAQ core. The potentials vary slightly depending mainly on the nature of substituent groups attached to TTFAQ. In comparison to TTFAQ core **197**, the dendrimer-functionalized TTFAQs all display higher oxidation potentials. This can be tied to the steric effects imposed by the dendron groups, since more energy is needed to obtain the required planar oxidation state from the highly distorted ground state as the size of substituents increases on the TTFAQ. In the negative potential window, **197** shows an irreversible reduction peak at -1.79 V, which is less negative relative to the dendrimer-functionalized TTFAQs (-2.00 V for **201** and -1.93 V **199**).

3.3.7 Characterizations of Dendrimer-Functionalized Linear OPEs

The molecular structures of dendrimer-functionalized OPEs were characterized by spectroscopic techniques, such as $^1\text{H-NMR}$, $^{13}\text{C-NMR}$, FT-IR, high resolution (HR) MALDI-TOF mass spectrometric measurements. The HR-MALDI-TOF mass spectra clearly showed the molecular ion peaks of these macromolecules. $^1\text{H-NMR}$ characterization offered unambiguous evidence for the formation of triazole functional group, in addition to the IR absorptions at 2050-2150 cm^{-1} . $^{13}\text{C-NMR}$ also added irrefutable evidence for the identities of these molecules. It is interesting to notice from the $^1\text{H-NMR}$ data that the 1,2,3-triazole and benzylic protons show splitting phenomena, which is indicative of supramolecular aggregation in solution.³³

The optical properties of dendritic oligomers were examined by UV-Vis and fluorescence spectroscopy and are compared against those of their unsubstituted

counterparts. In the absorption spectra, the λ_{max} (in CHCl_3) for various dendritic oligomers appear at almost similar wavelength with variation of $\pm 2-3$ nm). These λ_{max} values are blue-shifted by 2–5 nm relative to their OPE precursor, which can be rationalized by the increased steric crowding of the dendritic groups that force the backbone of π -oligomer to adopt a non-planar ground-state structure. The insertion of two electron-deficient triazole rings on these molecules via CuAAC reaction shows rather insignificant electronic effects on the electronic absorption behavior. The fluorescence behavior of these dendrimer-OPE derivatives shown in Figure 3.10 reveals the same trend of substituent effects as elicited from the UV-Vis characterization. The fluorescence quantum yields determined for pre- and post-functionalized OPEs are viturally unchanged, suggesting little effect of macromolecular aggregation.

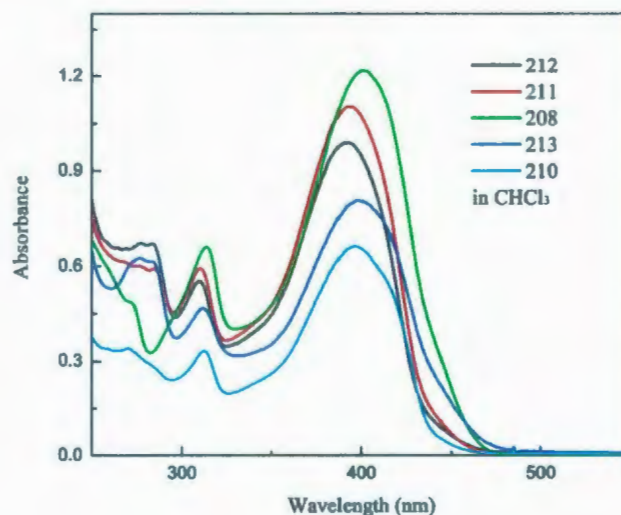


Figure 3.9: Absorption spectra of dendrimer and two dendrimer-functionalized OPEs 208-213.

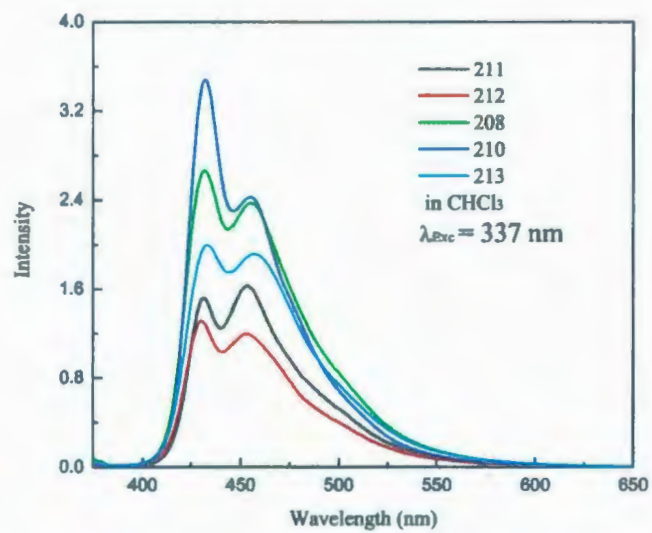


Figure 3.10: Emission spectra of dendrimer and two dendrimer functionalized-OPEs 208-213.

3.4 Conclusions

A series of dendrimer-functionalized conjugated macromolecules has been successfully synthesized using a modular protocol based on Sharpless' CuAAC click strategy. The yields of the click reactions demonstrated in this Chapter are satisfactory; however, the interference of other side reactions, such as oxidative homocoupling of alkynes, is also significant in the synthesis. Compared to numerous examples of click syntheses demonstrated in the literature, the synthetic results given in this chapter call for prudent planning and modest expectation of this popular synthetic paradigm in dealing with some highly π -conjugated systems. Nevertheless, it is irrefutable that the click philosophy has already been ingrained in the minds of the synthetic community, leading to the development of a large number of sophisticated macromolecular structures at an unprecedented speed. In this Chapter, access to new dendrimer-derived π -conjugated materials has not only delivered appealing systems for better understanding structure-property relationships, in particular, the complex effects stemming from dendrimers, but also presented novel properties that could eventually find applications in various molecular optoelectronic devices.

3.5 Experimental Part

General reagents, synthetic conditions and characterization techniques are the same as adopted in the experimental section of Chapter 2. Cyclic voltammetric analysis was performed on a BAS Epsilon electrochemical analyzer. UV-Vis absorption spectra were measured on a Cary6000i spectrophotometer. Fluorescence spectroscopy was

done on a PTI Quantmaster spectrofluorometer. For all UV-Vis and fluorescence experiments, samples were thoroughly de-oxygenated by means of vigorous bubbling with Ar before measurements.

Synthesis of *meso*-porphyrin **192**

To a 250 mL round-bottomed flask was added TMSA-benzaldehyde **186** (500 mg, 24.7×10^{-4} mol), pyrrole (166 mg, 24.7×10^{-4} mol) in glacial acetic acid (20 mL). The round-bottom flask was then fitted with a spiral condenser and heated up to 90-95 °C and kept stirring for 24-30 h. The reaction mixture was then cooled to room temperature, diluted with water (25 mL) and extracted three times with CHCl₃ (25 mL \times 3). The combined organic layer was washed with 5% aq. solution (w/w) of Na₂CO₃, dried over MgSO₄. The resulting solution was concentrated under vacuum and the crude mass was column chromatographed (hexanes/CHCl₃, 5:1) to yield compound **192** (1.78 g, 17.8×10^{-4} mol, 72%) as a shiny deep-brown needles (like iodine pellets). IR (neat): 2957, 2924, 2854, 2157, 1501, 1474, 1249 cm⁻¹; ¹H NMR (500 MHz, CDCl₃): δ 8.84 (s, 8H, alkenyl *H*), 8.17 (d, *J* = 8.0 Hz, 8H, Ar-*H*), 7.90 (d, *J* = 7.7 Hz, 8H, Ar-*H*), 0.4 (s, 36H); ¹³C NMR (125 MHz, CDCl₃): δ 142.7, 134.8, 130.8, 123.2, 120.0, 105.3, 100.0, 96.1, 32.0, 0.5; HR-EI-TOF MS (positive mode) *m/z* calcd C₆₄H₆₂N₄Si₄ 998.4052, found 998.4052 [M]⁺.

Synthesis of **194**

To a 100 mL round-bottomed flask was added a solution of **192** (181 mg, 1.81×10^{-4} mol) in dry THF (10 mL) and was cooled to 0 °C in an ice-bath. To this was then dropwise added a dilute solution TBAF (0.08 mL, 1.00 M solution in hexane) in dry THF (5 mL). The reaction mixture was stirred for 5 min and solvent was

removed. The resulting solid mass was taken in CHCl_3 , and washed with H_2O . The organic layer was then dried over MgSO_4 , filtered and solvent was removed to get compound **193** as a shiny deep-brown solid, which was kept at $0\text{ }^\circ\text{C}$ prior to use. Compound **183d** (726 mg, 7.48×10^{-4} mol), CuSO_4 (2.00 mg, 8.40×10^{-6} mol), and (+) sodium L-ascorbate (11.0 mg, 5.55×10^{-5} mol) were taken in 70 mL of THF/DMF (1:1) at $0\text{ }^\circ\text{C}$ in a 250 mL round-bottom flask. This was then evacuated under vacuum and purged with N_2 for several times and 2 mL of Et_3N was added to it. To this constantly stirred mixture, a solution of compound **193** in THF (20 mL) was slowly added for 0.5 h. The reaction mixture was stirred at room temperature for overnight, solvent (THF) was removed. The resulting solid mass was dissolved in CHCl_3 and washed with H_2O for several times. The organic layer was evaporated to dryness, and column chromatographed to afford compound **194** (76.3 mg, 1.66×10^{-5} mol, 46%) as a deep brownish-black solid. IR (neat): 2923, 2854, 2099, 1595, 1462, 1377, 1164, 1055 cm^{-1} ; ^1H NMR (500 MHz, CDCl_3): δ 6.61-6.27 (m, 64H), 4.99 (s, 16H), 4.29 (s, 8H), 3.98-3.93 (m, 32H), 1.82-1.79 (m, 32H), 1.77-1.46 (m, 32H), 1.35-1.32 (m, 192H), 0.92 (t, $J = 6.9$ Hz, 48H); ^{13}C NMR (125 MHz, CDCl_3): δ 161.0, 160.8, 160.7, 160.6, 143.8, 140.4, 139.2, 138.0, 108.0, 107.6, 107.4, 106.1, 102.3, 101.3, 98.9, 68.5, 68.4, 68.3, 57.6, 55.3, 32.3, 30.0, 29.8, 29.75, 29.7, 26.5, 23.1, 22.2, 14.5; HR-MALDI-TOF MS (dithranol as the matrix) m/z calcd for $\text{C}_{296}\text{H}_{422}\text{N}_{16}\text{O}_{24}$ 4596.6107, found 4596.1545 $[\text{M}]^+$.

Synthesis of 195

To a 250 mL round-bottomed flask was then added a solution of compound **183h** (48.3 mg, 6.28×10^{-5} mol), CuSO_4 (2.00 mg, 8.40×10^{-6} mol), (+) sodium L-

ascorbate (11.0 mg, 5.55×10^{-5} mol) in 60 mL THF/DMF (1:1) at 0 °C. The reaction vessel was then evacuated and purged with N₂ and 2 mL of Et₃N was added. To this constantly stirred mixture, a solution of **193** (10.0 mg, 1.42×10^{-5}) in THF (20 mL) was added for 0.5 h and then stirred at room temperature for overnight. Solvent (THF) was removed under vacuum and the resulting solid mass was dissolved in CHCl₃. The solution was washed with H₂O for several times. The organic layer was evaporated to dryness and column chromatographed to yield compound **195** (9.87 mg, 1.66×10^{-6} mol, 47%) as a deep brownish-black solid. IR (neat): 2922, 2855, 2099, 1595, 1454, 1369, 1162, 1053 cm⁻¹; ¹H NMR (500 MHz, CDCl₃): δ 7.50-6.62 (m, 144H), 5.10-4.31 (m, 56H); ¹³C NMR (125 MHz, CDCl₃): δ 160.7, 160.6, 139.6, 138.2, 137.3, 129.1, 129.05, 128.5, 128.04, 128.0, 107.7, 106.8, 102.3, 102.1, 70.6, 70.5, 55.3; HR-MALDI-TOF MS (dithranol as the matrix) *m/z* calcd for C₂₄₈H₂₀₂N₁₆O₂₄ 3789.5145, found 3789.1442 [M]⁺.

Synthesis of **196**

To a 100 mL round-bottomed flask was added a solution of **192** (100 mg, 1.00×10^{-4} mol) in dry THF (10 mL) and cooled to approximately 0 °C. To this was then dropwise added a dilute solution TBAF (0.08 mL, 1.00 M solution in hexane) in dry THF (5 mL) and was stirred for 5 min. The solvent was removed and the resulting solid mass was taken in CHCl₃, and washed with H₂O. The organic layer was then dried over MgSO₄, filtered and solvent was removed to get compound **193** as a shiny deep-brown solid, which was kept at 0 °C prior to use. To a 250 mL round-bottom flask was then added a solution of compound **183d** (830 mg, 4.12×10^{-4} mol), CuSO₄ (2.00 mg, 8.40×10^{-6} mol), (+) sodium L-ascorbate (11.0 mg, 5.55×10^{-5} mol) in

60 mL of THF/DMF (1:1) at 0 °C. The flask was then evacuated and purged with N₂ and 2 mL of Et₃N was added. To this constantly stirred mixture, a solution of **193** in THF (20 mL) was added for 0.5 h and stirred at temperature for overnight. Solvent (THF) was removed under vacuum and the resulting solid mass was dissolved in CHCl₃ and washed with H₂O for several times. The organic layer was evaporated to dryness and column chromatographed to yield compound **196** (485 mg, 5.50 × 10⁻⁵ mol, 55%) as a deep brownish-black solid. IR (neat): 2923, 2853, 2100, 1595, 1454, 1369, 1162, 1053 cm⁻¹; ¹H NMR (500 MHz, CDCl₃): δ 7.83 (s, 4H), 6.70-6.43 (m, 100H), 5.05-4.96 (m, 56H), 4.29 (s, 2H), 3.97-3.95 (m, 64H), 1.78-1.71 (m, 64H), 1.46-1.22 (m, 448H), 0.93-0.89 (m, 96H); ¹³C NMR (125 MHz, CDCl₃): δ 161.0, 160.9, 160.6, 139.5, 139.4, 138.1, 107.7, 106.8, 106.1, 102.2, 102.1, 101.3, 70.6, 70.5, 68.5, 55.2, 32.4, 30.0, 29.9, 29.8, 29.7, 26.5, 23.1, 14.6; MALDI-TOF MS (dithranol as the matrix) *m/z* calcd for C₅₆₈H₈₄₂N₁₆O₅₆ 8789.37, found 8789.03 [M]⁺.

Synthesis of deprotected ex-TTF oligomer **198**

A solution of linear OPE **197** (50.0 mg, 3.48 × 10⁻⁵ mol) in dry THF (5mL) was taken in a 100 mL round-bottomed flask. The flask was evacuated and purged with N₂ for several times and a dilute solution of TBAF (0.04 mL of 1 M solution) in THF (2 mL) was added dropwise to it. The reaction mixture was sonicated for 5 min, diluted with H₂O and extracted with CHCl₃. The organic layer was dried over MgSO₄, filtered and solvent was removed to afford compound **198** (35.1 mg, 2.44 × 10⁻⁵ mol, 77%) as a deep-yellow solid. ¹H NMR (500 MHz, CDCl₃): δ 7.72-7.48 (m, 6H), 7.06 (s, 2H), 7.02 (s, 2H), 4.07-4.03 (m, 8H), 3.38 (s, 2H), 2.44 (s, 6H), 2.43 (s, 6H), 1.89-1.83 (m, 8H), 1.60-1.49 (m, 8H), 1.44-1.28 (m, 48H), 0.97-0.88 (m,

12H); ^{13}C NMR (125 MHz, CDCl_3): δ 154.6, 154.0, 135.0, 134.8, 133.4, 127.0, 125.9, 121.8, 118.3, 117.3, 115.0, 113.1, 95.4, 87.0, 82.8, 80.4, 70.12, 70.10, 32.3, 30.0, 29.83, 29.80, 29.7, 29.6, 26.5, 26.4, 23.1, 19.5, 14.6, 14.5; MALDI-TOF MS (dithranol as the matrix) m/z calcd for $\text{C}_{84}\text{H}_{108}\text{O}_4\text{S}_8$ 1437.60, found 1437.67 $[\text{M}]^+$.

Synthesis of dendrimer G1-C10 functionalized ex-TTF oligomer 199

To a 250 mL round-bottomed flask, were added a solution of **182d** (94.5 mg, 9.75×10^{-5} mol), CuSO_4 (2.00 mg, 8.40×10^{-6} mol), (+) sodium L-ascorbate (15.5 mg, 7.82×10^{-5} mol) in 50 mL of THF/DMF (1:1) at 0 °C. The round-bottom flask was evacuated and purged with N_2 for several times and 2 mL of Et_3N was added to it with the help of a syringe. To this constantly stirred mixture, a solution of **198** (56.2 mg, 3.91×10^{-5} mol) was added dropwise for 0.5 h and then stirred at room temperature for overnight. The solvent was removed, and the resulting solid mass was dissolved in CHCl_3 and washed with H_2O for several times. The organic layer was evaporated to dryness, and column chromatographed to give compound **199** (71.3 mg, 2.11×10^{-5} mol, 54%) as a deep-yellow oil. IR (neat): 2923, 2853, 2100, 1596, 1494, 1379, 1164 cm^{-1} ; ^1H NMR (500 MHz, CDCl_3): δ 8.08 (s, 1H), 7.99(s, 1H), 7.74-7.07 (m, 10H), 6.58-6.42 (m, 18H, dendritic Ar-H), 5.76-4.94 (m, 12H, benzylic Ar-H, splitting due to aggregation), 4.33-3.94 (m, 24H, O- CH_2), 2.44-2.43 (2s, 12H), 2.44-1.24 (m, 192H), 0.95-0.87 (m, 36H); ^{13}C NMR (125 MHz, CDCl_3): δ 161.0, 160.9, 160.6, 139.1, 136.9, 106.2, 106.1, 101.3, 70.6, 70.1, 68.5, 32.3, 30.1, 29.9, 29.8, 29.7, 29.1, 26.5, 26.4, 23.1, 14.4; HR-MALDI-TOF MS (dithranol as the matrix) m/z calcd for $\text{C}_{206}\text{H}_{306}\text{O}_{16}\text{S}_8\text{N}_6$ 3379.1844, found 3379.0769 $[\text{M}]^+$.

Synthesis of G2-C10 functionalized ex-TTF oligomer 201

To a 250 mL round-bottomed flask was added a solution of **183d** (150 mg, 7.43×10^{-5} mol), CuSO_4 (2.00 mg, 8.40×10^{-6} mol), (+) sodium L-ascorbate (12.0 mg, 6.03×10^{-5} mol) in 60 mL of THF/DMF (1:1) at 0 °C. The flask was evacuated and purged with N_2 for several times and 2 mL of Et_3N was added to it. To this constantly stirred mixture, a solution of **198** (43.0 mg, 2.99×10^{-5} mol) was added dropwise for 0.5 h and then stirred at room temperature for overnight and solvent (THF) was removed under vacuum. The resulting solid mass was dissolved in CHCl_3 and washed with H_2O for several times. The organic layer was evaporated to dryness, and column chromatographed to give compound **201** (118 mg, 2.15×10^{-5} mol, 72%) as a deep-yellow oil. IR (neat): 2922, 2853, 2099, 1595, 1454, 1375, 1163, 1054 cm^{-1} ; ^1H NMR (500 MHz, CDCl_3): δ 8.08 (s, 1H), 7.99 (s, 1H), 7.73-6.70 (m, 10H), 6.70-6.43 (m, 42H, dendritic Ar-H), 5.53-4.29 (m, 28H, benzylic Ar-H, splitting due to aggregation), 4.29-3.95 (m, 40H, O- CH_2), 2.44-2.43 (s, 12H), 1.79-1.73 (m, 40H), 1.59-1.30 (m, 280H), 0.92-0.87 (m, 60H); ^{13}C NMR (125 MHz, CDCl_3): δ 160.93, 160.92, 160.90, 160.57, 139.4, 139.3, 139.24, 139.20, 138.0, 107.6, 106.7, 106.1, 102.2, 102, 101, 70.6, 70.5, 68.5, 55.2, 32.3, 29.8, 29.75, 29.74, 29.7, 26.5, 23.1, 14.6; MALDI-TOF MS (dithranol as the matrix) m/z calcd for $\text{C}_{342}\text{H}_{514}\text{O}_{32}\text{S}_8\text{N}_6$ 5478.3, found 5478.8 $[\text{M}]^+$.

Synthesis of G2-H functionalized ex-TTF oligomer **200**

To a 250 mL round-bottomed flask were added a solution of G2-H **183h** (47.7 mg, 6.20×10^{-5} mol), CuSO_4 (2.00 mg, 8.40×10^{-6} mol), (+) sodium L-ascorbate (11.0 mg, 5.55×10^{-5} mol) in 70 mL of THF/DMF (1:1) at 0 °C. The round-bottom flask was evacuated and purged with N_2 for several times and 2 mL of Et_3N was added to it with the help of a syringe. To this constantly stirred mixture, a solution of compound

198 (39.9 mg, 2.77×10^{-5} mol) was slowly added for 0.5 h and then stirred at room temperature for overnight. The solvent (THF) was removed under vacuum. The resulting solid mass was dissolved in CHCl_3 and washed with H_2O for several times. The organic layer was evaporated to dryness, and column chromatographed to obtain compound **200** (71.3 mg, 2.11×10^{-5} mol, 67%) as a deep-yellow oil. IR (neat): 2922, 2852, 2099, 1594, 1496, 1455, 1377, 1152, 1043 cm^{-1} ; ^1H NMR (500 MHz, CDCl_3): δ 7.71-7.69 (m, 2H), 7.43-6.70 (m, 10H), 7.38-7.06 (m, 40H), 6.58-6.47 (m, 18H, dendritic Ar-*H*), 5.59-4.28 (m, 12H, benzylic *H*, splitting due to aggregation), 4.04-3.94 (m, 8H, O- CH_2), 2.44-2.43 (m, 12H), 1.89-1.86 (m, 8H), 1.84-1.28 (m, 56H), 0.91-0.87 (m, 12H); ^{13}C NMR (125 MHz, CDCl_3): δ 160.6, 139.1, 137.13, 129.0, 128.4, 128.0, 127.97, 127.94, 106.8, 106.7, 102.0, 100.0, 70.53, 70.5, 70.4, 30.1, 29.95, 29.85, 29.8, 29.75, 29.7, 29.65, 26.5, 26.3, 23.1, 14.54, 14.52; HR-MALDI-TOF MS (dithranol as the matrix) m/z calcd for $\text{C}_{184}\text{H}_{194}\text{O}_{16}\text{S}_8\text{N}_6$ 2978.0384, found 2979.2105 $[\text{M} + \text{H}]^+$.

Synthesis of 1,4-bis(decyloxy)benzene (**203**)

To a 250 mL round-bottomed flask was added a solution of 1,4-dihydroquinone (**202**) (4.40 g, 40.0 mmol) and solid KOH pellets (5.61 g, 1.00 mol) in EtOH (20 mL). This was then stirred at room temperature for 5-10 min (the color of reaction mixture changed to purple at this stage). A solution of *n*-decyl bromide (17.7 g, 40.0 mmol) in EtOH (20 mL) was added dropwise and then refluxed overnight. The reaction mixture was cooled to room temperature and 150 mL of CH_2Cl_2 was added to it. The whole mass was transferred to a separatory funnel and washed with H_2O . The organic layer was evaporated to dryness and the resulting solid mass was recrystallized from MeOH to afford compound **203** (14.9 g, 38.1 mmol, 95%) as a white shiny needle-like crystals.

Mp 69-71 °C; IR (neat): 2954, 2933, 2918, 2872, 2850, 1558, 1029 cm^{-1} ; ^1H NMR (500 MHz, CDCl_3): δ 6.88 (s, 4H, Ar-H), 3.94 (t, $J = 6.6$ Hz, 4H), 1.81-1.76 (m, 4H), 1.51-1.45 (m, 4H), 1.38-1.23 (m, 24H), 0.93 (t, $J = 7.0$ Hz, 6H); ^{13}C NMR (125 MHz, CDCl_3): δ 153.7 (Ar C-O), 115.8, 69.1, 32.3, 30.1, 29.8, 29.6, 29.5, 26.5, 23.2, 14.5; APCI-MS (positive mode) m/z calcd for $\text{C}_{26}\text{H}_{46}\text{O}_2$ 390.0, found 390.0 $[\text{M}]^+$.

Synthesis of 1,4-bis(decyloxy)-2,5-diiodobenzene (204)

A mixture of compound **203** (12.0 g, 30.7 mmol), I_2 (19.5 g, 76.8 mmol), and $\text{Hg}(\text{OAc})_2$ (24.5 g, 76.8 mmol) were dissolved in 100 mL of CH_2Cl_2 in a 250 mL round-bottomed flask, equipped with a magnetic stirrer. The reaction mixture was stirred at room temperature for 20 h and then passed through a celite plug. The solution was transferred to a separatory funnel and washed sequentially with satd $\text{Na}_2\text{S}_2\text{O}_3$ (3 times) solution, then satd NaHCO_3 solution and finally with H_2O (the original deep-purple color of the solution faded to colorless at this stage). The organic portion was dried over MgSO_4 , filtered and solvent was removed to give the product as a pale brown solid, which was recrystallized from MeOH to afford compound **204** (17.7 g, 27.6×10^{-3} mol, 90%) as a white amorphous solid. Mp 50-51 °C; IR (neat): 2975, 2956, 2944, 2851, 1496, 1388, 1039 cm^{-1} ; ^1H NMR (500 MHz, CDCl_3): δ 7.18 (s, 2H, Ar-H), 3.92 (t, $J = 6.4$ Hz, 4H), 1.83-1.77 (m, 4H), 1.55-1.47 (m, 4H), 1.37-1.28 (m, 24H), 0.89 (t, $J = 7.0$ Hz, 6H); ^{13}C NMR (125 MHz, CDCl_3): δ 152.5, 122.0, 86.8 (Ar-I carbons), 70.8 (two CH_2O), 32.4, 30.1, 29.8, 29.6, 29.5, 26.4, 23.2, 14.5; APCI-MS (positive mode) m/z calcd for $\text{C}_{26}\text{H}_{44}\text{O}_2\text{I}_2$ 642.0, found 642.0 $[\text{M}]^+$.

Synthesis 1,4-bis(decyloxy)-2-iodo-5-(trimethylsilylethynyl)benzene (205)

A mixture of 1,4-bis(decyloxy)-2,5-diiodobenzene (**204**) (2.00 g, 3.12 mmol),

Pd(PPh₃)₂Cl₂ (66.0 mg, 9.41 × 10⁻⁵ mol), and CuI (59.0 mg, 3.10 × 10⁻⁴ mol) were added in 50 mL of dry THF/Et₃N (1:1) in a 100 mL round-bottomed flask equipped with a magnetic stirrer. The flask was then evacuated under vacuum and purged with N₂ for several times to remove O₂. To this constantly stirred mixture, was then dropwise added a solution of TMSA (214 mg, 2.18 mmol, 0.7 mol equivalent to that of **204**) in dry THF (5mL) (the color of the reaction mixture quickly turned to dark-brown at this stage). The reaction mixture was then stirred at room temperature for 24 h. The solvent was removed under vacuum and the resulting solid mass was dissolved in CHCl₃ and washed with H₂O. The organic layer was dried over MgSO₄, filtered and finally column chromatographed (hexanes/CH₂Cl₂, 10:1) to afford compound **205** (638 mg, 1.04 mmol, 62%) as a colorless solid. Mp 37-38 °C; IR (neat): 2978, 2919, 2849, 2133, 1582, 1526, 1343, 1039 cm⁻¹; ¹H NMR (500 MHz, CDCl₃): δ 7.31 (s, 2H), 6.87 (s, 2H), 4.02-3.91 (m, 4H), 1.86-1.79 (m, 4H), 1.58-1.49 (m, 4H), 1.35-1.29 (m, 24H), 0.92 (t, *J* = 5.0 Hz, 6H), 0.27 (s, 9H); ¹³C NMR (125 MHz, CDCl₃): δ 155.3, 152.1, 124.6, 116.6, 113.9, 101.2, 99.9, 88.3, 70.5, 70.3, 32.4, 32.3, 30.1, 30.07, 30.05, 30.0, 29.9, 29.85, 29.80, 29.79, 29.75, 29.70, 29.69, 26.5, 26.4, 23.2, 14.5, 0.1; APCI-MS (positive mode) *m/z* calcd for C₃₆H₆₂O₂Si₂ 612.0, found 612.3 [M]⁺.

Synthesis 1,4-bis(decyloxy)-2,5-bis(trimethylsilylethynyl)benzene (**206**)

A mixture of 1,4-bis(decyloxy)-2,5-diiodobenzene (**204**) (3.20 g, 4.98 mmol), Pd(PPh₃)₄ (298 mg, 2.50 × 10⁻⁴ mol), and CuI (95.0 mg, 5.00 × 10⁻⁴ mol) were taken in 50 mL of dry THF/Et₃N (1:1) in a 100 mL round-bottomed flask. The flask was evacuated under vacuum and purged with N₂ for several times to remove O₂ as much

as possible. To this constantly stirred mixture was then dropwise added a solution of TMSA (3.91 g, 39.8 mmol) in THF (5 mL) and stirred at room temperature for 24 h. The solvent was removed and the resulting solid mass was dissolved in CHCl_3 and washed with H_2O . The organic layer was then dried over MgSO_4 , filtered and finally column chromatographed (hexanes/ CH_2Cl_2 , 5:1) to give compound **206** (2.65 g, 4.55 mmol, 92%) as a pale-yellow solid. IR (neat): 3031, 2978, 2919, 2849, 2133, 1582, 1525, 1377, 1039 cm^{-1} ; ^1H NMR (500 MHz, CDCl_3): δ 6.91 (s, 2H), 3.97 (t, $J = 6.3$ Hz, 4H), 1.82-1.79 (m, 4H), 1.56-1.50 (m, 4H), 1.35-1.29 (m, 24H), 0.91 (t, $J = 6.9$, 6H), 0.27 (s, 18H); ^{13}C NMR (125 MHz, CDCl_3): δ 154.7, 119.5, 114.2, 101.5, 100.1, 70.0, 32.4, 32.3, 30.1, 30.07, 30.05, 30.0, 29.9, 29.85, 29.80, 29.79, 29.75, 29.70, 29.69, 26.5, 26.4, 23.2, 14.5, 0.1; APCI-MS (positive mode) m/z calcd for $\text{C}_{36}\text{H}_{62}\text{O}_2\text{Si}_2$ 582.0, found 582.5 $[\text{M}]^+$.

Synthesis 1,4-bis(decyloxy)-2,5-bis(ethynyl)benzene (207)

A solution of **206** (1.20 g, 2.06 mmol) in dry THF (5 mL) was taken in a 100 mL round-bottomed flask. To this was then added dropwise a dilute solution of TBAF (0.05 mL of 1 M solution) in THF (2 mL) and then sonicated for 5 min. The reaction mixture was diluted with H_2O and extracted with CHCl_3 . The organic layer was dried over MgSO_4 , filtered and solvent was removed to afford compound **207** (902 mg, 2.06 mmol, 95%) as a pale-yellow solid. IR (neat): 3285, 2982, 2959, 2942, 2850, 2142, 1540, 1500, 1384, 1028 cm^{-1} ; ^1H NMR (500 MHz, CDCl_3): δ 6.98 (s, 2H), 3.99 (t, $J = 6.7$ Hz, 4H), 3.35 (s, 2H), 1.85-1.79 (m, 4H), 1.52-1.46 (m, 4H), 1.39-1.30 (m, 24H), 0.92-0.89 (t, $J = 6.9$ Hz, 6H); ^{13}C NMR (125 MHz, CDCl_3): δ 154.2, 118.2, 113.5, 82.4, 80.3, 70.1, 32.5, 32.3, 30.1, 30.0, 29.9, 29.85, 29.80, 29.79, 26.5, 26.4, 23.2,

14.5; APCI-MS (positive mode) m/z calcd for $C_{30}H_{46}O_2$ 438.0, found 439.0 $[M + H]^+$.

Synthesis of linear OPE 208

To a 100 mL round-bottomed flask was added compound **205** (550 mg, 8.98×10^{-4} mol), $Pd(PPh_3)_2Cl_2$ (12.8 mg, 1.82×10^{-5} mol), and CuI (6.90 mg, 3.63×10^{-5} mol) in 60 mL of dry THF/ Et_3N (1:1) at 0 °C. The flask was evacuated and purged with N_2 for several times to remove O_2 as much as possible. To this constantly stirred mixture, a solution of 1,4-bis(decyloxy)-2,5-bis(ethynyl)benzene (**207**) (160 mg, 3.65×10^{-4} mol) in Et_3N (5 mL) was added dropwise for 0.5 h. The reaction mixture was then stirred overnight and solvent was removed under vacuum. The resulting solid mass was dissolved in $CHCl_3$ and washed with aq HCl (1%). The organic layer was dried over $MgSO_4$, filtered and solvent was removed to dryness and finally column chromatographed (hexanes/ $CHCl_3$, 5:1) to yield compound **208** (489 mg, 3.47×10^{-4} mol, 95%) as a deep-yellow solid. IR (neat): 2952, 2922, 2850, 2150, 1653, 1533, 1385, 1221 cm^{-1} ; 1H NMR (500 MHz, $CDCl_3$): δ 7.01 (s, 2H), 6.98 (s, 2H), 6.96 (s, 2H), 4.05-3.97 (m, 12H), 1.87-1.81 (m, 12H), 1.56-1.51 (m, 12H), 1.37-1.27 (m, 72H), 0.92-0.88 (m, 18H), 0.30 (s, 18H); ^{13}C NMR (125 MHz, $CDCl_3$): δ 154.6, 153.9, 153.8, 117.9, 117.7, 117.5, 115.1, 114.8, 114.1, 101.6, 100.5, 92.0, 91.8, 70.2, 70.1, 69.9, 32.4, 32.3, 30.1, 30.07, 30.05, 30.0, 29.9, 29.85, 29.80, 29.79, 29.75, 29.70, 29.69, 26.5, 26.4, 23.2, 14.5; APCI-MS (positive mode) m/z calcd for $C_{92}H_{150}O_6Si_2$ 1408.0, found 1408.0 $[M]^+$.

Synthesis of deprotected linear OPE 209

A solution of compound **208** (69.0 mg, 4.90×10^{-5} mol) in dry THF (5 mL)

was taken in a 100 mL round-bottomed flask. To this was added dropwise a dilute solution of TBAF (0.05 mL of 1 M solution) in THF (2 mL) and then sonicated for 5 min at 0-5 °C. The reaction mixture was diluted with H₂O and extracted with CHCl₃. The organic layer was dried over MgSO₄, filtered and solvent was removed to give compound **209** (60.0 mg, 4.74×10^{-5} mol, 95%) as deep-yellow solid. IR (neat): 3315, 2922, 2851, 2145, 2106, 1600, 1497, 1387, 1218 cm⁻¹; ¹H NMR (500 MHz, CDCl₃): δ 7.02 (s, 2H), 7.01 (s, 2H), 7.00 (s, 2H), 4.04-3.98 (m, 12H), 3.36 (s, 2H), 1.88-1.83 (m, 12H), 1.55-1.51 (m, 12H), 1.39-1.27 (m, 72H), 0.91-0.89 (m, 18H); ¹³C NMR (125 MHz, CDCl₃): δ 154.6, 154.0, 153.8, 118.5, 117.7, 117.4, 115.4, 114.7, 113.0, 92.0, 91.7, 82.7, 80.4, 70.2, 70.1, 70.0, 32.2, 30.1, 30.07, 30.05, 30.0, 29.9, 29.85, 29.80, 29.79, 29.75, 29.70, 29.69, 26.5, 26.4, 23.2, 14.5; MALDI-TOF MS (dithranol as the matrix) *m/z* calcd for C₈₆H₁₃₄O₆ 1263.02, found 1263.46 [M]⁺.

Synthesis of G1-C10 functionalized linear oligomer **211**

To a 250 mL round-bottomed flask were added a solution of compound **182d** (22.0 mg, 2.27×10^{-5} mol), CuSO₄ (20.0 mg, 8.50×10^{-5} mol), and (+) sodium L-ascorbate (30.0 mg, 8.50×10^{-4} mol) in 70 mL of THF/DMF (1:1) at 0 °C. The flask was evacuated under vacuum and purged with N₂ for several times and 2 mL of Et₃N was added. To this constantly stirred mixture, a solution of compound **209** (15.0 mg, 1.19×10^{-5} mol) was slowly added for 0.5 h. The reaction mixture was then stirred at room temperature for overnight, then the solvent (THF) was removed. The resulting solid mass was dissolved in CHCl₃ and washed with H₂O for several times. The organic layer was evaporated to dryness, and column chromatographed to give compound **211** (25.5 mg, 8.00×10^{-6} mol, 65%) as a yellowish green oil. IR

(neat): 2974, 2929, 2850, 2100, 1689, 1248 cm^{-1} ; ^1H NMR (500 MHz, CDCl_3): δ 8.06 (s, 1H), 7.97 (s, 1H), 7.11-7.05 (m, 6H), 6.60-6.42 (m, 12H, dendritic Ar-*H*), 4.95-4.93 (m, 12H, benzylic *H*), 4.18-3.90 (m, O-*CH*₂, 28H), 1.89-1.43 (m, 56H), 1.36-1.29 (m, 168H), 0.91-0.88 (m, 42H); ^{13}C NMR (125 MHz, CDCl_3): δ 160.9, 160.6, 137.0, 136.0, 107.0, 106.0, 103.0, 102.0, 70.2, 68.2, 67.0, 54.5, 32.3, 30.1, 30.07, 30.05, 30.0, 29.9, 29.85, 29.80, 29.79, 29.75, 29.70, 29.69, 26.5, 26.4, 23.2, 14.5; MALDI-TOF MS (dithranol as the matrix) *m/z* calcd for $\text{C}_{208}\text{H}_{330}\text{O}_{18}\text{N}_6$ 3202.5, found 3202.5 $[\text{M}]^+$.

Synthesis of G1-H functionalized linear oligomer 210

To a 250 mL round-bottomed flask were added a solution of compound **182h** (22.0 mg, 2.27×10^{-5} mol), CuSO_4 (2.00 mg, 8.40×10^{-6} mole), and (+) sodium L-ascorbate (11.3 mg, 5.70×10^{-5} mol) in 70 mL of THF/DMF (1:1) at 0 °C. The flask was evacuated and purged with N_2 for several times. To this constantly stirred mixture, a solution of compound **209** (15.0 mg, 1.18×10^{-5} mole) in THF (5 mL) was added slowly for 0.5 h and then stirred at room temperature for overnight and solvent (THF) was removed. The resulting solid mass was dissolved in CHCl_3 and washed with H_2O for several times. The organic layer was evaporated to dryness and column chromatographed to afford compound **210** (25.5 mg, 7.96×10^{-6} mol, 70%) as a yellowish-green oil. IR (neat): 2974, 2929, 2100, 1595, 1478, 1392, 1162 cm^{-1} ; ^1H NMR (500 MHz, CDCl_3): δ 8.06 (s, 1H), 7.97 (s, 1H), 7.50-7.01 (m, 6H), 6.60-6.42 (m, 18H, Ar-*H*), 4.98-4.93 (m, 12H, benzylic *H*), 4.18-3.90 (m, 28H), 1.89-1.49 (m, 56H, O-*CH*₂), 1.46-1.29 (m, 168H), 0.91-0.89 (m, 42H); ^{13}C NMR (125 MHz, CDCl_3): δ 161.0, 157.4, 137.8, 136.0, 107.0, 105.7, 102.3, 101.5, 69.9, 68.5, 55.3, 32.3, 30.0, 29.81, 29.8, 29.7, 29.4, 26.5, 23.1, 14.5; MALDI-TOF MS (dithranol as the matrix)

m/z calcd for $C_{208}H_{332}O_{18}N_6$ 3202.57, found 3202.51 $[M]^+$.

Synthesis of G2-C10 functionalized linear oligomer 213

To a 250 mL round-bottomed flask were added a solution of compound **183d** (116.0 mg, 5.75×10^{-5} mol), $CuSO_4$ (2.00 mg, 8.40×10^{-6} mol), and (+) sodium L-ascorbate (11.3 mg, 5.70×10^{-5} mol) in 80 mL of THF/DMF (1:1) 0 °C. The flask was evacuated and purged with N_2 for several times. To this constantly stirring mixture, a solution of compound **209** (36.0 mg, 2.85×10^{-5} mol) in THF (5 mL) was added slowly for 0.5 h. The reaction mixture was stirred at room temperature overnight and solvent (THF) was removed under vacuum. The resulting solid mass was dissolved in $CHCl_3$ and washed with H_2O for several times. The organic layer was evaporated to dryness and column chromatographed to afford compound **213** (108 mg, 2.04×10^{-5} mol, 72%) as a deep yellowish-green oil. IR (neat): 2974, 2929, 2100, 1595, 1478, 1392, 1162 cm^{-1} ; 1H NMR (500 MHz, $CDCl_3$): δ 8.20 (s, 1H), 7.98 (s, 1H), 7.5-7.01 (m, 6H), 6.67-6.42 (m, 42H, Ar-*H*), 4.97-4.96 (m, 28H, benzylic *H*), 4.03-3.94 (m, 44H), 1.86-1.52 (m, 88H, O- CH_2), 1.46-1.29 (m, 264H), 0.91-0.89 (m, 66H); ^{13}C NMR (125 MHz, $CDCl_3$): δ 160.92, 160.9, 160.6, 160.5, 139.3, 107.1, 106.1, 70.6, 68.5, 32.3, 30.0, 29.81, 29.8, 29.74, 29.72, 29.7, 26.4, 23.1, 14.5; MALDI-TOF MS (dithranol as the matrix) m/z calcd for $C_{344}H_{540}O_{34}N_6$ 5300.07, found 5298.54 $[M]^+$.

Synthesis of G2-H functionalized linear oligomer 212

To a 250 mL round-bottomed flask were added a solution of compound **183h** (22.0 mg, 2.27×10^{-5} mol), $CuSO_4$ (20.0 mg, 8.50×10^{-5} mol), and (+) sodium L-ascorbate (30.0 mg, 8.50×10^{-4} mol) in 75 mL of THF/DMF (1:1) at 0 °C. The flask

was then evacuated and purged with N₂ for several times. To this constantly stirred mixture, a solution of compound **209** (15.0 mg, 1.19 × 10⁻⁵ mol) in THF (5.00 mL) was added slowly for 0.5 h and was stirred at room temperature for overnight. The solvent (THF) was removed under vacuum. The resulting solid mass was dissolved in CHCl₃ and then washed with H₂O for several times. The organic layer was evaporated to dryness and column chromatographed to yield compound **212** (25.5 mg, 8.00 × 10⁻⁶ mol, 67%) as a deep yellowish-green oil. IR (neat): 2974, 2929, 2850, 2100, 1689, 1248 cm⁻¹; ¹H NMR (500 MHz, CDCl₃): 8.06 (s, 1H), 7.97 (s, 1H), 7.11-7.05 (m, 6H), 6.60-6.42 (m, 12H, dendritic Ar-*H*), 4.95-4.93 (m, 12H, benzylic *H*), 4.18-3.90 (m, O-CH₂, 28H), 1.89-1.43 (m, 56H), 1.36-1.29 (m, 168H), 0.89 (m, 42H); ¹³C NMR (125 MHz, CDCl₃): 160.9, 160.6, 137.0, 136.0, 107, 106, 103, 102, 70.2, 68.2, 67.0, 54.5, 32.3, 30.1, 30.07, 30.05, 30.0, 29.9, 29.85, 29.80, 29.79, 29.75, 29.70, 29.69, 26.5, 26.4, 23.2, 14.5; MALDI-TOF MS (dithranol as the matrix) *m/z* calcd for C₁₈₄H₂₁₈O₁₈N₆ 2801.6, found 2801.5 [M]⁺.

Synthesis of 1,4-bis(methoxy)-2,5-diiodobenzene (**214**)

A mixture of 1,4-bis(methoxy)benzene (**202a**) (4.00 g, 28.9 mmol), I₂ (18.4 g, 72.4 mmol), and Hg(OAc)₂ (23.1 g, 72.4 mmol) were taken in 100 mL of CH₂Cl₂ in a 250 mL round-bottomed flask equipped with a magnetic stirrer. The reaction mixture was stirred at room temperature for 24 h and then passed through a celite plug. The solution was sequentially washed with satd. Na₂S₂O₃ (3 times), then satd. NaHCO₃ (10% w/w aq.) and finally with H₂O (the original deep-purple color of the organic solution became almost colorless). The solution was then dried over MgSO₄, filtered and solvent was removed. It was then recrystallized from MeOH to afford compound

214 (10.7 g, 27.5 mmol, 99%) as a shiny white needle-like crystalline solid. IR (neat): 3007, 2932, 2832, 1482, 1061, 1016 cm^{-1} ; ^1H NMR (500 MHz, CDCl_3): δ 7.22 (s, 2H, Ar-*H*), 3.85 (s, 6H); ^{13}C NMR (125 MHz, CDCl_3): δ 153.8, 122.0, 85.9, 57.6 (Ar-I *C*).

Synthesis of 1,4-bis(methoxy)-2,5-bis(silylethynyl)benzene (**215**)

A mixture of 1,4-bis(methoxy)-2,5-diiodobenzene (**214**) (1.00 g, 2.56 mmol), $\text{Pd}(\text{PPh}_3)_4$ (90.0 mg, 1.28×10^{-4} mol), CuI (48.0 mg, 2.53×10^{-4} mol) were added in 50 mL of dry THF/ Et_3N (1:1) in a 100 mL round-bottomed flask and cooled to 0 $^\circ\text{C}$. The flask was evacuated under vacuum and purged with N_2 for several times to remove O_2 as much as possible. To this constantly stirred mixture, was then added dropwise a solution of TMSA (1.51 g, 15.4 mmol) in dry THF (5 mL) and stirred at room temperature for 4 h. The solvent was removed to dryness. The resulting solid mass was dissolved in CHCl_3 and washed with H_2O . The organic layer was dried over MgSO_4 , filtered and absorbed on silica gel and finally column chromatographed (hexanes/ CH_2Cl_2 , 10:1) to yield compound **215** (754 mg, 2.28 mmol, 89%) as pale yellow solid. IR (neat): 2957, 2897, 2842, 2151, 1592, 1490, 1372 cm^{-1} ; ^1H NMR (500 MHz, CDCl_3): δ 6.94 (s, 2H, Ar-*H*), 3.86 (s, 6H), 0.29 (s, 18H); ^{13}C NMR (125 MHz, CDCl_3): δ 154.6, 116.6, 113.8, 101.2, 100.8, 56.8; GC-MS m/z (%) calcd for $\text{C}_{18}\text{H}_{26}\text{O}_2\text{Si}_2$ 330.1, found 330.0 (100) $[\text{M}]^+$, 315 (16) $[\text{M} - \text{CH}_3]^+$.

Synthesis of 1,4-bis(methoxy)-2,5-bis(ethynyl)benzene (**216**)

A solution of 1,4-bis(methoxy)-2,5-bis(ethynyl)benzene (**215**) (1.00 g, 3.02 mmol) and K_2CO_3 (1.67 g, 12.1 mmol) were added in a 25 mL of THF/ $\text{MeOH}/\text{CHCl}_3$ (1:1:1) in a 100 mL round-bottomed flask. The reaction mixture was stirred for 6 h, and the

solvent was removed. The resulting solid mass was dissolved in CHCl_3 and washed with H_2O . The organic layer was dried over MgSO_4 , filtered and solvent was removed to afford compound **216** (517 mg, 2.78×10^{-3} mol, 92%) as pale-yellow solid. IR (neat): 3285, 3014, 2976, 2945, 2850, 2105, 1553, 1454, 1388, 1327, 1035 cm^{-1} ; ^1H NMR (500 MHz, CDCl_3): δ 6.98 (s, 2H, Ar-H), 3.86 (s, 6H, O- CH_3), 3.40 (s, 2H, ethynyl H); ^{13}C NMR (125 MHz, CDCl_3): δ 154.8, 116.6, 113.1, 83.2, 83.1, 80.1, 56.8; GC-MS m/z (%) calcd for $\text{C}_{12}\text{H}_{10}\text{O}_2$ 186.1, found 186.0 (100, $[\text{M}]^+$), 171.0 (16, $[\text{M}-\text{CH}_3]^+$).

Synthesis of linear OPE 217

To a 100 mL round-bottomed flask was added a solution of compound **205** (600 mg, 9.80×10^{-4} mol), $\text{Pd}(\text{PPh}_3)_2\text{Cl}_2$ (34.0 mg, 4.84×10^{-5} mol), CuI (18.6 mg, 9.78×10^{-5} mol) in 60 mL of dry THF (70 mL). It was cooled to -78°C , evacuated under vacuum and purged with N_2 for several times to remove O_2 as much as possible. To this constantly stirred mixture, 1,4-bis(ethynyl)-2,5-bis(methoxy)benzene (**216**) (75.0 mg, 4.03×10^{-4} mol) in Et_3N (15 mL) was added dropwise for 0.5 h. The mixture was then stirred at room temperature overnight and solvent was removed. The resulting solid mass was dissolved in CHCl_3 and washed with H_2O for several times. The organic layer was dried over MgSO_4 , filtered and solvent was removed to dryness and then flash chromatographed (hexanes/ CHCl_3 , 5:1) to yield compound **217** (315 mg, 2.59×10^{-4} mol, 68%) as deep-yellow solid. IR (neat): 2921, 2850, 2155, 1511, 1495, 1386, 1274 cm^{-1} ; ^1H NMR (500 MHz, CDCl_3): δ 7.04 (s, 2H), 7.01 (s, 2H), 6.97 (s, 2H), 4.04-3.99 (m, 8H), 3.91 (s, 6H), 1.91-1.80 (m, 8H), 1.54-1.38 (m, 8H), 1.31-1.19 (m, 48H), 0.92-0.88 (m, 12H), 0.29 (s, 18H); ^{13}C NMR (125 MHz,

CDCl₃): δ 154.6, 154.3, 153.9, 117.7, 117.3, 116.7, 116.0, 114.7, 114.3, 114.0, 113.9, 112.8, 101.6, 100.5, 99.8, 92.1, 91.7, 70.0, 69.9, 56.8, 32.0, 30.1, 30.0, 29.85, 29.83, 29.8, 29.70, 26.5, 25.7, 14.5; MALDI-TOF MS (dithranol as the matrix) m/z calcd for C₇₄H₁₁₄O₆Si₂ 1154.82, found 1154.42 [M]⁺.

Synthesis of deprotected OPE 218

A solution of compound **217** (100 mg, 8.66×10^{-5} mol) in dry THF (5 mL) was taken in a 100 mL round-bottomed flask. To this was then added dropwise a dilute solution of TBAF (0.10 mL of 1 M solution) in THF (5 mL) and then sonicated for 5 min at 0-5 °C. The reaction mixture was diluted with H₂O, and extracted with CHCl₃. The organic layer was dried over MgSO₄, filtered and solvent was removed to give compound **218** (80.0 mg, 7.92×10^{-5} mol, 91%) as deep-yellow solid. IR (neat): 3289, 2921, 2851, 2104, 1601, 1495, 1466, 1385, 1222 cm⁻¹; ¹H NMR (500 MHz, CDCl₃): δ 7.05 (s, 2H), 7.04 (s, 2H), 7.0 (s, 2H), 4.03 (t, $J = 6.3$ Hz, 8H), 3.92 (s, 6H), 3.37 (s, 2H), 1.89-1.81 (m, 12H), 1.56-1.47 (m, 8H), 1.38-1.27 (m, 48H), 0.92-0.88 (m, 12H); ¹³C NMR(125 MHz, CDCl₃): δ 154.6, 154.3, 153.9, 118.2, 117.3, 116.1, 115.0, 114.1, 113.1, 91.9, 91.7, 80.4, 77.7, 77.4, 77.2, 70.1, 70.0, 32.3, 30.0, 29.9, 29.80, 29.6, 26.3, 23.08, 23.07, 14.51; MALDI-TOF MS (dithranol as the matrix) m/z calcd for C₆₈H₉₈O₆ 1011.50, found 1011.91 [M]⁺.

Synthesis of G1-H functionalized OPE 219

To a 250 mL round-bottomed flask were added a solution of compound **182h** (26.0 mg, 7.53×10^{-5} mol), CuSO₄ (2.00 mg, 8.40×10^{-6} mol), (+) sodium L-ascorbate (11.0 mg 5.51×10^{-5} mol) in 70 mL of THF/DMF (1:1). This was then cooled to -78 °C and evacuated under vacuum. The flask was purged with N₂ and 2 mL of Et₃N

was added with the help of a syringe. To this constantly stirred mixture, a solution of compound **218** (28.0 mg, 2.76×10^{-5} mol) in THF (10 mL) was slowly added for 0.5 h and then stirred at room temperature overnight. The solvent (THF) was removed and the resulting solid mass was dissolved in CHCl_3 and washed with H_2O for several times. The organic layer was dried over MgSO_4 , filtered and evaporated to dryness and finally column chromatographed to yield compound **219** (92.0 mg, 5.43×10^{-5} mol, 67%) as a deep yellowish-green oil. IR (neat): 2923, 2854, 2099, 1595, 1464, 1373, 1164, 1155 cm^{-1} ; ^1H NMR (500 MHz, CDCl_3): δ 8.04 (s, 1H), 7.98 (s, 1H), 7.40-7.31 (m, 20H, dendritic peripheral Ar-H), 7.15-7.05 (m, 6H, oligomer Ar-H), 6.60-6.54 (m, 6H, dendrimeric core Ar-H), 5.60-5.02 (m, 12H, benzylic H), 4.96-3.77 (m, O- CH_2 , 8H), 3.68 (s, 6H), 2.07-1.39 (m, 16H), 1.36-1.26 (m, 48H), 0.92-0.88 (m, 12H); ^{13}C NMR (125 MHz, CDCl_3): 160.8, 160.6, 154.3, 137.0, 136.8, 129.0, 128.5, 127.94, 127.9, 114.3, 107.4, 100, 70.6, 56.9, 32.3, 30.0, 29.8, 29.7, 29.6, 26.3, 23.09, 23.07, 14.5; MALDI-TOF MS (dithranol as the matrix) m/z calcd for $\text{C}_{110}\text{H}_{136}\text{O}_{10}\text{N}_6$ 1702.29, found 1703.87 $[\text{M} + \text{H}]^+$.

Synthesis of G2-H functionalized OPE 221

To a 250 mL round-bottomed flask was added a solution of compound **183h** (96.0 mg, 1.25×10^{-4} mol), CuSO_4 (3.00 mg, 1.27×10^{-5} mol), and (+) sodium L-ascorbate (18.8 mg, 9.40×10^{-5} mol) in 80 mL of THF/DMF (1:1). This was then cooled to -78 $^\circ\text{C}$, evacuated under vacuum and purged with N_2 and 2 mL of Et_3N was added to it. To this constantly stirring mixture, a solution of compound **218** (48.0 mg, 4.74×10^{-5} mol) in THF (5 mL) was added for 0.5 h and stirred at room temperature overnight and the solvent (THF) was removed. The resulting solid mass was dissolved

in CHCl_3 and washed with H_2O for several times. The organic layer was evaporated to dryness and column chromatographed to afford compound **221** (84.7 mg, 3.31×10^{-5} mol, 70%) as a deep yellowish-green oil. IR (neat): 2974, 2929, 2100, 1595, 1478, 1392, 1162 cm^{-1} ; ^1H NMR (500 MHz, CDCl_3): δ 8.06 (s, 1H), 7.97 (s, 1H), 7.44-7.34 (m, 40H), 7.08-7.03 (m, 6H), 6.70-6.54 (m, 18H, Ar-H) 5.52-4.28 (m, 28H, benzylic *H*), 4.23-3.99 (m, 8H), 3.94 (s, 6H), 1.66-1.39 (m, 16H), 1.38-1.25 (m, 48H), 0.91-0.86 (m, 12H); ^{13}C NMR (125 MHz, CDCl_3): δ 160.6, 160.5, 139.5, 138.1, 137.14, 137.12, 129.0, 128.4, 128.0, 127.96, 107.1, 102.7, 102.1, 70.53, 70.51, 70.43, 55.2, 32.33, 32.31, 30.0, 29.7, 26.5, 23.11, 23.09, 14.5; MALDI-TOF MS (dithranol as the matrix) m/z calcd for $\text{C}_{166}\text{H}_{184}\text{O}_{18}\text{N}_6$ 2551.3, found 2552.0 $[\text{M}]^+$.

Synthesis of G1-C10 functionalized OPE **220**

To a 250 mL round-bottomed flask were added a solution of **182d** (50.0 mg, 5.15×10^{-5} mol), CuSO_4 (2.0 mg, 8.4×10^{-6} mol), and (+)sodium L-ascorbate (10.2 mg, 5.14×10^{-5} mol) in 80 mL of THF/DMF (1:1). The flask was cooled to -78°C , evacuated under vacuum and purged with N_2 and 2 mL of Et_3N was added to it. To this constantly stirred mixture, a solution of **218** (26.0 mg, 2.57×10^{-5} mol) in CH_2Cl_2 (5 mL) was slowly added for 0.5 h and then stirred at room temperature overnight. The solvent (THF) was removed under vacuum. The resulting solid mass was dissolved in CHCl_3 and washed with water for several times and evaporated to dryness and flash chromatographed to afford compound **220** (49.4 mg, 1.67×10^{-5} mol, 72%) as a deep yellowish-green oil. IR (neat): 2923, 2854, 2099, 1595, 1463, $1164, 1054 \text{ cm}^{-1}$; ^1H NMR (500 MHz, CDCl_3): 8.07 (s, 1H), 7.98 (s, 1H), 7.07-7.01 (m, 6H), 6.57-6.60 (m, 18H, dendritic Ar-H), 5.60-4.88 (s, 12H, benzylic *H*), 4.04-3.88

(m, 27H), 1.70-1.07 (m, 192H), 0.92-0.86 (m, 36H); ^{13}C NMR (125 MHz, CDCl_3): δ 161.0, 160.7, 139.2, 138.0, 107.6, 106.1, 102.3, 101.3, 70.6, 68.5, 55.3, 32.3, 29.8, 29.74, 29.72, 29.7, 23.1, 14.51, 14.49; MALDI-TOF MS (dithranol as the matrix) m/z calcd for $\text{C}_{190}\text{H}_{296}\text{O}_{18}\text{N}_6$ 2950.24, found 2950.0 $[\text{M}]^+$.

Synthesis of G2-C10 functionalized OPE 222

To a 250 mL round-bottomed flask was added a solution of compound **183d** (140 mg, 6.93×10^{-5} mol), CuSO_4 (2.00 mg, 8.40×10^{-6} mol), and (+) sodium L-ascorbate (13.7 mg, 6.91×10^{-5} mol) in 80 mL of THF/DMF (1:1). The flask was cooled to -78°C , evacuated under vacuum, and purged with N_2 for several times and 2 mL of Et_3N was added to it. To this constantly stirred mixture, a solution of compound **218** (35.0 mg, 3.46×10^{-5} mol) in THF (5 mL) was slowly added for 0.5 h and was then stirred at room temperature overnight and solvent (THF) was removed. The resulting solid mass was dissolved in CHCl_3 and washed with H_2O for several times. The organic layer was dried over MgSO_4 , filtered and evaporated to dryness and column chromatographed to yield compound **222** (103 mg, 2.04×10^{-5} mol, 59%) as a deep yellowish-green oil. IR (neat): 2923, 2854, 2099, 1595, 1453, 1162, 1054 cm^{-1} ; ^1H NMR (500 MHz, CDCl_3): δ 8.08 (s, 1H), 7.99 (s, 1H), 7.11-6.45 (m, 6H), 6.71-6.44 (m, 42H, Ar-H), 5.54-4.30 (m, 28H, benzylic protons), 4.09-3.81 (m, 46H), 1.83-1.77 (m, 40H, O- CH_2 H), 1.51-1.45 (m, 40H), 1.38-1.32 (m, 240H), 0.94-0.91 (t, $J = 7.1$ Hz, 60H); ^{13}C NMR (125 MHz, CDCl_3): δ 160.96, 160.95, 160.9, 160.6, 139.4, 139.3, 139.28, 139.2, 138.1, 138, 107.64, 107.6, 106.8, 106.2, 106.1, 102.2, 102.1, 101.3, 101.27, 70.6, 70.5, 68.5, 32.3, 30.1, 30.0, 29.83, 29.8, 29.7, 26.5, 23.1, 14.5; MALDI-TOF MS (dithranol as the matrix) m/z calcd for $\text{C}_{326}\text{H}_{504}\text{O}_{34}\text{N}_6$

5047.79, found 5047.45 [M]⁺.

Synthesis of 1,3,5-tris(silylethynyl)benzene (**224**)

To a 100 mL round-bottomed flask was added a mixture of 1,3,5-tribromobenzene (**223**) (1.00 g, 3.20 mmol), Pd(PPh₃)₂Cl₂ (66.9 mg, 9.50 × 10⁻⁵ mol), CuI (181.0 mg, 95.2 × 10⁻⁵ mol) in 60 mL of dry Et₃N/toluene (1:1). The round-bottomed flask was evacuated under vacuum and purged with N₂ for several times. To this constantly stirred mixture, a solution of TMSA (4.68 g, 47.6 mmol) in Et₃N (3 mL) was slowly added for 0.5 h and then stirred at 50-55 °C overnight. After the completion of reaction, the solvent was evaporated off to yield a deep-yellow mixture, which was flash chromatographed (hexanes/CH₂Cl₂, 15:1) to afford compound **224** (1.06 g, 2.89 mmol, 92%) as pale-yellow crystalline solid. IR (neat): 2959, 2899, 2163, 1579, 1411, 1250, 1110 cm⁻¹; ¹H NMR (500 MHz, CDCl₃): δ 7.51 (s, 3H), 0.25 (s, 27H); ¹³C NMR (125 MHz, CDCl₃): δ 135.3, 124.0, 103.5, 96.0, 0.4; GC-MS *m/z* calcd for C₂₁H₃₀Si₃ 366.0, found 366.0 [M]⁺.

Synthesis of 1,3,5-tris(ethynyl)benzene (**225**)

A solution of trimer **224** (150 mg, 4.10 × 10⁻⁴ mol) in 30 mL of THF/MeOH (1:1) was added in a 100 mL round-bottomed flask. To this was then added K₂CO₃ (226 mg, 1.64 mmol) and stirred overnight. After completion of reaction, the solvent was removed. The resulting solid mass was dissolved in CHCl₃ and washed with H₂O. The organic layer was dried over MgSO₄, filtered and solvent was removed to yield compound **225** (61.0 mg, 4.03 × 10⁻⁴ mol, 98.6%) as a pale-yellow solid. IR (neat): 3296, 3278, 3064, 2957, 2924, 2871, 2111, 1580, 1558, 1363 cm⁻¹; ¹H NMR (500 MHz, CDCl₃): δ 7.49 (s, 3H), 3.03 (s, 3H); ¹³C NMR (125 MHz, CDCl₃): δ 136.0, 123.3,

82.0, 79.1.

Synthesis of compound 226

To a 250 mL round-bottomed flask were added a solution of **205** (457 mg, 7.46×10^{-4} mol), Pd(PPh₃)₂Cl₂ (8.90 mg, 1.26×10^{-5} mol), and CuI (4.05 mg, 2.36×10^{-5} mol) in 100 mL of dry THF/Et₃N (1:1) at 0 °C. The flask was evacuated under vacuum and purged with N₂ for several times. To this constantly stirred mixture, a solution of 1,3,5-tris(ethynyl)benzene (**225**) (32.0 mg, 2.13×10^{-4} mol) in Et₃N (3 mL) was added slowly for 0.5 h, followed by the addition of 5 drops of DBU. The mixture was stirred at room temperature overnight. After completion of the reaction, the solvent was evaporated off to give a deep-yellow mixture, which after flash chromatography (hexanes/CH₂Cl₂, 5:1) yielded compound **226** (291.0 mg, 1.81×10^{-4} mol, 85%) as a pale-yellow solid. IR (neat): 2923, 2854, 2153, 1579, 1498, 1213 cm⁻¹; ¹H NMR (500 MHz, CDCl₃): δ 7.64 (s, 3H), 6.98 (s, 3H), 6.97 (s, 3H), 4.04-3.97 (m, 12H), 1.89-1.81 (m, 12H), 1.54-1.42 (m, 12H), 1.35-1.26 (m, 72H), 0.91-0.85 (m, 18H), 0.30 (s, 27H); ¹³C NMR (125 MHz, CDCl₃): δ 154.6, 154.0, 134.3, 124.6, 117.8, 117.4, 114.6, 114.2, 101.5, 100.7, 87.5, 70.1, 70.0, 32.3, 30.02, 30.00, 29.96, 29.81, 29.75, 29.72, 26.5, 23.1, 23.07, 14.51, 14.50, 0.4; MALDI-TOF MS (dithranol as the matrix) *m/z* calcd for C₁₀₅H₁₆₅O₆Si₃ 1607.69, found 1606.18 [M]⁺.

Synthesis of deprotected OPE 227

A solution of oligomer **226** (55.0 mg, 3.42×10^{-5} mol) in dry THF (5 mL) was taken in a 100 mL round-bottomed flask. To this was added dropwise a dilute solution of TBAF (0.03 mL of 1 M solution) in THF (5 mL) and then sonicated for 5 min at 0-5 °C. The reaction mixture was diluted with water and was extracted with CHCl₃.

The organic layer was dried over MgSO_4 , filtered and solvent was removed to give compound **227** (44.5 mg, 3.20×10^{-5} mol, 94%) as deep-yellow solid. IR (neat): 3313, 2923, 2851, 2213, 2106, 1603, 1579, 1387, 1214 cm^{-1} ; ^1H NMR (500 MHz, CDCl_3): δ 7.7 (s, 3H), 7.01 (s, 3H), 7.0 (s, 3H), 4.03 (t, $J = 6.6$ Hz, 12H), 3.4 (s, 3H), 1.89-1.82 (m, 12H), 1.58-1.48 (m, 12H), 1.41-1.21 (m, 72H), 0.92-0.84 (m, 18H); ^{13}C NMR (125 MHz, CDCl_3): δ 154.5, 154.0, 134.4, 124.6, 118.3, 117.4, 114.6, 113.5, 93.6, 87.3, 70.12, 70.1, 30.02, 30.0, 29.8, 29.73, 29.70, 29.6, 26.5, 26.3, 23.09, 23.07, 14.51, 14.50; MALDI-TOF MS (dithranol as the matrix) m/z calcd for $\text{C}_{96}\text{H}_{138}\text{O}_6$ 1388.12, found 1387.27 $[\text{M}]^+$.

Synthesis of **228**

To a round-bottomed flask were added a solution of compound **205** (120 mg, 1.96×10^{-4} mol), $\text{Pd}(\text{PPh}_3)_2\text{Cl}_2$ (4.00 mg, 5.60×10^{-6} mol), and CuI (1.00 mg, 5.20×10^{-6} mol) in dry Et_3N (60 mL) and was cooled to -78 $^\circ\text{C}$. The flask was evacuated and purged with N_2 for several times. To this constantly stirred mixture, compound **227** (77.7 mg, 5.60×10^{-5} mol) in Et_3N (3 mL) was added slowly for 0.5 h, followed by addition of 5 drops of DBU. The reaction mixture was warmed slowly and stirred at room-temperature for overnight. After completion of the reaction, the solvent was evaporated off to give a deep yellow mixture, which was flash chromatographed (hexanes/ CH_2Cl_2 , 4:1) to afford compound **228** (129.0 mg, 4.53×10^{-4} mol, 81%) as pale-yellow solid. IR (neat): 2923, 2853, 2209, 2152, 1579, 1505, 1387, 1157 cm^{-1} ; ^1H NMR (500 MHz, CDCl_3): δ 7.65 (s, 3H), 7.03-6.97 (m, 12H), 4.07-3.86 (m, 24H), 1.90-1.81 (m, 24H), 1.55-1.49 (m, 24H), 1.37-1.28 (m, 144H), 0.91-0.84 (m, 36H), 0.29 (s, 27H); ^{13}C NMR (125 MHz, CDCl_3): δ 154.6, 154.2, 153.9, 153.8, 135.7, 135.6, 128.0,

124.6, 117.5, 115.1, 114.9, 114.2, 114.0, 101.6, 100.5, 93.6, 91.8, 87.6, 70.2, 70.12, 70.1, 69.9, 53.8, 32.3, 30.02, 30.00, 29.8, 29.7, 26.5, 23.1, 23.07, 14.5, 0.4; MALDI-TOF MS (dithranol as the matrix) m/z calcd for $C_{189}H_{294}O_{12}Si_3$ 2842.61, found 2842.25 $[M]^+$.

Chapter 4

Synthesis and Properties of Electroactive Polyynes

4.1 Introduction

Carbynes are a hypothetical 1-D carbon allotrope, although their existence has been a matter of debate for more than 100 years.¹²² Naturally occurring carbynes may or may not exist, but various defined length oligomers like polyynes/oligoynes have close structural similarities to those of carbynes. For example, like carbynes, they are also chain-like molecules and have continuous connection of acetylenic units. It is believed that the properties of carbynes could be understood by extrapolating the spectroscopic, crystallographic, and photophysical data of a series of structurally related polyynes.¹²³

Polyynes are a group of organic compounds having alternating single and triple bonds, which are distinct from other organic chains by their structural rigidity.

Polynes have been detected in outer space for a long time. For example, the octatetraynyl and hexatriynyl radicals were detected in interstellar molecular clouds in the early 1970s (see Figure 4.1).¹²⁴

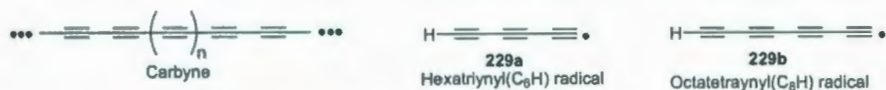


Figure 4.1: Structure of carbynes and polyynyl radicals **229**.

Polynes are *sp*-hybridized carbon oligomers having interesting optical, physical and electronic properties. Their one-dimensional molecular wire behavior, unique solid-state reactivities, and rich optoelectronic activities are particularly useful for the development of thin-film transistors (TFTs), organic light-emitting diodes (OLEDs), and non linear optical (NLO) media. Moreover, an important feature of carbyne chemistry lies in its ability to be transformed into diamond under high-pressure and temperature.¹²² Unlike graphite, polyynes can form diamond structures without catalyst, resulting in ultra-pure diamond materials.¹²²

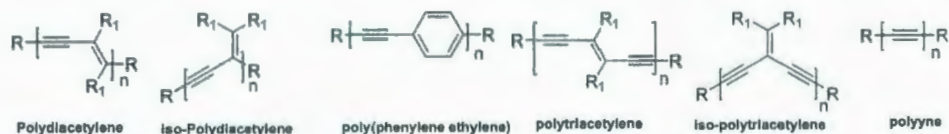


Figure 4.2: Common oligo-/polymeric systems based on acetylenic building blocks.

One way that property optimization of organic materials could be obtained is through the synthesis and study of some series of structurally related oligomers, where the degree of conjugation is controlled by the number of repeating units. For example, in the other types of π -conjugated oligomers, structure-activity relationships are

usually elucidated by studying the trends in HOMO-LUMO gap variation. Acetylenic units offer an important building block to assemble various linear conjugated polymeric frameworks as shown in Figure 4.2. By varying the substituents and spacer units in these structures, interesting molecular properties could be discovered.

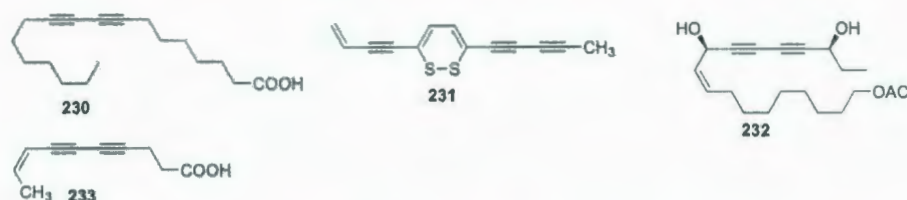


Figure 4.3: Examples of naturally occurring polyynes.

Synthetic chemists have been attempting to synthesize “carbyne-type” chain-like molecules for around 125 years.¹²² The credit for the first attempt to synthesize these chain-like molecules goes to A. von Baeyer back in 1885. Unfortunately, following step-wise synthetic procedures, he was not able to isolate the product “tetraacetylene” due to its instability. This critical problem led Baeyer to develop a “strain theory”, in which he postulated that it was impossible to make chain-like carbon. Baeyer’s reputation effectively dampened the interest of other synthetic chemists to make polyynes for few decades. But soon some medicinally important natural polyynes were isolated and characterized (from plant and fungi).^{122,123} For example, the acetylenic fatty acid **230** (see Figure 4.3) having anti-cancer properties, was isolated from the legume *Paramacrolobium caeruleum*.¹²³ The plants containing the pigment thiarubrine **231** have been used by people for treating skin infections and intestinal parasites in remote area of Africa and Canada. Polyne **232** was obtained from the bark and roots of Devil’s club, and has been used by the Red-Indians to

treat a variety of ailments. Polyynes **233**, obtained from the soldier beetle, has also shown medicinal importance.¹²³

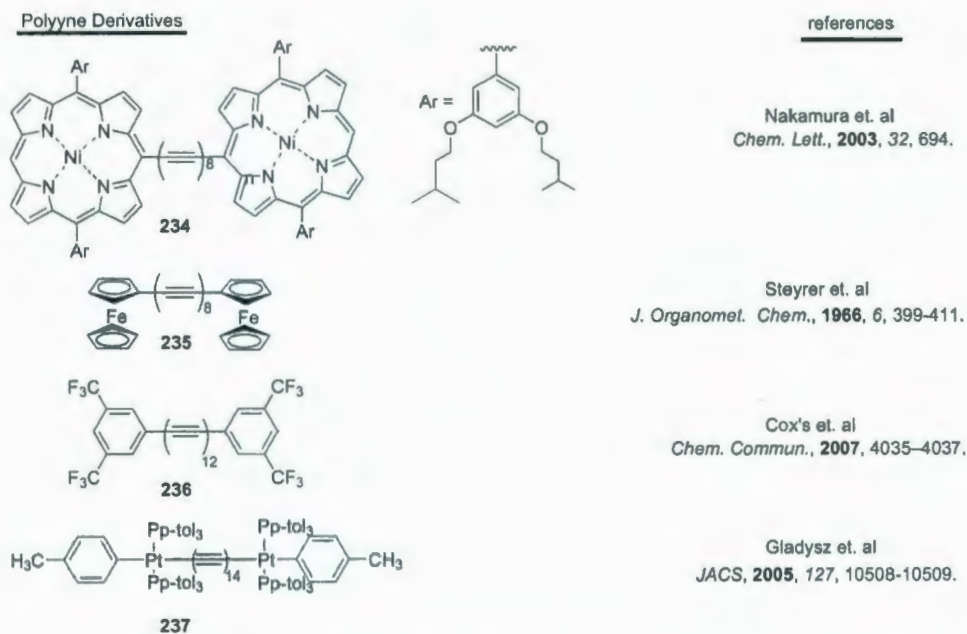


Figure 4.4: Some interesting endcapped polyynes synthesized by various groups.

At this point, synthetic chemists were greatly stimulated by the discoveries of these medicinally important, naturally occurring polyynes with a hope to replicate their syntheses on the industrial scale. Over the past 50-60 years, a significant number of polyynes have been synthesized (see Figure 4.4). In most of the cases, polyynes having 2 to 12 acetylenic units have been obtained; however, longer homolog could only be identified by UV-Vis and IR-spectroscopy due to their kinetic instability.¹²⁵ The recent trends of extended polyynes syntheses focus mainly on two goals: (a) to fully explore the properties of polyynes by modern analytical techniques, and (b) to study polyynes with a broad range of end-functionality. These continued

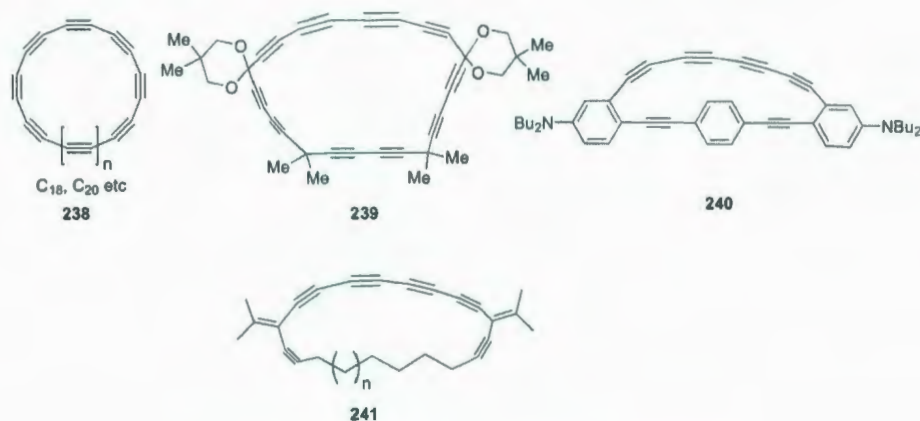
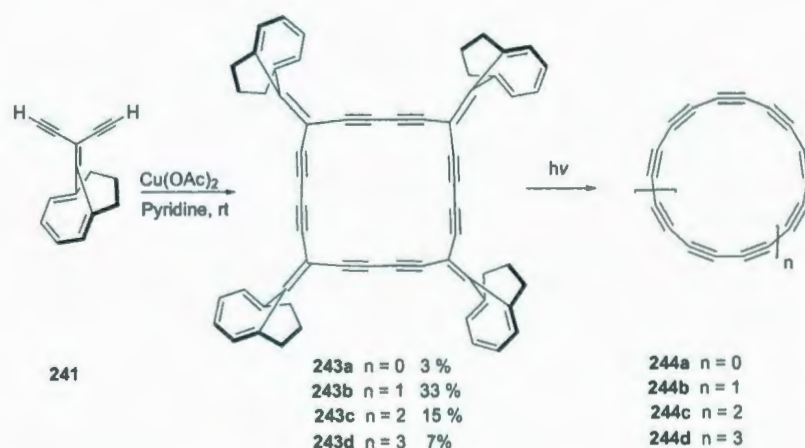


Figure 4.5: Examples of strained polyynes.

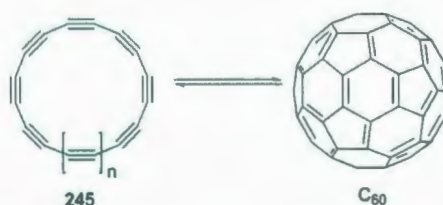
efforts have resulted in the synthesis and property elucidation of a diverse range of polyyne structures; for example iodine, chalcogen, tetrathiafulvalene (TTFs), various metals, porphyrins, polyether, and dendrimer end-capped polyynes are among a few of the examples (see Scheme 4.4). The credit for synthesis of the longest polyyne so far goes to Gladysz *et al.* (see Figure 4.4). Some structurally diverse “strained polyynes”, the synthesis of which poses further challenge, have also been realized (see Scheme 4.5).¹²⁶ Among these “strained polyyne“, cyclic polyynes deserve some special category (see Scheme 4.1). The discovery of C₆₀ as a stable carbon allotrope is a milestone in polyyne chemistry, as strained cyclic polyynes were supposed to be a possible intermediate in the formation of [60]fullerene (see Scheme 4.5).^{125,126}

Among various ways to synthetically assemble polyyne chains, the two most popular methods are Cu(I/II)-catalyzed oxidative homocoupling (such as, Eglinton, Glaser, Hay coupling) and carbene/carbenoid rearrangement (see Scheme 4.3).¹²⁵

Tetrathiafulvalene (TTF) is a stable and reversible two electron donor system (see Figure 4.6) and has been the subject of enormous research interest to mate-

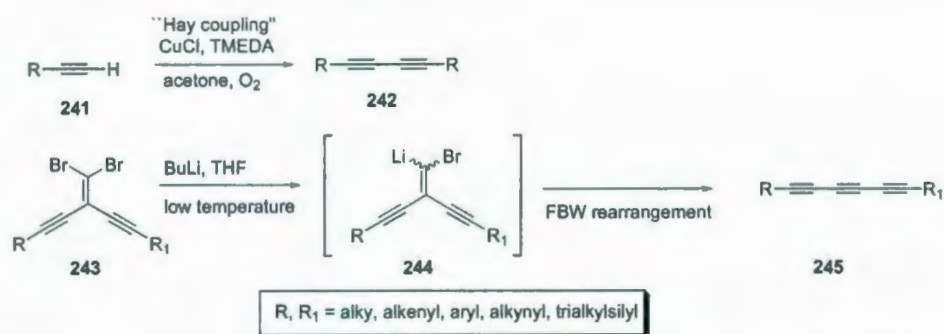


Scheme 4.1: Tobe's synthesis of cyclo[n]carbons (**243ad**) by laser-desorption time-of-flight.



Scheme 4.2: Cyclic polyynes were supposed as intermediates of [60] fullerenes.

rials chemist for more than four decades.¹²⁷ They have application potentials in organic conductors, charge-transfer complexes, supramolecular chemistry, and various molecular switches and locks, to name a few. Materials chemists are interested in further extending the conjugation in TTF, since π -extended TTF analogues (exTTFs) have the potentials to produce exceptional nonlinear optical, photophysical and electrochemical properties. In recent years, the combination of TTF with various linear π -conjugated oligomers has been a topical research. Growing efforts have been made towards the synthesis of new extended TTFs and D- π -A dyads based on acetylenic spacers in order to exploit their unique optical properties and redox



Scheme 4.3: Two polyynes synthetic approaches via Hay coupling and a modified Fritsch-Buttenberg-Wiechell (FBW) rearrangement.

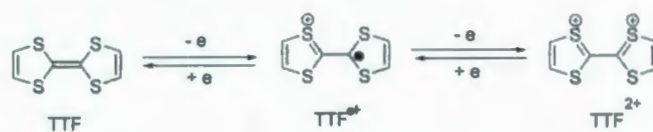


Figure 4.6: Sequential single-electron transfers on TTF.

behavior.

4.2 Objectives of the Project

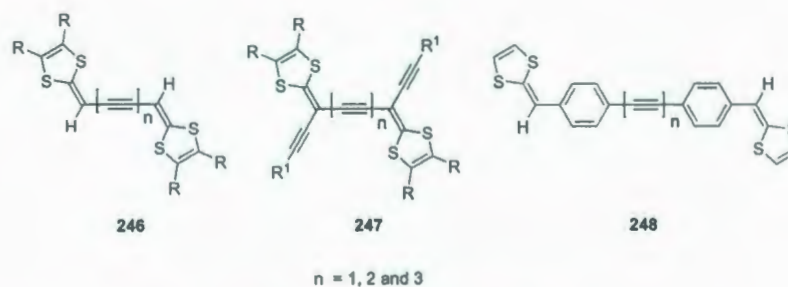


Figure 4.7: Polyynes-extended TTF analogues.

The incorporation of acetylene based π -spacers into TTF could offer a versatile approach to attain novel TTF-based conjugated oligomeric systems, which could

eventually lead to new functional materials. It was therefore planned in the beginning of this project to prepare various polyynes-extended TTFs for the study of their molecular properties. In this context, TTF-polyynes **246** and **247** (see Scheme 4.7), have already been investigated by Gorgues, Diederich, Nielsen, and others.¹²⁸⁻¹³⁰ However, analogous systems, such as **248**, have not been given any attention, although the structure of **248** represents an interesting TTF-acetylene hybrids with versatile reactivities and molecular properties. First, aryl-substituted dithiafulvenes have been reported to readily dimerize upon oxidation to produce electroactive TTF vinylogue (TTFV) products.^{131,132} Second, the polyynes units can undergo topochemical polymerization under various conditions, such as heat, light, pressure and γ -ray irradiation.¹³³ In this chapter, polyynes derivatives (**249-251**) endcapped with strong electron-donating groups (see Figure 4.8) were targeted in order to address the issues mentioned above.

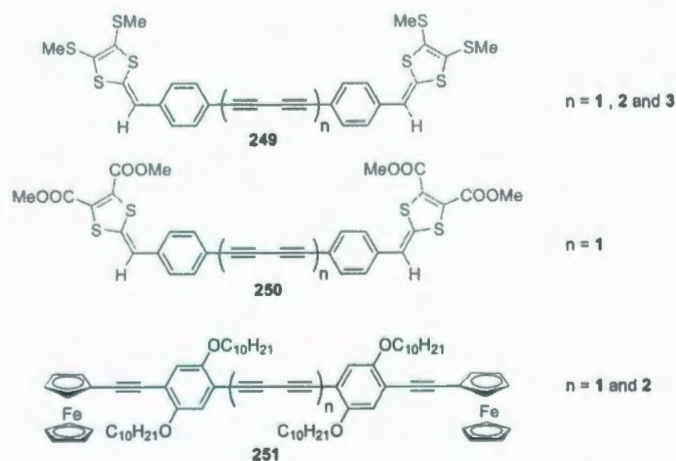
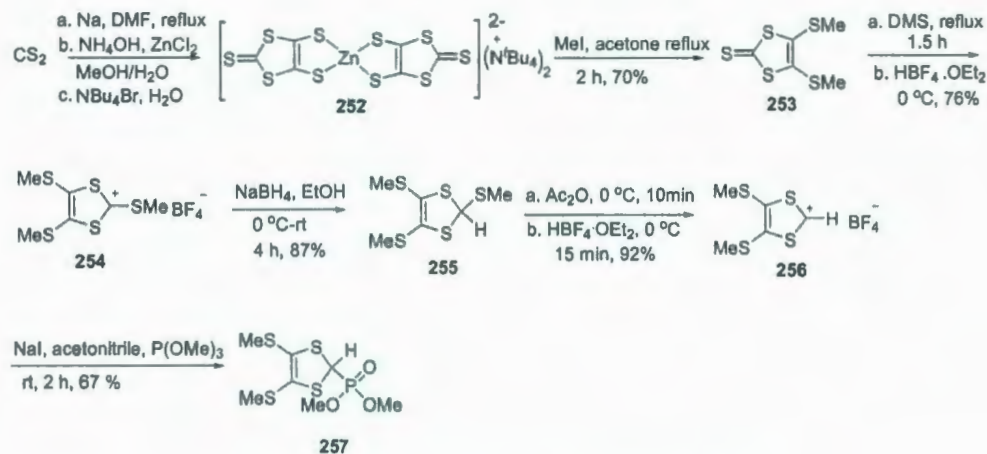


Figure 4.8: The synthesized electro-active polyynes **249-251**.

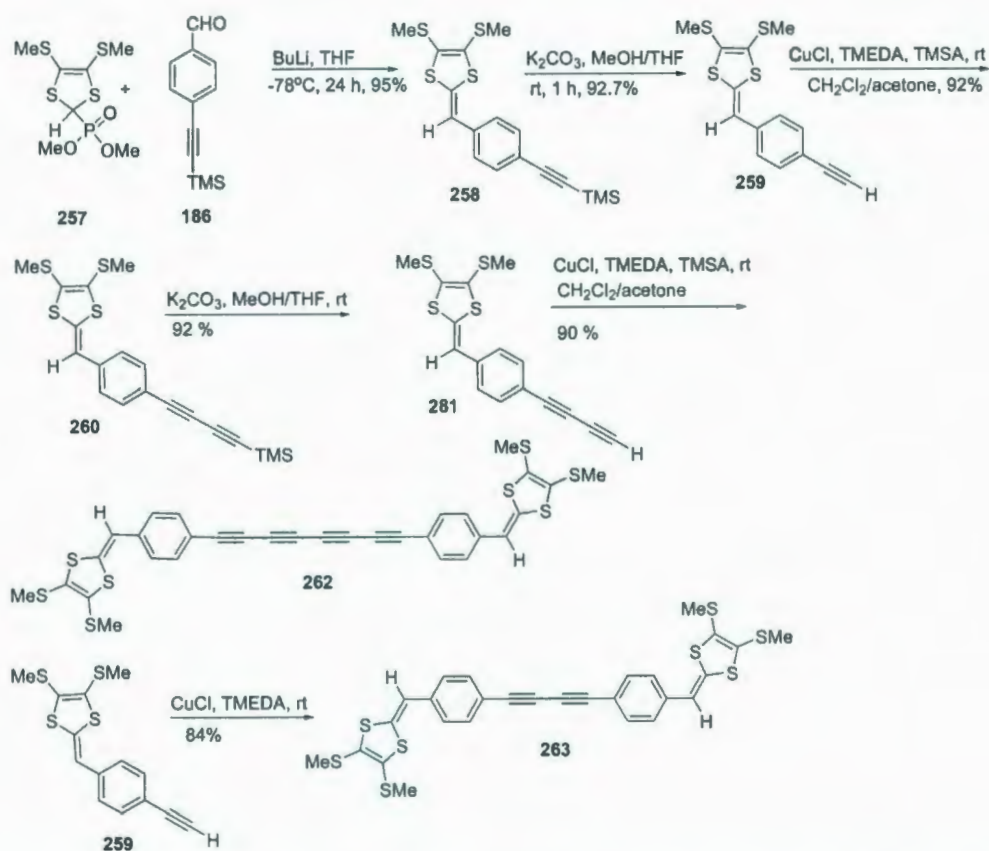
4.3 Results and Discussions

4.3.1 Synthesis



Scheme 4.4: Synthesis of phosphonate **257**.

The dithiafulvenyl (DTF) endcapped polyynes were synthesized mainly by iterative Pd-catalyzed cross-coupling and Cu(I)-catalyzed homo-coupling reactions. Different synthetic strategies were followed to prepare different polyynes. For example, to obtain polyyne **249**, the synthesis of an important precursor, *S*-methyl phosphonate **257** was conducted following the literature procedure.¹¹⁸ As shown in Scheme 4.4, the reaction of finely-cut metallic sodium with dry CS₂ followed by immediate zinc chelation with ZnCl₂ produced a deep-red dithiolate zincate salt **252**, which was methylated by MeI in refluxing acetone to yield *S*-methyl thione **253** as a deep-yellow solid. Compound **253** was subjected to another methylation reaction by refluxing in neat dimethyl sulfate, followed by slow addition of tetrafluoroboric acid-etherate complex to produce salt **254**, which was subsequently reduced by NaBH₄ in

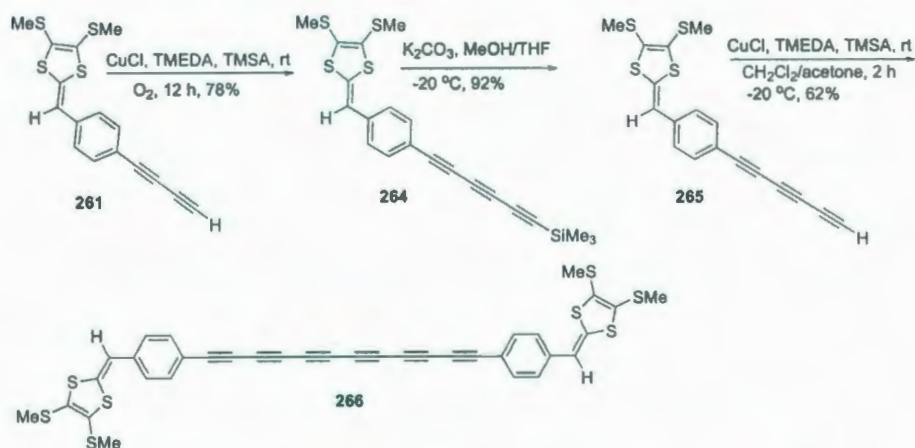


Scheme 4.5: Synthesis of dithiafulvenyl (DTF) endcapped tetrayne **262** and diyne **263**.

absolute ethanol to afford **255**. Compound **255** was then converted to phosphonate **257** in two steps. First, dissolution of **255** in Ac₂O at 0 °C, followed by slow addition of tetrafluoroboric acid-etherate complex produced an unstable salt **256**. Intermediate **256** was immediately treated with a NaI solution in dry acetonitrile, and then subjected to slow addition of P(OMe)₃, producing *S*-methyl phosphonate **257** as a deep-red solid.

TMSA benzaldehyde **186** was synthesized through a Pd-catalyzed Sonogashira reaction in 88% yield (see Chapter 2). Horner-Emmons-Wadsworth (HWE) reaction

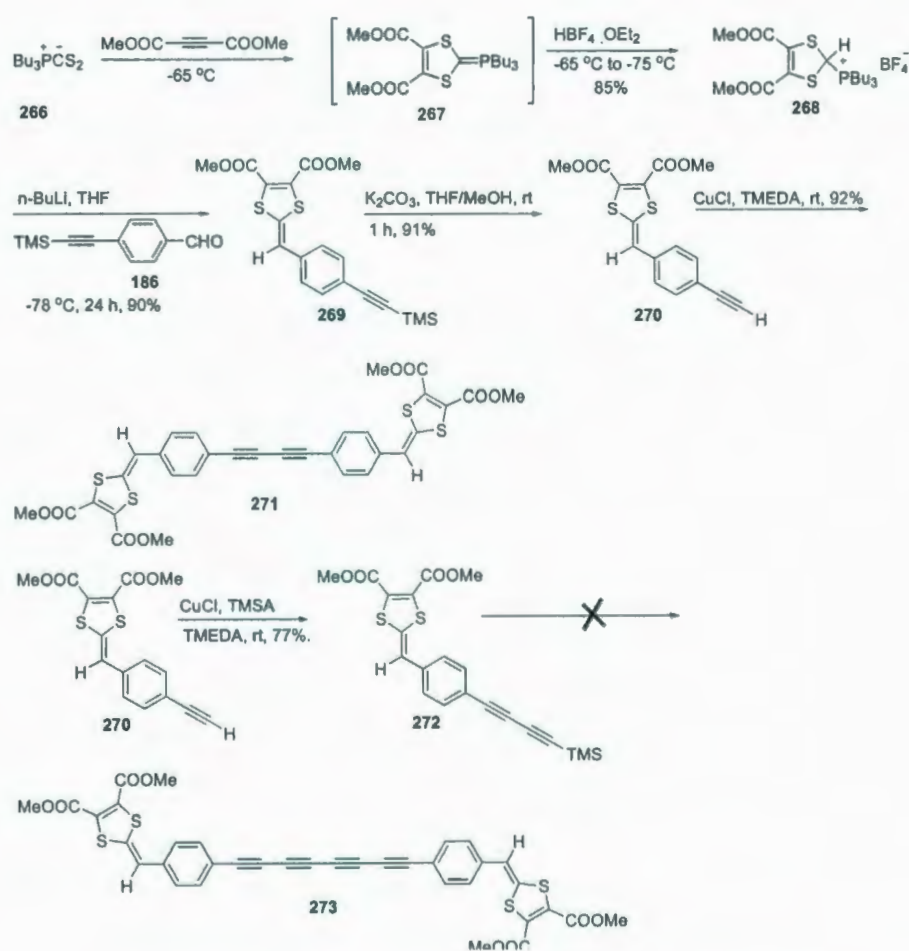
of **186** with *S*-methyl phosphonate at $-78\text{ }^{\circ}\text{C}$ in the presence of *n*-BuLi gave **258** in 95% yield (see Scheme 4.5). The aryl-substituted dithiafulvene **258** was desilylated with K_2CO_3 to afford **259** in 93% yield. Compound **259** was then subjected to a Hay coupling with excess TMSA to give diyne **260** in 92% yield. Compound **260** was deprotected with K_2CO_3 to get **261**. Finally a homocoupling reaction of **261** produced compound **262** in 90% yield. In the same fashion, dithiafulvenyl endcapped diyne **263** was prepared in 84% yield using another Hay coupling.



Scheme 4.6: Synthesis of DTF endcapped hexaynes **266**.

The hexayne-centered exTTF **265** was also prepared using the same strategy applied in the synthesis of diyne and tetrayne (see Scheme 4.5). First diyne **261** was reacted with TMSA under Hay coupling conditions to provide silyl protected triyne **264**. The silyl group was deprotected at low temperature using K_2CO_3 , and the resulting terminal alkyne **265** was immediately homocoupled under the catalysis of Cu(I) to afford hexayne **265** in 62% yield.

In view of the tedious and costly synthesis of methylthiol-substituted dithiole

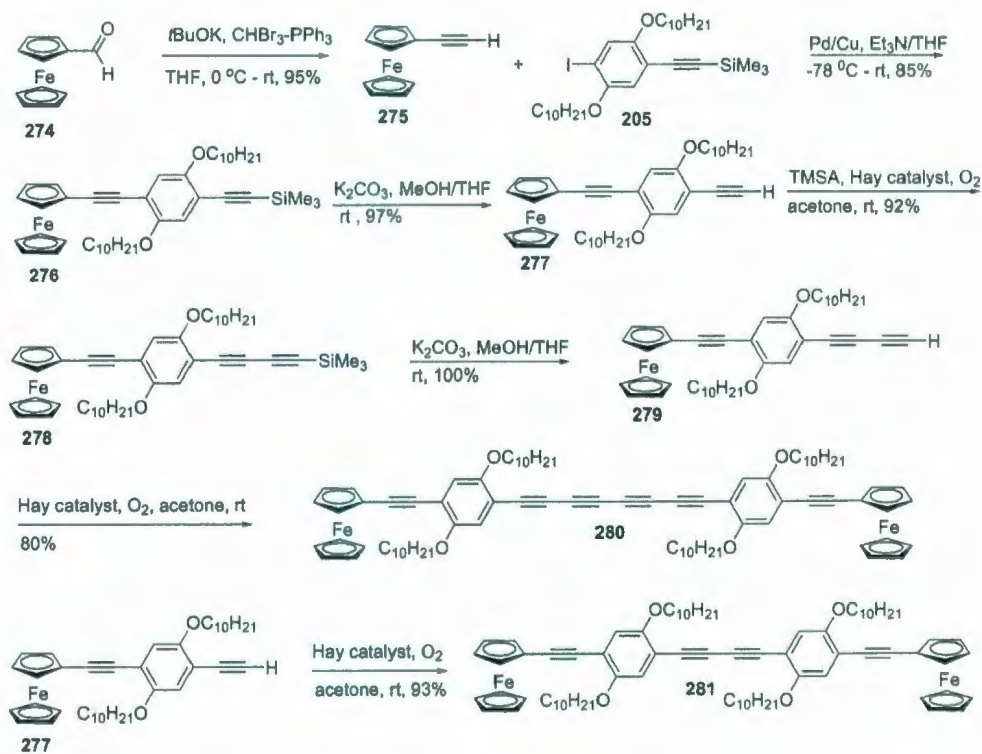


Scheme 4.7: Synthesis of DTF endcapped diynes **271**.

phosphonate precursor **257**, another set of dithiafulvene terminated oligoynes was explored. In these compounds, ester groups were incorporated and the preparation of relevant precursor **268** was relatively concise and less expensive.

Electroactive polyynes **250** was synthesized using the same procedures as for the synthesis of **249**. First, the tributyl phosphine-tetrafluoroborate salt **268** was prepared (see Scheme 4.7) with 85% yield following the literature procedure.¹³⁴ Compound **268** was then coupled with aldehyde **186** via a HWE reaction at -78°C to yield

compound **269** in 90% yield. The TMS group was deprotected by K_2CO_3 , and the resulting alkyne was homocoupled in the next step under Hay coupling conditions to give diyne **271** in 92% yield. Diyne **270** was subjected to Hay coupling again with excess TMSA to afford silyl protected diyne **272** in 77% yield. In the next step, the TMS group was deprotected using K_2CO_3 (see Scheme 4.7). However, the ester appendages were also hydrolyzed. Other attempts (TBAF at lower temperature, even at $-78\text{ }^\circ\text{C}$, Lewis acid conditions, K_2CO_3 at lower temperature) to selectively deprotect the silyl group failed as well.



Hay catalyst: **CuCl/TMEDA**

Scheme 4.8: Synthesis of ferrocenyl endcapped polyynes.

Finally, a series of ferrocene endcapped oligoynes was explored in view of the electron-donating and robust redox behavior of ferrocene. The synthesis of these compounds is outlined in Scheme 4.8. Ferrocene carboxaldehyde **274** was subjected to a modified Corey-Fuchs reaction to give ferrocene alkyne **275**. Pd-catalyzed Sonogashira reaction between **275** and **205** at $-78\text{ }^{\circ}\text{C}$ produced compound **276**. The TMS group of **276** was deprotected by K_2CO_3 in THF/MeOH to yield alkyne **277** in 97% yield. In the next step, **277** was coupled with excess TMSA in the presence of Hay catalyst to afford compound **278** in 92% yield. The TMS group of **278** was deprotected with K_2CO_3 to afford free diyne **279** in quantitative yield. Compound **279** was subjected to another Hay coupling to give ferrocene end-capped hexayne **280** in 80% yield. In a similar manner, compound **277** was homocoupled to give tetrayne **281** in 93% yield.

4.3.2 Characterizations

The molecular structures of the synthesized polyynes (**249-251**) were characterized by $^1\text{H-NMR}$, $^{13}\text{C-NMR}$, FT-IR spectroscopy, and high-resolution mass spectrometry. The high-resolution mass spectra clearly showed the molecular ion peaks of these polyynes and the precursors, whereas $^1\text{H-NMR}$, $^{13}\text{C-NMR}$, FT-IR also provided unambiguous evidence for structure identification.

The electrochemical redox properties of diyne **263** and tetrayne **262** were studied by cyclic voltammetry (CV). Figure 4.9 shows the cyclic voltammograms of **263** and **262** measured upon repetitive cycling of the potential of a glassy carbon working electrode over a range of 0.0 to +1.4 V.

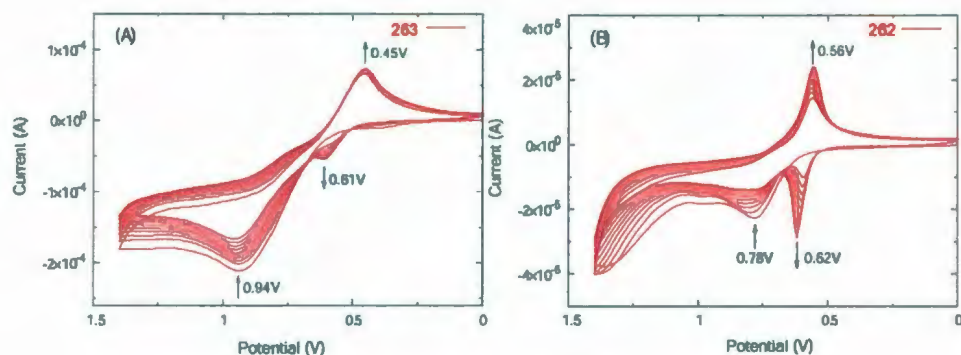
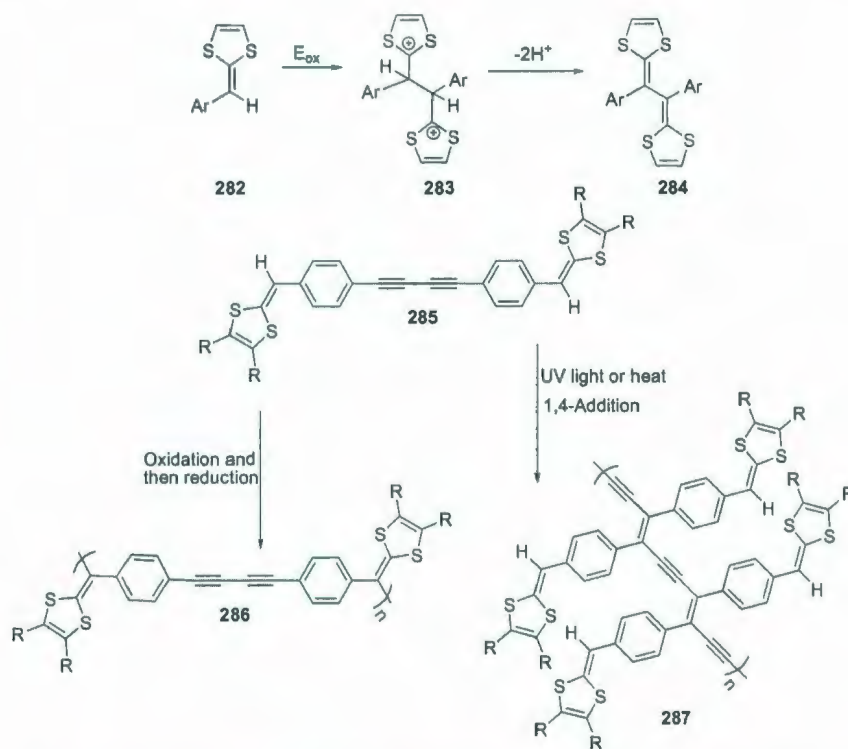


Figure 4.9: CV results of diyne **263** and tetrayne **262**.

Compound **263** showed an anodic peak at +0.94 V and a cathodic peak at +0.45 V in the very first scan (see Figure 4.9A). Interestingly, after the first cycle of scan, a new anodic peak at +0.61 V begins to develop. The anodic peak at +0.94 V is seen to decrease steadily, while the cathodic peak at +0.45 V increases slightly. From previous literature results, the new anodic peak at +0.61 V is assigned to $[\text{TTFV}]^{2+}$,^{131,135} hence the CV data shown in Figure 4.9A is indicative of electropolymerization of diyne **263** as proposed in Scheme 4.9. Almost similar voltammogram patterns corresponding to electropolymerization of tetrayne **262** can be observed in Figure 4.9B, in which an anodic peak at +0.78 V decreases and two peaks at +0.62 V (anodic) and +0.56 V (cathodic) increase continually with increasing scan cycles.

After multi-cycle CV scans of compounds **263** and **262**, electroactive dark-greenish thin films were formed on the surfaces of the working electrode. To investigate the properties of these electrogenerated polymer films, repetitive CV scans were performed on glass substrates coated with ITO in a similar manner to the above CV experiments. The CV data for the resulting polymer films measured in an electrolyte solution are shown in Figure 4.10. The polymer electrochemically



Scheme 4.9: Proposed polymerization pathways for **285** via oxidative coupling or topochemically controlled 1,4-addition.

generated from diene **263** gives rise to a pair of reversible waves at +0.51 and +0.68 V, which could be assigned to the TTFV units.¹³⁶ Two irreversible anodic peaks appear at +1.03 V and +1.20 V, the origins of which is likely due to the oxidation processes at the dithiafulvene and the phenylene butadiynylene moieties. The electrogenerated polymer resulting from tetrayne **262** shows a different CV pattern compared to that of **263**. Of particular interest is that the first anodic peak of **262** at +0.85 V is greatly shifted to more positive direction relative to that of diene **263**. A plausible explanation for this observation is that after the electrochemical polymerization of oligoyne-TTF **262**, a topochemical polymerization of the tetrayne moieties might

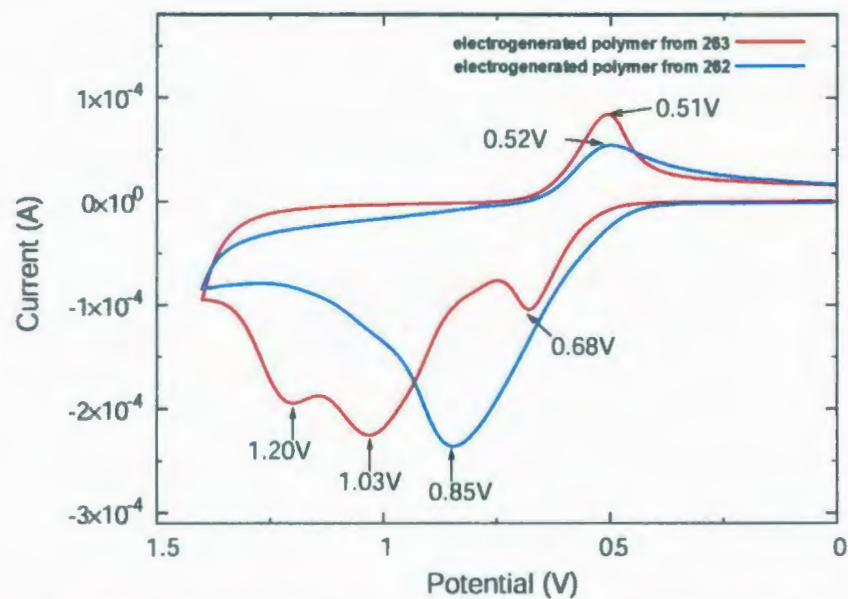


Figure 4.10: Film on ITO surface: Cyclic voltammograms of the electrochemically generated polymers from **263** and **262** on an ITO glass electrode. Scan rate: 0.1 V s^{-1} .

ensue to form a complex, heavily crosslinked polymeric network. The increased structural rigidity of the resulting polymer backbone thus hindered the oxidation of the TTFV groups embedded in it.

The electronic properties of ex-TTFs **263** and **262** have also been investigated by spectroelectrochemical experiments, where UV-Vis spectra were recorded using a 1 mm cell, which was subjected to varying applied potentials by means of a Pt-mesh electrode immersed in it. The detailed spectral data are shown in Figure 4.11. When the applied potentials are in the range of +0.1 to +0.5 V, the UV-Vis spectra of **263** show a virtually identical profile, featuring a maximum absorption band at 412 nm. In the voltage range from +0.6 to +1.4 V, the absorption band at 412 nm starts to decrease, while a new broad absorption band centered at 651 nm grows steadily with

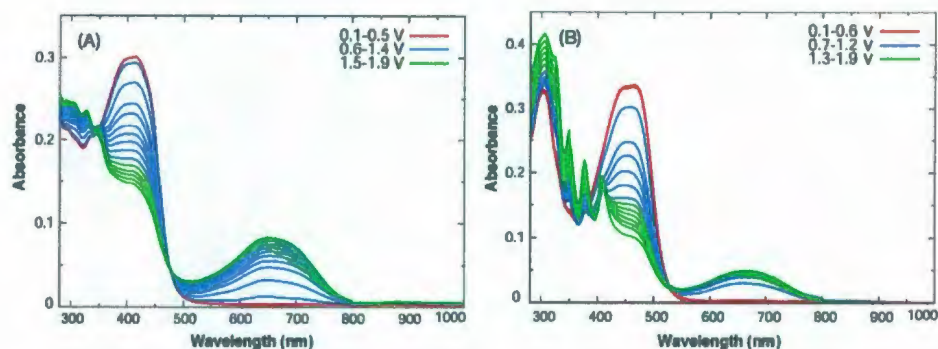


Figure 4.11: UV-Vis spectral changes of diyne **263** and tetrayne **262** in association with varying applied electrode potentials.

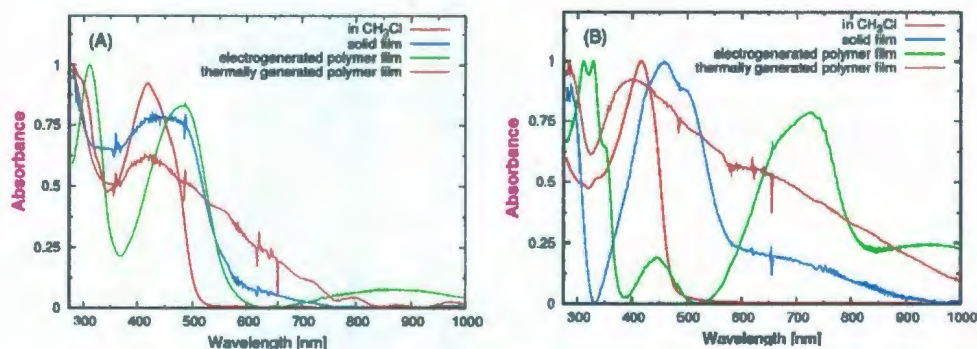


Figure 4.12: UV-Vis spectra of diyne **263** (left) and tetrayne **262** (right) measured under different conditions.

increasing voltage. In addition to that, the absorption in the high-energy region of 250 to 350 nm increases in intensity as well. When the applied potential is in the range of +1.5 to +1.9 V, the spectra of **263** change rather insignificantly. From Figure 4.11A, two isosbestic points are clearly observed at 350 and 477 nm. The emerging band at 651 nm can be attributed to the electrochemically generated polymer in the cationic form, given the fact that the radical-cation of dithiafulvene tends to react rapidly in solution.¹³⁵ In Figure 4.11B, the spectra of compound **262** remain unchanged, with

two absorption bands at 303 and 450 nm, when the applied potentials are in the range of +0.1 to +0.6 V. From +0.7 to +1.2 V, the spectra of **262** shows a steadily growing broad absorption band centered at 653 nm that is ascribed to the formation of cationic polymer. Meanwhile, the absorption at 450 nm drops considerably with increasing potentials. From +1.3 to +1.9 V, the absorption band at 653 nm decreases slightly. It could be due to decomposition at higher voltage. The absorption band at 450 nm continues to decrease, while a multitude of high-energy bands at 303, 324, 348, 376, and 406 nm appear to grow significantly. However, only one isosbestic point at 530 nm can be clearly identified in Figure 4.11B.

The electronic absorption spectra of polymer films electrochemically generated from **263** and **262** on ITO glass were also investigated by UV-Vis spectroscopy. For comparison purposes, polymers derived from the solid-state polymerization of oligoynes under thermal conditions (150 °C, 30 min) were also examined. The UV spectra of these polymers, together with the spectra of **263** are shown in Figure 4.12.

Figure 4.12 shows a pronounced low-energy absorption peak at ca. 728 nm in the spectrum of the electrogenerated polymer from **262**, which is consistent with the absorption band arising from thermally induced tetrayne polymerization. This band is, however, absent in the case of **263**, indicating that most probably diyne-TTF **263** was polymerized mainly through dithiafulvenyl dimerization process during the electrodeposition, whereas tetrayne-TTF **262** appears to undergo a twofold polymerization involving both oxidative dimerization and topochemical polymerization.

From the UV-Vis spectra of various polyynes, we see the difference in shift of λ_{max}

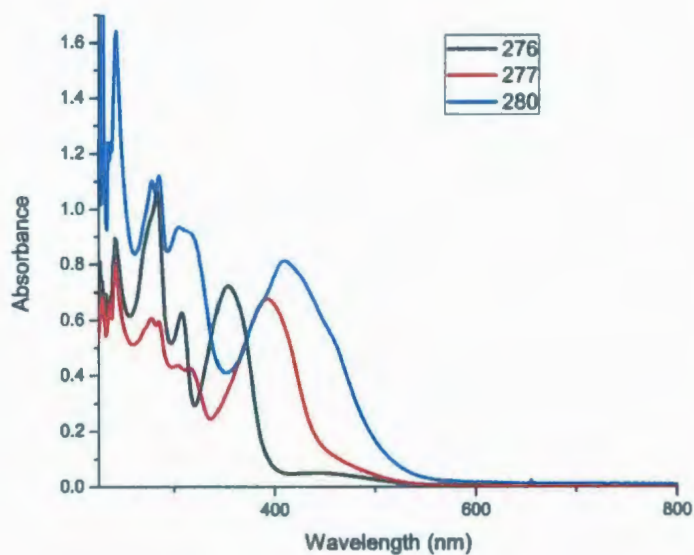


Figure 4.13: UV-Vis spectra of ferrocenyl endcapped oligynes.

depending upon the electron-donating abilities of end-functionalities (see Figures 4.15, 4.16 and 4.13). For the case of polyynes having electron donating ferrocenyl groups the red shift is around 50 nm, which is consistent with the Lewis-Calvin relationship for $E_g \sim n^{-0.5}$ usually observed for many polyenic materials.¹²⁴ However the shift is little bit lower for the polyyne series having methylthiol groups, which are not strong electron donors as ferrocenyl compounds (see Figures 4.16 and 4.13).

The fluorescence spectra of the series of polyynes having TTF or ferrocenyl end-functionalities were measured and shown in Figures 4.17 and 4.18; however, the spectral features are rather complex and difficult to explain.

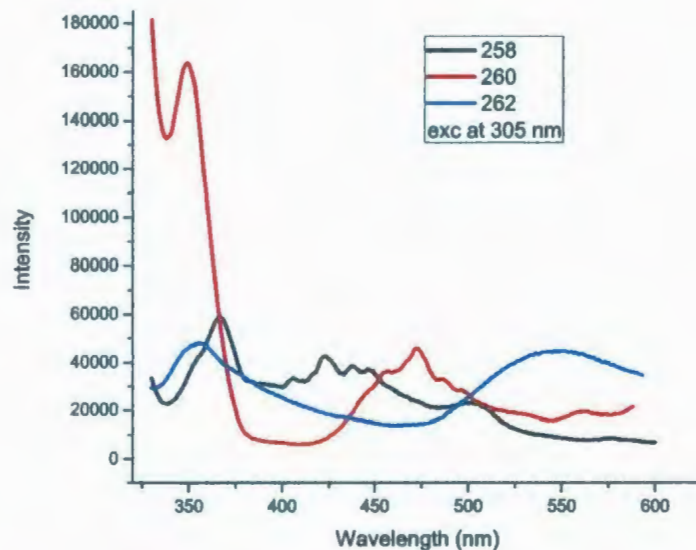


Figure 4.14: Fluorescence spectra of ferrocenyl endcapped oligoynes.

4.4 Conclusions

A new class of oligoynes-expanded TTF analogues has been synthesized and characterized. Particularly interesting in this regard is that the oligoynes-TTF derivatives could be used as precursors to generate electroactive polymers through a facile electrodeposition process. This finding could eventually lead to new methodologies for the preparation of TTF and polyynes containing functional polymers and related molecular devices. More research activity in this direction is currently underway in Zhao group.

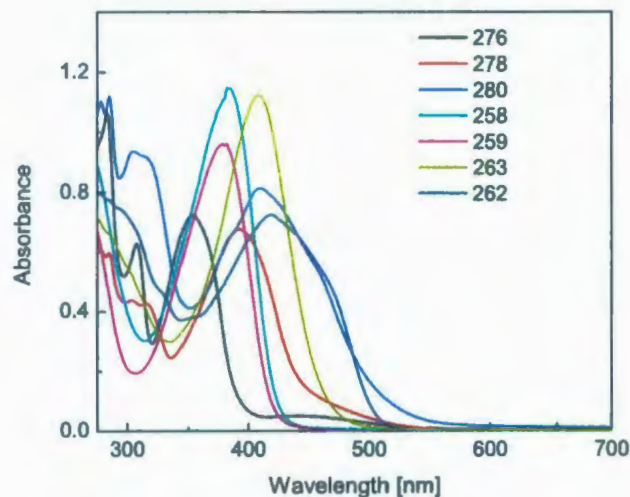


Figure 4.15: UV-Vis absorption spectra of all polyynes synthesized in this chapter.

4.5 Experimental Part

General reagents, synthetic conditions and characterization techniques are the same as adopted in the experimental sections of Chapters 2 and 3.

Synthesis of bis(tetrabutylammonium) bis(1,3-dithiole-4,5-dithiolate)zincate (252)¹¹⁸

Finely cut metallic Na (6.80 g, 300 mmol) and CS₂ (60 mL, 1.00 mol) were added to an oven-dried 250 mL round-bottom flask fitted with a reflux condenser and sealed with a septum. The flask was purged with N₂ for several times and refluxed for 20 min under N₂ protection. Dry DMF (20 mL) was added dropwise over a period of 20 min via a syringe. The mixture was refluxed for another 2 h, cooled to room temperature and then concentrated in a rotatory evaporator. The residual solid mass was then cooled in an ice-bath, and MeOH (40 mL) was slowly added. After filtration,

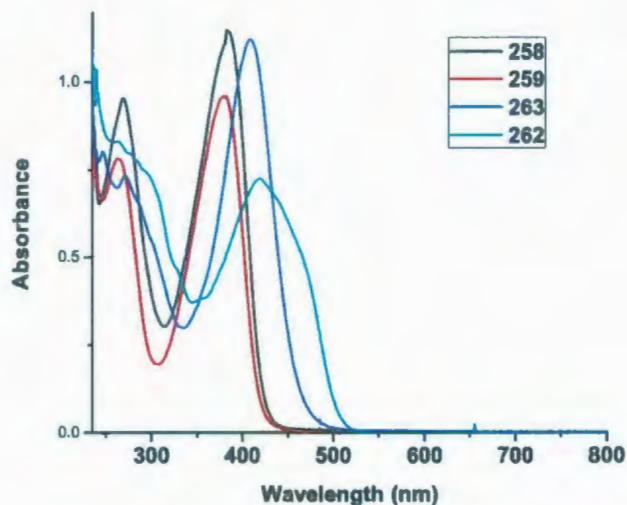


Figure 4.16: UV-Vis absorption spectra of all TTF tetraynes synthesized in this chapter.

a solution of ZnCl_2 (7.00 g, 51.3 mmol) in 120 mL of $\text{MeOH}/\text{NH}_4\text{OH}$ (1:1) was added slowly and carefully to the filtrate. To the resulting mixture, $n\text{-Bu}_4\text{NBr}$ (30.6 g, 95.0 mmol) in H_2O (80 mL) was added. The mixture was then left standing overnight. After filtration the residue was sequentially washed with H_2O and Et_2O to yield compound **252** (31.1 g, 33.0 mmol, 88%) as a deep-red solid. Mp 203-204 °C.

Synthesis of 4,5-bis(methylthio)-1,3-dithiol-2-thione (**253**)¹¹⁸

To a solution of **252** (4.00 g, 4.24 mmol) in acetone (45 mL) was added MeI (2.71 g, 1.20 mL, 19.1 mmol) in an oven-dried 100 mL round-bottom flask. The temperature was gradually increased to around 45-50 °C. The mixture was then refluxed for 2.5 h, cooled to room temperature, and evaporated under vacuum. The residue was dissolved in CH_2Cl_2 , washed with H_2O , dried over MgSO_4 , and evaporated under

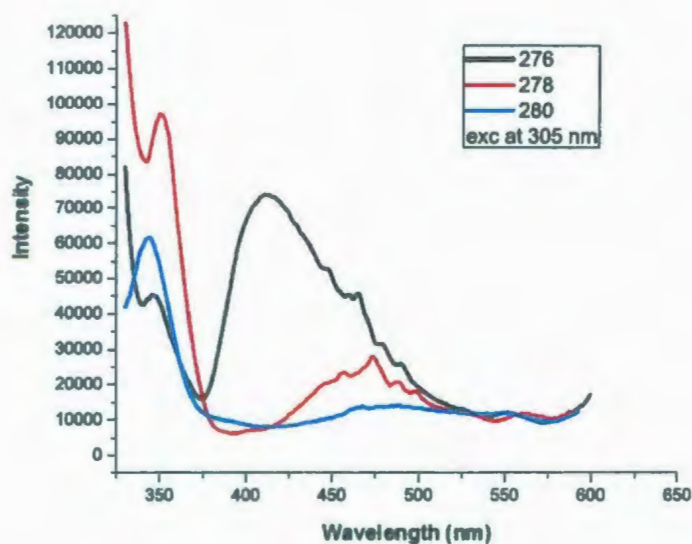


Figure 4.17: Fl spectra of all Fc tetraynes.

vacuum. The resulting precipitated solid was recrystallized from MeOH (35 mL) to afford an orange crystalline solid **253** (671 mg, 2.97 mmol, 70 %). Mp 107-108 °C; IR (neat): 2958, 2910, 2872, 1783, 1468, 1418, 1055, 1032 cm^{-1} ; ^1H NMR (500 MHz, CDCl_3): δ 2.52 (s, 6H); ^{13}C NMR (125 MHz, CDCl_3): δ 211.3, 136.3, 19.7, 14.2.

Synthesis of 4,5-bis(methylthio)-1,3-dithiol-2-ium tetrafluoroborate (**254**)¹¹⁸

A mixture of thione **253** (3.37 g, 14.9 mmol) and dimethyl sulfate (14.2 mL, 14.9 mmol) was heated in an oven-dried 100 mL round-bottom flask at 100-105 °C and stirred for 1.5 h. The mixture was cooled in an ice-bath, and $\text{HBF}_4 \cdot \text{Et}_2\text{O}$ (3.25 mL, 31.6 mmol) was added to it, followed by the addition of AcOH (15.0 mL, 342 mmol). After 10 min, Et_2O (100 mL) was added. The round-bottom flask was then kept in a freezer for 0.5 h (brown solid was separated out at this stage). The product was collected by gravity filtration and washed with Et_2O to afford compound **254** (3.01 g, 11.4 mmol, 76%) as a light-brown solid. Mp 66-68 °C; IR (neat): 3035, 2983, 1680,

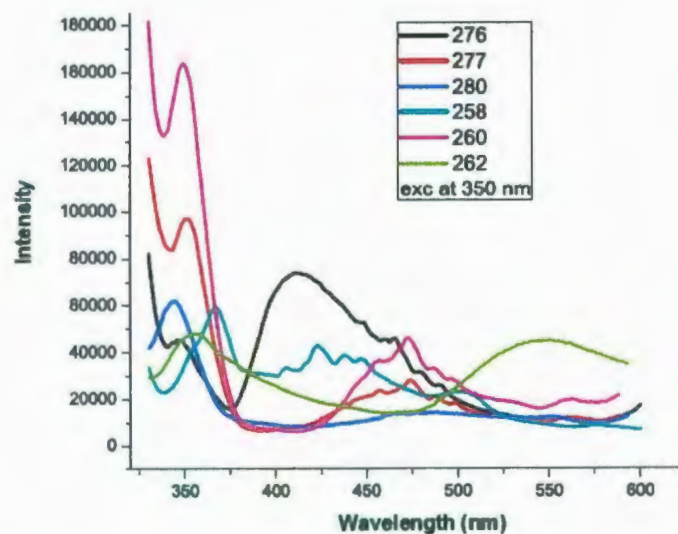


Figure 4.18: Fl spectra of all polyynes.

1464, 1433, 1030 cm^{-1} ; ^1H NMR (500 MHz, CDCl_3): δ 3.25 (s, 3H), 2.77 (s, 6H); ^{13}C NMR (125 MHz, CDCl_3): δ 147.8, 60.9, 23.4, 20.4.

Synthesis of 4,5-bis(methylthio)-2-(methylthio)-1,3-dithiole (**255**)¹¹⁸

To a solution of compound **254** (7.00 g, 19.1 mmol) in EtOH (80 mL), was added NaBH_4 (2.80 g, 74.1 mmol) in an oven-dried 100 mL round-bottom flask kept in an ice-bath. After 15 min the mixture was warmed up to room temperature and stirred for another 3 h. The mixture was then evaporated under vacuum. The round-bottom flask was kept in an ice-bath and slowly H_2O (20 mL) was added to the solid mass. The product was collected by filtration and washed with Et_2O to yield compound **255** (6.11 g, 16.6 mmol, 87%) as a pale orange solid. IR (neat): 2982, 2916, 1418, 1103 cm^{-1} ; ^1H NMR (500 MHz, CDCl_3): δ 5.83 (s, 1H), 2.45 (s, 6H), 2.30 (s, 3H); ^{13}C NMR (125 MHz, CDCl_3): δ 124.8, 62.6, 57.5, 19.67, 19.66, 13.31, 13.3; APCI-MS

(negative mode) m/z (%) calcd for $C_6H_{10}S_5$ 241.9 found 240.9 (9) $[M - H]^-$, 194.9 (100).

Synthesis of *S*-methyl phosphonate **257**¹¹⁸

A solution of **255** (2.85 g, 7.77 mmol) in Ac_2O (25 mL) was added to an oven-dried 100 mL round-bottom flask and cooled to 0 °C. The reaction mixture was stirred for 10 min and $HBF_4 \cdot OEt_2$ was then added to the flask at this temperature for 5 min. It was then stirred for another 15 min followed by slow addition of Et_2O . The round-bottom flask was then kept in a freezer for 0.5 h and the precipitated mass was filtered off to give compound **256** as a pale greenish-yellow solid. Compound **256** was immediately dissolved in acetonitrile (50 mL) in an oven-dried 100 mL round-bottom flask and to this was added NaI (4.00 g, 26.7 mmol) under N_2 , followed by the addition of $P(OMe)_3$ (3.30 mL, 28.0 mmol). The mixture was stirred for 3 h and then evaporated under vacuum. The resulting solid mass was dissolved in CH_2Cl_2 and washed with H_2O , dried over $MgSO_4$, and evaporated under vacuum and finally column chromatographed (ethyl acetate/hexanes, 1:5) to afford compound **257** (1.70 g, 5.60 mmol, 72%) as a dark-red liquid, which solidified when kept at 0 °C. IR (neat): 2922, 2852, 1429, 1181, 1023 cm^{-1} ; 1H NMR (500 MHz, $CDCl_3$): δ 4.75 (d, $J = 5.5$ Hz, 1H), 3.90 (d, $J = 10.0$ Hz, 6H), 2.44 (s, 6H); ^{13}C NMR (125 MHz, $CDCl_3$): δ 125.6, 54.8, 42.4, 41.1, 19.2; APCI-MS (positive mode) m/z (%) calcd for $C_7H_{13}S_4P$ 304.4, found 305.0 (12) $[M + H]^+$, 194.9 (100).

Synthesis of dimethyl tetrathiafulvene **258**

To an oven-dried 250 mL round-bottom flask was added a solution of **257** (1.00 g, 3.29 mmol) in dry THF (60 mL) and was sealed with a septum. This was evacuated

and purged with N₂ for several times and then cooled to -78 °C using a dry ice/acetone bath. *n*-BuLi (1.32 mL of 2.5 M in hexanes, 3.29 mmol) was then slowly added to this solution for 15 min (color changed to deep-purple). After the addition of *n*-BuLi, the reaction mixture was stirred at 0 °C for 10 min. A solution of **186** (670 mg, 3.31 mmol) in THF (20 mL) was added to the reaction mixture for 10 min and stirred at room temperature for another 24 h. H₂O was added to quench excess *n*-BuLi, and the solvent was removed. The resulting solid mass was dissolved in CH₂Cl₂ and washed with H₂O. The organic layer was dried over MgSO₄, filtered and absorbed on silica gel and column chromatographed to yield compound **258** (1.191 g, 3.12 mmol, 95%) as a deep-purple liquid. IR (KBr): 2954, 2920, 2149, 1563, 1540, 1499, 1247 cm⁻¹; ¹H NMR (500 MHz, CDCl₃): δ 7.45 (d, *J* = 8.3 Hz, 2H), 7.13 (d, *J* = 8.3 Hz, 2H), 6.43 (s, 1H), 2.44 (s, 3H), 2.43 (s, 3H), 0.29 (s, 9H); ¹³C NMR (125 MHz, CDCl₃): δ 136.7, 134.2, 132.5, 128.1, 126.9, 124.7, 120.5, 114.3, 105.8, 95.1, 19.5, 19.3, 0.5; HR-EI-TOF MS (positive mode) *m/z* calcd for C₁₇H₂₁S₄Si 381.0295, found 381.0306 [M]⁺.

Synthesis of TTF-alkyne **259**

To an oven-dried 100 mL round-bottom flask was added a solution of compound **258** (420 mg, 1.10 mmol) in 20 mL of THF/MeOH (1:1). To this was then added K₂CO₃ (575 mg, 4.17 mmol) and stirred at room temperature for 1 h. The solvent was removed under vacuum and the resulting solid mass was dissolved in CH₂Cl₂ and washed with H₂O. The organic layer was dried over MgSO₄, filtered and the solvent was removed to afford compound **259** (316 mg, 1.02 mmol, 93%) as a deep-purple solid. IR (KBr): 3295, 2923, 2854, 2105, 1599, 1385 cm⁻¹; ¹H NMR (500 MHz,

CDCl₃): δ 7.49 (d, $J = 8.3$ Hz, 2H), 7.18 (d, $J = 8.3$ Hz, 2H), 6.48 (s, 1H), 3.13 (s, 1H), 2.47 (s, 3H), 2.46 (s, 3H); ¹³C NMR (125 MHz, CDCl₃): δ 137.0, 134.4, 132.7, 128.1, 126.9, 124.8, 119.4, 114.2, 84.2, 78.0, 19.5, 19.3; HR-EI-TOF MS (positive mode) m/z calcd for C₁₄H₁₃S₄ 308.9900, found 308.9904 [M]⁺.

Synthesis of TTF-diynes **260**

To an oven-dried 100 mL round-bottom flask was added a solution of **259** (300 mg, 9.71×10^{-4} mol) and TMSA (574 mg, 5.84 mmol) in 20 mL of CH₂Cl₂/acetone (1:1). To this was then added 1 mL of a freshly prepared Hay catalyst. The mixture was stirred at room temperature for 2 h. The solvent was removed under vacuum. The resulting solid mass dissolved in CH₂Cl₂ and washed with H₂O. The organic layer was dried over MgSO₄, filtered and solvent was removed and finally column chromatographed to afford compound **260** (362 mg, 8.94 mmol, 92%) as a deep-purple liquid. IR (KBr): 2923, 2854, 2199, 2102, 1564, 1385 cm⁻¹; ¹H NMR (500 MHz, CDCl₃): δ 7.45 (d, $J = 8.4$ Hz, 2H), 7.13 (d, $J = 8.4$ Hz, 2H), 6.43 (s, 1H), 2.43 (s, 3H), 2.42 (s, 3H), 0.23 (s, 9H); ¹³C NMR (125 MHz, CDCl₃): δ 137.7, 135.6, 133.5, 128.3, 127.1, 125.1, 118.6, 114.2, 91.7, 88.7, 77.9, 75.2, 19.7, 19.6, 0.1; HR-EI-TOF MS (positive mode) m/z calcd for C₁₉H₂₁S₄Si 405.0295, found 405.0299 [M]⁺.

Synthesis of TTF-bisalkyne **261**

To an oven-dried 100 mL round-bottom flask was added a solution of compound **260** (410 mg, 1.01 mmol) in 20 mL of THF/MeOH (1:1). To this was then added K₂CO₃ (560 mg, 4.06 mmol) and stirred at room temperature for 2 h. The solvent was removed under vacuum. The resulting solid mass was dissolved in CH₂Cl₂ and washed with H₂O. The organic layer was dried over MgSO₄, filtered and the solvent

was removed to afford compound **261** (318 mg, 9.61×10^{-4} mol, 95%) as a bright-orange solid. IR (KBr): 3274, 3032, 2993, 2919, 2201, 1624, 1597, 1563, 1384 cm^{-1} ; ^1H NMR (500 MHz, CDCl_3): δ 7.50 (d, $J = 8.3$ Hz, 2H), 7.17 (d, $J = 8.3$ Hz, 2H), 6.46 (s, 1H), 2.54 (s, 1H), 2.47 (s, 3H), 2.46 (s, 3H); ^{13}C NMR (125 MHz, CDCl_3): δ 137.7, 135.5, 133.4, 128.3, 126.9, 124.9, 118.0, 113.9, 76.1, 74.4, 72.1, 68.7, 19.5, 19.3; HR-EI-TOF MS (positive mode) m/z calcd for $\text{C}_{16}\text{H}_{12}\text{S}_4$ 331.9822, found 331.9823 $[\text{M}]^+$.

Synthesis of the compound **262**

To an oven-dried 100 mL round-bottom flask was added a solution of compound **261** (287 mg, 8.67×10^{-4} mol) in 20 mL of THF/MeOH (1:1). To this was then dropwise added 1.5 mL of a freshly prepared Hay catalyst and stirred at room temperature for 2 h. The solvent was removed under vacuum and the resulting solid mass was dissolved in CH_2Cl_2 and washed with H_2O . The organic layer was dried over MgSO_4 , filtered and the solvent was removed and finally column chromatographed to yield compound **262** (362 mg, 3.92×10^{-4} mol, 90%) as orange flakes. IR (KBr): 2959, 2925, 2854, 2195, 1637, 1618, 1385 cm^{-1} ; ^1H NMR (500 MHz, CDCl_3): δ 7.53 (d, $J = 8.3$ Hz, 4H), 7.18 (d, $J = 8.3$ Hz, 4H), 6.48 (s, 2H), 2.48 (s, 6H), 2.47 (s, 6H); ^{13}C NMR (125 MHz, CDCl_3): δ 138.2, 136.7, 133.9, 128.7, 127.1, 125.4, 117.6, 114.1, 79.2, 76.5, 69.0, 65.3, 19.6, 19.5; HR-MALDI-TOF MS m/z calcd for $\text{C}_{32}\text{H}_{22}\text{S}_8$ 661.9487, found 661.9619 $[\text{M}]^+$.

Synthesis of compound **263**

To an oven-dried 100 mL round-bottom flask was added a solution of compound **259** (250 mg, 8.10×10^{-4} mol) in 20 mL of CH_2Cl_2 /acetone (1:1). To this was then

added 1.5 mL of a freshly prepared Hay catalyst and stirred at room temperature for 2 h. The solvent was removed and solid mass dissolved in CH_2Cl_2 and washed with H_2O . The organic layer was dried over MgSO_4 , filtered and the solvent was removed and then column chromatographed to give compound **263** (210 mg, 3.41×10^{-4} mol, 84%) as a yellow flake-type solid. IR (KBr): 2923, 2856, 1653, 1621, 1385 cm^{-1} ; ^1H NMR (500 MHz, CDCl_3): δ 7.51 (d, $J = 8.2$ Hz, 4H), 7.18 (d, $J = 8.2$ Hz, 4H), 6.48 (s, 2H), 2.47 (s, 6H), 2.46 (s, 6H); ^{13}C NMR (125 MHz, CDCl_3): δ 137.3, 135.3, 133.1, 128.3, 127.0, 125.0, 119.0, 114.2, 83.0, 75.4, 19.5, 19.3; HR-MALDI-TOF MS m/z calcd for $\text{C}_{28}\text{H}_{22}\text{S}_8$ 613.9580, found 614.9582 $[\text{M} + \text{H}]^+$.

Synthesis of compound 264

To an oven-dried 100 mL round-bottom flask was added a solution of **261** (225 mg, 6.78×10^{-4} mol) and TMSA (199 mg, 2.03 mmol) in 20 mL of CH_2Cl_2 /acetone (1:1). To this was then added 1.50 mL of a freshly prepared Hay catalyst and the reaction mixture stirred at room temperature for 2 h. Then solvent was removed and resulting solid mass dissolved in CHCl_3 . The organic layer was washed with H_2O , dried over MgSO_4 , filtered and the solvent was removed. Column chromatography afforded compound **264** (227 mg, 5.30×10^{-4} mol, 78%) as a bright orange solid. IR (KBr): 3034, 2957, 2916, 2163, 2072, 1595, 1566 cm^{-1} ; ^1H NMR (500 MHz, CDCl_3): δ 7.51 (d, $J = 8.4$ Hz, 2H), 7.17 (d, $J = 8.4$ Hz, 2H), 6.47 (s, 1H), 2.47 (s, 3H), 2.46 (s, 3H), 0.25 (s, 9H); ^{13}C NMR (125 MHz, CDCl_3): δ 137.9, 135.9, 133.7, 126.9, 126.3, 125.0, 117.7, 113.9, 89.7, 88.6, 75.4, 67.7, 62.2, 19.5, 19.3, 0.4; HR-EI-TOF MS (positive mode) m/z calcd for $\text{C}_{21}\text{H}_{20}\text{SiS}_4$ 428.0217, found 428.0215 $[\text{M}]^+$.

Synthesis of bis-TTF-hexaynes 266

To an oven-dried 100 mL round-bottom flask kept in an dry ice-acetone bath, was added a solution of **264** (160 mg, 3.74×10^{-4} mol) in 20 mL of THF/MeOH (1:1). To this was then added K_2CO_3 (103 mg, 7.48×10^{-4} mol) and the resulting mixture was stirred at $-20^\circ C$ for 6 h. The solvent was then removed and the resulting solid was dissolved in 20 mL of CH_2Cl_2 and washed with cold H_2O . 20 mL acetone was immediately added to it and again cooled to $-20^\circ C$. Then 1.00 mL of a freshly prepared Hay catalyst was added dropwise to this and stirred at $-20^\circ C$ for 2 h. The solvent was removed and the resulting solid mass was dissolved in CH_2Cl_2 (20 mL) and washed with H_2O . The organic layer was dried over $MgSO_4$, filtered and the solvent was removed and finally column chromatographed to give compound **265** (77.1 mg, 1.08×10^{-4} mol, 58%) as a shiny-orange solid. IR (KBr): 3037, 2994, 2917, 2196, 2120, 2079, 1652, 1595, 1331 cm^{-1} ; 1H NMR (500 MHz, CD_2Cl_2): δ 7.53 (d, $J = 8.3$ Hz, 4H), 7.23 (d, $J = 8.3$ Hz, 4H), 6.51 (s, 2H), 2.51 (s, 6H), 2.50 (s, 6H); ^{13}C NMR (125 MHz, $CDCl_3$): δ 138.1, 136.6, 133.9, 128.7, 127.1, 125.4, 117.6, 114.0, 79.2, 77.9, 77.5, 76.4, 69.0, 65.3, 19.6, 19.5; HR-MALDI-TOF MS (positive mode) m/z calcd for $C_{36}H_{22}S_8$ 709.9487, found 711.9647 $[M]^+$.

Synthesis of tributyl phosphine salt **268**

An oven-dried 100 mL round-bottom flask was purged with N_2 and kept in a dry ice/acetone bath to maintain temperature as low as $-65^\circ C$ to $-78^\circ C$. Dry Et_2O (50 mL) was added to the round-bottomed flask followed by the addition of 5 mL of tributylphosphine (4.10 g, 20.3×10^{-3} mol) and 12 mL of reagent grade CS_2 (15.2 g, 200 mmol). The flask was again purged with N_2 and stirred for 15 min at around $-78^\circ C$ (a deep-red reaction mixture formed at this stage). To this constantly stirred

mixture, were then added a portion of 2.70 mL of $\text{HBF}_4 \cdot \text{OEt}_2$ complex (3.51 g, 26.2 mmol), and then 2.5 mL of dimethyl acetylenedicarboxylate (2.90 g, 20.4 mmol) (gummy sticky solid precipitated out immediately). The reaction mixture was then manually stirred for another 0.5 h at low temperature. The upper colorless solution was decanted and the sticky mass was recrystallized using $\text{CH}_3\text{CN}/\text{Et}_2\text{O}$ (1:7) to yield compound **268** (7.96 g, 17.2×10^{-3} mol, 85%) as a cotton-like white solid. IR (neat): 2962, 2937, 2875, 1718, 1576, 1061 cm^{-1} ; ^1H NMR (500 MHz, CDCl_3): δ 6.19 (s, 1H), 3.87 (s, 6H), 2.46-2.40 (m, 6H), 1.69-1.62 (m, 6H), 1.57-1.51 (m, 6H), 1.0 (t, $J = 7.4$ Hz, 9H); ^{13}C NMR (125 MHz, CDCl_3): δ 160.0, 131.9, 54.1, 43.4, 43.0, 24.6, 24.44, 24.40, 17.1, 16.8, 13.6.

Synthesis of 4,5-bis(methoxycarbonyl)-1,3-dithiolytributylphosphonium tetrafluoroborate **269**

To an oven-dried 250 mL round-bottom flask was added a solution of compound **268** (1.71 g, 3.69 mmol) in dry THF (25 mL) and the flask was sealed with a septum. This was evacuated and purged with N_2 for several times and then cooled to approximately -78 °C using dry ice/acetone bath. *n*-BuLi (1.48 mL in hexane, 3.69 mmol) was then slowly added to this, which resulted in a color change of the reaction mixture to deep-purple. After addition of *n*-BuLi, the mixture was stirred at 0 °C for 10 min. A solution of **186** (746 mg, 3.69 mmol) in THF (20 mL) was dropwise added to this for 10 min and stirred at room temperature for another 24 h. A few mL of H_2O was added to quench excess *n*-BuLi and the solvent was removed. The resulting dry mass was dissolved in CH_2Cl_2 and then washed with H_2O . The organic layer was dried over MgSO_4 , filtered and adsorbed on silica gel and column chromatographed

to give compound **269** (1.341 g, 3.32 mmol, 90%) as a deep-purple solid. IR (KBr): 2955, 2924, 2853, 2155, 1732, 1541, 1252 cm^{-1} ; ^1H NMR (500 MHz, CDCl_3): δ 7.46 (d, $J = 8.3$ Hz, 2H), 7.15 (d, $J = 8.3$ Hz, 2H), 6.43 (s, 1H), 3.88 (s, 3H), 3.87 (s, 3H), 0.28 (s, 9H); ^{13}C NMR (125 MHz, CDCl_3): δ 160.5, 160.0, 136.1, 132.0, 126.9, 115.1, 105.4, 95.5, 53.8, 53.7, 0.38; HR-Cl-TOF MS (positive mode) m/z calcd for $\text{C}_{19}\text{H}_{20}\text{SiS}_2\text{O}_4$ 404.0572, found 404.0578 $[\text{M}]^+$.

Synthesis of the compound **271**

To an oven-dried 100 mL round-bottom flask was added a solution of **270** (200 mg, 6.02×10^{-4} mol) in 20 mL of CH_2Cl_2 /acetone (1:1). To this was then added 1.50 mL of a freshly prepared Hay catalyst and the resulting mixture was stirred at room temperature for 2 h. Then solvent was removed and solid mass was dissolved in CH_2Cl_2 and washed with H_2O . The organic layer was dried over MgSO_4 , filtered and solvent was removed and finally column chromatographed to yield compound **271** (210 mg, 3.41×10^{-4} mol, 92%) as a deep-red solid. IR (KBr): 2958, 2925, 2855, 1730, 1557, 1264 cm^{-1} ; ^1H NMR (500 MHz, CDCl_3): δ 7.53 (d, $J = 8.3$ Hz, 4H), 7.20 (d, $J = 8.3$ Hz, 4H), 6.47 (s, 2H), 3.90 (s, 6H), 3.89 (s, 6H); ^{13}C NMR (125 MHz, CDCl_3): δ 160.5, 159.9, 136.8, 133.2, 129.7, 127.1, 119.7, 114.7, 82.6, 75.3, 53.9, 53.7; HR-Cl-TOF MS (positive mode) m/z calcd for $\text{C}_{32}\text{H}_{23}\text{O}_8\text{S}_4$ 663.0276, found 663.0281 $[\text{M}]^+$.

Synthesis of **272**

To an oven-dried 100 mL round-bottomed flask was added a solution of compound **270** (51.0 mg, 1.54×10^{-4} mol), and TMSA (30.0 mg, 3.05×10^{-4} mol) in 20 mL of CH_2Cl_2 /acetone (1:1). To this was then added 1.00 mL of a freshly prepared

Hay catalyst and stirred at room temperature for 2 h. The solvent was removed and the resulting solid mass was dissolved in CH_2Cl_2 and washed with H_2O . The organic layer was dried over MgSO_4 , filtered, solvent was removed and finally column chromatographed to give compound **272** (51.0 mg, 1.19×10^{-4} mol, 77%) as a deep-purple solid. IR (KBr): 2956, 2924, 2853, 2195, 2098, 1754, 1722, 1586, 1562, 1385, 1230 cm^{-1} ; ^1H NMR (500 MHz, CDCl_3): 7.49 (d, $J = 8.3$ Hz, 2H), 7.17 (d, $J = 8.3$ Hz, 2H), 6.44 (s, 1H), 3.89 (s, 3H), 3.87 (s, 3H), 0.26 (s, 9H); ^{13}C NMR (125 MHz, CDCl_3): δ 160.4, 159.9, 136.9, 133.9, 129.7, 128.6, 127.0, 119.2, 114.7, 91.7, 88.3, 77.2, 75.4, 53.9, 53.7, 0.1; HR-EI-TOF MS (positive mode) m/z calcd for $\text{C}_{19}\text{H}_{20}\text{O}_4\text{Si}_4$ 404.5752, found 381.0295 $[\text{M}-\text{CH}_3]^+$.

Synthesis of the ferrocene-alkyne **275**

To an oven-dried 100 mL round-bottomed flask was added a solution of $\text{Ph}_3\text{P}\cdot\text{CHBr}_3$ salt (4.00 g, 7.77 mmol) and compound **274** (836 mg, 3.91 mmol) in dry THF (50 mL) and the resulting mixture was cooled to 0 °C. To this was then added a suspension of *t*-BuOK (896 mg, 7.98 mmol) in dry THF and the reaction mixture was stirred at 0 °C for 5 min and then warmed to room temperature and stirred for a further 0.5 h. The solvent was removed in vacuum and the resulting solid was dissolved in CHCl_3 and washed with cold 1% HCl solution. The organic layer was dried over MgSO_4 , filtered, the solvent was removed. Column chromatography (hexanes/ CH_2Cl_2 , 4:1) yielded compound **275** (779 mg, 3.71 mmol, 95%) as a pale-yellow liquid which was immediately used in next step without characterization.

Synthesis of **276**

An oven-dried 100 mL round-bottom flask was purged with N_2 and to this was

then added compound **205** (612 mg, 1.00 mmol), Pd(PPh₃)₂Cl₂ (35.1 mg, 5.0 × 10⁻⁵ mol), CuI (19.0 mg, 1.0 × 10⁻⁴ mol) in 30 mL of dry THF/Et₃N (1:1). The flask was sealed with a septum, evacuated under vacuum, and purged with N₂. The reaction mixture was cooled to -78 °C. To this constantly stirred mixture, a solution of the compound **275** (210 mg, 1.00 mmol) in Et₃N (3 mL) was then added dropwise for 0.5 h and stirred for 2 h. The reaction mixture was warmed to room temperature and stirred overnight. The solvent was evaporated under vacuum. The resulting solid mass was dissolved in CHCl₃ and washed sequentially with 1.0% HCl, and satd NH₄Cl solution to give a deep-red organic layer which was concentrated to dryness and then flash chromatographed (hexanes/CH₂Cl₂, 5:1) to yield compound **276** (660 mg, 9.5 × 10⁻⁴ mol, 95%) as deep-yellow solid. IR (KBr): 2959, 2922, 2852, 2105, 1638, 1617, 1508, 1385, 1214 cm⁻¹; ¹H NMR (500 MHz, CDCl₃): δ 6.96 (s, 1H), 6.95 (s, 1H), 4.55-4.27 (m, 9H), 4.04-4.00 (m, 4H), 1.92-1.81 (m, 4H), 1.58-1.52 (m, 4H), 1.39-1.32 (m, 24H), 0.93-0.91 (m, 6H), 0.31 (s, 9H); ¹³C NMR (125 MHz, CDCl₃): δ 154.6, 153.8, 117.6, 117.4, 115.4, 113.4, 101.8, 100.1, 94.3, 82.3, 69.3, 65.7, 32.3, 29.84, 29.83, 29.8, 29.7, 26.5, 23.1, 14.53, 14.52, 0.41.

Synthesis of **277**

A solution of compound **276** (200 mg, 2.88 × 10⁻⁴ mol) in 20 mL of THF/MeOH (1:1) was added to an oven-dried 100 mL round-bottom flask. K₂CO₃ (159 mg, 1.15 × 10⁻³ mol) was added to it and then stirred overnight at room temperature. Solvent was removed under vacuum and the resulting solid mass was dissolved in CHCl₃, dried over MgSO₄, filtered and solvent was removed to afford compound **277** (179 mg, 2.88 × 10⁻⁴ mol, 100%) as a pale-yellow solid. ¹H NMR (500 MHz, CDCl₃): δ 6.99 (s,

1H), 6.98 (s, 1H), 4.55-4.28 (m, 9H), 4.04-4.02 (m, 4H), 3.37 (s, 1H), 1.89-1.82 (m, 4H), 1.50-1.32 (m, 28H), 0.94-0.91 (m, 6H); ¹³C NMR (125 MHz, CDCl₃): δ 154.6, 153.8, 118.1, 117.3, 115.8, 112.3, 94.5, 82.4, 69.3, 65.66, 65.63, 65.63, 32.3, 30.1, 30.0, 29.96, 29.8, 29.7, 26.5, 23.1, 14.6, 14.5.

Synthesis of 278

A solution of ferrocene alkyne **277** (100 mg, 1.61×10^{-4} mol) and TMSA (94.0 mg, 9.57×10^{-4} mol) in acetone (20 mL) was added to an oven-dried 100 mL round-bottom flask. To this was then added 1.50 mL of a freshly prepared Hay catalyst and stirred at room temperature for 24 h. Then solvent was removed and the resulting solid mass was dissolved in CH₂Cl₂ and washed sequentially with satd NH₄Cl solution, and H₂O. The organic layer was dried over MgSO₄, filtered and solvent was removed and finally column chromatographed (hexanes/CH₂Cl₂, 5:1) to give compound **278** (56.5 mg, 7.86×10^{-5} mol, 92%) as a bright-orange solid. IR (KBr): 2959, 2922, 2852, 2105, 1638, 1617, 1385 cm⁻¹; ¹H NMR (500 MHz, CDCl₃): δ 6.96 (s, 1H), 6.95 (s, 1H), 4.54-4.27 (m, 9H), 4.03-3.95 (m, 4H), 1.90-1.82 (m, 4H), 1.56-1.50 (m, 4H), 1.38-1.32 (m, 24H), 0.94-0.91 (m, 6H), 0.27 (s, 9H); ¹³C NMR (125 MHz, CDCl₃): δ 155.8, 153.7, 138.2, 118.3, 117.3, 116.5, 111.6, 95.3, 92.1, 88.6, 77.2, 70.5, 70.46, 69.4, 65.5, 30.0, 29.84, 29.79, 29.77, 29.76, 29.6, 26.5, 26.4, 23.12, 23.11, 14.5, 0.1; HR-MALDI-TOF MS (dithranol as the matrix) *m/z* calcd for C₄₅H₆₂O₂SiFe 718.9031, found 718.6600 [M]⁺.

Synthesis of 280

To an oven-dried 100 mL round-bottom flask was added a solution of **278** (225 mg, 3.12×10^{-4} mol), and K₂CO₃ (172 mg, 1.25 mmol) in 20 mL of THF/MeOH (1:1).

This was then stirred at room temperature for 1 h. The solvent was removed under vacuum and the resulting solid mass was dissolved in Et₂O and washed sequentially with satd NH₄Cl solution, and H₂O. The organic layer was dried over MgSO₄, filtered and solvent was removed to afford **279** as an orange solid. Compound **279** was immediately dissolved in 50 mL of acetone in a 100 mL round-bottom flask and to this was then dropwise added 1.00 mL of a freshly prepared Hay catalyst and stirred at room temperature for 4 h. The solvent was removed and the resulting solid mass was dissolved in CH₂Cl₂ and washed with H₂O. The organic layer was dried over MgSO₄, filtered and solvent was removed and finally column chromatographed (hexanes/CH₂Cl₂, 5:1) to afford compound **280** (323 mg, 2.50 × 10⁻⁴ mol, 80%) as a shiny-orange solid. IR (KBr): 2962, 2928, 2858, 2194, 1652, 1503, 1261 cm⁻¹; ¹H NMR (500 MHz, CDCl₃): δ 6.98 (s, 2H), 6.96 (s, 2H), 4.55-4.28 (m, 18H), 4.04-4.0 (m, 8H), 1.89-1.80 (m, 8H), 1.52-1.41 (m, 8H), 1.40-1.32 (m, 48H), 0.95-0.91 (m, 12H); ¹³C NMR (125 MHz, CDCl₃): δ 156.7, 153.7, 118.2, 117.4, 117.1, 110.5, 96.1, 79.6, 75.1, 69.1, 65.4, 65.1, 32.4, 29.84, 29.79, 29.76, 29.53, 26.5, 26.4, 23.14, 23.11, 14.6, 14.5; MALDI-TOF MS (dithranol as the matrix) *m/z* calcd for C₈₄H₁₀₆O₄Fe₂ 1291.68, found 1291.00 [M]⁺.

Synthesis of **281**

To an oven-dried 100 mL round-bottom flask was added a solution of **277** (300 mg, 4.82 × 10⁻⁴ mol) in 20 mL of CH₂Cl₂/acetone (1:1). To this was then dropwise added 1.50 mL of a freshly prepared Hay catalyst and stirred at room temperature for 2 h. The solvent was removed and the resulting solid mass was dissolved in CH₂Cl₂ and washed with H₂O. The organic layer was dried over MgSO₄, filtered and solvent

was removed and finally column chromatographed to afford compound **281** (558 mg, 4.49×10^{-4} mol, 93%) as a deep-yellow solid. IR (KBr): 2921, 2898, 2866, 2216, 2104, 1653, 1599, 1531, 1105 cm^{-1} ; ^1H NMR (500 MHz, CDCl_3): δ 7.00 (s, 2H), 6.97 (s, 2H), 4.56-4.28 (m, 18H), 4.06-4.01 (m, 8H), 1.94-1.87 (m, 8H), 1.85-1.24 (m, 56H), 0.93-0.89 (m, 12H); ^{13}C NMR (125 MHz, CDCl_3): δ 155.6, 153.9, 118.8, 117.9, 116.6, 112.2, 82.4, 79.5, 69.4, 65.6, 32.3, 30.0, 29.85, 29.76, 29.75, 29.60, 26.5, 23.1, 14.52; MALDI-TOF MS (dithranol as the matrix) m/z calcd for $\text{C}_{80}\text{H}_{106}\text{O}_4\text{Fe}_2$ 1243.39, found 1243.08 $[\text{M}]^+$.

Chapter 5

Design and Synthesis of π -Conjugated Polymers and Task-specific Ionic Liquids for Carbon Nanotube Functionalization

5.1 Introduction

Carbon nanotubes (CNTs) are fascinating quasi-one-dimensional nanomaterials, the structure of which can be perceived as being formed from rolling up graphitic sheets into a cylindrical shape.¹³⁷ The exceptional properties of CNTs, including electrical and thermal conductivity, extra-ordinary strength (e.g. tensile strength is as high

as 1 TPA) and stiffness, electronic bandgap properties, and extraordinary aspect ratio, make them suitable for various device applications in molecular electronics, conductive fillers for the development of electrically/thermally conductive polymer-based composites, energy storage, nanomedicine, sensing devices, and many others.⁷⁸

Although CNTs have unique properties and promising application potentials, the direct application of raw, as-produced CNTs in device fabrication is problematic. This challenge is especially significant for single-walled carbon nanotubes (SWNTs). Commercially available SWNTs are produced as mixtures, consisting of various electronic types (metallic and semiconducting), diameters, and chiral indices. Multi-walled CNTs, other carbonaceous impurities, and transition metal catalysts (Fe, Co, Ni) are also present. Moreover, SWNTs have a strong tendency to aggregate in the solid state due to van der Waals forces or π - π stacking. Whatever the reason, the compositional heterogeneity of various SWNTs samples has greatly limited their application potentials, because many SWNT-based devices (e.g. field effect transistors, sensors, and molecular wires) have particular requirements for the electronic type and structure of nanotubes in operation.¹³⁸ Preparation of structurally homogenous SWNTs in a scalable and cost-effective way is thus the most urgent demand in the advance of SWNT-based technologies.

High-quality and structurally homogenous carbon nanotubes (CNTs) could be obtained by refining production techniques. However, practical approaches have not been achieved yet. The alternate ways could be various post-production methods to functionalize as-prepared CNTs. Three types of functionalization methods have been developed for SWNTs: covalent functionalization, non-covalent functionalization, and the endohedral filling/pouring of the inner empty cavity of

SWNTs.¹³⁷ Covalent functionalization gives rise to effective surface modification by using chemical reactions between SWNTs and various chemical reagents and compounds. This approach produces highly soluble and debundled SWNTs in a variety of solvents. The resultant solubility of some chemically functionalized SWNTs have attained as high as 0.6 mg/mL.¹³⁹ In some cases, electronic-type dependent reactivities could also be used to isolate SWNTs of a particular electronic type.¹⁴⁰ However, chemical functionalization suffers from a major disadvantage; any covalent attachment to the pristine SWNTs would invariably disrupt the π -delocalization among the sp^2 hybridized carbons on SWNTs, and therefore result in the loss of structural integrity.¹³⁹

The non-covalent approach is free from the problem of structural damage, since it utilizes relatively weak physical interactions, such as π -stacking or van der Waals forces, to bind various macromolecular moieties with SWNTs. Because of its non-destructive nature, the non-covalent approach is deemed to be advantageous over the covalent functionalization in the applications where electrical conductivity or optical properties are of prime importance.¹⁴¹

Considerable attention have been given to non-covalently functionalize SWNTs in recent studies. The methods range from coating the nanotubes with surfactants (e.g. sodium dodecyl sulfonate), polymers, and large biomolecules (DNA/RNA, proteins, carbohydrates).^{138,142,143} The coating of SWNTs with either surfactants or π -conjugated polymers, produces a weak inter-nanotube repulsion that enables the formation of a metastable suspension of nanotube complexes in common solvents.^{138,142}

Most recently, rationally designed macromolecular systems have been reported

to show selectivity in dispersion of SWNTs based on discriminative non-covalent supramolecular interactions, and this research topic has been of significantly growing interest. For example, a series of fluorene-based polymers was utilized by Nicholas and co-workers to achieve good diameter selectivity in dispersing HiPCO and CoMoCAT SWNTs.¹³⁸ In this work, the origin of selectivity was ascribed to the formation of self-assembled intermolecular structures with an n -fold symmetry, derived from a simplified molecular mechanics simulation. Chen *et al.* investigated another series of fluorene-based aromatic polymers that could selectively interact with SWNTs of different chiral angles.¹⁴⁴ As a result, they were able to enrich certain chiral nanotubes from a small-diameter SWNT sample (Co-MCM-41). Menuier and co-workers explored the use of discriminative π -stacking interactions between SWNTs and amphiphilic pentacene and quaterrylene derivatives to achieve selectivity toward armchair and zigzag types from as-produced SWNTs.¹⁴⁵ Komatu's group designed and prepared a group of optically pure dimeric porphyrin molecules that could discriminate left- and right-handed chiral nanotubes in solution.¹⁴⁶ In spite of these successes, there still remains a big question: "whether these subtly biased supramolecular interactions are sufficient enough to produce structurally homogeneous SWNTs from as-produced SWNTs." To shed more light to this issue, it is helpful to use systematically designed dispersants, for example, π -conjugated polymers, to probe and understand the supramolecular effects on the dissolution outcomes of SWNTs in solution.

Generally speaking, both the non-covalent and covalent functionalization methods for SWNTs have pros and cons. Although the covalent approach has been reported to disrupt the structural integrity of SWNTs, chemical reactions on SWNTs typically

result in a highly localized transformation of the electronic structure of the nanotubes. If the experimental conditions are carefully controlled, the change of the entire bulk properties can be insignificant.¹³⁷ On the other hand, the covalent approach can efficiently introduce a wide range of functional groups on the surface of carbon nanotubes, while the resulting functionalized nanotubes are substantially more stable and less cytotoxic than most of non-covalently functionalized ones.^{82,137} For instance, the cytotoxicity of functionalized SWNTs has been found to decrease with an increasing degree of covalent functionalization.⁸² There have been many attempts to chemically functionalize SWNTs, but the results using common organic or aqueous solvents under typical reaction conditions are not satisfactory. A main reason for this is because of the poor solubility/dispersity of SWNTs in these solvents.

Room-temperature ionic liquids (RTILs) have emerged as unique solvents for a variety of synthetic applications.¹⁴⁷ In particular, it has been of great interest to obtain air-stable RTILs composed of asymmetric *N,N'*-dialkylimidazolium cations with a variety of bulky counter anions, such as PF_6^- and BF_4^- . These ionic liquids display high thermal stability, a large liquid range, and negligible vapor pressure,¹⁴⁷ which make them potentially attractive for use in the so called "sonochemical reactions".¹⁴⁸ It was reported by several groups that SWNTs, when suspended in imidazolium ion based ionic liquids, formed gels ("bucky gels") wherein SWNTs were effectively debundled.¹⁴⁸ This finding hence suggests that ionic liquids could serve as better media for covalent functionalization of SWNTs.

5.2 Objectives of the Project

The main aim of this project was to develop a suitable method for producing structurally homogenous SWNTs in a scalable and cost-effective way. The first objective of this project is to synthesize novel conjugated polymers for SWNT dispersion and purification. Previously, the Zhao group has reported that linear arylene polymers, such as poly(phenylene ethynylene)s (PPEs **291** and **292**), poly(*p*-phenylene vinylene)s (PPVs, **293**, and **294**), and poly(phenylene butadiynylene)s (PPBs) are capable of dispersing as-produced SWNTs in organic solvents. The most interesting manifestation from our previous investigations is that the effectiveness of SWNTs dispersion is related to the nature of the polymer dispersant.¹⁴⁹

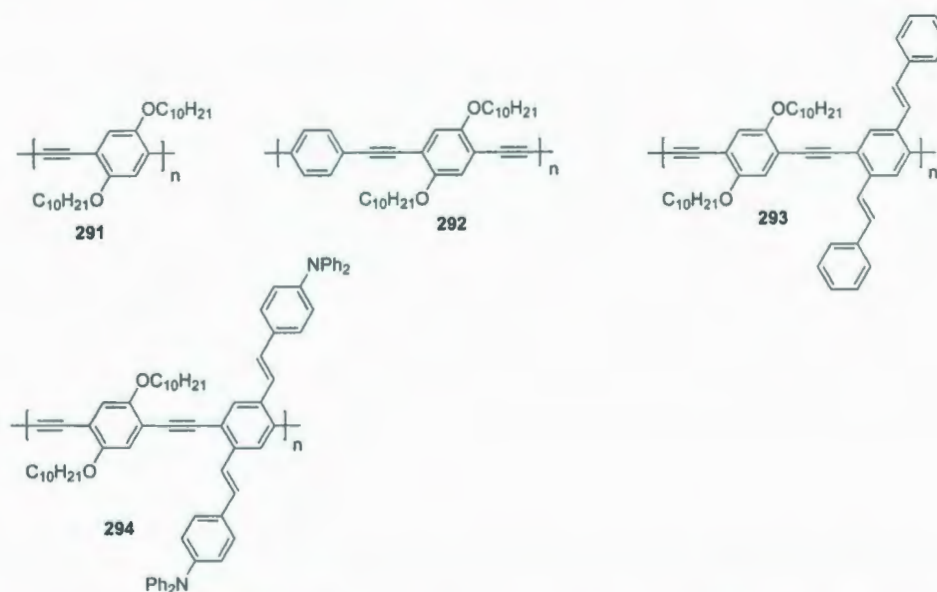


Figure 5.1: Polymers **291-294** previously reported by the Zhao group for SWNT functionalization.

Although there have been some successes so far in non-covalent SWNT separation

and sorting as reported by various research groups, the physical origins and mechanisms of these non-covalent interactions are still obscured and ill-defined. A reasonable approach to overcome these hurdles is to investigate the structure-property relationships using systematically designed models. In this regard, a series of polymers bearing different appendages, such as **288**, **289**, and **290** have been synthesized (see Figure 5.2).

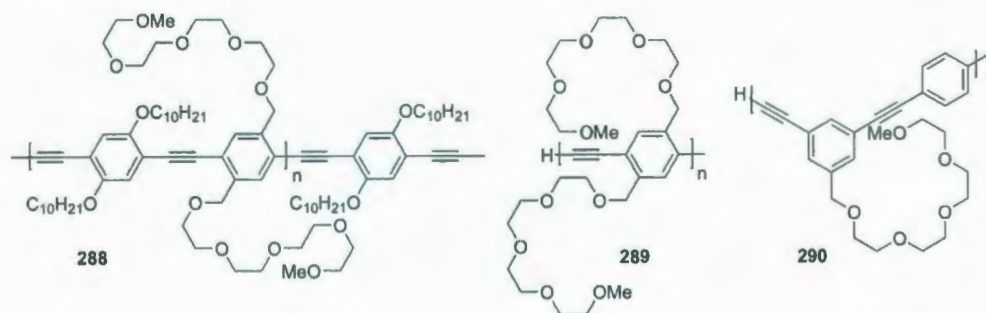


Figure 5.2: Polymers **288**, **289**, and **290** were targeted in this chapter.

In addition to the polymer-based functionalization, a series of amide-containing imidazolium ionic liquids and one pyrene-attached analogue were prepared in the second part of this thesis, with the intention of developing new strategies for SWNT functionalization (see Figure 5.3). The focus on these compounds originated from two known facts: (1) amide solvents are known to perform much better than other solvents in terms of dispersing SWNTs, and (2) pyrene shows irreversible adsorption on the surface of SWNTs. Based on these considerations, the imidazolium ion based targets shown in Figure 5.3 were anticipated to serve as a springboard toward the development of effective and environmentally friendly SWNT functionalization methods.

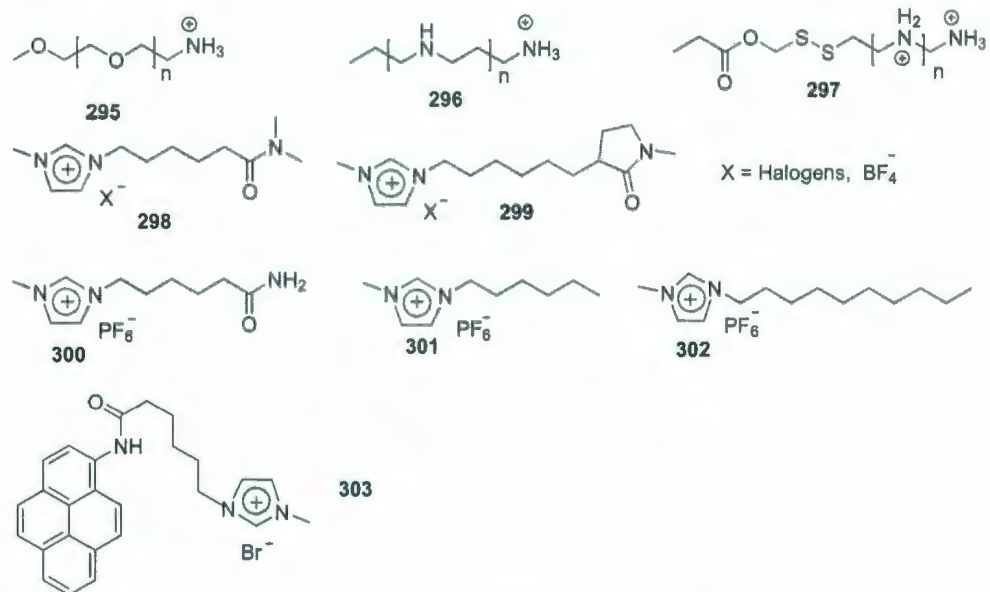
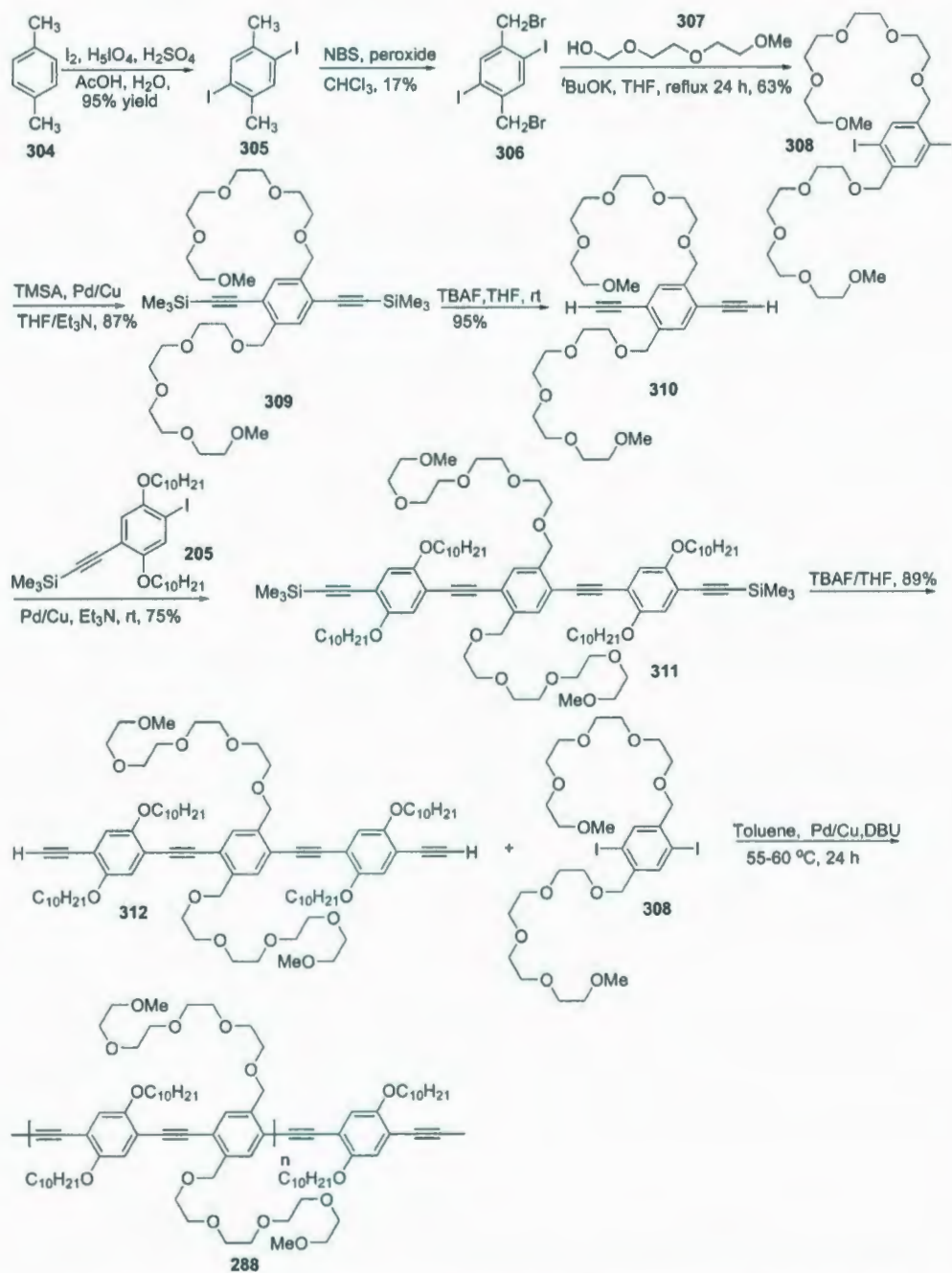


Figure 5.3: Task-specific ionic-liquids **300-303** to be investigated for SWNT functionalization.

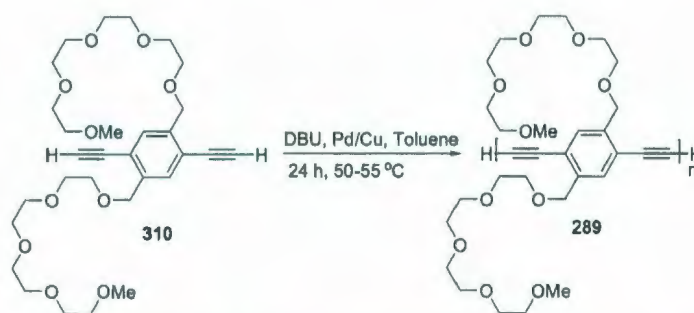
5.3 Results and Discussions

5.3.1 Synthesis of Ethylene Glycol Functionalized Phenylene Ethynylene Polymers

The synthesis of ethylene glycol ether attached PPEs is described in Scheme 5.1. It started with acid-catalyzed iodination of *p*-xylene **304** by molecular iodine and periodic acid, which resulted in the formation of compound **305** with an excellent yield of 95%. The diiodo compound **305** was then subjected to a modified Wurtz radical bromination using NBS in the presence of dibenzoyl peroxide and a trace amount of molecular bromine to afford compound **306** in 17% yield. Compound **306** then reacted with the alkoxide derived from tetra(ethylene glycol) monomethyl ether (**307**) to produce compound **308**. Compound **308** was then subjected to a Pd-catalyzed Sonogashira reaction with TMSA to afford compound **309** in 87% yield. The silyl protected ethynyl groups were deprotected by TBAF in THF at low temperature to give compound **310** in 95% yield. Compound **310** was then coupled with 1,4-bis(decyloxy)-2-iodo-5-(trimethylsilylethynyl)benzene (**205**) in another Sonogashira reaction to form OPE **311** in 75% yield. Deprotection of the TMS groups in compound **311** by TBAF at low temperature yielded oligomer **312**, which was then subjected to a Pd-catalyzed polymerization reaction to afford the desired polymer **288**.



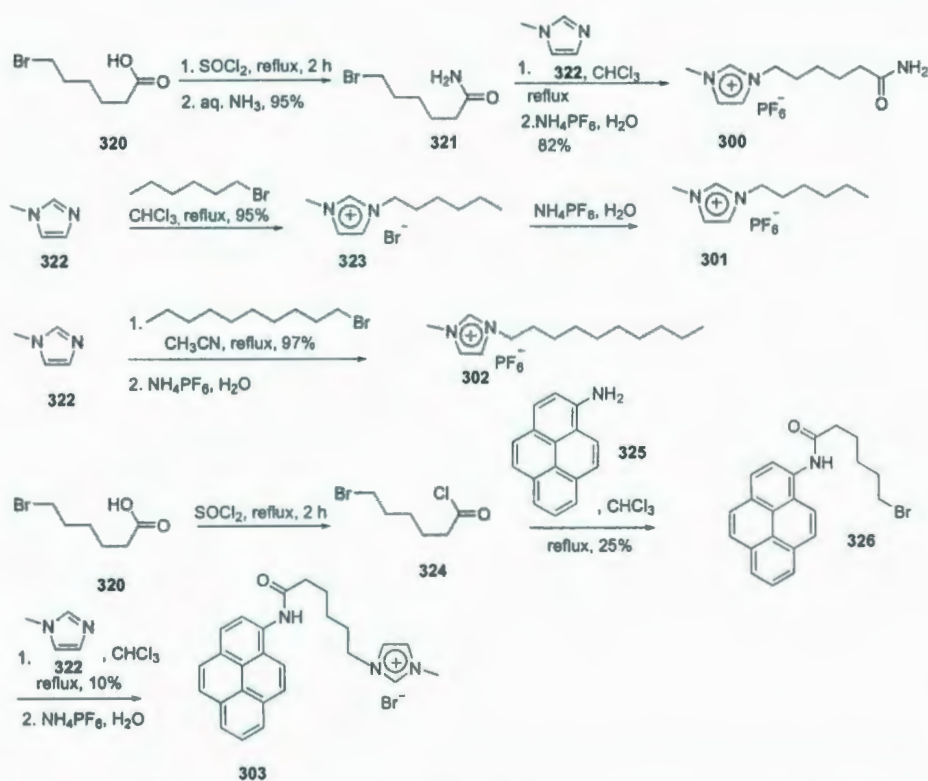
Scheme 5.1: Synthesis of ethylene glycol ether functionalized PPE **288**.



Scheme 5.2: Synthesis of ethylene glycol ether functionalized PPB **289**.

Compound **310** could also be polymerized through an oxidative homocoupling approach under the catalysis of Pd/Cu and DBU.¹⁵⁰ The synthesis is described in Scheme 5.2, wherein a phenylene butadiynylene polymer, PPB **289**, was obtained.

In addition to the above two linear polymers, a *meta*-phenylene based polymer **290** was also prepared, with the aim to investigate polymer folding,¹⁵¹ and its effects on SWNTs interactions. The synthesis (see Scheme 5.3) started from 3,5-diaminobenzoic acid (**313**), which was subjected to an acid-catalyzed esterification reaction with MeOH to form **314** in quantitative yield. In the next step, a Sandmeyer reaction was executed to yield diiodo compound **315** in 66% yield. Compound **315** was then coupled with TMSA through Sonogashira reaction to yield compound **316**. The ester functional group of **316** was reduced by LiAlH₄ at low temperature to give benzyl alcohol **317** in 98% yield. The benzyl alcohol functional group of compound **317** was transformed into benzyl bromide **318** via an Appel reaction using CBr₄ and PPh₃. Compound **318** was then subjected to alkylation reaction with tetra(ethylene glycol) monomethylether (**307**) in the presence of *t*-BuOK to produce **319**. Compound **319** was polymerized with dibromobenzene under Sonogashira conditions to give polymer **290**.



Scheme 5.4: Synthesis of imidazolium and pyrene containing ionic liquids.

ions, such as BF_4^- and PF_6^- , via anion metathesis.

5.3.3 Supramolecular Interactions Between SWNTs and Conjugated Polymers

Polymers **288**, **289**, and **290** were characterized by ^1H NMR, and FT-IR spectroscopy to verify their molecular structures. The following spectroscopic and microscopic characterizations were conducted in collaboration with N. Rice during her B.Sc. (honors) thesis study. For a comprehensive discussion on these characterizations, readers are referred to the B.Sc. (honors) thesis by N. Rice.¹⁵³

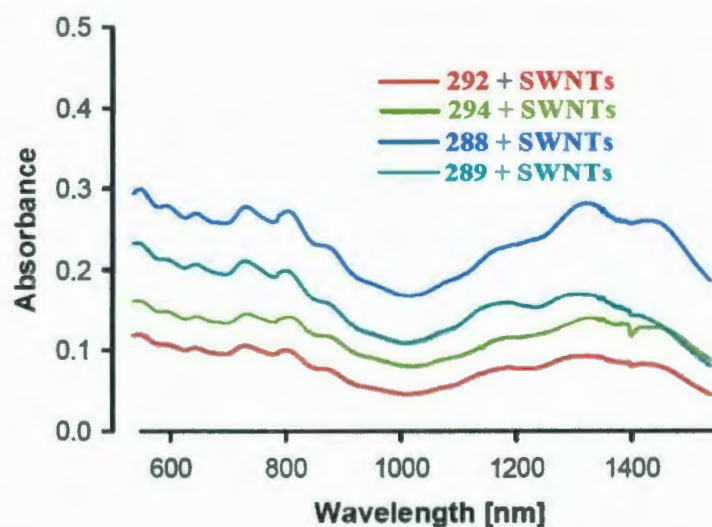


Figure 5.4: UV-Vis-NIR absorption spectra of polymer and HiPCO-NT complexes.

The dispersion of SWNTs in an organic solvent (CHCl_3) with the assistance of polymers **288-300** was undertaken by sonication. It should be mentioned here that the dispersion method was used in a similar manner to an ancient Egyptian recipe, first used 5000 years ago for the preparation of carbon black ink.¹⁵⁴ The suspensions of SWNTs in polymers **288**, **289**, and **300** were found to be stable. There was no obvious precipitation of SWNTs observed, and distinctive SWNT bands were detected in the UV-Vis-NIR absorption spectra. As shown in Figure 5.4, a multitude of absorption peaks are seen, which are due to the characteristic interband electronic transitions of HiPCO-NTs. The well-resolved spectral envelopes indicate that the nanotubes dispersed in solution are debundled. The debundling is also supported by atomic force microscopic (AFM) evidence (see Figure 5.5).

Evidence for selective dispersion of SWNTs by the polymers according to nanotube diameter was obtained from examining the radial breathing mode (RBM) region of the

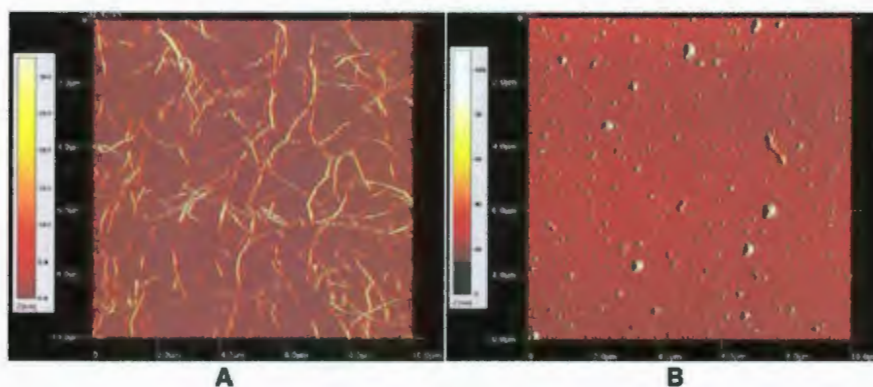


Figure 5.5: AFM images of SWNT-polymer complexes spincoated on mica surface. Left: polymer **289** with HiPCO-NTs; right: polymer **288** with CoMoCAT-NTs.

Raman spectra (see Figures 5.6 and 5.7). In general, the RBM frequency (ω_{RBM}) is inversely proportional to the NTs diameter, expressed by $\omega_{\text{RBM}} = A/d_t + B$, where A and B are constants depending on the experimental conditions used, and d_t denotes the diameter of nanotube. In the spectra, the RBM bands of pristine HiPCO sample displays two major groups of peaks centered around 181 and 269 cm^{-1} respectively. By adopting the two constants, $A = 223.5 \text{ nm cm}^{-1}$ and $B = 12.5 \text{ cm}^{-1}$,¹³⁸ the mean diameters for the two groups of nanotubes existing in HiPCO-NTs could be estimated as 1.33 and 0.87 nm. The RBM spectral patterns in Figure 5.6 clearly show that polymers **288** and **289**, both bearing ethylene glycol side chains, give rise to almost exclusive selection to smaller tubes ($d_t = 0.87 \text{ nm}$), while polymer **294** shows high selectivity for larger tubes ($d_t = 1.33 \text{ nm}$). The Raman spectrum for polymer **292** and HiPCO-NT complexes shows peaks at 181 and 269 cm^{-1} with unequal intensities. This result suggests that polymer **292** is more selective for smaller tubes instead of larger ones, but the diameter selectivity displayed by **292** is not as prominent as those of polymers **289** and **288**.

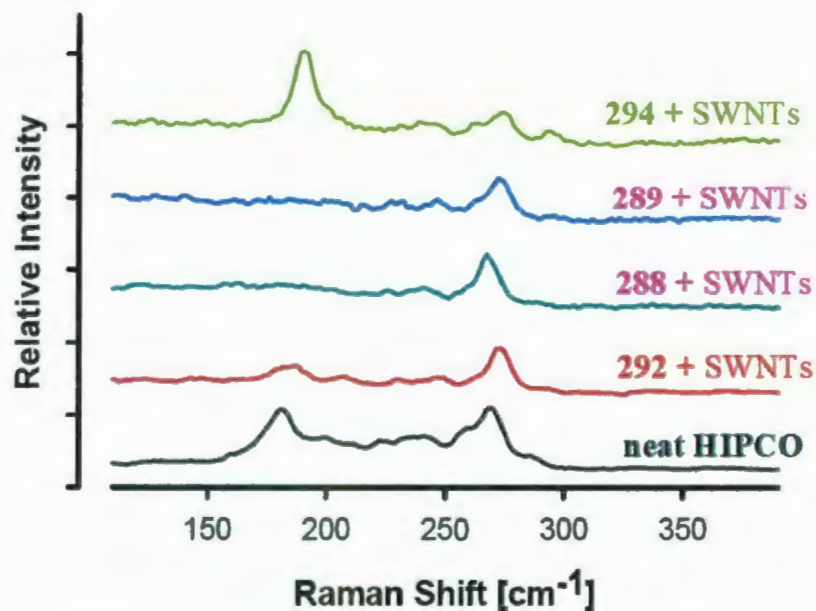


Figure 5.6: Raman spectra for polymer and HiPCO-NT composites in the RBM region.

The Raman spectra for polymer and CoMoCAT-NT complexes are given in Figure 5.7. The spectral envelopes observed in the Raman spectra, particularly in the RBM region, offer evidence for chirality discrimination. In the RBM region, the composites involving polymers **289** and **292-294** show three major bands at 273, 290, and 310 cm^{-1} . On the other hand, the composite of polymer **288** and nanotubes shows only two significant bands at 186 and 273 cm^{-1} . Compared to the neat CoMoCAT-NT sample, each of the polymers obviously shows some extent of selectivity to nanotubes of certain types. Detailed assignments of chiral indices on these Raman bands, however, cannot be convincingly made at this stage. Further characterization in collaboration with other groups equipped with photoluminescence and Raman instruments with variable excitation lasers is underway.

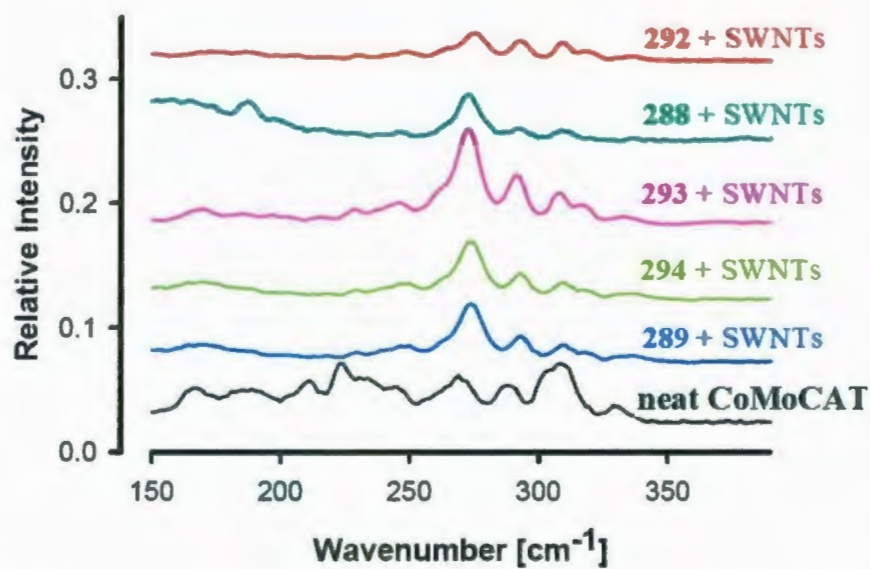


Figure 5.7: Raman spectra of polymers and CoMoCAT-NT composites in the RBM region.

5.4 Conclusions

It has been demonstrated that phenylene-based conjugated polymers upon suitable structural tailoring can effectively act as dispersants to form stable and highly debundled suspensions of SWNTs in common organic solvents. The supramolecular interactions originate mainly from π -stacking between these polymers and SWNTs. However, other non-covalent binding forces such as van der Waals, charge-transfer, and electrostatic interactions may also play significant roles, as manifested by the factor that ethylene glycol ether chains greatly improve the solubility and selectivity. Raman analyses suggest that polar poly(ethylene glycol) groups give rise to selectivity towards small diameter tubes in the HiPCO sample, whereas electron-rich aromatic groups cause preferable interactions with the large-diameter tubes. For the dispersion

of CoMoCAT-CNTs, enrichments of (6,5) and (7,6) nanotubes have been achieved by using different phenylene polymers, indicating a promising step to ultimate purification of structurally homogeneous SWNTs.

5.5 Experimental Part

General procedures and methods

The phenylene-based polymers were synthesized using the the literature procedures with suitable modifications.^{74,155} Two commercially available SWNT samples, namely HiPCO-NTs and CoMoCAT-NTs, were purchased from Carbon Nanotechnologies Inc. (Houston, TX) and SouthWest Nanotechnologies Inc. (Norman, OK), respectively.

Dispersion of SWNTs in polymer solutions was performed using our previously developed procedure: a suitable amount (0.5-1.0 mg) of as-produced SWNT sample was added to a saturated polymer solution in chloroform (ca. 2 mL), and the mixture was sonicated until a stable back suspension was formed (it could take a few minutes to hours). The resultant suspension was filtered through a tightly packed cotton plug, made on a medium-sized glass-pipette to remove any undissolved particles, affording almost clear suspension of SWNTs in chloroform.

Raman analysis was done on the thin films of polymer-SWNT complex drop-casted on glass substrates by using a confocal LabRAM instrument ($\lambda_{ex} = 532.1$ nm). Surface morphological studies were conducted on a QSCOPE 250 scanning probe microscope (SPM). Samples for AFM imaging (tapping mode) were prepared by first spin-coating dilute suspensions of SWNT in polymeric solution. Polymer

complexes (in chloroform) on freshly cleaved mica surfaces were spin-coated at 2,000 rpm, and then the surface were rinsed with pure chloroform three times while spinning in the spin-coater.

Chemicals and reagents were purchased from commercial suppliers and used without further purification. *p*-Xylene, PPh₃, TMSA were purchased from Fischer Scientific International Inc. MeOH, EtOH, Et₂O, CH₂Cl₂, CHCl₃ were of reagent grade and used directly. THF was distilled with sodium/benzophenone and subsequently purified. Et₃N, benzene, and toluene were dried by distilling with LiH. All reactions were performed in standard, dry glassware and palladium-catalyzed Sonogashira reactions were done under a N₂ atmosphere. Evaporation and concentration was done at H₂O-aspirator pressure. Flash column chromatography was carried out with silica gel 60 (230-400 mesh) from VWR International. Thin-layer chromatography (TLC) was carried out with silica gel 60 F₂₅₄ covered on plastic sheets and visualized by UV light or KMnO₄ stain. Melting points (m.p.) were measured with a Fisher-Johns melting point apparatus and are uncorrected. ¹H and ¹³C NMR spectra were measured on the Bruker Avance 500 MHz spectrometer. Chemical shifts are reported in ppm downfield from the signal of the internal reference SiMe₄. Coupling constants (*J*) are given in Hz. Infrared spectra (IR) were recorded on a Bruker Tensor 27 spectrometer. UV-Vis spectra were recorded on an Agilent 8453 spectrophotometer. AP-CI mass spectra were measured on an Agilent 1100 series LCMSD spectrometer, and high-resolution MALDI-TOF mass spectra on an Applied Biosystems Voyager instrument with dithranol as the matrix.

Synthesis of 1,4-diiodoxylene (305)

p-Xylene **304** (10.0 g, 9.43×10^{-2} mol), iodine (24.0 g, 9.43×10^{-2} mol) and periodic acid (8.95 g, 3.93×10^{-2} mol) were added in an oven-dried 250 mL round-bottom flask. The flask was placed in a water bath. Acetic acid (85 mL), H₂SO₄ (8.50 mL) and H₂O (10.0 mL) were added. The reaction mixture became hot at the beginning. After being stirred at room temperature for 0.5 h, the water bath was removed, followed by heating up to 85-90 °C for 24 h in an oil bath. The reaction mixture was then cooled to room temperature and poured into a 500 mL beaker half full of ice. The mixture was stirred for 0.5 h. Brown crystals were separated out of the solution. The crystals were collected by suction filtration. Recrystallization from acetone afforded compound **305** (27.8 g, 7.76×10^{-2} mol, 82%) as a white crystalline solid. IR (neat): 2974, 2946, 2912, 1555, 1487, 1040 cm⁻¹; ¹H NMR (500 MHz, CDCl₃): δ 7.69 (s, 2H), 2.38 (s, 6H); ¹³C NMR (125 MHz, CDCl₃): δ 141.0, 139.7, 129.4, 101.1, 27.3; APCI-LC-MS (positive mode) *m/z* calcd for C₈H₈I₂ 357.9, found 357.9 [M]⁺.

Synthesis of 1,1'-dibromo-1,4-diiodoxylene (**306**)

Compound **305** (12.0 g, 3.35×10^{-2} mol), NBS (26.8 g, 1.51×10^{-2} mol), benzoyl peroxide (649 mg, 2.68 mmol) were dissolved in 125 mL of dry CHCl₃ in an oven-dried 250 mL round-bottom flask, and to this was added 2-3 drops of molecular bromine. The mixture was refluxed under visible light irradiation for 8 h. The reaction was cooled to room temperature and excess bromine was quenched with satd Na₂S₂O₃ solution and the mixture was washed with satd NH₄Cl solution. The organic layer was kept in a freezer overnight to recrystallize. The white solid mass that formed was collected by suction filtration and column chromatographed to give compound **306**

as cotton-like crystals (3.02 g, 5.85 mmol, 17%). IR (neat): 3067, 3027, 2972, 2845, 1466, 1431, 1347, 1215, 1049 cm^{-1} ; ^1H NMR (500 MHz, CDCl_3): δ 7.94 (s, 2H), 4.52 (s, 4H); ^{13}C NMR (125 MHz, CDCl_3): δ 142.6, 141.4, 100.3, 100.0, 36.9; APCI-MS (positive mode) m/z calcd for $\text{C}_8\text{H}_4\text{Br}_2\text{I}_2$ 512.7/514.7/516.7, found 530.7/532.7/534.7 $[\text{M} + \text{H}_2\text{O}]^+$.

Synthesis of 1,1'-bis-tetra(ethylene glycol) monomethyl ether)-1,4-diiodoxylene (308)

Tetra(ethylene glycol) monomethyl ether **307** (591 mg, 2.84 mmol) in dry THF was added to an oven-dried 100 mL round-bottom flask kept in an ice-bath. To this was then added *t*-BuOK (317 mg, 2.84 mmol) and the flask was sealed with a septum, evacuated and purged with N_2 several times. The reaction mixture was then stirred at room temperature for 15 min, followed by heating at 60 $^\circ\text{C}$ for another 15 min. It was then cooled to room temperature. A solution of compound **306** (732 mg, 1.42 mmol) in dry THF was then added dropwise. The reaction mixture was then heated to 55 $^\circ\text{C}$ and stirred at this temperature for 24 h. The reaction was cooled to room temperature and solvent was removed under vacuum. The resulting solid mass was dissolved in CHCl_3 and washed with water. The organic layer was dried over MgSO_4 and concentrated under vacuum. The crude product was column chromatographed (hexanes/ CHCl_3 /MeOH, 40:40:1) to yield compound **308** (688 mg, 8.93×10^{-4} mol, 63%) as a pale-yellow liquid. IR (neat): 2869, 1454, 1350, 1199, 1042 cm^{-1} ; ^1H NMR (500 MHz, CDCl_3): δ 7.82 (s, 2H), 4.43 (s, 4H), 3.69-3.50 (m, 32H), 3.33 (s, 6H); ^{13}C NMR (125 MHz, CDCl_3): 141.8, 138.8, 97.4 (3 Ar-C), 76.3, 72.3, 71.1, 71.02, 71.0, 70.92, 70.9, 70.7 (8 ethylene C, instead of 9), 59.4; APCI-MS (positive mode) m/z

calcd for $C_{26}H_{44}O_{10}I_2$ 770.1, found 788.1 $[M + H_2O]^+$.

Synthesis of 1,1'-bis-tetra(ethylene glycol) monomethyl ether-1,4-bis(trimethylsilyl acetylene)xylene (309)

To an oven dried 100 mL round-bottom flask were added 1,1'-bis-tetra(ethylene glycol) monomethyl ether-1,4-diiodoxylene (**308**) (500 mg, 6.49×10^{-4} mol), $Pd(PPh_3)_2Cl_2$ (27.4 mg, 3.90×10^{-5} mol), CuI (25.0 mg, 1.31×10^{-4} mol) in dry THF (25 mL). The flask was purged with N_2 twice and cooled to $-78^\circ C$. To this mixture was added 10 drops of 1,8-diazabicyclo[5, 4, 0]undec-7-ene (DBU). TMSA (509 mg, 5.18 mmol) in Et_3N (5 ml) was then added dropwise for 0.5 h. The mixture was stirred for 2 h at this temperature, and then warmed up to room temperature under stirring overnight. The solvent was removed in vacuo and the resulting solid mass was dissolved in ethyl acetate and washed with 1% HCl. The organic layer was then washed with saturated NH_4Cl solution to give a deep-red organic layer, which was concentrated to dryness and then flash chromatographed (hexanes/ethyl acetate/diethyl ether, 10:1:1) to yield compound **309** (401 mg, 5.64×10^{-4} mol, 87%) as a brown liquid. IR (neat): 2957, 2921, 2871, 2152, 1621, 1384, 1109 cm^{-1} ; 1H NMR (500 MHz, $CDCl_3$): δ 7.56 (s, 2H Ar-H), 4.68 (s, 4H), 3.72-3.39 (m, 32H), 3.38 (s, 6H), 0.27 (s, 18H); ^{13}C NMR (125 MHz, $CDCl_3$): 139.8, 131.4, 122.1 (3 Ar-C), 102.7, 101.3 ($C\equiv C$), 72.3, 71.07, 71.02, 71.01, 70.93, 70.92, 70.91, 70.9, 70.5 (ethylene glycol and benzyl C), 59.4, 0.35; APCI-MS (positive mode) m/z calcd for $C_{36}H_{62}O_{10}Si_2$, 710.4 found 728.3 $[M + H_2O]^+$.

Synthesis of 1,1'-bis(tetraethyleneglycol monomethylether)-1,4-bis(ethynyl)xylene (310)

To an oven-dried 100 mL round-bottomed flask was added **309** (138.8 mg, 1.95×10^{-4} mol) in dry THF (20 mL). To this was then added TBAF (0.2 mL, 1 M solution in hexane) and sonicated at room temperature for 5 min. Slowly H₂O was added, and the solvent was then removed. The resulting solid mass was dissolved in diethyl ether and washed with satd. NH₄Cl solution. The organic layer was dried over MgSO₄, filtered and concentrated to afford compound **310** as a pale-brown liquid (105 mg, 1.85×10^{-4} mol, 95%). ¹H NMR (500 MHz, CDCl₃): δ 7.62 (s, 2H), 4.70 (s, 4H), 3.70-3.54 (m, 32H), 3.40 (s, 2H), 3.38 (s, 6H); ¹³C NMR (125 MHz, CDCl₃): δ 140.2, 131.8, 121.4 (3 Ar-C), 83.8, 81.2 (C \equiv C), 72.3, 71.1, 71.02, 71.01, 71.0, 70.95, 70.9, 70.8, 70.5 (ethyleneglycol and benzyl C), 59.4; APCI-MS (positive mode) *m/z* calcd for C₃₀H₄₆O₁₀ 566.3, found 584.4 [M + H₂O]⁺.

Synthesis of compound **311**

An oven-dried 100 mL round-bottom flask was purged with N₂ and to this were added compound **205** (57.3 mg, 9.36×10^{-5} mol), Pd(PPh₃)₂Cl₂ (2.60 mg, 3.70×10^{-6} mol), CuI (9.00 mg, 4.73×10^{-5} mol) in dry THF (50 mL). The round-bottom flask was purged with N₂ and cooled to -78 °C. Ten drops of DBU was then added. To this constantly stirred mixture, a solution of compound **310** (25.0 mg, 4.41×10^{-5} mol) in Et₃N (5 mL) was then added dropwise for 0.5 h. The mixture was stirred for 2 h at this temperature and then warmed up to room temperature under stirring overnight. The solvent was evaporated off and the resulting solid mass was dissolved in ethyl acetate and washed sequentially with 1% HCl, and satd. NH₄Cl to yield a deep-red organic layer, which was concentrated to dryness. Flash chromatography (hexanes/ethyl acetate/diethyl ether, 10:1:1) yielded compound **311** (51.0 mg, 3.32

$\times 10^{-5}$ mol, 75%) as a brown liquid. IR (neat): 2924, 2856, 2152, 1502, 1468, 1386, 1104 cm^{-1} ; ^1H NMR (500 MHz, CDCl_3): δ 7.68 (s, 2H, Ar-H), 6.98 (s, 2H, Ar-H), 6.95 (s, 2H, Ar-H), 4.84 (s, 4H), 4.01-3.99 (m, 8H), 3.73-3.52 (m, 32H), 3.37 (s, 6H), 1.93-1.81 (m, 8H), 1.56-1.47 (m, 8H), 1.37-1.26 (m, 48H), 0.91-0.87 (m, 12H), 0.29 (s, 18H); ^{13}C NMR (125 MHz, CDCl_3): 154.5, 153.8, 139.5, 131.0, 122.1, 117.2, 117.1, 114.4, 114.2 (9 Ar-C), 101.5, 100.7, 92.9, 92.6 ($\text{C}\equiv\text{C}$), 72.3, 71.02, 71.0, 70.96, 70.95, 70.3, 69.9, 69.7 (8 ethylene glycol and benzyl C signals instead of 9), 59.4, 32.3, 29.81, 29.8, 29.75, 29.74, 29.72, 26.5, 26.4, 23.1, 14.5, 0.4; MALDI-TOF MS (dithranol as the matrix) m/z calcd for $\text{C}_{92}\text{H}_{150}\text{O}_{14}\text{Si}_2$ 1536.34, found 1536.41 $[\text{M}]^+$.

Synthesis of compound 312

To an oven-dried 100 mL round-bottom flask was added **311** (50.0 mg, 3.25×10^{-5} mol) in dry THF (20 mL). To this was then added TBAF (0.03 mL, 1 M solution in hexanes, 2 drops) and the mixture was sonicated at room temperature for 5 min. H_2O was added slowly, then solvent was removed under vacuum. The resulting solid mass was dissolved in CHCl_3 and washed with satd. NH_4Cl solution. The organic layer was dried over MgSO_4 , filtered and evaporated to give compound **312** as a pale-brown solid (40.0 mg, 2.87×10^{-5} mol, 89%). ^1H NMR (500 MHz, CDCl_3): δ 7.69 (s, 2H, Ar-H), 7.01 (s, 2H, Ar-H), 6.99 (s, 2H, Ar-H), 4.84 (s, 4H), 4.04-4.0 (m, 8H), 3.66-3.52 (m, 32H), 3.37 (s, 8H, 2 OCH_3 and 2 ethynyl protons), 1.89-1.82 (m, 8H), 1.48-1.37 (m, 8H), 1.33-1.26 (m, 48H), 0.91-0.87 (m, 12H); ^{13}C NMR (125 MHz, CDCl_3): 154.5, 153.8, 139.5, 131.0, 122.2, 117.7, 117.3, 114.6, 113.3 (9 Ar-C), 92.9, 92.4, 82.8, 80.4 ($\text{C}\equiv\text{C}$), 72.3, 71.03, 71.00, 70.96, 70.95, 70.9, 70.3, 70.2, 69.8 (9 signals from ethyleneglycol and benzyl C), 59.3, 32.3, 29.75, 29.73, 29.72, 29.7,

29.6, 26.4, 23.1, 23.07, 14.5; MALDI-TOF MS (dithranol as the matrix) m/z calcd for $C_{86}H_{134}O_{14}$ 1391.98, found 1392.10 $[M]^+$.

Synthesis of PPE 288

An oven-dried 100 mL round-bottom flask was purged with N_2 and to this was then added **312** (45.4 mg, 3.26×10^{-5} mol), 1,1'-bis(tetraethyleneglycol monomethylether)-1,4-diiodoxylylene **308** (25.1 mg, 3.26×10^{-5} mol), $Pd(PPh_3)_2Cl_2$ (2.30 mg, 3.28×10^{-6} mol), CuI (12.0 mg, 6.32×10^{-5} mol) in dry toluene (50 mL). The flask was and purged with N_2 twice and cooled to -78 °C. Ten drops of DBU was then added and the content was heated up to $55-60$ °C. The reaction mixture was stirred for 24 h at this temperature and then cooled to room temperature. The solvent was evaporated off under vacuum and the residual solid mass was dissolved in $CHCl_3$ and washed sequentially with 1% HCl and satd. NH_4Cl solution to give a deep-red organic layer, which was concentrated to dryness to yield polymer **288** (38.0 mg) as a deep-red solid. IR (neat): 3387, 2921, 1649, 1559, 1106 cm^{-1} ; 1H NMR (500 MHz, $CDCl_3$): δ 7.85 (s, 1H), 7.66-7.01 (m, 16H), 4.84 (m, 8H), 4.46-3.05(m, 140H), 2.37-0.88(m, 200H), 1.84-1.34 (m, 50H), 1.34-1.26 (m, 110H), 0.88 (m, 30H).

Synthesis of polymer 289

An oven-dried 100 mL round-bottom flask was purged with N_2 , and to this were added compound **310** (105 mg, 1.85×10^{-4} mol), $Pd(PPh_3)_2Cl_2$ (5.00 mg, 7.10×10^{-6} mol), CuI (7.00 mg, 3.68×10^{-5} mol) in dry toluene (50 mL). The flask was purged with N_2 twice and then cooled to -78 °C. Ten drops of DBU was then added and heated up to $54-55$ °C. The mixture was stirred for 24 h at this temperature and then cooled to room temperature. The solvent was removed. The residual solid mass

was dissolved in CHCl_3 , washed sequentially with 1% HCl, and satd. NH_4Cl solution to give a deep-red organic layer, which was concentrated to dryness to afford polymer **289** (36.8 mg) as a deep-red solid. IR (neat): 2866, 1643, 1452, 1350, 1093 cm^{-1} ; ^1H NMR (500 MHz, CDCl_3): δ 7.73-7.48(m, 2H), 4.76 (m, 4H), 3.78-3.55 (m, 36H), 3.39 (s, 8H).

Synthesis of Synthesis of 3,5-diaminobenzoic acid ester (**314**)

To a 100 mL round-bottom flask was added compound **313** (2.00 g, 1.32×10^{-2} mol) in MeOH (30 mL). The mixture was sonicated for 0.5 h to form a suspension. Ten drops of 35% HCl was added to it, and the mixture was heated to reflux overnight. The reaction mixture was then cooled to room temperature and solvent was removed in vacuo to afford compound **314** (2.18 g, 1.31×10^{-2} mol, 100%) as a pale-brown precipitate. ^1H NMR (500 MHz, D_2O): δ 7.86 (d, $J = 2.0$ Hz, 2H, Ar-H), 7.54 (t, $J = 1.5$ Hz, 1H, Ar-H), 3.75 (s, 3H) (ammonium protons were not observed due to rapid exchange with D_2O); ^{13}C NMR (125 MHz, D_2O): δ 167.7, 134.2, 133.3, 124.1, 53.1; APCI-MS (positive mode) m/z calcd for $\text{C}_8\text{H}_{10}\text{O}_2\text{N}_2$ 166.2, found 167.1 [$\text{M} + \text{H}$] $^+$.

Synthesis of 3,5-diiodobenzoic acid ester (**315**)

To a 250 mL beaker was added compound **314** (3.00 g, 1.80×10^{-2} mol) in 35% HCl (8 mL). The mixture was vigorously shaken with a glass rod. The reaction mixture was cooled to 0 $^\circ\text{C}$, and then an aqueous solution (10 mL) of NaNO_2 (2.46 g, 3.57×10^{-2} mol) was slowly added to it. The reaction mixture was manually stirred at 0 $^\circ\text{C}$ for 0.5 h. Color changed to pale yellow at this stage. Another 10 mL of aqueous solution of KI (5.93 g, 3.57×10^{-2} mol) was then dropwise added to it

with vigorously shaking by the glass rod (violet vapor of I₂ released with each drop of addition). When KI addition was complete, the reaction mixture was stirred at room temperature for 15 min and then heated at 80 °C for 1 h. The reaction mixture was cooled to room temperature, and 10 mL of a saturated solution of Na₂S₂O₃ was added to it upon vigorously shaking. The solution became colorless at this stage. The compound was extracted with CHCl₃ (20 mL × 3). The combined organic layer was washed with satd. NaCl, dried in vacuo, and then recrystallized from MeOH to afford compound **315** (4.63 g, 1.19 × 10⁻² mol, 66%) as a white amorphous solid. IR (neat): 3065, 2955, 1721, 1542, 1264, 874; ¹H NMR (500 MHz, CDCl₃): δ 8.34 (d, *J* = 5.0 Hz, 2H, Ar-H), 8.26-8.25 (m, 1H, Ar-H), 3.94 (s, 3H); ¹³C NMR (125 MHz, CDCl₃): δ 164.6, 149.6, 138.1, 133.7, 94.7, 53.1; HR-EI-TOF MS (positive mode) *m/z* calcd for C₈H₆O₂I₂ 387.8457, found 387.8454 [M]⁺.

Synthesis of 3,5-bis(silylethynyl)benzoic acid ester (**316**)

To an oven-dried 100 mL round-bottom flask were added 3,5-diiodobenzoic acid methyl ester (**315**) (1.00 g, 2.58 mmol), Pd(PPh₃)₂Cl₂ (181 mg, 2.58 × 10⁻⁴ mol), CuI (98.0 mg, 5.16 × 10⁻⁴ mol) in dry THF (25 mL). The flask was evacuated and purged with N₂ twice and cooled to -78 °C. To this constantly stirred mixture TMSA (509 mg, 5.18 mmol) in Et₃N (5 mL) was added dropwise in 0.5 h. The mixture was stirred for 2 h at this temperature and then warmed up to room temperature and stirred overnight. The solvent was evaporated off. The residual mass was dissolved in ethyl acetate, washed sequentially with 1% HCl, and satd. NH₄Cl to give a deep-red organic layer, which was concentrated to dryness and then flash chromatographed (hexanes/CH₂Cl₂, 4:1) to yield compound **316** (700 mg, 2.13 × 10⁻³ mol, 83%) as

a brown solid. IR (neat): 2959, 2900, 2159, 1731, 1588, 1428, 1163 cm^{-1} ; ^1H NMR (500 MHz, CDCl_3): δ 8.00 (d, $J = 5.0$ Hz, 2H Ar-H), 7.68 (m, 1H, Ar-H), 3.87 (s, 3H), 0.24 (s, 18H); ^{13}C NMR (125 MHz, CDCl_3): δ 166.1, 139.4, 133.0, 130.9, 124.3, 103.3, 96.5, 52.8, 0.2; HR-EI-TOF MS (positive mode) m/z calcd for $\text{C}_{18}\text{H}_{24}\text{O}_2\text{Si}_2$ 328.1315, found 328.1309 $[\text{M}]^+$.

Synthesis of 3,5-bis(silylethynyl)benzyl alcohol (317)

A solution of **316** (900 mg, 2.74×10^{-3} mol) in dry THF (40 mL) was added to an oven-dried 100 mL round-bottom flask cooled at 0°C . A pre-cooled slurry of LiAlH_4 (226 mg, 5.97×10^{-3} mol) in dry THF (10 mL) was then added dropwise. After addition of LiAlH_4 , the reaction mixture was stirred at room temperature for 2 h, then a small amount of H_2O was added to quench excess LiAlH_4 , followed by neutralization with 1% HCl. The solvent THF was removed in vacuo, and the resulting content was extracted with ethyl acetate and washed with satd. NH_4Cl . The organic layer was dried over MgSO_4 and filtered. Evaporation of the solvent in vacuo afforded compound **317** (801 mg, 2.66 mmol, 98%) as a white solid. IR (neat): 3418, 3067, 2954, 2871, 2112, 1589, 1280, 1115 cm^{-1} ; ^1H NMR (500 MHz, CDCl_3): δ 7.54 (s, 1H, Ar-H), 7.44 (s, 2H, Ar-H), 4.68 (s, 2H), 0.28 (s, 18H), (OH proton was not observed due to rapid proton exchange); ^{13}C NMR (125 MHz, CDCl_3): δ 141.6, 134.8, 130.5, 124.0, 104.3, 95.5, 64.7, 0.3.

Synthesis of 3,5-bis(trimethylsilylethynyl)benzyl bromide (318)

A solution of **317** (780 mg, 2.59 mmol) and CBr_4 (3.56 g, 3.89 mmol) in CH_2Cl_2 (30 mL) was added in an oven-dried 100 mL round-bottom flask, and to this mixture was added dropwise a solution of PPh_3 (1.03 g, 3.89 mmol) in CH_2Cl_2 at 0°C . The content

was kept under stirring at room temperature for 3 h. The solvent was removed in vacuo and the residue was purified by flash chromatography (hexanes/CH₂Cl₂, 10:1) to yield compound **318** (859 mg, 2.33 mmol, 100%) as a white solid. IR (neat): 2959, 2899, 2163, 1586, 1441, 1215, 1164 cm⁻¹; ¹H NMR (500 MHz, CDCl₃): δ 7.54 (s, 1H, Ar-H), 7.45 (s, 2H, Ar-H), 4.39 (s, 2H), 0.29 (s, 18H); ¹³C NMR (125 MHz, CDCl₃): δ 138.5, 135.5, 132.7, 124.4, 103.8, 96.0, 32.1, 0.3.

Synthesis of **319**

Tetraethyleneglycol monomethyl ether **307** (524 mg, 1.42 mmol) in dry THF (50 mL) was added to an oven-dried 100 mL round-bottom flask kept in an ice-bath. To this was then added *t*-BuOK (317 mg, 2.84 × 10⁻³ mol), and the round-bottom flask was sealed with a septum and evacuated and purged with N₂ for several times to remove O₂ thoroughly. The reaction mixture was stirred at room temperature for 15 min, followed by heating at 60 °C for another 15 min. It was then cooled to room temperature, then a solution of **318** (270 mg, 1.30 × 10⁻³ mol) in dry THF was added dropwise. The reaction mixture was heated to 50-55 °C and stirred for 24 h. Afterwards the mixture was cooled to room temperature, and concentrated in vacuo. The resulting solid mass was dissolved in CHCl₃ and washed with H₂O. The organic layer was dried over MgSO₄, concentrated and finally column chromatographed to get compound **319** (420 mg, 1.21 mmol, 85%) as a pale-yellow liquid. IR (neat): 3234, 2869, 1454, 1350, 1199, 1042 cm⁻¹; ¹H NMR (500 MHz, CDCl₃): δ 7.40 (s, 1H, Ar-H), 7.34 (s, 2H, Ar-H), 4.40 (s, 2H), 3.56-3.41 (m, 16H), 3.25 (s, 3H), 3.10 (s, 2H, alkynyl protons); ¹³C NMR (125 MHz, CDCl₃): δ 139.6, 134.9, 131.6, 122.9, 82.9, 78.7, 72.3, 72.2, 72.1, 71.0, 70.9, 70.89, 70.8, 70.2, 70.1, 59.2.

Synthesis of polymer 290

An oven-dried 100 mL round-bottom flask was purged with N₂ and to this was then added compound **319** (116 mg, 3.35×10^{-4} mol), 1,4-dibromobenzene (79.0 mg, 3.04×10^{-4} mol), Pd(PPh₃)₂Cl₂ (5.00 mg, 7.10×10^{-6} mol), and CuI (7.00 mg, 3.68×10^{-5} mol) in dry toluene (25 mL). The flask was purged with N₂ twice. Five drops of DBU was then added and the mixture was heated up to 55-60 °C and stirred for 24 h at this temperature. The mixture was cooled to room temperature. The solvent was removed in vacuo. The resulting solid mass was dissolved in CHCl₃, washed sequentially with 1% HCl, and satd. NH₄Cl to give a deep-red organic layer, which was concentrated to dryness to yield polymer **290** (36.8 mg) as a deep-red solid. IR (neat): 3246, 2922, 2866, 2245, 1590, 1509 cm⁻¹; ¹H NMR (500 MHz, CDCl₃): δ 7.73-7.27 (m, 6H, Ar-H), 4.61 (s, 2H), 3.72-3.56 (m, 16H), 3.40 (s, 1H), 3.39 (s, 3H).

Synthesis of *N*-methyl imidazolium *N*-hexyl amide IL 300

1-Bromohexanoic acid **320** (4.00 g, 2.05×10^{-2} mol) was dissolved in SOCl₂ (9 mL) in an oven-dried 50 mL round-bottom flask, and the reaction was kept under reflux for 1 h. The reaction mixture was then cooled to room temperature, and excess SOCl₂ was removed by evaporation in rotary to give the acid chloride product as a liquid, which was dropwise added to a solution of aq. NH₄OH (20 mL) kept at 0 °C. The precipitated solid was washed with ice-cold water and dried in vacuo to get compound **321** (1.99 g, 1.02×10^{-2} mol, 50%) as a white solid (Mp 108 °C). A mixture of *N*-methylimidazole **322** (1.00 g, 1.22×10^{-2} mol) and compound **321** (2.37 g, 1.22×10^{-2} mol) was refluxed in dry acetonitrile (50 mL) in a 100 mL round-bottom flask overnight. After cooling, acetonitrile was evaporated off and the

resulting crude product was washed with cold ethyl acetate and dried under vacuum. To this was then added a solution of NH_4PF_6 (2.70 g, 2.57×10^{-2} mol) in dry acetone and the mixture was refluxed for 2 h. The white precipitate thus formed was filtered off and washed with acetone, and dried under high vacuum to give compound **300** (2.83 g, 1.0×10^{-2} mol, 82%) as a colorless solid. Mp 72 °C; IR (neat): 3426, 2957, 2932, 2861, 1629, 1572, 1466, 1168, 1056 cm^{-1} ; ^1H NMR (500 MHz, CDCl_3): δ 8.63 (s, 1H), 7.42 (s, 1H), 7.38 (s, 1H), 4.15-4.13 (m, 2H), 3.84 (m, 2H, NH_2), 3.84 (s, 3H), 2.24-2.19 (m, 2H), 1.85-1.81 (m, 2H), 1.57-1.32 (m, 2H), 1.30-1.27 (m, 2H); ^{13}C NMR (125 MHz, CDCl_3): δ 180.2, 136.2, 123.9, 122.6, 49.7, 36.0, 35.1, 29.3, 25.2, 24.8.

Synthesis of *N*-methylimidazole IL 301

N-Methylimidazole **322** (2.00 g, 2.44×10^{-2} mol) and *n*-hexyl bromide (4.02 g, 2.44×10^{-2} mol) were refluxed overnight in dry acetonitrile (50 mL) in a 100 mL round-bottom flask. Acetonitrile was evaporated off and the resulting viscous liquid was washed several times with cold ethyl acetate and dried in vacuo. To this was then added KPF_6 (7.50 g, 4.07×10^{-2} mol) in dry acetone and refluxed for 2 h. The white precipitate thus formed was filtered off and washed with acetone to give compound **301** (3.22 g, 1.04×10^{-2} mol, 85%) as a colourless viscous liquid. IR (neat): 3077, 2956, 2930, 2859, 1628, 1570, 1465, 1167 cm^{-1} ; ^1H NMR (500 MHz, CDCl_3): δ 9.11 (s, 1H), 7.39 (s, 1H), 7.33 (s, 1H), 4.23 (t, $J = 7.5$ Hz, 2H), 4.02 (s, 3H), 1.94-1.88 (m, 2H), 1.34-1.32 (m, 6H) 0.91 (t, $J = 7.1$ Hz, 3H); ^{13}C NMR (125 MHz, CDCl_3): δ 136.9, 124.2, 122.6, 50.4, 37.0, 36.8, 30.4, 26.1, 22.6, 14.2.

Synthesis of *N*-methylimidazole IL 302

N-Methylimidazole **322** (2.00 g, 2.44×10^{-2} mol) and *n*-decyl bromide (5.33 g,

2.44×10^{-2} mol) were refluxed overnight in dry acetonitrile (50 mL) in a 100 mL round-bottom flask. Acetonitrile was evaporated off and the resulting viscous liquid was washed several times with cold ethyl acetate and dried in vacuo. To this was then added KPF_6 (7.50 g, 4.07×10^{-2} mol) in dry acetone and refluxed for 2 h. The white precipitate thus formed was filtered off and washed with acetone to give compound **302** (5.53 g, 1.04×10^{-2} mol, 63%) as a colourless viscous liquid. IR (neat): 3070, 2924, 2854, 1570, 1516, 1167 cm^{-1} ; ^1H NMR (500 MHz, CDCl_3): δ 7.46 (s, 1H), 7.34 (s, 1H), 7.06-6.90 (m, 1H), 4.33 (t, $J = 7.5$ Hz, 2H), 4.15 (s, 3H), 1.95-1.90 (m, 2H), 1.34-1.26 (m, 14H), 0.89 (t, $J = 6.9$ Hz, 3H); ^{13}C NMR (125 MHz, CDCl_3): δ 138.0, 123.9, 122.2, 50.6, 37.2, 32.2, 30.7, 29.8, 29.7, 29.6, 29.4, 26.6, 23.0, 14.5.

Synthesis of 6-bromopyrene amide (**326**)

To an oven-dried 50 mL round-bottom flask was charged with 6-bromohexanoic acid (**320**) (899 mg, 4.61 mmol) and the flask was sealed with a septum and purged with N_2 several times. With the help of a syringe, SOCl_2 (10 mL) was added dropwise. The reaction mixture was then stirred at room temperature for 1 h. To this was added dropwise a solution of 2-aminopyrene (**325**) (1.00 g, 4.61×10^{-3} mol) in dry acetonitrile (25 mL). This was then stirred for 2 h, and refluxed overnight. After cooling, acetonitrile was evaporated off. The resulting solid was dissolved in CHCl_3 and washed with H_2O , and finally recrystallized from MeOH to yield compound **326** as a black crystalline solid (440 mg, 1.16 mmol, 25%). Mp >200 $^\circ\text{C}$; IR (neat): 3241, 3041, 2948, 2852, 1660, 1620, 1600, 1549, 1278 cm^{-1} ; ^1H NMR (500 MHz, CDCl_3): δ 8.44-7.77 (m, 9H, pyrene), 3.52-3.50 (m, 2H), 2.69-2.66 (m, 2H), 2.02-1.95 (m, 4H), 1.74-1.66 (m, 2H). Due to solubility problem meaningful ^{13}C NMR spectrum could

not be obtained.

Synthesis of pyrene containing amide **IL 303**

A mixture of *N*-methylimidazole **322** (1.00 g, 12.2 mmol) and pyrene **325** (4.63 g, 12.2 mmol) in dry acetonitrile (25 mL) was refluxed overnight. After cooling, acetonitrile was evaporated off. The resulting solid was washed with cold ethyl acetate and dried in vacuo to afford compound **303** as a black crystalline solid (460 mg, 1.21 mmol, 10%). Mp >200 °C; IR (neat): 3282, 2833, 1648, 1599, 1267 cm⁻¹; ¹H NMR (500 MHz, CDCl₃): δ 9.26 (s, 1H), 8.22-7.89 (m, 9H), 7.37 (s, 1H) 7.10 (s, 1H), 4.02 (s, 3H), 3.75 (s, 1H, NH), 3.63-1.28 (m, 10H). Due to solubility problem, meaningful ¹³C NMR spectrum could not be obtained for compound **303**.

Chapter 6

Conclusions and Future Work

The unifying theme of this thesis work is to develop efficient synthetic access to novel π -conjugated organic materials with the intention to benefit relevant research on biological chemistry, materials science, and engineering. In this sense, the design and synthesis of various functional carbon-rich molecular systems have been given the most attention, given their widespread application in molecular electronic/photonic devices and supramolecular chemistry. The synthetic work was followed by investigations on the interrelationships between molecular structure and property/reactivity using various state-of-the-art instrumental analyses. With such knowledge, device fabrications based on these materials are envisioned in the future work mainly through collaboration with other research teams.

In terms of synthetic methodologies, this thesis work demonstrates the efficiency of using the CuAAC reaction (a click reaction) to attach functional groups to various conjugated π -building blocks, ranging from [60]fullerene, porphyrin, tetrathiafulvalene derivatives, and linear and star-shaped conjugated oligomers. In almost all of

experiments, the yields of CuAAC reactions were found around 60-80%, which is less than the expected quantitative yield for general click reaction. Nevertheless, the click strategy still demonstrated superior advantages over other synthetic methods, given the structural complexity of the dendrimer hybrids reported in this thesis. In addition, the synthetic route to a class of electron-rich polyynes has also been explored. Redox properties of these polyynes were studied and the results showed the potential of these materials to attain electrochemically active conjugated polymer materials. Various polyethyleneglycol functionalized conjugated polymers (PPE, PPB and meta-phenylene PPE) and imidazolium and pyrene containing amide ionic liquids have also been synthesized to facilitate the functionalization of SWNTs.

In terms of property studies, the most significant results are from; (i) investigations of the interfacial self-assembly of dendrofullerene. From detailed examination of surface morphology, it is believed that under different conditions, dendro[60]fullerenes could give four different self-assembly morphologies, namely, multilayered cylinder, lamella, monolayer spherical micelle, and multilayered spherical micelle. This finding obviously presents a very useful bottom-up approach to construct uniform functional nanomaterial. Further exploration along this direction would benefit the research of C_{60} and dendrimer based functional nanomaterials; (ii) interesting electrochemical and spectroscopic behavior for a variety of new compounds (TTF, polyynes, TTFAQs, porphyrins, linear and star-shaped oligomers; (iii) discriminative control over supramolecular interactions between rationally designed polymers and SWNTs.

Overall, the synthetic work of my PhD study is aimed at offering reasonable models for better understanding the control and manipulation of functional nanomaterials.

The numerous compounds prepared in this research work, although have offered useful information in this respect, are still insufficient in delineating clear structure-property relationships. Future research should therefore be focused on continued design and synthesis of analogous molecular structures, more detailed property and mechanistic investigations, and device fabrication based on extensive collaboration with other groups.

Bibliography

- [1] Husanu, M.; Baibarac, M.; Baltog, I. *Physica E* **2008**, 66–69.
- [2] Stupp, S. I. *Chem. Rev.* **2005**, 105, 1023–1024.
- [3] Hawker, C. J.; Wooley, K. L. *Science* **2005**, 309, 1200–1205.
- [4] Lo, S.-C.; Burn, P. L. *Chem. Rev.* **2007**, 107, 1097–1116.
- [5] Brusso, J. L.; Hirst, O. D.; Dadvand, A.; Ganesan, S.; Cicoira, F.; Robertson, C. M.; Oakley, R. T.; Rosei, F.; Perepichka, D. F. *Chem. Mater.* **2008**, 20, 2484–2494.
- [6] Zang, L.; Che, Y.; Moore, J. S. *Acc. Chem. Res.* **2008**, 41, 1596–1608.
- [7] Kolb, H. C.; Finn, M. G.; Sharpless, B. *Angew. Chem. Int. Ed.* **2001**, 40, 2004–2021.
- [8] Kolb, H. C.; Sharpless, K. B. *DDT* **2003**, 8, 1128–1137.
- [9] Bock, V. D.; Hiemstra, H.; van Maarseveen, J. H. *Eur. J. Org. Chem.* **2006**, 51–68.
- [10] Jørgensen, K. A. *Angew. Chem. Int. Ed.* **2000**, 39, 3558–3588.

- [11] Kolb, H. C.; VanNieuwenhze, M. S.; Sharpless, K. B. *Chem. Rev.* **1994**, *94*, 2483–2547.
- [12] Ohno, H.; Aso, A.; Kadoh, Y.; Fujii, N.; Tanaka, T. *Angew. Chem. Int. Ed.* **2007**, *46*, 6325–6328.
- [13] Dondoni, A. *Angew. Chem. Int. Ed.* **2008**, *47*, 8995–8997.
- [14] Rostovtsev, V. V.; Green, L. G.; Fokin, V. V.; Sharpless, K. B. *Angew. Chem. Int. Ed.* **2002**, *41*, 2596–2599.
- [15] Lee, B.-Y.; Park, S. R.; Jeon, H. B.; Kim, K. S. *Tetrahedron Lett.* **2006**, *47*, 5105–5109.
- [16] Appukkuttan, P.; Dehaen, W.; Fokin, V. V.; der Eycken, E. V. *Org. Lett.* **2004**, *6*, 4223–4225.
- [17] Wu, P.; Fokin, V. *Aldrichimica Acta* **2007**, *40*, 7–17.
- [18] Binder, W. H.; Sachsenhofer, R. *Macromol. Rapid Comm.* **2008**, *29*, 952–981.
- [19] Chan, T. R.; Hilgraf, R.; Sharpless, K. B.; Fokin, V. V. *Org. Lett.* **2004**, *6*, 2853–2855.
- [20] Himo, F.; Lovell, T.; Hilgraf, R.; Rostovtsev, V. V.; Noodleman, L.; Sharpless, K. B.; Fokin, V. V. *J. Am. Chem. Soc.* **2005**, *127*, 210–216.
- [21] Golas, P. L.; Tsarevsky, N. V.; Sumerlin, B. S.; Matyjaszewski, K. *Macromolecules* **2006**, *39*, 6451–6457.

- [22] Zhan, W.-H.; Barnhill, H. N.; Sivakumar, K.; Tiana, H.; Wang, Q. *Tetrahedron Lett.* **2005**, *46*, 1691–1695.
- [23] Orgueira, H. A.; Fokas, D.; Isome, Y.; Chan, P. C.-M.; Baldino, C. M. *Tetrahedron Lett.* **2005**, *46*, 2911–2914.
- [24] Hein, C. D.; Liu, X.-M.; Wang, D. *Pharm. Res.* **2008**, *25*, 2216–2230.
- [25] Rondelez, Y.; Marie-Noëlle Rager, A. D.; Reinaud, O. *J. Am. Chem. Soc.* **2002**, *124*, 1334–1340.
- [26] Chassaing, S.; Kumarraja, M.; Sido, A. S. S.; Pale, P.; ; Sommer, J. *Org. Lett.* **2007**, *9*, 883–886.
- [27] Tron, G. C.; Pirali, T.; Billington, R. A.; Canonico, P. L.; Sorba, G.; Genazzani, A. A. *Med. Res. Rev.* **2008**, *28*, 278–308.
- [28] Horne, W. S.; Stout, C. D.; Ghadiri, M. R. *J. Am. Chem. Soc.* **2003**, *125*, 9372–9376.
- [29] Hawker, C. J.; Fokin, V. V.; Finn, M. G.; Sharpless, K. B. *Aust. J. Chem.* **2007**, *60*, 381–383.
- [30] Helms, B.; Meijer, E. W. *Science* **2006**, *313*, 929–930.
- [31] Wu, P.; Malkoch, M.; Hunt, J. N.; Vestberg, R.; Kaltgrad, E.; Finn, M. G.; Valery V. Fokin, K. B. S.; Hawker, C. J. *Chem. Commun.* **2005**, 5775–5777.
- [32] Lutz, J.-F. *Angew. Chem. Int. Ed.* **2007**, *46*, 1018–1025.

- [33] Englert, B. C.; Bakbak, S.; Bunz, U. H. F. *Macromolecules* **2005**, *38*, 5868–5877.
- [34] Daugaard, A. E.; Hvilsted, S.; Hansen, T. S.; Larsen, N. B. *Macromolecules* **2008**, *41*, 4321–4327.
- [35] Gil, M. V.; Arévalo, M. J.; López, O. *Synthesis* **2007**, 1589–1620.
- [36] Boydston, A. J.; Holcombe, T. W.; Unruh, D. A.; Fréchet, J. M. J.; Grubbs, R. H. *J. Am. Chem. Soc.* **2009**, *131*, 5388–5389.
- [37] Trooper, F. D.; Romanowska, A.; Roy, R. *Meth. Enzym.* **1994**, *242*, 257–271.
- [38] Moses, J. E.; Moorhouse, A. D. *Chem. Soc. Rev.* **2007**, *36*, 1249–1262.
- [39] Ladmiral, V.; Mantovani, G.; Clarkson, G. J.; Cauet, S.; Irwin, J. L.; Haddleton, D. M. *J. Am. Chem. Soc.* **2006**, *128*, 4823–4830.
- [40] Wang, J.; Matyjaszewski, K. *J. Am. Chem. Soc.* **1995**, *117*, 5614–5615.
- [41] Tsarevsky, N. V.; Sumerlin, B. S.; Matyjaszewski, K. *Macromolecules* **2005**, *38*, 3558–3561.
- [42] Riva, R.; Schmeits, S.; Jérôme, C.; Jérôme, R.; Lecomte, P. *Macromolecules* **2007**, *40*, 796–803.
- [43] Durmaz, H.; Dag, A.; Altintas, O.; Erdogan, T.; Hizal, G.; Tunca, U. *Macromolecules* **2007**, *40*, 191–198.
- [44] Laurent, B. A.; Grayson, S. M. *J. Am. Chem. Soc.* **2006**, *128*, 4238–4239.

- [45] Carroll, J. B.; Jordan, B. J.; Xu, H.; Erdogan, B.; Lee, L.; Cheng, L.; Tiernan, C.; Cooke, G.; Rotello, V. M. *Org. Lett.* **2005**, *7*, 2551–2554.
- [46] Hilf, S.; Hanik, N.; Kilbinger, A. F. M. *J. Polym. Sci. Part A: Polym. Chem.* **2008**, 2913–2921.
- [47] Binder, W. H.; Kluger, C. *Curr. Org. Chem.* **2006**, *10*, 1791–1815.
- [48] Collman, J. P.; Devaraj, N. K.; Chidsey, C. E. D. *Langmuir* **2004**, *20*, 1051–1053.
- [49] Zirbs, R.; Kienberger, F.; Hinterdorfer, P.; Binder, W. H. *Langmuir* **2005**, *21*, 8414–8421.
- [50] Such, G. K.; Quinn, J. F.; Quinn, A.; Tjipto, E.; Caruso, F. *J. Am. Chem. Soc.* **2006**, *128*, 9318–9319.
- [51] Yang, M.; Sheehan, P. E.; King, W. P.; Whitman, L. J. *J. Am. Chem. Soc.* **2006**, *128*, 6774–6775.
- [52] Bakbak, S.; Leech, P. J.; Carson, B. E.; Saxena, S.; King, W. P.; Bunz, U. H. F. *Macromolecules* **2006**, *39*, 6793–6795.
- [53] Hassane, F. S.; Frisch, B.; Schuber, F. *Bioconjugate Chem.* **2006**, *17*, 849–854.
- [54] Ossipov, D. A.; Piskounova, S.; Hilborn, J. *Macromolecules* **2008**, *41*, 3971–3982.
- [55] Sinaga, A.; Hatton, T. A.; Tam, K. C. *Macromolecules* **2007**, *40*, 9064–9073.

- [56] Malkoch, M.; Vestberg, R.; Gupta, N.; Mespouille, L.; Dubois, P.; Malson, A. F.; Hedrick, J. L.; Liao, Q.; Frank, C. W.; Kingsbury, K.; Hawker, C. *Chem. Commun.* **2006**, 2774–2776.
- [57] Tzokova, N.; Fernyhough, C. M.; Topham, P. D.; Sandon, N.; Adams, D. J.; Butler, M. F.; Armes, S. P.; Ryan, A. J. *Langmuir* **2009**, *25*, 2479–2485.
- [58] Crescenzi, V.; Cornelio, L.; Meo, C. D.; Nardecchia, S.; Lamanna, R. *Biomacromolecules* **2007**, *8*, 1844–1850.
- [59] Nierengarten, J.-F.; Gutiérrez-Nava, M.; Zhang, S.; Masson, P.; Oswald, L.; Bourgogne, C.; Rio, Y.; Accorsi, G.; Armaroli, N.; Setayesh, S. *Carbon* **2004**, *42*, 1077–1083.
- [60] Mahmud, I. M.; Zhou, N.; Zhao, Y. *Tetrahedron* **2008**, *64*, 11420–11432.
- [61] Kong, J.; Franklin, N. R.; Zhou, C.; Chapline, M. G.; Peng, S.; Cho, K.; Dai, H. *Science* **2000**, *287*, 622–625.
- [62] Kong, J.; Chapline, M. G.; Dai, H. *Adv. Mater.* **2001**, *13*, 1384–1386.
- [63] Avouris, P. *Acc. Chem. Res.* **2002**, *35*, 1026–1034.
- [64] Plank, N.; Cheung, R. *Microelec. Eng.* **2004**, *7374*, 578–582.
- [65] Choi, W. B.; Chung, D. S.; Kang, J. H.; Kim, H. Y.; Jin, Y. W.; Han, I. T.; Lee, Y. H.; Jung, J. E.; Lee, N. S.; Park, G. S.; Kim, J. M. *Appl. Phys. Lett.* **1999**, *75*, 3129–3131.

- [66] Dresselhaus, M.; Dresselhaus, G.; Avouris, P. *Carbon Nanotubes: Synthesis, Structure, Properties and Applications.*; Springer: Berlin, 2001.
- [67] Dai, H. *Surf. Sci.* **2002**, *500*, 218–241.
- [68] Dai, L.; Patil, A.; Gong, X.; Guo, Z.; Liu, L.; Liu, Y.; Zhu, D. *ChemPhysChem* **2003**, *4*, 1150–1169.
- [69] Huang, Y.; Duan, X.; Wei, Q.; Lieber, C. M. *Science* **2001**, *291*, 630–633.
- [70] Tasis, D.; Tagmatarchis, N.; Georgakilas, V.; Prato, M. *Chem. Eur. J.* **2003**, *9*, 4000–4008.
- [71] Li, H.; Cheng, F.; Duft, A. M.; Adronov, A. *J. Am. Chem. Soc.* **2005**, *127*, 14518–14524.
- [72] Cheng, F.; Imin, P.; Maunders, C.; Botton, G.; Adronov, A. *Macromolecules* **2008**, *41*, 2304–2308.
- [73] Valentini, L.; Armentano, I.; Ricco, L.; Alongi, J.; Pennelli, G.; Mariani, A.; Russo, S.; Kenny, J. *Diamond Rel. Mater.* **2006**, *15*, 95–99.
- [74] Chen, J.; Liu, H.; Weimer, W. A.; Halls, M. D.; Waldeck, D. H.; Walker, G. C. *J. Am. Chem. Soc.* **2002**, *124*, 9034–9035.
- [75] Cheng, F.; Adronov, A. *Chem. Eur. J.* **2006**, *12*, 5053–5059.
- [76] Hirsch, A. *Angew. Chem. Int. Ed.* **2002**, *41*, 1853–1859.
- [77] Niyogi, S.; Hamon, M. A.; Hu, H.; Zhao, B.; Bhowmik, P.; Sen, R.; Itkis, M. E.; Haddon, R. C. *Acc. Chem. Res.* **2002**, *35*, 1105–1113.

- [78] Sun, Y.-P.; Fu, K.; Lin, Y.; Huang, W. *Acc. Chem. Res.* **2002**, *35*, 1096–1104.
- [79] Banerjee, S.; Hemraj-Benny, T.; Wong, S. S. *Adv. Mater.* **2005**, *17*, 17–29.
- [80] Zeng, Y.-L.; Huang, Y.-F.; Jiang, J.-H.; Zhang, X.-B.; Tang, C.-R.; Shen, G.-L.; Yu, R.-Q. *Electrochem. Commun.* **2007**, *9*, 185–190.
- [81] Maurizio Prato, K. K.; Bianco, A. *Acc. Chem. Res.* **2008**, *41*, 60–68.
- [82] Guo, Z.; Liang, L.; Liang, J.-J.; Ma, Y.-F.; Yang, X.-Y.; Ren, D.-M.; Chen, Y.-S.; Zheng, J.-Y. *J. Nanopart. Res.* **2008**, *10*, 1077–1083.
- [83] Liu, J.; Nie, Z.; Gao, Y.; Adronov, A.; Li, H. *J. Polym. Sci. Part A: Polym. Chem.* **2008**, *46*, 7187–7199.
- [84] Lehn, J. M. *Supramolecular Chemistry*; VCH Press: New York, 1995.
- [85] Palmer, L. C.; Stupp, S. I. *Acc. Chem. Res.* **2008**, *41*, 1674–1684.
- [86] Trabolsi, A.; Elhabiri, M.; Urbani, M.; de la Cruz, J. L. D.; Ajamaa, F.; Solladié, N.; Albrecht-Gary, A.-M.; Nierengarten, J.-F. *Chem. Commun.* **2005**, 5736–5738.
- [87] Fernández, G.; Pérez, E. M.; Sánchez, L.; Martín, N. *J. Am. Chem. Soc.* **2008**, *130*, 2410–2411.
- [88] Moon, K.-S.; Lee, E.; Lee, M. *Chem. Commun.* **2008**, 3061–3063.
- [89] Kennedy, R. D.; Ayzner, A. L.; Wagner, D. D.; Day, C. T.; Halim, M.; Khan, S. I.; Tolbert, S. H.; Schwartz, B. J.; Rubin, Y. *J. Am. Chem. Soc.* **2008**, *130*, 17290–17292.

- [90] Lin, N.; Langner, A.; Tait, S. L.; Rajadurai, C.; Ruben, M.; Kern, K. *Chem. Commun.* **2007**, 4860–4862.
- [91] Isobe, H.; Cho, K.; Solin, N.; Werz, D. B.; Seeberger, P. H.; Nakamura, E. *Org. Lett.* **2007**, *9*, 4611–4614.
- [92] Hahn, U.; Cardinaliy, F.; Nierengarten, J.-F. *New J. Chem.* **2007**, *31*, 1128–1138.
- [93] Hahn, U.; González, J. J.; Huerta, E.; Segura, M.; Eckert, J.-F.; Cardinali, F.; de Mendoza, J.; Nierengarten, J.-F. *Chem. Eur. J.* **2005**, *11*, 6666–6672.
- [94] Cassell, A. M.; Asplund, C. L.; Tour, J. M. *Angew. Chem. Int. Ed.* **1999**, *38*, 2403–2405.
- [95] Rio, Y.; Accorsi, G.; Nierengarten, H.; Rehspringer, J.-L.; Hönerlage, B.; Kopitkovas, G.; Chugreev, A.; Dorsselaer, A. V.; Armaroli, N.; ; Nierengarten, J.-F. *New J. Chem.* **2002**, *26*, 1146–1154.
- [96] Hager, K.; Hartnagel, U.; Hirsch, A. *Eur. J. Org. Chem.* **2007**, 1942–1956.
- [97] de Freitas, R. P.; Iehl, J.; Delavaux-Nicot, B.; Nierengarten, J.-F. *Tetrahedron* **2008**, *64*, 11409–11419.
- [98] Iehl, J.; de Freitas, R. P.; Delavaux-Nicot, B.; Nierengarten, J.-F. *Chem. Commun.* **2008**, 2450–2452.
- [99] Echegoyen, L.; Echegoyen, L. E. *Acc. Chem. Res.* **1998**, *31*, 593–601.

- [100] Wang, J. *Analytical Electrochemistry*; John Wiley & Sons, Inc.: Hoboken, NJ, 2006.
- [101] Araki, Y.; Kunieda, R.; Fujitsuka, M.; Ito, O.; Motoyoshiya, J.; Aoyama, H.; Takaguchi, Y. *C. R. Chimie* **2006**, *9*, 1014–1021.
- [102] Guldi, D. M.; Prato, M. *Acc. Chem. Res.* **2000**, *33*, 695–703.
- [103] Clifford, J. N.; Gégout, A.; Zhang, S.; de Freitas, R. P.; Urbani, M.; Holler, M.; Ceroni, P.; Nierengarten, J.-F.; Armaroli, N. *Eur. J. Org. Chem.* **2007**, 5899–5908.
- [104] Guldi, D. M.; Zerbetto, F.; Georgakilas, V.; Prato, M. *Acc. Chem. Res.* **2005**, *38*, 38–43.
- [105] Partha, R.; Lackey, M.; Hirsch, A.; Ward Casscells, S.; Conyers, J. L. *J. Nanobiotech.* **2007**, *5*, 1–11.
- [106] Nandi, N.; Vollhardt, D. *Acc. Chem. Res.* **2007**, *40*, 351–360.
- [107] Tsonchev, S.; Schatz, G. C.; ; Ratner, M. A. *Nano Lett.* **2003**, *3*, 623–626.
- [108] Stupp, S. I.; LeBonheur, V.; Walker, K.; Li, L. S.; Huggins, K. E.; Keser, M.; Amstutz, A. *Science* **1997**, *276*, 384–389.
- [109] Jiang, D.-L.; Aida, T. *Nature* **1997**, *388*, 454–456.
- [110] Loiseau, F.; Campagna, S.; Hameurlaine, A.; Dehaen, W. *J. Am. Chem. Soc.* **2005**, *127*, 11352–11563.

- [111] Schenning, A. P. H. J.; Peeters, E.; Meijer, E. W. *J. Am. Chem. Soc.* **2000**, *122*, 4489–4495.
- [112] Moore, J. S. *Acc. Chem. Res.* **1997**, *30*, 402–413.
- [113] Günes, S.; Neugebauer, H.; Sariciftci, N. S. *Chem. Rev.* **2007**, *107*, 1324–1338.
- [114] Murphy, A. R.; Fréchet, J. M. J. *Chem. Rev.* **2007**, *107*, 1066–1096.
- [115] Meiyer, H.; Lehmann, M.; Kolb, U. *Chem. Eur. J.* **2000**, *6*, 2462–2469.
- [116] Jiang, Y.; Lu, Y.-X.; Cui, Y.-X.; Zhou, Q.-F.; Ma, Y.; Pei, J. *Org. Lett.* **2007**, *9*, 4539–4542.
- [117] Hoeben, F. J. M.; Jonkheijm, P.; Meijer, E.; Schenning, A. P. H. J. *Chem. Rev.* **2005**, *105*, 1491–1546.
- [118] Chen, G.; Zhao, Y. *Tetrahedron Lett.* **2006**, *47*, 5069–5073.
- [119] Jiang, L.; Jiu, T.; Li, Y.; Li, Y.; Yang, J.; Li, J.; Li, C.; Liu, H.; Song, Y. *J. Phys. Chem. B* **2008**, *112*, 756–759.
- [120] Larsen, J.; Andersson, J.; ás, T.; Polívka,; Sly, J.; Crossley, M. J.; Sundström, V.; Åkesson, E. *Chem. Phys. Lett.* **2005**, *403*, 205–210.
- [121] Punidha, S.; Sinha, J.; Kumar, A.; Ravikanth, M. *J. Org. Chem.* **2008**, *73*, 323–326.
- [122] Kudryavtsev, Y. P.; Evsyukov, S. E.; Guseva, M. B.; Babaev, V. G.; Khvostov, V. V. *Russ. Chem. Bull.* **1993**, *42*, 399–413.

- [123] Shun, A. L. K. S.; Tykwinski, R. R. *Angew. Chem. Int. Ed.* **2006**, *45*, 1034–1057.
- [124] Chalifoux, W. A.; Tykwinski, R. R. *Chem. Rec.* **2006**, *6*, 169–182.
- [125] Spantulescu, A.; Luu, T.; Zhao, Y.; McDonald, R.; Tykwinski, R. R. *Org. Lett.* **2008**, *10*, 609–612.
- [126] Chalifoux, W. A.; Tykwinski, R. R. *Compt. Rend. Chim.* **2009**, *12*, 341–358.
- [127] Bendikov, M.; Wudl, F.; Perepichka, D. F. *Chem. Rev.* **2004**, *104*, 4891–4946.
- [128] Khanous, A.; Gorgues, A.; Jubault, M. *Tetrahedron Lett.* **1990**, *31*, 7307.
- [129] Nielsen, M. B.; Moonen, N. N. P.; Boudon, C.; Gisselbrecht, J.-P.; Seiler, P.; Gross, M.; Diederich, F. *Chem. Commun.* **2001**, 1848–1849.
- [130] Nielsen, M. B.; Utesch, N. F.; Moonen, N. N. P.; Boudon, C.; Gisselbrecht, J.-P.; Concilio, S.; Piotta, S. P.; Seiler, P.; Günter, P.; Gross, M.; Diederich, F. *Chem. Eur. J.* **2002**, *8*, 3601–3613.
- [131] Roncali, J. *J. Mater. Chem.* **1997**, *7*, 2307–2321.
- [132] Guerro, M.; Pham, N. H.; Massue, J.; Bellec, N.; Lorcy, D. *Tetrahedron* **2008**, *64*, 5285–5290.
- [133] Enkelmann, V. *Chem. Mater.* **1994**, *6*, 1337–1340.
- [134] Sato, M.; Gonnella, N. C.; Cava, M. P. *J. Org. Chem.* **1979**, *44*, 930–934.
- [135] Bellec, N.; Boubekeur, K.; Carlier, R.; Hapiot, P.; Lorcy, D.; Tallec, A. *J. Phys. Chem. A* **2000**, *104*, 9750–9759.

- [136] Inagi, S.; Naka, K.; Chujo, Y. *J. Mater. Chem.* **2007**, *17*, 4122–4135.
- [137] Tasis, D.; Tagmatarchis, N.; Bianco, A.; Prato, M. *Chem. Rev.* **2006**, *106*, 1105–1136.
- [138] Zhao, Y.; Rice, N. A.; Zhou, N.; Mahmud, I. *ECS Trans.* **2008**, *13*, 31–41.
- [139] Dyke, C. A.; Tour, J. M. *Chem. Eur. J.* **2004**, *10*, 812–817.
- [140] Strano, M. S.; Dyke, C. A.; Usrey, M. L.; Barone, P. W.; Allen, M. J.; Shan, H.; Kittrell, C.; Hauge, R. H.; Tour, J. M.; Smalley, R. E. *Science* **2003**, *301*, 1519–1522.
- [141] Star, A.; Liu, Y.; Grant, K.; Ridvan, L.; Stoddart, J. F.; Steuerman, D. W.; Diehl, M. R.; Boukai, A.; Heath, J. R. *Macromolecules* **2003**, *36*, 553–560.
- [142] Ortiz-Acevedo, A.; Xie, H.; Zorbas, V.; Sampson, W. M.; Dalton, A. B.; Baughman, R. H.; Draper, R. K.; Musselman, I. H.; Dieckmann, G. R. *J. Am. Chem. Soc.* **2005**, *127*, 9512–9517.
- [143] Yang, H.; Wang, S. C.; Merciera, P.; Akins, D. L. *Chem. Commun.* **2006**, 1425–1427.
- [144] Chen, F.; Wang, B.; Chen, Y.; Li, L.-J. *Nano Lett.* **2007**, *7*, 3013–3017.
- [145] Marquis, R.; Greco, C.; Sadokierska, I.; Lebedkin, S.; Kappes, M. M.; Michel, T.; Alvarez, L.; Sauvajol, J.-L.; Meunier, S.; Mioskowski, C. *Nano Lett.* **2008**, *7*, 1830–1835.

- [146] Peng, X.; Komatsu, N.; Bhattacharya, S.; Shimawaki, T.; Aonuma, S.; Kimura, T.; Osuka, A. *Nature Nanotech.* **2007**, *2*, 361–365.
- [147] Oxley, J. D.; Prozorov, T.; Suslick, K. S. *J. Am. Chem. Soc.* **2003**, *125*, 11138–11139.
- [148] Aida, T.; Fukushima, T. *Phil. Trans. R. Soc. A* **2007**, *365*, 1539–1552.
- [149] Rice, N. A.; Soper, K.; Zhou, N.; Merschrod, E.; Zhao, Y. *Chem. Commun.* **2006**, 4937–4939.
- [150] Zhou, Q.; Swager, T. M. *J. Am. Chem. Soc.* **1995**, *117*, 12593–12602.
- [151] Smaldone, R. A.; Moore, J. S. *Chem. Eur. J.* **2008**, *14*, 2650–2657.
- [152] Welton, T. *Chem. Rev.* **1999**, *99*, 2071–2083.
- [153] Rice, N. A. M.Sc. thesis, Department of Physics and Physical Oceanography, Memorial University of Nfld., 2008.
- [154] Bandyopadhyaya, R.; Nativ-Roth, E.; Regev, O.; Yerushalmi-Rozen, R. *Nano Lett.* **2002**, *2*, 25–28.
- [155] Jiang, Y.; Perahia, D.; Wang, Y.; Bunz, U. H. F. *Macromolecules* **2006**, *39*, 4941–4944.



